TAMPEREEN TEKNILLINEN YLIOPISTO
TAMPERE UNIVERSITY OF TECHNOLOGY

Janis Werner

Directional Antenna System-Based DoA/RSS Estimation, Localization and Tracking in Future Wireless Networks: Algorithms and Performance Analysis

Julkaisu 1350 • Publication 1350

Tampere 2015

Tampereen teknillinen yliopisto. Julkaisu 1350
Tampere University of Technology. Publication 1350

Janis Werner

Directional Antenna System-Based DoA/RSS Estimation, Localization and Tracking in Future Wireless Networks: Algorithms and Performance Analysis

Thesis for the degree of Doctor of Science in Technology to be presented with due permission for public examination and criticism in Tietotalo Building, Auditorium TB224, at Tampere University of Technology, on the 23rd of November 2015, at 12 noon.

Tampereen teknillinen yliopisto - Tampere University of Technology
Tampere 2015

Supervisor

Mikko Valkama, Professor
Department of Electronics and Communications Engineering
Tampere University of Technology
Tampere, Finland

Pre-examiners

Magnus Jansson, Professor
Department of Signal Processing
KTH – Royal Institute of Technology
Stockholm, Sweden

Kaushik Roy Chowdhury, Associate Professor
Department of Electrical and Computer Engineering
Northeastern University
Boston, USA

Opponent

Emil Björnson, Assistant Professor
Department of Electrical Engineering
Linköping University
Linköping, Sweden

ISBN 978-952-15-3634-2 (printed)
ISBN 978-952-15-3653-3 (PDF)
ISSN 1459-2045

Abstract

Location information plays an important role in many emerging technologies such as robotics, autonomous vehicles, and augmented reality. Already now the majority of smartphone owners use their devices' localization capabilities for a broad range of location-based services. Currently, location information in smartphones is mostly obtained in a device-centric approach, where the device to be localized, here referred to as the target node (TN), estimates its own location using, for example, the global positioning system (GPS). However, TNs with wireless communication capabilities can be localized based on their transmitted signals by a third party. In particular, localization can be implemented as a functionality of a wireless network. Depending on the application area and implementation, this network-centric approach has several advantages compared to device-centric localization, such as reducing the energy consumption within the TNs, enabling localization of non-cooperative TNs, and making location information available in the network itself. Current generation wireless networks are already capable of coarse localization. However, these existing localization capabilities do not suffice for the challenging demands of future applications. The majority of approaches moreover does not exploit the fact that an increasing number of base stations (BSs) and user devices are equipped with directional antennas. However, directional antennas enable direction of arrival (DoA) estimation that can, in turn, serve as the basis for advanced localization and location tracking. In this thesis, we thus study the application of directional antennas for localization and location tracking in future generation wireless networks. The contributions of this thesis can be grouped into two topics.

First, this thesis provides a detailed study of DoA/received signal strength (RSS) estimation and localization with a group of directional antennas herein denoted as sectorized antennas. This group of antennas is of particular interest as it encompasses a broad range of directional antennas that can be implemented with a single RF front-

end. Thus, the hardware complexity of sectorized antennas is low in comparison to the conventionally used antenna arrays that require multiple transceiver branches. However, at the same time this means that DoA estimation with sectorized antennas has to be implemented in a fundamentally different way. In order to address these differences, the study of sectorized antennas in this thesis includes the derivation of Cramer-Rao bounds (CRBs) for DoA/RSS estimation and localization, the proposal of three different DoA/RSS estimators, as well as numerical and analytical performance evaluations of DoA/RSS estimation and localization using sectorized antennas.

Second, this thesis deals with localization based on the fusion of DoA and RSS estimates as well as DoA and time of arrival (ToA) estimates. It is shown that the combination of these estimates can result in a much increased localization performance compared to a localization based on one of these estimates alone. For the localization based on DoA/RSS estimates, a mechanism explaining this improvement is revealed by means of a CRB analysis. Thereafter, DoA/RSS-based fusion is further studied using an extended Kalman filter (EKF) as an example location tracking algorithm. Finally, an EKF is proposed that tracks the location of a TN by fusing DoA and ToA estimates. Apart from a significantly improved tracking performance, this joint DoA/ToA-EKF moreover provides estimates for the TN device clock offset and is able to localize the TN in situations where a classical DoA-only EKF fails to provide a location estimate altogether.

Overall, this thesis thus provides insights into benefits of localization and location tracking using directional antennas, accompanied by specific DoA/RSS estimation, localization and location tracking solutions, as well as design guidelines for implementing localization systems in future generation wireless networks.

Preface

This thesis is based on research work carried out during the years 2011–2015 at the Department of Electronics and Communications Engineering, Tampere University of Technology, Tampere, Finland.

First and foremost, I would like to express my deepest gratitude to my supervisor, Prof. Mikko Valkama for providing me the opportunity to work in his team and for his invaluable guidance during all these years. His hard-working nature, extensive knowledge and experience in this field and research in general have been an incredible support in this part of my education. My gratitude extends to Prof. Danijela Cabric, who has hosted me in her research group at the University of California Los Angeles and whose support and suggestions have been very important for this thesis as well. For the highly beneficial collaboration with the Huawei Research Center, I would like to express my gratitude to Kari Leppänen. I would also like to thank Prof. Markku Renfors for his tremendous influence in making our current and former department such a pleasant place to work, as well as for sharing his vast knowledge in the area of digital communications.

I am grateful to Prof. Kaushik Roy Chowdhury and Prof. Magnus Jansson for acting as pre-examiners for this thesis. Moreover, I would like to express my gratitude to Prof. Emil Björnson for agreeing to act as the opponent at my defense.

For the financial support, I would like to thank the following organizations and funds: the Doctoral Programme of the President of Tampere University of Technology, the Tuula and Yrjö Neuvo Fund, the Nokia Foundation, and the Finnish Funding Agency for Technology and Innovation (Tekes, under the projects "Reconfigurable Antenna-based Enhancement of Dynamic Spectrum Access Algorithms" and "5G Networks and Device Positioning").

During the time of the research leading to this thesis, I had plenty of productive and downright enjoyable discussions with my co-authors Aki Hakkarainen, Jun Wang,

and Mário Costa. This has been a very important contribution and I am very thankful for that. Further, I am very fortunate to have been working in a research environment with such a great atmosphere and so many nice people. I would like to thank my current and former roommates Adnan Kiayani, Jaakko Marttila, and Simran Singh. For the countless discussions, lunches, dinners, coffees, evenings and laughs shared, I would like to thank the aforementioned as well as Dani Korpi, Pedro Figueiredo e Silva, Mahmoud Abdelaziz, Timo Huusari, Joonas Säe, Ahmet Hasim Gokceoglu, Paschalis Sofotasios, Sener Dikmese, Yaning Zou, Jukka Talvitie, Markus Allén, Matias Turunen, Lauri Anttila, Toni Levanen, Tero Isotalo, Ville Syrjälä, Vesa Lehtinen, and everyone else whom I had the pleasure of meeting in these years.

I also would also like to acknowledge all the people here at Tampere University of Technology who have helped me with practical matters. Specifically, I would like to thank Tarja Erälaukko, Soile Lönnqvist, Ulla Siltaloppi, Heli Ahlfors, and Elina Orava.

I am also grateful to my friends from outside of work. In particular, I would like to thank my climbing friends who have been instrumental in the important task of helping me to forget this work altogether every once in a while.

My education would not have been possible without my family. I am so very grateful to all of them, in particular to my parents and sisters who have been a tremendous support throughout my whole life.

Last but not least, I would like to express my deepest gratitude to my dear girlfriend Katja Kekki for her love, understanding, and support during all these years that we have shared together.

Tampere, October 2015,

Janis Werner

Table of Contents

List of Publications

This thesis is a compound thesis based on the following seven publications.

[P1] J. Werner, A. Hakkarainen, J. Wang, D. Cabric, and M. Valkama, "Performance and Cramer-Rao bounds for DoA/RSS estimation and transmitter localization using sectorized antennas," accepted for publication in *IEEE Transactions on Vehicular Technology*, 2015.

[P2] J. Werner, A. Hakkarainen, J. Wang, N. Gulati, D. Patron, D. Pfeil, K. Dandekar, D. Cabric, and M. Valkama, "Sectorized antenna-based DoA estimation and localization: Advanced algorithms and measurements," in *IEEE Journal on Selected Areas in Communications*, vol. 33, pp. 2272–2286, Nov. 2015.

[P3] J. Werner, A. Hakkarainen, and M. Valkama, "Estimating the primary user location and transmit power in cognitive radio systems using extended Kalman filters," in *Proceedings of the 10th Annual Conference on Wireless On-Demand Network Systems and Services (WONS)*, Banff, AB, 2013, pp. 155–161.

[P4] J. Werner, A. Hakkarainen, J. Wang, D. Cabric, and M. Valkama, "Primary user localization in cognitive radio networks using sectorized antennas," in *Proceedings of the 10th Annual Conference on Wireless On-Demand Network Systems and Services (WONS)*, Banff, AB, 2013, pp. 68–73.

[P5] J. Werner, A. Hakkarainen, J. Wang, D. Cabric, and M. Valkama, "Primary user DoA and RSS estimation in cognitive radio networks using sectorized antennas," in *Proceedings of the 8th International Conference on Cognitive Radio Oriented Wireless Networks (CROWNCOM)*, Washington, DC, 2013, pp. 43–48.

[P6] J. Werner, A. Hakkarainen, and M. Valkama, "Cramer-Rao bounds for hybrid RSS-DOA based emitter location and transmit power estimation in cognitive radio networks," in *Proceedings of the IEEE 78th Vehicular Technology Conference (VTC fall)*, Las Vegas, NV, 2013, pp. 1–7.

[P7] J. Werner, M. Costa, A. Hakkarainen, K. Leppänen, and M. Valkama, "Joint user node positioning and clock offset estimation in 5G ultra-dense networks," accepted for publication in *Proceedings of the IEEE Global Communications Conference (GLOBECOM), San Diego, CA, 2015.*

Abbreviations

5G	Fifth generation
ACF	Autocorrelation function
AN	Access node
AoA	Angle of arrival
AR	Auto-regressive
AWGN	Additive white Gaussian noise
BS	Base station
CR	Cognitive radio
CRB	Cramer-Rao bound
D2D	Device-to-device
DBS	Different beamwidth sectors
DC-CDMA	Direct sequence code division multiple access
DCAA	Digitally controlled antenna array
DFU	DoA fusion
DoA	Direction of arrival
E-OTD	Enhanced observed time difference
E911	Enhanced 911
EBS	Equal beamwidth sectors
EKF	Extended Kalman filter
ESA	Equal sector antenna
ESPAR	Electronically steerable parasitic array radiator
EW	Equal weighting
FIM	Fisher information matrix
GNSS	Global navigation satellite system
GPS	Global positioning system

ITU	International telecommunication union
LMMSE	Linear minimum mean-square error
LoS	Line of sight
LS	Least squares
LTE	Long term evolution
LWA	Leaky-wave antenna
METIS	Mobile and wireless communications enablers for the twenty-twenty information society
MGSCM	METIS geometry-based stochastic channel model
MIMO	Multiple-input multiple-output
ML	Maximum likelihood
MMSE	Minimum mean-square error
MSE	Mean-squared error
MVUE	Minimum variance unbiased estimator
NLoS	Non line of sight
OFDM	Orthogonal frequency-division multiplexing
ON	Observing node
OTDoA	Observed time difference of arrival
PDF	Probability density function
ppm	Parts per million
PU	Primary user
PW	Power weighting
RMSE	Root-mean-squared error
RRMSE	Relative root-mean-squared error
RSS	Received signal strength
RToA	Round-trip time of arrival
SBS	Switched-beam system
SDE	Sector-pair DoA estimation
SINR	Signal-to-interference-plus-noise ratio
SLS	Simplified least squares
SNR	Signal-to-noise ratio
SSL	Sector selection
SSP	Side-sector suppression
STD	Standard deviation
SU	Secondary user
TDoA	Time difference of arrival
TN	Target node
ToA	Time of arrival
TSLS	Three-stage SLS
UN	User node

VW	Variance weighting
WCL	Weighted centroid localization
WLAN	Wireless local area network

Symbols and Notations

a_s	Side-sector suppression (SSP)
α	Path-loss coefficient
c	Speed of light
d_k	Euclidean distance between target node (TN) and observing node (ON) k
$\delta(t)$	Dirac delta function
ϵ	Sector power
γ	Received signal strength (RSS)
φ	(Azimuth) direction of arrival (DoA)
ρ	Radiation pattern in power domain
τ	Time of arrival (ToA)
x	x-coordinate of target node (TN)
Δx_k	$\Delta x_k = x - x_k$
x_k	x-coordinate of observing node (ON) k
y	y-coordinate of target node (TN)
Δy_k	$\Delta y_k = y - y_k$

y_k	y-coordinate of observing node (ON) k

CHAPTER 1

Introduction

1.1 Background and Research Motivation

With the rise of smartphones and other handheld devices equipped with global positioning system (GPS) receivers, the number of location-based services has increased significantly over the previous years. It was recently estimated that nowadays three quarters of smartphone owners actively use the location capabilities of their phones for navigation, in order to obtain location-based recommendations or to mark their location in social networks [122]. Apart from these basic services, location information also plays an important role in many emerging technologies such as robotics [100], autonomous vehicles [11], and augmented reality [78], among others. In fact, the indoor location market alone is expected to be worth over $4 billion by the year 2019 [4].

A lot of recent research also suggests that enhanced location awareness in future generation wireless networks will enable several advanced functionalities in the networks internally. In cognitive radio (CR) networks, knowledge about the primary user (PU) locations will make it possible to implement functionalities such as intelligent location aware power control and routing [108], spatio-temporal sensing, as well as spectrum policy enforcement [22]. In fifth generation (5G) mobile networks accurate estimation, tracking and prediction of user node (UN) locations is expected to facilitate advanced interference mitigation, an improved utilization of the available radio resources, and proactive radio resource management, among others [31, 43]. If accurate UN location information is obtained within the networks, it can be provided to third parties, such as intelligent transportation services, thereby opening new business opportunities for the network operators [31, 43].

While the available localization technologies are constantly improving, we also experience increasingly demanding applications and requirements. For E911 emergency calls,

for example, the federal communications commission specified in 1999 that network-based localization should be capable of delivering an accuracy of less than 100 m for 67 % of the time, and less than 300 m for 95 % of the time [1]. Now in 2015, we face proposals that the upcoming 5G networks should be able to localize the UNs with an accuracy in the sub-meter range [6, 71]. Clearly, this accuracy cannot be achieved with existing technologies.

Network-aided UN localization schemes, such as localization with enhanced observed time difference (E-OTD) [85, 97], uplink-time difference of arrival [44, 85], and observed time difference of arrival (OTDoA) [5, 65, 85, 97], achieve accuracies of a few tens of meters. Higher accuracies can be achieved with global navigation satellite system (GNSS) solutions ($\approx$ 5 m [28]) or WiFi fingerprinting (3 – 4 m [61]). However, fingerprinting requires the creation and maintenance of large databases [47], whereas GNSS solutions require a clear view to the sky and are thus not universally applicable [28,42]. In addition, GNSS receivers have a very high energy consumption, meaning that GNSS cannot serve as the basis for continuous location tracking on handheld devices. The GPS receivers on modern smartphones, as an example, consume 100 mW – 150 mW [25]. Finally, neither GNSS solutions nor fingerprinting alone will meet the targeted accuracy requirements for 5G. On the other hand, PU localization in CR networks does not have the same stringent accuracy requirements. However, in contrast to UNs in a 5G network, PUs do not cooperate with the secondary users (SUs) [19]. This poses enormous constraints on the PU localization process, which have to be taken into account in the development of corresponding localization and location tracking solutions.

UN localization schemes specified in 2G, 3G and 4G cellular communication standards are mainly based on received signal strength (RSS) or propagation time measurements [27, 120]. However, in modern wireless communication networks, an increasing number of access nodes (ANs) and even UNs are equipped with multiple antennas [15, 68]. In fact, the massive multiple-input multiple-output (MIMO) approach, where the number of antennas at the ANs is significantly larger than the number of served users, is often considered a key technology for the upcoming 5G networks [15, 104]. Primarily intended to increase the networks capacity [114], this widespread availability of multi-antenna devices further enables a localization using direction of arrival (DoA) estimates obtained at individual multi-antenna devices. Apart from equipping devices with multiple antennas, the network capacity can also be improved by using other directional antennas such as reconfigurable antennas [16, 52, 80]. Compared to multi-antenna systems, some other directional antennas require a smaller number of RF chains and can even be implemented using a single RF front-end only. As such, they may be the preferable antenna choice for applications where AN or UN devices are subject to stringent cost or size limitations [40, 95]. Now, independent of the type of directional antenna available at the network devices, directionality can always be exploited for localization. This,

of course, results in enormous opportunities for the development of localization and location tracking solutions in future generation wireless networks.

1.2 Thesis Scope and Objectives

The main objective of this thesis is to propose and investigate different solutions for DoA/RSS estimation, localization and location tracking with directional antennas in future generation wireless networks. This thesis focuses on two main research topics. The first focus lays on the study of sectorized antennas, which is a class of antennas encompassing directional antennas with a low hardware complexity, such as reconfigurable antennas. More specifically, the objective is to develop and analyze algorithms and ultimate performance bounds for low complexity DoA estimation and localization with sectorized antennas. The second focus is on the fusion of heterogeneous measurements for localization and location tracking. In this context, the aim is to analyze different fusion mechanisms and to develop suitable location tracking algorithms specifically targeted for future generation wireless networks.

1.3 Outline and Main Results of the Thesis

The main outcomes of this thesis are

- definition and motivation of the sectorized antenna model [P1], [P2], [P4], [P5]
- derivation of performance bounds for DoA/RSS estimation as well as localization with sectorized antennas, including an asymptotic analysis [P1]
- proposal of three different low-complexity DoA estimators and two different low-complexity RSS estimators for sectorized antennas [P4], [P5], [P2]
- extensive numerical as well as analytical performance evaluation of the proposed estimators along with a brief complexity analysis [P1], [P2], [P4], [P5]
- numerical study and measurement example for localization with sectorized antennas [P1], [P2], [P4]
- study of hybrid DoA/RSS-based localization through derivation of a performance bound [P6] and development of an example location tracking algorithm [P3]
- proposal and analysis of an algorithm for joint location and clock offset tracking using DoA and time of arrival (ToA) estimates, specifically developed for an application in 5G ultra-dense networks [P7]

The thesis is organized as follows. In Chapter 2 the most important topics of estimation theory are briefly discussed. Chapter 3 consists of a short overview of important concepts for localization and tracking in wireless networks. The actual contributions of this thesis are then presented in Chapters 4 and 5. More specifically, Chapter 4 covers the contributions to DoA/RSS estimation and localization with sectorized antennas, whereas Chapter 5 presents the contributions related to localization and location tracking through fusion of DoA estimates with RSS or ToA estimates. Finally, a summary and the conclusions of the thesis can be found in Chapter 6.

1.4 Author's Contributions to the Publications

The research leading to this thesis was started in the context of the Tekes-funded project "Reconfigurable Antenna-based Enhancement of Dynamic Spectrum Access Algorithms." This project inspired the author's interest in the topic area of this thesis. Another Tekes-funded project entitled "5G Networks and Device Positioning" later served as additional inspiration. The ideas for the publications [P1]–[P7] all stem from the author. Similarly, the vast majority of the implementation, analysis, and writing leading to publications [P1]–[P7] were also done by the author. However, the measurements in [P2] were obtained during a research visit of Aki Hakkarainen at Drexel University and without direct involvement of the author in the measurement process. In addition, the channel model implementation used in [P7] was provided by D.Sc. Mário Costa from the Huawei research center in Finland. General guidance and valuable suggestions for the research topics and the publications came from Prof. Mikko Valkama, who also initiated the Tekes-funded projects. The research area of the latter project was also partly suggested by D.Sc. Kari Leppänen from the Huawei Research Center in Finland. Additional guidance and valuable suggestions came from Prof. Danijela Cabric ([P1],[P2], [P4], [P5]) from the University of California Los Angeles (UCLA). Moreover, the research was discussed in detail with Dr. Jun Wang ([P1],[P2], [P4], [P5]), D.Sc. Mário Costa ([P7]), and Aki Hakkarainen ([P1]–[P7]). All these persons also contributed to the final appearance of the respective publications.

1.5 Mathematical Notation

Throughout this thesis, vectors and matrices are written as boldface letters. The $N \times N$ identity matrix is written as $\mathbf{I}_N$, whereas $\mathbf{1}_{M\times N}$ and $\mathbf{0}_{M\times N}$ denote the $M \times N$ matrices where all elements are equal to ones and zeros, respectively. Similarly, $\mathbf{1}_M$ and $\mathbf{0}_M$ denote the $M \times 1$ column vectors where all elements are equal to ones and zeros, respectively. When the dimensions are clear from the context, we sometimes write those matrices and vectors simply as $\mathbf{I}$, $\mathbf{1}$ and $\mathbf{0}$. $\mathbf{M}^{\mathrm{T}}$, $\mathbf{M}^{\mathrm{H}}$, and $\mathbf{M}^{-1}$ represent the transpose, conjugate

transpose and inverse of the matrix $\mathbf{M}$, respectively. $\mathbf{M} = \mathrm{diag}(\mathbf{x})$ is a diagonal matrix composed of the elements of vector $\mathbf{x}$ on its diagonal and $\mathbf{A} \circ \mathbf{B}$ is the Hadamard product of the matrices $\mathbf{A}$ and $\mathbf{B}$ with equal dimensions. Moreover, $|\mathbf{M}|$ and $\mathrm{tr}(\mathbf{M})$ denote the determinant and trace of matrix $\mathbf{M}$, respectively.

For two real scalars $x \in \mathbb{R}$ and $y \in \mathbb{R}$, $\mathrm{mod}_y(x)$, $\min(x, y)$, and $\max(x, y)$ denote the remainder of the division x/y, the minimum, and the maximum of x and y, respectively. The error function for a real scalar $x \in \mathbb{R}$ is defined as

$$\mathrm{erf}(x) = \frac{2}{\sqrt{\pi}} \int_0^x e^{-t^2} dt, \tag{1.1}$$

whereas the imaginary error function is defined as [3]

$$\mathrm{erfi}(x) = -i\,\mathrm{erf}(ix) = \frac{2}{\sqrt{\pi}} \int_0^x e^{t^2} dt. \tag{1.2}$$

For a complex number $z \in \mathbb{C}$, z^* denotes its complex conjugate and $|z|$ its absolute value. The absolute difference of two integer circular values $i, j \in \{1, 2, \ldots, M\}$ is denoted as

$$|i - j|_M = \min[\mathrm{mod}_M(i - j), \mathrm{mod}_M(j - i)] \tag{1.3}$$

and the function

$$\mathcal{M}(\varphi') = \mathrm{mod}_{2\pi}(\varphi' + \pi) - \pi \tag{1.4}$$

wraps the real value φ' from $\mathbb{R}$ to $[-\pi; \pi)$. Expressions involving angular quantities, such as DoAs, are generally stated assuming that the angular quantities are given in radiants, while numerical examples of angular quantities are mostly given in degrees for ease of interpretation. The partial derivative of a function $f : \mathbb{R} \to \mathbb{R}$ w.r.t the scalar x is written in short as

$$[f]_x = \frac{\partial f(x)}{\partial x}. \tag{1.5}$$

Derivatives of vector functions are always element-wise.

For a random vector $\mathbf{X} \in \mathbb{R}^N$ with probability density function (PDF) $p(\mathbf{x})$, the expected value is defined as

$$\mathrm{E}[\mathbf{X}] = \int_{-\infty}^{\infty} \mathbf{x}\, p(\mathbf{x})\, d\mathbf{x}, \tag{1.6}$$

whereas the corresponding variance is defined individually for each of the elements X_i, $i = 1 \dots N$ of $\mathbf{X}$ as

$$\mathrm{var}[X_i] = \mathrm{E}\big[(X_i - \mathrm{E}[X_i])^2\big]. \tag{1.7}$$

Correspondingly, the covariance matrix of two vectors $\mathbf{X}_1, \mathbf{X}_2 \in \mathbb{R}^N$ is defined as

$$\mathrm{cov}[\mathbf{X}_1, \mathbf{X}_2] = \mathrm{E}\big[(\mathbf{X}_1 - \mathrm{E}[\mathbf{X}_1])(\mathbf{X}_2 - \mathrm{E}[\mathbf{X}_2])^T\big]. \tag{1.8}$$

$\mathbf{X} \sim \mathcal{N}(\boldsymbol{\mu}_x, \mathbf{Q}_x)$ denotes a Gaussian distributed real-valued random vector with mean vector $\boldsymbol{\mu}_x$ and covariance matrix $\mathbf{Q}_x = \mathrm{cov}[\mathbf{X}, \mathbf{X}]$, and $\mathbf{Z} \sim \mathcal{CN}(0, \mathbf{Q}_z)$ denotes a circular symmetric complex Gaussian distributed random vector with covariance $\mathbf{Q}_z = \mathrm{E}[\mathbf{Z}\mathbf{Z}^{\mathrm{H}}]$. A real random variable uniformly distributed on the interval $[a; b)$ is denoted by $X \sim \mathcal{U}(a; b)$.

CHAPTER 2

Estimation Theory Essentials

In estimation theory, the aim is to infer a parameter θ or parameter vector $\boldsymbol{\theta}$ from some measurement data $\mathbf{x}$. Towards that end, it is necessary to first find a good mathematical model for the data. In classical estimation theory, the parameters are assumed to be deterministic but unknown. Thus, the data can be described using the family of PDFs $p(\mathbf{x};\boldsymbol{\theta})$. In Bayesian estimation theory, in contrast, the unknown parameter to be estimated is assumed to be a realization of a random variable. Consequently, the data is described by the joint PDF $p(\mathbf{x},\boldsymbol{\theta}) = p(\mathbf{x}|\boldsymbol{\theta})p(\boldsymbol{\theta})$ composed of the prior PDF $p(\boldsymbol{\theta})$ and the conditional PDF $p(\mathbf{x}|\boldsymbol{\theta})$. In this chapter, we will shortly discuss the aspects of estimation theory that are most important for this thesis. In Chapter 2.1 aspects of classical estimation theory will be discussed, whereas Chapter 2.2 is dedicated to Bayesian estimation theory. In this thesis, we will be mostly dealing with real measurements and parameters. For simplicity, the following discussion therefore assumes $\mathbf{x} \in \mathbb{R}^N$ and $\boldsymbol{\theta} \in \mathbb{R}^K$.

2.1 Classical Estimation Theory

2.1.1 Performance Metrics and Unbiased Estimators

For a given estimation problem, it is possible to find a large variety of estimators. In order to enable a comparison of various estimators it is thus necessary to define some performance metrics. The two most widely used performance metrics are the bias and

mean-squared error (MSE). The bias of an estimator $\hat{\boldsymbol{\theta}}$ is defined as

$$\text{bias}[\hat{\boldsymbol{\theta}}] = \text{E}[\hat{\boldsymbol{\theta}}] - \boldsymbol{\theta} \tag{2.1}$$

and is thus a measure of how much an estimator deviates *on average* from the true value of the parameter. An estimator is called unbiased if

$$\text{E}[\hat{\boldsymbol{\theta}}] = \boldsymbol{\theta} \tag{2.2}$$

or equally $\text{bias}[\hat{\boldsymbol{\theta}}] = 0$ *for all possible parameter vectors* $\boldsymbol{\theta}$. Unbiasedness is thus a very desirable property as it tells us that an estimator will yield the correct value on average. The second metric, i.e., the MSE is defined element-wise as

$$\text{MSE}[\hat{\theta}_i] = \text{E}\Big[(\hat{\theta}_i - \theta_i)^2\Big] \tag{2.3}$$

which can easily be shown to be equal to

$$\text{MSE}[\hat{\theta}_i] = \text{var}[\hat{\theta}_i] + \Big(\text{bias}[\hat{\theta}_i]\Big)^2. \tag{2.4}$$

Hence, for unbiased estimators the MSE is indeed identical with the variance.

2.1.2 Cramer-Rao Bound

Besides comparing estimators against each other, it is of particular interest to evaluate an estimator in comparison to the ultimately achievable performance. The performance of unbiased estimators is therefore often compared to the Cramer-Rao bound (CRB). Given that the PDF $p(\mathbf{x};\boldsymbol{\theta})$ fulfills weak regularity conditions [56, p. 44], the CRB theorem states that the covariance $\mathbf{C}_{\hat{\boldsymbol{\theta}}}$ of any unbiased estimator $\hat{\boldsymbol{\theta}}$ is lower bounded by

$$\mathbf{C}_{\hat{\boldsymbol{\theta}}} - \mathbf{F}^{-1}(\boldsymbol{\theta}) \geq \mathbf{0} \tag{2.5}$$

where $\geq \mathbf{0}$ denotes that $\mathbf{C}_{\hat{\boldsymbol{\theta}}} - \mathbf{F}^{-1}(\boldsymbol{\theta})$ is positive semidefinite. In (2.5) $\mathbf{F}^{-1}(\boldsymbol{\theta})$ is known as the CRB, which is obtained as the inverse of the Fisher information matrix (FIM) $\mathbf{F}(\boldsymbol{\theta})$ with elements equal to

$$[\mathbf{F}(\boldsymbol{\theta})]_{ij} = -\,\text{E}\left[\frac{\partial^2 \ln p(\mathbf{x};\boldsymbol{\theta})}{\partial\theta_i\theta_j}\right]. \tag{2.6}$$

It follows from (2.5) that the variance of individual elements of $\hat{\boldsymbol{\theta}}$ are lower-bounded by [56]

$$\text{var}[\hat{\theta}_i] \geq [\mathbf{F}(\boldsymbol{\theta})^{-1}]_{ii}. \tag{2.7}$$

In general, it is not guaranteed that an estimator exists that achieves equality in (2.5). However, if such an estimator exists it is said to be *efficient*. The estimator resulting in the lowest variance for all elements and all possible values of the parameter vector $\boldsymbol{\theta}$ is called the minimum variance unbiased estimator (MVUE) [56, p. 116]. Conversely, if an efficient estimator exists it is the MVUE. However, not even the existence of the MVUE is guaranteed as there might not exist a *single* unbiased estimator that achieves the lowest variance for all values of the parameter vector.

A list of important properties for the CRB can be found in [119]. Note that for a given bias, the CRB can be modified to lower bound all estimators with that specific bias as shown in [102, p. 147]. In that case, the CRB is a lower bound on the MSE.

2.1.3 Maximum Likelihood Estimator

Even if the MVUE exists, it is in general not easy to find [56, p. 83]. In practice, estimators are therefore often determined using the maximum likelihood (ML) approach (see, e.g., [37, 62, 92, 93, 99]). The ML estimator is defined as the estimator maximizing

$$\hat{\boldsymbol{\theta}}_{\mathrm{ML}} = \arg\max_{\boldsymbol{\theta}} p(\mathbf{x};\boldsymbol{\theta}), \tag{2.8}$$

which can be found from

$$\frac{\partial \ln p(\mathbf{x};\boldsymbol{\theta})}{\partial \boldsymbol{\theta}} = \mathbf{0}. \tag{2.9}$$

Using the ML approach, we are thus able to obtain an estimator according to a well-defined principle. More importantly, the ML estimator is asymptotically for large data records unbiased and efficient, i.e.,

$$\lim_{N\to\infty} \hat{\boldsymbol{\theta}}_{\mathrm{ML}} \sim \mathcal{N}\big(\boldsymbol{\theta}, \mathbf{F}^{-1}(\boldsymbol{\theta})\big) \tag{2.10}$$

where $\mathbf{F}(\boldsymbol{\theta})$ is the FIM and N is the length of the data $\mathbf{x}$. Moreover, it can be shown that the ML estimator is always the efficient estimator if such an estimator exists at all [56, p. 187].

2.1.4 Least Squares Estimator

Another class of estimators frequently used in practice are the least squares (LS) estimators [89, 111, 113]. In contrast to ML estimators, the LS approach makes no assumptions about the statistics of the data, but only about the signal model. More specifically, it is assumed that the data is related to the parameters via a known function $\mathbf{s}(\boldsymbol{\theta})$. However, the exact dependency of $\mathbf{x}$ on $\boldsymbol{\theta}$ including, e.g., measurement noise is not assumed to be known. This, of course, makes the LS approach very practical in

situations where the noise statistics are not exactly known or where the signal model is only an approximation. At the same time, however, it also means that the LS approach is generally not optimal. The LS estimator is obtained by minimizing the norm

$$\hat{\boldsymbol{\theta}}_{\mathrm{LS}} = \arg\min_{\boldsymbol{\theta}} J_{\mathrm{LS}} \tag{2.11}$$

given by

$$J_{\mathrm{LS}} = (\mathbf{x} - \mathbf{s}(\boldsymbol{\theta}))^T (\mathbf{x} - \mathbf{s}(\boldsymbol{\theta})). \tag{2.12}$$

In case of a linear LS problem, we have $\mathbf{s}(\boldsymbol{\theta}) = \mathbf{H}\boldsymbol{\theta}$, which can be solved in closed-form as [56, p. 225]

$$\hat{\boldsymbol{\theta}}_{\mathrm{LS}} = (\mathbf{H}^T\mathbf{H})^{-1}\mathbf{H}^T\mathbf{x}. \tag{2.13}$$

Interestingly, if the measurement noise is *iid* zero-mean additive white Gaussian noise (AWGN), i.e., $\mathbf{x} - \mathbf{s}(\boldsymbol{\theta}) \sim \mathcal{N}(\mathbf{0}, \sigma^2\mathbf{I})$ then the LS estimator is equal to the ML estimator [56, p. 254].

2.2 Bayesian Estimation Theory

2.2.1 Minimum Mean Square Error Estimator

The calculation of the Bayesian MSE differs from the calculation of the classical MSE. In the Bayesian framework, the expected value in (2.3) is evaluated w.r.t. $p(\mathbf{x}, \theta_i)$, yielding the Bayesian MSE given by [56, p. 346]

$$\mathrm{MSE}[\hat{\theta}_i] = \int\int (\hat{\theta}_i - \theta_i)^2 \, p(\mathbf{x}, \theta_i) \, d\mathbf{x} \, d\theta_i \tag{2.14}$$

whereas in classical estimation theory the MSE is calculated as

$$\mathrm{MSE}[\hat{\theta}_i] = \int (\hat{\theta}_i - \theta_i)^2 \, p(\mathbf{x}; \theta_i) \, d\mathbf{x}. \tag{2.15}$$

Now, (2.14) can be shown to be minimized by the minimum mean-square error (MMSE) estimator defined as

$$\hat{\boldsymbol{\theta}}_{\mathrm{MMSE}} = \mathrm{E}[\boldsymbol{\theta}|\mathbf{x}] \tag{2.16}$$

which is element-wise calculated as

$$\hat{\theta}_{\mathrm{MMSE},i} = \int \theta_i \, p(\theta_i|\mathbf{x}) d\theta_i \tag{2.17}$$

where $p(\theta_i|\mathbf{x})$ is obtained by averaging over all θ_j, $j \neq i$ according to

$$p(\theta_i|\mathbf{x}) = \int \ldots \int \int \ldots \int p(\boldsymbol{\theta}|\mathbf{x}) \, d\theta_1 \ldots d\theta_{i-1} d\theta_{i+1} \ldots d\theta_p. \tag{2.18}$$

The integration involved in MMSE estimation is often difficult in practice. For the special case of jointly Gaussian $\boldsymbol{\theta}$ and $\mathbf{x}$, (2.16) can be solved in closed-form as [56, p. 325]

$$\hat{\boldsymbol{\theta}}_{\mathrm{MMSE,G}} = \mathrm{E}[\boldsymbol{\theta}] + \mathbf{C}_{\boldsymbol{\theta}\mathbf{x}} \mathbf{C}_{\mathbf{x}\mathbf{x}}^{-1} (\mathbf{x} - \mathrm{E}[\mathbf{x}]) \tag{2.19}$$

with $\mathbf{C}_{\boldsymbol{\theta}\mathbf{x}} = \mathrm{cov}[\boldsymbol{\theta}, \mathbf{x}]$ and $\mathbf{C}_{\mathbf{x}\mathbf{x}} = \mathrm{cov}[\mathbf{x}, \mathbf{x}]$. In many cases, however, the integrals in (2.16) cannot be solved in closed form and a numerical solution may be too computationally complex. One solution is then to resort to the linear minimum mean-square error (LMMSE) estimator, which is defined as the linear estimator

$$\hat{\theta}_{\mathrm{LMMSE},i} = \sum_{n=0}^{N-1} a_{in} x[n] + a_{iN} \tag{2.20}$$

minimizing the Bayesian MSE. This estimator is generally not optimal in the MMSE sense, but it can be solved in closed-form and is identical to (2.19) [56, p. 382]. Conversely, this means that jointly Gaussian $\boldsymbol{\theta}$ and $\mathbf{x}$ is a special case where the LMMSE estimator is in fact optimal in the MMSE sense.

2.2.2 Kalman Filter

So far we have reviewed different approaches for dealing with the estimation of fixed parameters. In tracking, however, parameters are assumed to evolve in time. To clearly distinguish between fixed parameters and those that evolve in time, the latter ones are often referred to as a state. The task in tracking is then to infer the state $\mathbf{s}[n]$ from the measurements $\mathbf{y}[n]$ taken at time-step n. Obviously, we could implement tracking by estimating states at every time-step individually, using some of the earlier discussed methods. However, if an estimate $\hat{\mathbf{s}}[n-1]$ is available at time-step n, this estimate can often be used as prior information for the estimation of $\hat{\mathbf{s}}[n]$. When tracking the location of a pedestrian, as an example, the change in location is clearly determined by the pedestrian's velocity. Thus, if we have obtained an estimate for the pedestrian's location and velocity at time-step $n-1$, we can already estimate the pedestrian's location at time-step n without taking any measurements. In order to exploit such knowledge, we obviously need a good model for the evolution of the state. In Kalman filtering this

model is often referred to as the state transition and is given by

$$\mathbf{s}[n] = \mathbf{F}\,\mathbf{s}[n-1] + \mathbf{w}[n] \tag{2.21}$$

The state transition (2.21) consists of the the state transition matrix $\mathbf{F}$ and the zero-mean driving noise $\mathbf{w}[n]$ with covariance matrix $\mathrm{E}[\mathbf{w}[n]\mathbf{w}^T[m]] = \delta_{m-n}\mathbf{R}[n]$ where δ_{i-j} is the Kronecker delta function. Note that (2.21) is a linear state transition as required in conventional Kalman filtering. Extensions for nonlinear models exist [91, p. 407]. However, in this thesis all state transitions will be of the above form.

In order to infer the state from the measurements, we have to find a model for the measurement equation

$$\mathbf{y}[n] = \mathbf{h}(\mathbf{s}[n]) + \mathbf{u}[n] \tag{2.22}$$

where $\mathbf{u}[n]$ is the zero-mean measurement noise with a covariance equal to $\mathrm{E}[\mathbf{u}[n]\mathbf{u}^T[m]] = \delta_{m-n}\mathbf{Q}[n]$. Note that we do not state the measurement equation in its most general form (see [91, p. 407]). However, in contrast to the linear state transition we now enable nonlinear relationships between the state and the measurements via the vector function $\mathbf{h}$. We allow this nonlinear relationship since all the measurements considered in this thesis depend nonlinearly on the location that we track.

In cases where both the state transition as well as the measurement equations are linear, i.e., $\mathbf{y}[n] = \mathbf{H}[n]\mathbf{s}[n] + \mathbf{u}[n]$ it is possible to obtain state estimates using the iterative Kalman filter. The Kalman filter is optimal in the MMSE sense if $\mathbf{w}[n]$ and $\mathbf{u}[n]$ are jointly Gaussian. And if the Gaussian assumption does not hold, the Kalman filter is still the optimal LMMSE estimator. However, as noted above the measurement equations are often nonlinear. Thus, in practice we often use the so-called extended Kalman filter (EKF) instead of the conventional Kalman filter. The main idea of the EKF is to linearize the nonlinear parts of the models using the current state estimate. As such, we generally cannot make any claims regarding optimality.

For each time-step n, the EKF consists of an *a priori* and an *a posteriori* estimation stage. In the *a priori* stage, we estimate the state $\hat{\mathbf{s}}^-[n]$ and covariance of the state estimate $\mathbf{P}^-[n]$ at time-step n using all measurements up to but excluding $\mathbf{y}[n]$. The estimation is given by

$$\hat{\mathbf{s}}^-[n] = \mathbf{F}\hat{\mathbf{s}}^+[n-1] \tag{2.23}$$

$$\mathbf{P}^-[n] = \mathbf{F}\mathbf{P}^+[n-1]\mathbf{F}^T + \mathbf{R}[n]. \tag{2.24}$$

In the *a posteriori* estimation stage, we estimate the state $\hat{\mathbf{s}}^+[n]$ and covariance of the state estimate at time-step n using all measurements up to and including $\mathbf{y}[n]$. The

calculation in the *a posteriori* estimation stage is according to

$$\mathbf{K}[n] = \mathbf{P}^{-}[n]\mathbf{H}[n]^{T}(\mathbf{H}[n]\mathbf{P}^{-}[n]\mathbf{H}^{T}[n] + \mathbf{Q}[n])^{-1} \tag{2.25}$$

$$\hat{\mathbf{s}}^{+}[n] = \hat{\mathbf{s}}^{-}[n] + \mathbf{K}[n]\big[\mathbf{y}[n] - \mathbf{h}(\hat{\mathbf{s}}^{-}[n])\big] \tag{2.26}$$

$$\mathbf{P}^{+}[n] = (\mathbf{I} - \mathbf{K}[n]\mathbf{H}[n])\mathbf{P}^{-}[n] \tag{2.27}$$

with the Jacobian matrix $\mathbf{H}[n] = \frac{\partial \mathbf{h}[n]}{\partial \mathbf{s}[n]}$ evaluated at $\hat{\mathbf{s}}^{-}[n]$. Interestingly, the EKF provides the possibility of state prediction. By executing the *a priori* estimation stage N times without the *a posteriori* stage, we are able to obtain a prediction $\hat{\mathbf{s}}^{\mathrm{p}}[n+N]$ using only measurements up to time-step n.

Note that the EKF is not the only approach for nonlinear filtering. An overview of other popular approaches such as unscented Kalman filters or particle filters can be found, for example, in [91]. Note, moreover, that the CRB discussed in Section 2.1.2 does not lower-bound the performance of Bayesian estimators such as the EKF. Sometimes, we can learn certain general properties of the estimation problem by deriving the classical CRB and benefit from the knowledge of these properties also in Bayesian estimation (see Section 5.1 for an example). However, if we are interested in a lower performance bound for, e.g., an EKF we have to refer to the so-called posterior CRB [101].

CHAPTER 3

Localization and Tracking in Wireless Networks

The aim of localization or positioning is to estimate the location $\boldsymbol{\ell} = [x, y]^T$ of a TN. In this thesis, we generally assume that this task is achieved by a set of K collaborating ONs in a wireless network. In accordance with the discussion in Section 1.1, we moreover assume that each of the ONs is equipped with some sort of a directional antenna as depicted in Figure 3.1. In order to localize the TN, each ON k, $k = 1 \dots K$ makes a measurement Ψ_k based on the TN signal and communicates this measurement to the fusion center, where the measurements from all K ONs are combined into a TN location estimate. In contrast to localization, we talk about location tracking when we estimate the evolution of the TN location over time. In the following discussion, we will mostly discuss localization. However, the majority of the topics discussed in this chapter also apply to location tracking.

This chapter is organized as follows. In Section 3.1 we discuss important properties of wireless networks, the ON devices, and the TN as well as their implications for localization and location tracking. Thereafter, in Section 3.2 we discuss measurements commonly used for localization in detail. Finally, in Section 3.3 we summarize the Stansfield fusion algorithm.

3.1 Properties of Wireless Networks and Implications for Localization and Location Tracking

In a practical wireless network, the choice of measurements for localization and location tracking as well as the fusion mechanisms are confined by the network properties, the ON devices and the nature of the TN. For time-based measurements the synchronization

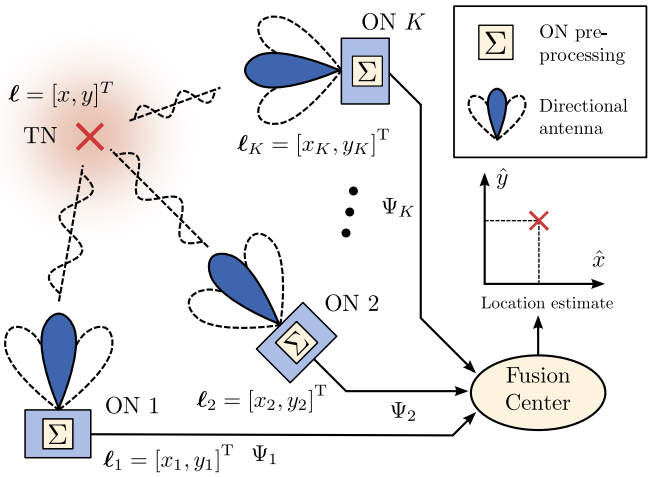

Fig. 3.1. Considered localization system where the observing nodes (ONs) collaborate to estimate or track the location of the target node (TN). ONs are assumed to be equipped with directional antennas.

of the network is of particular importance. In the best-case scenario, the clocks of the ONs are perfectly synchronized with the TN clock. In that case the distance d_k can be extracted directly from the ToA estimates (see Section 3.2.3). However, already very small synchronization errors significantly increase the ToA estimation error, which is related to the relative clock offsets via the speed of light, $c \approx 3 \times 10^8$ m/s. In many networks, a sufficiently accurate synchronization with the TN is not assumed to be given. Thus, location estimates are often obtained by fusing time difference of arrival (TDoA) estimates instead [5, 46]. However, utilizing TDoA estimates for localization still requires synchronization of the ONs. Without any synchronization in the network, the propagation time can be exploited using the so-called round-trip time of arrival (RToA) [29, 117]. In order to measure the RToA, an ON sends a packet to the TN. Once the TN receives the packet, it responds by sending the packet back to the ON [117]. The time between transmission and reception at the ON is then approximately equal to $2\,d_k/c$. However, RToA estimation obviously requires dedicated two-way localization signaling, which may not be feasible in networks that are primarily designed for communication purposes, such as the 5G network considered in [57] that also forms the basis for the localization system proposed in [P7].

Apart from synchronization, the nature of the TN has important implications for the applicability of time-based measurements. In PU localization, spectrum policy enforcement, or military applications, the TN is generally non-cooperative [55, 79, 105–107,109]. This means that both ToA and RToA estimates are not available for localization. If, in addition, the network is unable to synchronize the ONs, TDoA estimates are also unavailable. In these cases, localization is generally based on RSS [64, 109] or DoA estimates [79, 105]. A problem arises when multiple non-cooperative TNs have to be

localized simultaneously. Distinguishing between the TNs with RSS measurements only is generally not possible. Thus, localization of multiple non-cooperative TNs is often performed using DoA estimates [30, 105]. However, in the fusion process DoAs estimates have to be associated to the TNs. This is commonly done using Bayesian methods [10] or by choosing the association that minimizes a given optimization criterion [30, 105].

In general, the fusion process can be implemented in a central or distributed fashion. In a classical cellular network architecture, a central fusion entity is readily available. However, for CR networks, as an example, it is often assumed that fusion has to be distributed among the CR devices [109]. Many centralized fusion algorithms such as the Kalman filter, weighted centroid localization [14] and the Stansfield algorithm [92] exist also in distributed versions [82,106,109] that achieve equal [82] or close to equal [106,109] performance as their centralized counterparts.

The antenna type employed at individual ONs influences the way DoA estimates can be obtained. Naturally, ONs need to be equipped with some sort of directional antenna in order to make DoA estimation possible in the first place [117]. Most flexibility is achieved when ONs are equipped with digitally controlled antenna arrays (DCAAs), which enables array processing techniques such as the MUSIC DoA estimator [88]. However, DoA estimators for other directional antennas exist as well. Later in Chapter 4, for example, we develop DoA estimators for the group of sectorized antennas. In fact these estimators could also be used with DCAAs if a less complex DoA estimation is desired. Low complexity might be required if the ONs are mobile devices with limited battery and/or computational resources. Such a scenario arises, e.g., in CR networks where the SU devices are involved in the PU localization [79, 105–107, 109] or in networks, where the UNs assist in the localization of another UN by means of device-to-device (D2D) communication [27]. In some cases it may even be required to select only a subset of all available ONs in order to reduce the overall energy consumption in the network. The selection of ONs employing DoA estimation, as an example, has been studied in [53, 55], taking into account that certain ONs-TN geometries produce better location estimates than others.

Note that the above discussion serves as an overview of topics that have been important in the making of this thesis. Therefore, it is not complete and the referenced literature by no means exhaustive. In general, it is also important to note that the discussed properties and implications are interdependent. In a network where the ONs are not synchronized, it could be possible to obtain synchronization by estimating the clock offsets of the ONs. However, this would probably increase the burden on the ON devices, which may again be prohibitive for resource limited ONs. Similarly, it was shown that it is possible to employ array processing techniques with certain sectorized antennas by letting the TN repetitively send the same signal [75,96,103]. Again, however, this is only an option if dedicated localization signaling is possible, which also always

implies a cooperative TN. A simplified summary of the discussion in this section can be found in Table 3.1.

3.2 Measurements for Localization and Tracking

3.2.1 Direction of Arrival (DoA)

In DoA estimation, the aim is to estimate the angle of an incoming signal. For a signal arriving from the line of sight (LoS) at an ON k, the DoA is equal to

$$\varphi_k = \arctan \frac{\Delta y_k}{\Delta x_k} \tag{3.1}$$

where $\Delta x_k = x - x_k$ and $\Delta y_k = y - y_k$. DoAs are sometimes also referred to as angle of arrivals (AoAs) or, especially in the past, as bearings. In the literature many different approaches for DoA estimation exist. For DCAAs, the most popular approaches such as MUSIC [88] and ESPRIT [86] are based on subspace processing requiring the estimation of the covariance matrix of the received signal. However, also other methods exist such as the RIMAX algorithm [99] that obtains the DoA from channel estimates using the ML approach.

When the focus is on the DoA fusion rather than on the estimation, DoA estimates are often modeled as [37, 92, 107]

$$\hat{\boldsymbol{\varphi}} = \boldsymbol{\varphi} + \delta\boldsymbol{\varphi} \tag{3.2}$$

where $\boldsymbol{\varphi} = [\varphi_1, \varphi_2, \ldots, \varphi_K]^T$ and $\delta\boldsymbol{\varphi}$ is the estimation error, assumed to be normally distributed $\delta\boldsymbol{\varphi} \sim \mathcal{N}(\mathbf{0}_K, \mathbf{Q}_\varphi)$ with covariance matrix $\mathbf{Q}_\varphi = \mathrm{diag}[\sigma^2_{\varphi,1}, \ldots, \sigma^2_{\varphi,K}]$. Modeling DoA estimation errors as normally distributed is motivated by the fact that many DoA estimators result in asymptotically normally distributed errors. This was shown for MUSIC in [93] and is, as discussed in Section 2.1.3, well known for any ML estimator such as RIMAX. Moreover, it is intuitively clear that DoA estimation errors of ONs with sufficient spatial separation are approximately uncorrelated, which, in turn, motivates the diagonal covariance matrix.

However, it is important to notice that the DoA is a circular quantity, defined on an (arbitrary) interval of 360° such as $\varphi \in [0°; 360°)$ or $\varphi \in [-180°; 180°)$. Consequently, adding 1° to a DoA of 359° would result in a DoA of 0° instead of 360° when using the former interval definition. In the development of DoA estimators the circular property of DoAs is generally ignored [86, 88, 99]. On the one hand, it is always possible to map DoA estimates $\varphi < 0°$ or $\varphi \geq 360°$ back to the correct interval, meaning that an estimate of 361° would simply become 1°. On the other hand, the mapping between the numerical values $[0°; 360°)$ and the actual physical angles is also arbitrary. Thus, by changing the

Tab. 3.1. Properties of wireless networks and implication on location estimation and tracking. Note that this table serves as a simplified summary of the discussion in Section 3.1 and some of the entries are a tendency rather than definite facts.

	Synchronization			**TN**		**Fusion**	
	none	ONs	ONs-TN	cooperative	non-cooperative	central	distributed
ToA	×	×	✓	✓	×	–	–
TDoA	×	✓	✓	–	–	–	–
RToA	–	–	–	✓	×	–	–
Req. data association	–	–	–	×	✓	–	–
Examples	[113]		[5, 46]	[75, 89, 96, 103, 113]	[10, 105–107, 109]	[8, 14, 37, 92]	[55, 106, 109]

	ON resources		**ON antennas**			**Localization signaling**	
	limited	not of primary concern	non-directional	sectorized	DCAAs	opportunistic	dedicated
DoA	–	–	×	✓	✓	–	–
Array processing	×	✓	×	×	✓	–	–
RToA	–	–	–	–	–	×	✓
Examples	[P1],[P2], [P4], [P5], [55]	[88]	[64, 109, 113]	[P1],[P2], [P4], [P5], [38, 75, 96, 103]	[86, 88, 93, 94]	[P1],[P2], [P4], [P5]	[75, 89, 96, 103]

mapping we can in practice often avoid DoAs $\varphi < 0°$ or $\varphi \geq 360°$ altogether. However, for the performance analysis of localization systems it may occasionally be necessary to model the DoA estimation error using directional statistics. Examples of popular directional distributions are the von Mises distribution [63, p. 36] and the wrapped normal distribution [63, p. 50]. Intuitively, modeling the DoA estimation error with directional statistics is only necessary when the estimation error is very large. This is supported by the fact that, for certain parameterizations, the von Mises distribution can be well approximated by a normal distribution [63, p. 41]. In cases where this is possible, the Gaussian distribution then always has a comparably small variance. As such it is not surprising that the localization CRBs derived assuming von Mises distributed DoA estimation errors and Gaussian distributed errors are approximately equal when the standard deviation (STD) of the errors is smaller than 57° [112]. Unless noted otherwise, we thus model DoAs as non-circular in this thesis.

By fusing DoAs from as little as two ONs, it is possible to localize a TN on a two-dimensional coordinate system. This process of DoA-based localization is also known as triangulation. Using the Gaussian DoA estimation error model, the FIM for DoAs-based localization can be expressed as (see, e.g., [79])

$$\mathbf{J}_{\mathrm{DoA}} = \begin{bmatrix} [\boldsymbol{\varphi}]_x^T \mathbf{Q}_\varphi^{-1} [\boldsymbol{\varphi}]_x & [\boldsymbol{\varphi}]_x^T \mathbf{Q}_\varphi^{-1} [\boldsymbol{\varphi}]_y \\ [\boldsymbol{\varphi}]_x^T \mathbf{Q}_\varphi^{-1} [\boldsymbol{\varphi}]_y & [\boldsymbol{\varphi}]_y^T \mathbf{Q}_\varphi^{-1} [\boldsymbol{\varphi}]_y \end{bmatrix} \tag{3.3}$$

where $[\boldsymbol{\varphi}]_x$ and $[\boldsymbol{\varphi}]_y$ are the partial derivatives of the DoA vector with respect to the x and y coordinates of the TN. These partial derivatives are given by

$$[\varphi_k]_x = -\frac{\Delta y_k}{d_k^2} \tag{3.4}$$

$$[\varphi_k]_y = \frac{\Delta x_k}{d_k^2}. \tag{3.5}$$

A popular DoA fusion method is the Stansfield algorithm that will be reviewed in Section 3.3. The Stansfield estimator assumes LoS links between the ONs and the TN. An algorithm for localization in a non line of sight (NLoS) condition was proposed in [89]. However, the algorithm in [89] relies on the availability of DoA estimates and ToA estimates at both link ends, i.e., at the ONs as well as at the TN.

3.2.2 Received Signal Strength (RSS)

Localization based on the RSS exploits the fact that electromagnetic signals are subject to a propagation loss that increases with the distance between the TN and the ONs.

The propagation loss is often modeled using the log distance path-loss model given by

$$\gamma_k = P - 10\alpha \lg(d_k/d_\mathrm{o}) + S_k \tag{3.6}$$

where γ_k is the RSS at ON k in dB, d_o is a reference distance (conveniently $d_\mathrm{o} = 1\,\mathrm{m}$), P is the transmit power at reference distance, and α is the path-loss coefficient. The path-loss coefficient is an environmental parameter that is, e.g., $\alpha = 2$ for propagation in a vacuum. In order to account for fluctuations in the path-loss, the model (3.6) moreover includes the random variable $S_i \sim \mathcal{N}(0, \sigma_\mathrm{f}^2)$ known as shadow fading. These fluctuations are caused, among others, by obstacles and reflections in the propagation environment. Therefore, the shadow fading for two closely located ONs k and l is generally correlated. Commonly, the correlation is modeled according to the Gudmundson model [39] which suggests a covariance

$$\operatorname{cov}[S_i, S_j] = \sigma_\mathrm{f}^2 \exp\left(-\frac{|\boldsymbol{\ell}_i - \boldsymbol{\ell}_j|}{d_\mathrm{c}}\right) \tag{3.7}$$

that depends on the distance $|\boldsymbol{\ell}_i - \boldsymbol{\ell}_j|$ relative to the so-called correlation distance d_c, which is again an environmental parameter. Note that apart from (3.6), other models, such as the ITU indoor propagation loss model [49], exist.

In general, the parameter P in (3.6) is unknown to the localization system. Thus, P has to be included in the estimation, even if we are primarily interested in the TN location. Parameters such as P that are not target of the estimation but an unknown part of the model are often referred to as nuisance parameters [56, p. 328]. For the estimation problem at hand, including P as a nuisance parameter results in a parameter vector $\boldsymbol{\theta} = [x, y, P]^T$. Based on this parameter vector, the FIM for localization using RSS estimates can be derived as [113]

$$\mathbf{J}_{\mathrm{RSS,u}} = \begin{bmatrix} [\boldsymbol{\gamma}]_x^T \mathbf{Q}_\gamma^{-1} [\boldsymbol{\gamma}]_x & [\boldsymbol{\gamma}]_x^T \mathbf{Q}_\gamma^{-1} [\boldsymbol{\gamma}]_y & [\boldsymbol{\gamma}]_x^T \mathbf{Q}_\gamma^{-1} [\boldsymbol{\gamma}]_P \\ [\boldsymbol{\gamma}]_x^T \mathbf{Q}_\gamma^{-1} [\boldsymbol{\gamma}]_y & [\boldsymbol{\gamma}]_y^T \mathbf{Q}_\gamma^{-1} [\boldsymbol{\gamma}]_y & [\boldsymbol{\gamma}]_y^T \mathbf{Q}_\gamma^{-1} [\boldsymbol{\gamma}]_P \\ [\boldsymbol{\gamma}]_x^T \mathbf{Q}_\gamma^{-1} [\boldsymbol{\gamma}]_P & [\boldsymbol{\gamma}]_y^T \mathbf{Q}_\gamma^{-1} [\boldsymbol{\gamma}]_P & [\boldsymbol{\gamma}]_P^T \mathbf{Q}_\gamma^{-1} [\boldsymbol{\gamma}]_P \end{bmatrix} \tag{3.8}$$

where the covariance matrix of RSS estimates $\mathbf{Q}_\gamma$ is given by (3.7) and where the partial derivatives of (3.6) are element-wise given by

$$[\gamma_k]_x = -\frac{10\alpha}{\ln 10} \frac{\Delta x_k}{d_k^2} \tag{3.9}$$

$$[\gamma_k]_y = -\frac{10\alpha}{\ln 10} \frac{\Delta y_k}{d_k^2} \tag{3.10}$$

$$[\gamma_k]_P = 1. \tag{3.11}$$

In the literature, different practical algorithms for localization based on RSS estimates exist. The simplest form of localization is based on the proximity of ONs to the TN [17,18]. Such solutions exploit that increasing distances eventually result in a path-loss so large that the ONs are unable to detect the TN signal. In centroid localization [18], as an example, the TN location is estimated as the average of all ON coordinates that can detect the TN signal. A refinement of this approach is known as weighted centroid localization, where the coordinates from each ON are weighted with a term relative to their RSS [14, 109]. Starting from a generic path-loss model comparable to (3.6), the authors in [113] derive a LS estimator for localization based on RSS estimates. Finally, a very popular approach for indoor localization based on RSS estimates is known as fingerprinting [54, 84]. Fingerprinting is commonly implemented in a device-centric approach and does not assume any specific model for the path-loss. Instead, the idea is to estimate the TN location by comparing RSS measurements from, e.g., WLAN access points to an existing database consisting of a mapping from RSS values to a geographical location. In that way fingerprinting is more robust to situations where path-loss models fail to describe the environment adequately [45, 76]. On the other hand, fingerprinting requires the creation and updating of the RSS database, which may be infeasible in some applications.

3.2.3 Time of Arrival (ToA)

In theory, the ToA can be estimated by very simple ON devices. In practice, however, the usefulness of ToA estimates is often limited by the synchronization in the network as discussed in Section 3.1. Given that an LoS connection between ON k and the TN exists, the ToA can be expressed as

$$\tau_k = \frac{d_k}{c}. \tag{3.12}$$

In contrast to the RSS that is in general readily available, the ToA has to be estimated. An overview of various ToA estimation approaches can be found in, e.g., [70]. For a unit-energy signal with spectrum $S(f)$ that is subject to AWGN, the CRB for ToA estimation is equal to (cf. [28])

$$\mathrm{CRB}_{\mathrm{ToA}} = \frac{1}{8\pi^2 \,\mathrm{SNR} \int\limits_{-\infty}^{\infty} f^2 |S(f)|^2 df} \tag{3.13}$$

where f is the frequency. Thus, from (3.13) we note that the performance of ToA estimation increases with an increasing signal-to-noise ratio (SNR) as well as with an increasing bandwidth of the signal. As a consequence, ToA-based localization is of particular interest in ultra-wideband communication systems [70, 90].

The process of fusing ToA estimates into a location estimate is also known as trilateration. CRBs for a localization based on ToA estimates can be found in [24, 51]. If a TN-ON synchronization does not exist, ToA estimates are often transformed into TDoA estimates defined as $\tau_i - \tau_j$, $i, j \in \{1 \dots K\}$, $i \neq j$. The fusion of TDoA estimates is also known as multilateration. An example algorithm that fuses TDoAs into a location estimate can be found in [46]. In practice, TDoA-based localization finds its application, e.g., in the OTDoA feature that is part of the LTE standard.

3.3 Fusion with the Stansfield Algorithm

The Stansfield algorithm is a popular fusion algorithm for localization with DoA estimates. It was first proposed in [92] and is an approximation of the ML estimator [37]. Assuming the DoA estimation model (3.2), the ML norm can be expressed as

$$J_{\mathrm{ML}} = \frac{1}{2} \sum_{k=1}^{K} \frac{f_k^2}{\sigma_{\varphi,k}^2} \tag{3.14}$$

where $f_k = \arctan\left(\frac{\Delta y_k}{\Delta x_k}\right) - \hat{\varphi}_k$ is the error of the individual DoA estimates. Now, (3.14) is a non-linear function of the TN location that can only be solved with iterative methods, which may be prone to divergence [37, 107]. However, for small DoA estimation errors, we can make the approximation $\sin(f_k) \approx f_k$, which leads to an ML norm equal to

$$J_{\mathrm{ML}} \approx J_{\mathrm{ST}} = \frac{1}{2} (\mathbf{A}\boldsymbol{\ell} - \mathbf{b})^T \mathbf{D}^{-1} \mathbf{Q}_{\varphi}^{-1} (\mathbf{A}\boldsymbol{\ell} - \mathbf{b}) \tag{3.15}$$

with

$$\mathbf{A} = \begin{bmatrix} \sin\hat{\varphi}_1 & -\cos\hat{\varphi}_1 \\ \vdots & \vdots \\ \sin\hat{\varphi}_K & -\cos\hat{\varphi}_K \end{bmatrix}; \quad \mathbf{b} = \begin{bmatrix} x_1 \sin\hat{\varphi}_1 - y_1 \cos\hat{\varphi}_1 \\ \vdots \\ x_K \sin\hat{\varphi}_K - y_K \cos\hat{\varphi}_K \end{bmatrix}, \tag{3.16}$$

and $\mathbf{D} = \mathrm{diag}[d_1^2, \dots, d_K^2]$. Apart from the multiplication with the diagonal matrix $\mathbf{D}^{-1}\mathbf{Q}_{\varphi}^{-1}$, the norm J_{ST} in (3.15) takes the form of the LS norm in (2.12). In fact, (3.15) can be interpreted as a weighted LS norm, which can be solved in closed-form [56, p. 226] and results in the Stansfield estimator

$$\hat{\boldsymbol{\ell}}_{\mathrm{ST}} = (\mathbf{A}^T \mathbf{D}^{-1} \mathbf{Q}_{\varphi}^{-1} \mathbf{A})^{-1} \mathbf{A}^T \mathbf{D}^{-1} \mathbf{Q}_{\varphi}^{-1} \mathbf{b}. \tag{3.17}$$

The Stansfield estimator in its conventional form depends on the the distances d_k via the matrix $\mathbf{D}$. If the Stansfield estimator is used in DoA-only fusion, the matrix $\mathbf{D}$ is

not available. However, already in [92] it was noted that J_{ST} is a weak function of $\mathbf{D}$. Thus, in practice $\mathbf{D}$ is often replaced with an identity matrix [107].

Overall, the Stansfield estimator has several advantages. First, it is a closed-form solution for DoA-based localization. Second, it has been studied extensively with several analytical approximations for its performance available in the literature [37, 106, 110]. Additionally, since the Stansfield algorithm is an approximation of the ML estimator, we know that it is asymptotically and for small errors efficient (see Section 2.1.3). This asymptotic efficiency has also been shown numerically for the modified Stansfield algorithm not relying on $\mathbf{D}$ [107]. Finally and as noted before, the Stansfield algorithm also exists in a distributed version resulting only in a small performance loss [106].

CHAPTER 4

DoA/RSS Estimation and Localization Using Sectorized Antennas

In this thesis, we define sectorized antennas as an abstract antenna model that helps us to develop and analyze performance of low-complexity DoA/RSS estimators and localization algorithms with a broad range of directional antennas. Our definition of the sectorized antenna model was first introduced in [P4]. Therein, a sectorized antenna was defined as an antenna structure that can receive energy selectively from a set of different sectors. More specifically, sectors were defined as a continuous range of angles, whereas selectivity implies a strong attenuation of signals arriving from outside of the activated sector. According to our definition, sectorized antennas are generally also incapable of receiving a signal within more than a single sector at a time. This last part of our definition is of particular importance as it indicates that a sectorized antenna can be implemented with a single RF front-end, which, in turn, implies a low hardware complexity as illustrated in Figure 4.1. Overall, the sectorized antenna model thus encompasses many directional antennas such as leaky-wave antennas (LWAs) [81], electronically steerable parasitic array radiators (ESPARs) [96] as well as switched-beam systems (SBSs) [38], i.e., antenna arrays with a single RF front-end. However, this also means that DoA estimation with sectorized antennas has to be implemented in a fundamentally different way compared to DoA estimation with DCAAs.

While DoA estimators for sectorized antennas exist in the literature, they are generally limited to a specific type of sectorized antenna, require a specific signal type, dedicated localization signaling, or a cooperative TN. In [7], the DoA is estimated with an LWA by continuously changing the antenna's main beam. As such, the approach is limited

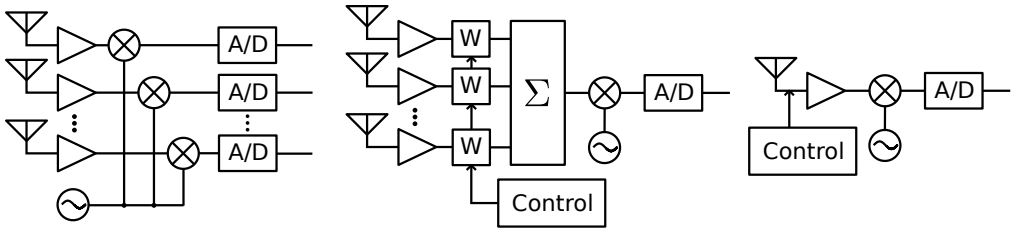

Fig. 4.1. Hardware required for different directional antenna types. Left: digitally controlled antenna array (DCAA), middle: switched-beam system (SBS), right: single RF front-end sectorized antenna.

to certain types of sectorized antennas and takes longer than a measurement in sectors (i.e. discrete steps). A DoA estimator that estimates the DoA of a wideband pulsed signal by exploiting the angle-dependent frequency response of an LWA was proposed in [118]. Through repetitively sending the same signal at the TN, ESPARs [96] or LWAs [75, 103] can be used to emulate DCAAs making MUSIC-based DoA estimation possible. However, such an approach obviously requires a cooperating TN and dedicated localization signaling. The authors of [38] propose an algorithm for estimating the DoAs of multiple DC-CDMA signals impinging on a base station (BS) equipped with an SBS. However, the estimator proposed in [38] requires either knowledge of the RSS at the BS or an additional omnidirectional BS antenna for proper normalization of the received signals.

In this chapter we will thus study DoA estimation and localization with sectorized antennas in a more generic framework. More specifically, we will derive performance bounds for DoA estimation with sectorized antennas, propose generic, low-complexity DoA estimators for sectorized antennas and study their performance in comparison to the bounds. Due to the directivity of sectorized antennas, the RSS at ONs equipped with sectorized antennas is not readily available. Therefore, we will also briefly discuss RSS estimation with sectorized antennas, albeit in much less detail compared to DoA estimation. Finally, we also derive performance bounds for localization with sectorized antennas and study the performance of a practical localization algorithm.

This chapter is organized as follows. In Section 4.1 we introduce our model for sectorized antennas in more detail. Section 4.2 is dedicated to DoA/RSS estimation with sectorized antennas, whereas localization with sectorized antennas is discussed in Section 4.3. This chapter concludes with a measurement example in Section 4.4 and a summary in Section 4.5.

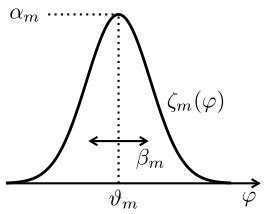

Fig. 4.2. Illustration of the Gaussian radiation pattern model $\zeta_m(\varphi)$ in (4.1). Every sector m is parameterized via the attenuation α_m, the beamwidth β_m, and the orientation ϑ_m.

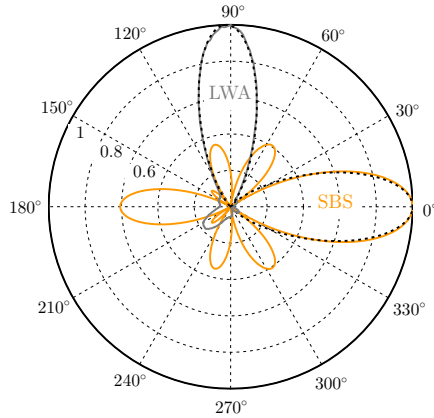

Fig. 4.3. Example for main beam approximation (dotted line) with Gaussian radiation pattern model (4.1). The example includes a) the measured radiation pattern of a sector with orientation $\vartheta = 90°$ from a leaky wave antenna (LWA) [81] and b) the theoretical radiation pattern of a sector with orientation $\vartheta = 0°$ from a SBS with an underlying uniform circular antenna array consisting of 8 antenna elements.

4.1 The Sectorized Antenna Model

4.1.1 Radiation Pattern Model

In this thesis we model a sectorized antenna via its radiation pattern. Towards that end, we approximate the main-beam in each of the sectors m, $m = 1, \ldots, M$ as

$$\zeta_m(\varphi) = \alpha_m \exp\left(-\frac{[\mathcal{M}(\varphi - \vartheta_m)]^2}{\beta_m^2}\right). \tag{4.1}$$

As illustrated in Figure 4.2, each sector m in (4.1) can be parameterized by the attenuation α_m, the orientation ϑ_m, and the beamwidth β_m. Due to this parameterization, the model (4.1) is also suitable for sectorized antennas such as the LWA [81], where the shape of the main-beam varies throughout the sectors. In this thesis, the model (4.1) simplifies the performance analysis of sectorized antenna-based processing significantly. Moreover, since a Gaussian curve as used in our and related models [2,64], describes the main beam of many practical sectorized antennas very well [41], the model (4.1) also serves as the basis for our algorithm development in Section 4.2. The excellent fit of our model (4.1) to practical sectorized antennas is also illustrated in Figure 4.3 using as examples the measured radiation pattern of the LWA [81] and the theoretical pattern of an SBS based on a circular antenna array.

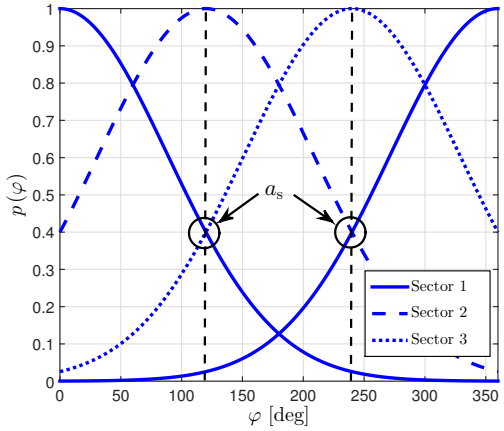

Fig. 4.4. Illustration of the side-sector suppression (SSP) for an equal sector antenna (ESA) with $M = 3$ sectors and $a_s = 0.4$

In the following, when considering a pair of sectors i and j, $i, j \in \{1, \ldots, M\}$ we will distinguish between the two cases

1. equal beamwidth sectors (EBS) $\beta_i = \beta_j$

2. different beamwidth sectors (DBS) $\beta_i \neq \beta_j$.

Moreover, we will denote antennas with $\alpha_i = \alpha_j = \alpha$, $\beta_i = \beta_j = \beta$ for all $i, j \in \{1, \ldots, M\}$, and $|\mathcal{M}(\vartheta_m - \vartheta_n)| = 2\pi/M = \Delta\vartheta$ for all neighboring sectors $|m - n|_M = 1$, $m, n \in \{1, \ldots, M\}$ as equal sector antennas (ESAs). A practical example of an ESA is the SBS based on a circular uniform antenna array depicted in Figure 4.3 that can be configured to fulfill all the above criteria. In this thesis we will parameterize ESAs via the so-called side-sector suppression (SSP), a_s. As illustrated in Figure 4.4, the SSP determines how much a signal is attenuated in the sectors $\mathrm{mod}_M(m) + 1$ and $\mathrm{mod}_M(m - 2) + 1$ when it arrives from the direction ϑ_m. This parameterization leads to a beamwidth equal to $\beta = 2\pi/[M\sqrt{\ln(1/a_s)}]$.

In order to simplify the presentation and without loss of generality, we assume in the following that the orientations ϑ_m $m = 1 \ldots M$ are the same at all ONs.

4.1.2 Sector-Powers

Our algorithm proposals and performance evaluations for sectorized antennas are based on so-called sector-powers. This was motivated in [P1] by showing that sector-powers form a sufficient statistic for DoA/RSS estimation as well as localization at individual ONs. We assume that sector-powers are calculated for every sector m, $m = 1, \ldots, M$ at

each ON k, $k = 1, \ldots, K$ as

$$\epsilon_{k,m} = \frac{1}{N} \sum_{n=0}^{N-1} |r_{k,m}[n]|^2 \tag{4.2}$$

where $r_{k,m}[n]$ results from sampling the time-continuous received signal $\tilde{r}_{k,m}(t)$ with sampling period T_s. In this thesis we consider, in general, cases where the LoS path is dominating the received signal. Then, we can express the received signal as

$$r_{k,m}[n] = \zeta_{k,m} s_{k,m}[n] + w_{k,m}[n] \tag{4.3}$$

where $w_{k,m}[n] \sim \mathcal{CN}(0, \sigma_\mathrm{w}^2)$ is additive noise, $\zeta_{k,m} = \zeta_m(\varphi_k)$, and $s_{k,m}[n]$ is the incoming signal in sector m, impinging with DoA φ_k. Here, we model the incoming signal as complex circular symmetric Gaussian distributed according to $s_{k,m}[n] \sim \mathcal{CN}(0, \gamma_k)$ where γ_k is the RSS at ON k. This is a common model in, e.g., the spectrum sensing literature [98] and a good approximation for OFDM-based transmission with a reasonable number of subcarriers, as an example. For simplicity, we moreover model signal samples at individual ONs k, $k = 1 \ldots K$ as uncorrelated in time, meaning that $\mathrm{E}[s_{k,i}[n] s_{k,j}[m]] = \delta_{m,n}\delta_{i,j}\rho_{k,m}\gamma_k$. Overall, this results in received signal samples distributed as $r_{k,m}[n] \sim \mathcal{CN}(0, \rho_{k,m}\gamma_k)$ where $\rho_{k,m} = \zeta_{k,m}^2$. For moderate to large numbers of samples N, the sector-powers at individual ONs k are then approximately normally distributed according to $\epsilon_{k,m} \sim \mathcal{N}(g_{k,m}, \sigma_{k,m}^2)$ where $g_{k,m} = \rho_{k,m}\gamma_k + \sigma_\mathrm{w}^2$ and $\sigma_{k,m}^2 = \frac{1}{N}(\rho_{k,m}\gamma_k + \sigma_\mathrm{w}^2)^2$ with the property that $\mathrm{cov}[\epsilon_{k,i}, \epsilon_{k,j}] = \delta_{i,j}\sigma_{k,i}^2$ [P1] [P5].

Thus far, our sector-power model considers sector-powers at the ONs individually. Hence, the model as such will serve as the basis for our development and analysis of DoA/RSS estimators. However, in order to derive the localization CRB, where sector-powers from multiple ONs have to be considered jointly, the above model has to be extended. In particular, we cannot assume that sector-powers from different ONs are uncorrelated. In order to illustrate that, let us first write (4.3) in its time-continuous form, taking also the influence of the channel h_k from TN to ON k into account. This yields

$$\tilde{r}_{k,m}(t) = \zeta_{k,m} h_k \tilde{s}(t - \eta_k - (m-1)T_\mathrm{a}) + \tilde{w}_{k,m}(t) \tag{4.4}$$

with the propagation delay $\eta_k = d_k/c$, the sector switching period $T_\mathrm{a} = NT_\mathrm{s}$, and the TN signal $\tilde{s}(t)$ related to the incoming signal in (4.3) through

$$s_{k,m}[n] = h_k \tilde{s}(nT_\mathrm{s} - \eta_k - (m-1)T_\mathrm{a}). \tag{4.5}$$

For simplicity, we assume that h_k remains constant during the observation period and state the localization CRB for a given channel. In order to fulfill $s_{k,m}[n] \sim \mathcal{CN}(0, \gamma_k)$

we then have $\tilde{s}(t) \sim \mathcal{N}(0, \sigma_{\mathrm{s}}^2)$ and $\gamma_k = h_k^2 \sigma_{\mathrm{s}}^2$. Next, consider the sector-powers $\epsilon_{k,m}$ and $\epsilon_{l,m}$ from two ONs k and l, $k \neq l$ located on a circle around the TN. These sector-powers are composed of the received signal samples $r_{k,m}[n]$ and $r_{l,m}[n]$, which in turn originate from the TN signal $\tilde{s}(t)$ sampled at the exact same moment since $\eta_k = \eta_l$ in (4.5). Hence, the resulting sector-powers of ONs k and l are correlated. Obviously, a situation where $d_k = d_l$ will practically not occur. However, d_k can be arbitrarily close to d_l meaning that $\tilde{s}(t)$ is sampled at arbitrarily close time instants at ONs k and l. Thus, for $r_{k,m}[n]$ and $r_{l,m}[n]$ to be uncorrelated in all cases except $d_k = d_l$, the time-continuous TN signal $\tilde{s}(t)$ would have to be white, meaning an autocorrelation function (ACF) $u_{\tilde{s}}(\tau) = \mathrm{E}[\tilde{s}(t)\tilde{s}^*(t-\tau)] = \delta(\tau)$. At the same time, this also implies a signal with an infinite bandwidth, whereas all practical communication signals are essentially bandlimited. We thus conclude that received signal samples at different ONs are correlated, meaning that sector-powers at different ONs are also correlated. In order to comply with our assumption of uncorrelated received signal samples at individual ONs, we have to assume that $u_{\tilde{s}}(nT_{\mathrm{s}}) = 0$ for $n = \pm 1, \pm 2, \ldots$. Apart from that, we do not restrict the ACF $u_{\tilde{s}}(\tau)$. However, in the evaluation of the localization CRB, we have to assume a specific ACF. As an example, we then consider a TN signal bandlimited to the frequencies $-B/2 < f < B/2$, where B denotes the physical bandwidth of the actual RF signal. Such a signal has an ACF equal to [20, pp. 416-418]

$$u_{\tilde{s}}(\tau) = \sigma_{\mathrm{s}}^2 \operatorname{sinc}(B\tau), \tag{4.6}$$

which fulfills $u_{\tilde{s}}(nT_{\mathrm{s}}) = 0$ if we do not oversample at the ONs, i.e., $T_{\mathrm{s}} = 1/B$.

With the above model, we can now express the distribution of sector-powers from multiple ONs as follows. First define the vector composed of the sector-powers from all ONs as $\boldsymbol{\epsilon} = [\boldsymbol{\epsilon}_1^T, \ldots, \boldsymbol{\epsilon}_K^T]^T$ with $\boldsymbol{\epsilon}_k = [\epsilon_{k,1}, \ldots, \epsilon_{k,M}]^T$. Similarly, define $\bar{\boldsymbol{\gamma}} = [\gamma_1 \mathbf{1}_{1\times M}, \gamma_2 \mathbf{1}_{1\times M}, \ldots, \gamma_K \mathbf{1}_{1\times M}]^{\mathrm{T}}$, $\boldsymbol{\rho} = [\boldsymbol{\rho}_1^{\mathrm{T}}, \boldsymbol{\rho}_2^{\mathrm{T}}, \ldots, \boldsymbol{\rho}_K^{\mathrm{T}}]^{\mathrm{T}}$ with $\boldsymbol{\rho}_k = [\rho_{k,1}, \rho_{k,2}, \ldots, \rho_{k,M}]^{\mathrm{T}}$, and $\mathbf{g}_k = [\mathbf{g}_1, \ldots, \mathbf{g}_K]^T$ with $\mathbf{g}_k = [g_{k,1}, \ldots, g_{k,M}]^T$. The vector $\boldsymbol{\epsilon}$ is then approximately distributed as [P1] $\boldsymbol{\epsilon} \sim \mathcal{N}(\mathbf{g}, \mathbf{Q})$ with

$$\mathbf{Q} = \boldsymbol{\rho}\boldsymbol{\rho}^{\mathrm{T}} \circ \bar{\boldsymbol{\gamma}}\bar{\boldsymbol{\gamma}}^{\mathrm{T}} \circ \mathbf{C} + \mathbf{D} \tag{4.7}$$

$$\mathbf{D} = \frac{\sigma_{\mathrm{w}}^2}{N}\left(2\,\mathrm{diag}(\boldsymbol{\rho} \circ \bar{\boldsymbol{\gamma}}) + \sigma_{\mathrm{w}}^2 \mathbf{I}\right) \tag{4.8}$$

and the $KM \times KM$ matrix $\mathbf{C}$ composed of the $M \times M$ submatrices

$$\boldsymbol{\Omega}_{ij} = \begin{pmatrix} c_{ij}(0) & c_{ij}(-1) & \ldots & c_{ij}(-(M-1)) \\ c_{ij}(1) & c_{ij}(0) & \ldots & c_{ij}(-(M-2)) \\ \vdots & \vdots & \ddots & \vdots \\ c_{ij}(M-1) & c_{ij}(M-2) & \ldots & c_{ij}(0) \end{pmatrix} \tag{4.9}$$

with $i, j = 1 \dots K$ and elements

$$c_{ij}(m) = \frac{1}{N}\mathcal{R}(\Delta\eta_{ij} + mT_\mathrm{a}) - 1 + \frac{1}{N^2}\sum_{p=1}^{N-1}(N-p)[\mathcal{R}(\Delta\eta_{ij} + mT_\mathrm{a} + pT_\mathrm{s}) + \mathcal{R}(\Delta\eta_{ij} + mT_\mathrm{a} - pT_\mathrm{s})] \quad (4.10)$$

that are dependent on the normalized ACF of the squared envelope

$$\mathcal{R}(\tau) = \frac{1}{\sigma_\mathrm{s}^4}\,\mathrm{E}[|\tilde{s}(t)|^2|\tilde{s}(t-\tau)|^2]. \quad (4.11)$$

Since we have assumed a zero-mean Gaussian TN signal, (4.11) can be expressed in terms of the TN signal ACF as [77, pp. 67-68]

$$\mathcal{R}(\tau) = 1 + \frac{1}{\sigma_\mathrm{s}^4}|u_{\tilde{s}}(\tau)|^2. \quad (4.12)$$

For the example signal with ACF (4.6), we obtain $\mathcal{R}(\tau) = 1 + \mathrm{sinc}^2(B\tau)$ and

$$c_{ij}(m) = \frac{1}{N}\,\mathrm{sinc}^2(t_{ij}(m)) + \frac{1}{N}\sum_{p=1}^{N-1}(N-p)\big[\mathrm{sinc}^2(t_{ij}(m) + pBT_\mathrm{s}) + \mathrm{sinc}^2(t_{ij}(m) - pBT_\mathrm{s})\big] \quad (4.13)$$

where $t_{ij}(m) = B\Delta\eta_{ij} + mBT_\mathrm{a}$. Note that in the following our numerical results will be based on the example ACF (4.6), whereas the expressions are for a generic ACF fulfilling $u_{\tilde{s}}(nT_\mathrm{s}) \approx 0$ for $n = \pm1, \pm2, \dots$.

4.2 DoA/RSS Estimation Using Sectorized Antennas

In the following section, we consider DoA/RSS estimation at an individual ON k, $k = 1 \dots K$. Therefore, we could technically drop the dependence of, e.g., $\epsilon_{k,m}$ on k and simply write ϵ_m. However, for notational consistency we write all equations explicitly in terms of ON k.

4.2.1 Cramer-Rao Bound

In theory, the estimation of DoAs and RSSs with sectorized antennas is inseparable, meaning that we always have to estimate both, even if we are interested only in one of them. Thus, the parameter vector of our estimation problem is given as $\boldsymbol{\theta} = [\varphi_k, \gamma_k]^T$.

Given the assumptions outlined in Section 4.1.2, the FIM for DoA/RSS estimation using sectorized antennas then becomes [P1]

$$\mathbf{\Gamma}_{11} = (N+2)\sum_{m=1}^{M} a_{k,m}\tilde{\rho}_{k,m}^2 \tag{4.14}$$

$$\mathbf{\Gamma}_{12} = \mathbf{\Gamma}_{21} = \frac{N+2}{\gamma_k}\sum_{m=1}^{M} a_{k,m}\tilde{\rho}_{k,m} \tag{4.15}$$

$$\mathbf{\Gamma}_{22} = \frac{N+2}{\gamma_k^2}\sum_{m=1}^{M} a_{k,m} \tag{4.16}$$

with

$$a_{k,m} = (\mathrm{SNR}_{k,m}^{-1}+1)^{-2} \tag{4.17}$$

where $\mathrm{SNR}_{k,m} = \rho_{k,m}\,\mathrm{SNR} = \frac{\rho_{k,m}\gamma_k}{\sigma_{\mathrm{w}}^2}$ is the SNR in sector m and $\tilde{\rho}_{k,m} = \frac{[\rho_{k,m}]_{\varphi}}{\rho_{k,m}}$. For the Gaussian radiation pattern $\tilde{\rho}_{k,m}$ becomes $\tilde{\rho}_{k,m} = -4\mathcal{M}(\varphi_k - \vartheta_m)/\beta^2$. With (4.14)–(4.16), the CRBs on the root-mean-squared error (RMSE) of DoA estimation, $\mathrm{RMSE}_{\mathrm{DoA}}$, and the relative root-mean-squared error (RRMSE) on RSS estimation, $\mathrm{RRMSE}_{\mathrm{RSS}} = \mathrm{RMSE}_{\mathrm{RSS}}/\gamma_k$, are obtained as [P1]

$$\mathrm{RMSE}_{\mathrm{DoA}} = \sqrt{\left(\mathbf{\Gamma}^{-1}\right)_{11}} \tag{4.18}$$

$$\mathrm{RRMSE}_{\mathrm{RSS}} = \frac{1}{\gamma_k}\sqrt{\left(\mathbf{\Gamma}^{-1}\right)_{22}}. \tag{4.19}$$

The above CRBs could be expressed explicitly using the well-known formula for the inversion of a 2×2 matrix. However, the result is not very intuitive. Instead, we can also approximate (4.18), (4.19) using the CRB for DoA estimation when the RSS is known and the CRB for RSS estimation when the DoA is known. These CRBs are given as [P1]

$$\mathrm{RMSE}_{\mathrm{DoA}}^{\mathrm{a}} = \sqrt{\mathbf{\Gamma}_{11}^{-1}} = \sqrt{\frac{1}{N+2}\left(\sum_{m=1}^{M} a_{k,m}\tilde{\rho}_{k,m}^2\right)^{-1}} \tag{4.20}$$

$$\mathrm{RRMSE}_{\mathrm{RSS}}^{\mathrm{a}} = \frac{1}{\gamma_k}\sqrt{\mathbf{\Gamma}_{22}^{-1}} = \sqrt{\frac{1}{N+2}\left(\sum_{m=1}^{M} a_{k,m}\right)^{-1}} \tag{4.21}$$

which are in fact slightly smaller than the bounds for the complete estimation problem, i.e., $\mathrm{RMSE}_{\mathrm{DoA}} > \mathrm{RMSE}_{\mathrm{DoA}}^{\mathrm{a}}$ and $\mathrm{RRMSE}_{\mathrm{RSS}} > \mathrm{RRMSE}_{\mathrm{RSS}}^{\mathrm{a}}$. However, as verified numerically in [P1] and partially also later in Section 4.2.4, $\mathrm{RMSE}_{\mathrm{DoA}} \approx \mathrm{RMSE}_{\mathrm{DoA}}^{\mathrm{a}}$ and

$\mathrm{RRMSE}_{\mathrm{RSS}} \approx \mathrm{RRMSE}^{\mathrm{a}}_{\mathrm{RSS}}$ with good approximation. Note that the above expressions are all stated in a generic form and without assuming a specific radiation pattern.

Next, let us study the asymptotic behavior of the CRBs (4.18)–(4.19). Towards that end, we have to assume a specific radiation pattern and model $\rho_{k,m} = \zeta^2_{k,m}$ according to the Gaussian pattern in (4.1). As we have shown in [P1], for asymptotically large $\mathrm{SNR} \to \infty$ we then obtain

$$\mathrm{RMSE}^{\mathrm{SNR}}_{\mathrm{DoA}} = \frac{\sqrt{3}\pi}{|\ln(a_{\mathrm{s}})|\sqrt{(M^5 - M^3)(N+2)}} \tag{4.22}$$

$$\mathrm{RRMSE}^{\mathrm{SNR}}_{\mathrm{RSS}} = \frac{1}{\sqrt{M(N+2)}}\sqrt{1 + \frac{3\,M^2\,[\mathcal{P}(\varphi_k)]^2}{\pi^2\,(M^2-1)}}, \tag{4.23}$$

where $\mathcal{P}(\varphi) = \mathrm{mod}_{\Delta\vartheta}(\varphi + \Delta\vartheta/2) - \Delta\vartheta/2$. So far, all the CRB expressions were stated for a given DoA. In order to understand the average DoA/RSS estimation performance, assume a uniformly distributed DoA $\varphi_k \sim \mathcal{U}(-\pi, \pi)$. Then, the asymptotic CRBs (4.22)-(4.23) become [P1]

$$\overline{\mathrm{RMSE}}^{\mathrm{SNR}}_{\mathrm{DoA}} = \mathrm{RMSE}^{\mathrm{SNR}}_{\mathrm{DoA}} \tag{4.24}$$

$$\overline{\mathrm{RRMSE}}^{\mathrm{SNR}}_{\mathrm{RSS}} = \frac{1}{\sqrt{(M - \frac{1}{M})(N+2)}}. \tag{4.25}$$

Obviously, $\overline{\mathrm{RMSE}}^{\mathrm{SNR}}_{\mathrm{DoA}}$ is equal to $\mathrm{RMSE}^{\mathrm{SNR}}_{\mathrm{DoA}}$ since (4.22) is independent of the DoA. Asymptotically, for a large number of samples $N \to \infty$ the CRBs (4.18)–(4.19) approach zero. They are thus independent of the DoA and consequently the average CRBs is equal zero as well, i.e.,

$$\mathrm{RMSE}^{N}_{\mathrm{DoA}} = \overline{\mathrm{RMSE}}^{N}_{\mathrm{DoA}} = 0 \tag{4.26}$$

$$\mathrm{RRMSE}^{N}_{\mathrm{RSS}} = \overline{\mathrm{RRMSE}}^{N}_{\mathrm{RSS}} = 0. \tag{4.27}$$

4.2.2 Practical DoA/RSS Estimators

4.2.2.1 Max-E

MaxE is a simple low-complexity DoA/RSS estimator for ESAs [P4], with a DoA estimation principle similar to the estimators in [7, 73]. The estimator's underlying principle is based on the fact that the largest sector-power occurs on average in the sector i with the orientation ϑ_i that is closest to the DoA among all orientations ϑ_m, $m = 1 \ldots M$. In mathematical terms, the MaxE DoA estimator can be expressed as

$$\hat{\varphi}_{k,\mathrm{m}} = \{\vartheta_i \,|\, i = \arg\max_i \epsilon_i\}, \tag{4.28}$$

whereas the RSS is estimated as the maximum difference between sector-power and noise variance, i.e.,

$$\hat{\gamma}_{k,\mathrm{m}} = \max_i \epsilon_i - \sigma_{\mathrm{w}}^2. \tag{4.29}$$

Obviously, the complexity of (4.28) and (4.29) is very low. In fact, as discussed in [P2], the complexity of MaxE overall is almost exclusively determined by the sector-power calculation (4.2). On the other hand, MaxE also has a performance far from the CRB as will be seen in our analytical evaluation in Section 4.2.3 and as was also shown numerically in [P5].

4.2.2.2 SLS

As will be discussed in more detail in Section 4.2.3, the performance of MaxE is limited due to the discretization of DoA estimation in (4.28). In [P5], we have thus proposed the simplified least squares (SLS) DoA/RSS estimator. Much like MaxE, SLS is a DoA/RSS estimator for ESAs. However, SLS results in continuous DoA estimates with much improved performance compared to MaxE.

SLS estimates the DoA in two steps. In the first step, SLS finds the two sector-powers $\epsilon_{k,i}$ and $\epsilon_{k,j}$ best suited for DoA estimation. Towards that end, SLS finds the two neighboring sectors $i, j \in 1 \dots M$, $|i-j|_M = 1$ such that $\epsilon_{k,i} + \epsilon_{k,j} > \epsilon_{k,m} + \epsilon_{k,n}$ for all other neighboring sectors $m, n \in 1 \dots M$, $n, m \neq i, j$, $|n-m|_M = 1$. For simplicity and without loss of generality, assume next that $\vartheta_i = \vartheta_j + \Delta\vartheta$, which guarantees $\vartheta_i > \vartheta_j$ on the one hand and, on the other hand, that we do not have to account for the wrapping of DoAs at the boarders of the interval $[-\pi; \pi)$. The selected sectors i and j then encompass, with high probability, the DoA φ_k, i.e., $\vartheta_i \geq \varphi_k \geq \vartheta_j$.

Given that the sectorized antenna has sufficient selectivity, sectors other than i and j measure the TN signal with a large attenuation. Thus, in the second step SLS estimates the DoA/RSS using only the sector-powers $\epsilon_{k,i}$ and $\epsilon_{k,j}$. Now, obtaining an estimator via a standard estimation approach like ML or LS would result in an iterative method since sector-powers depend nonlinearly on the DoAs. Moreover and as already discussed in Section 4.1.2, sector-powers depend on both the DoA and RSS. In order to avoid problems associated with iterative estimation in multiple parameters, such as divergence, we thus first calculate the noise-centered sector-powers

$$p_{k,m} = \epsilon_{k,m} - \sigma_{\mathrm{w}}^2 \tag{4.30}$$

for $m = i, j$. Thereafter, we calculate the ratio $p_{k,i}/p_{k,j}$ that is approximately independent of the RSS. Now we can formulate the so-called SLS metric

$$J_{\mathrm{SLS}} = \left(\frac{p_{k,i}}{p_{k,j}} - \frac{\rho_{k,i}}{\rho_{k,j}} \right)^2, \tag{4.31}$$

which leads to the SLS DoA estimator when minimized over the DoA. Note that (4.31) is also independent of the RSS, meaning that we are able to estimate the DoA individually and without estimating the RSS. That this is possible is also indicated by the fact that the DoA estimation CRBs for known and unknown RSS are approximately equal as discussed later in Section 4.2.4. Obviously, J_{SLS} is generally still a non-linear function of the DoA. Due to DoAs being defined on a closed interval, the minimization of J_{SLS} could be performed using a one-dimensional grid-search on the interval $\varphi_k \in [-\pi; \pi)$. Exploiting our earlier guess that $\vartheta_i \geq \varphi_k \geq \vartheta_j$, we could restrict the search interval even further to $\varphi_k \in [-\vartheta_j; \vartheta_i]$. However, recalling that the main beams of many practical sectorized antennas can be well approximated by the Gaussian radiation pattern (4.1), we can solve the minimization of (4.31) in closed-form as

$$\hat{\varphi}_{\mathrm{SLS},k} = \bar{\vartheta}_{ij} + \kappa(\ln p_{k,i} - \ln p_{k,j}), \tag{4.32}$$

where $\bar{\vartheta}_{ij} = \frac{1}{2}(\vartheta_i + \vartheta_j)$ and $\kappa = -\pi/(2M \ln a_{\mathrm{s}})$. Once we have calculated (4.32), we can proceed to estimate the RSS, which is related to the DoA and sector powers via the radiation pattern $\hat{\rho}_{k,m} = [\zeta(\hat{\varphi}_k - \vartheta_m)]^2$. Exploiting this relationship, SLS estimates the RSS as

$$\hat{\gamma}_{\mathrm{SLS},k} = \frac{1}{2}\left[\frac{\epsilon_{k,i} - \sigma_{\mathrm{w}}^2}{\hat{\rho}_{k,i}} + \frac{\epsilon_{k,j} - \sigma_{\mathrm{w}}^2}{\hat{\rho}_{k,j}} \right]. \tag{4.33}$$

In order to prevent large estimation errors when the TN signal is severely attenuated, SLS includes a validation check that reduces the estimation to MaxE in the following cases:

1. If $p_{k,i} < 0$ or $p_{k,j} < 0$, then the DoA estimation is according to (4.28).

2. If the inequality $\vartheta_i \geq \hat{\varphi}_{\mathrm{SLS},k} \geq \vartheta_j$ does not hold, then RSS estimation is according to (4.29).

4.2.2.3 TSLS

In the development of SLS, we had assumed that all but two sectors measure the TN signal with such a low SNR that we can exclude all but two sector-powers from DoA estimation. As will be seen in Section 4.2.4, this assumption holds well for ESAs with $a_{\mathrm{s}} = 0.4$ and low to moderate SNRs. However, for large SNR and/or a stronger overlap

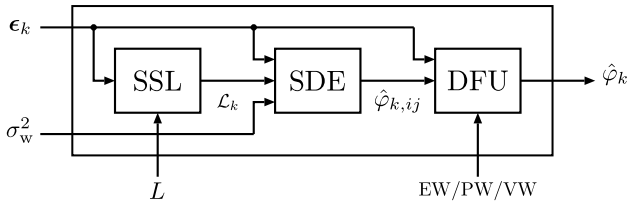

Fig. 4.5. The three stages of TSLS DoA estimation: sector selection (SSL), sector-pair DoA estimation (SDE), DoA fusion (DFU).

in the main beams, i.e. larger a_{s}, discarding all but two sector-powers results in a significant performance loss. Moreover, both MaxE and SLS are suitable for ESAs only. Thus, in order to address these shortcomings we have developed the three-stage SLS (TSLS) estimator in [P2]. In TSLS, we estimate the DoA in three stages and using L sectors as depicted in Figure 4.5. In the sector selection (SSL) stage, TSLS finds the subset $\mathcal{L}_k$ of L sectors best suited for DoA estimation. Pairs of the those L sectors are then used in the sector-pair DoA estimation (SDE) stage to estimate sector-pair DoAs. Finally, the sector-pair DoAs are fused into a final DoA estimate in the DoA fusion (DFU) stage. In the following we will be discussing each stage in detail.

Sector Selection (SSL)

Similarly to the selection of two sectors in SLS, the SSL stage in TSLS first finds two neighboring sectors such that $\epsilon_{k,q}\,\epsilon_{k,q+1} > \epsilon_{k,l}\,\epsilon_{k,l+1}$ for all other sector-pairs $(l, l+1)$, $l = 1, \ldots, M$, $l \neq q$. For antennas where α_m does not vary too strongly with m, we then have $\vartheta_q < \varphi_k < \vartheta_{q+1}$ with high probability. If L is even, the SSL stage is finished and returns the subset consisting of $\mathcal{L}_k = \{q - L/2 + 1, \ldots, q + L/2\}$. If L is odd, SSL first estimates whether φ_k is closer to ϑ_q or ϑ_{q+1} by comparing $\epsilon_{k,q}$ to $\epsilon_{k,q+1}$. If $\epsilon_{k,q} > \epsilon_{k,q+1}$ then it is likely that $|\varphi_k - \vartheta_q| < |\varphi_k - \vartheta_{q+1}|$ and SSL returns $\mathcal{L}_k = \{q - (L+1)/2 + 1, \ldots, q + (L-1)/2\}$. Otherwise, SSL returns $\mathcal{L}_k = \{q - (L-1)/2 + 1, \ldots, q + (L+1)/2\}$.

Note that for clarity of presentation, we have neglected the circularity of sector indices and DoAs in the above description. However, it is trivial to extend the above to take circularity into account. Note also that the SSL stage might have to be adapted for antennas other than the ones used in this thesis as discussed in more detail in [P2].

Sector-Pair DoA Estimation (SDE)

In the SDE stage, a sector-pair DoA is estimated for all sectors $i, j \in \mathcal{L}_k$, $i \neq j$. Towards that end, TSLS first calculates $p_{k,i}$ according to (4.30) for all $i \in \mathcal{L}_k$ and discards those sectors from $\mathcal{L}_k$ that have $p_{k,i} < 0$. Thereafter, for every sector-pair $i, j \in \mathcal{L}_k$, $i \neq j$ the sector-pair DoA $\hat{\varphi}_{k,ij}$ is obtained as the angle minimizing the corresponding J_{SLS}

metric, i.e.,

$$\hat{\varphi}_{k,ij} = \arg\min_{\varphi} \left(\frac{p_{k,i}}{p_{k,j}} - \frac{\rho_{k,i}(\varphi)}{\rho_{k,j}(\varphi)} \right)^2. \tag{4.34}$$

Making again use of our assumption that the main beam of our antenna can be approximated by (4.1), then (4.34) can be solved in closed-form. However, the solution is different for EBS and DBS.

1. *Equal beamwidth sectors:* For EBS, the sector-pair DoA is estimated as

$$\hat{\varphi}_{k,ij} = \bar{\vartheta}_{ij} + \kappa_{ij} \left(\ln \frac{p_{k,i}}{p_{k,j}} - 2 \ln \frac{\alpha_i}{\alpha_j} \right) \tag{4.35}$$

   where $\bar{\vartheta}_{k,ij} = \frac{1}{2}(\vartheta_i + \vartheta_j)$ and $\kappa_{ij} = \frac{\beta^2}{4(\vartheta_i - \vartheta_j)}$. For ESAs this solution is in fact equal to the DoA estimation in SLS.

2. *Different beamwidth sectors:* Solving (4.34) for DBS results in a quadratic equation. Hence, initially TSLS has to calculate two DoAs per DBS sector-pair according to

$$\hat{\varphi}_{k,ij}^{[1/2]} = \lambda_{ij} \pm b_{ij} g(p_{k,i}, p_{k,j}) \tag{4.36}$$

   with

$$g(p_{k,i}, p_{k,j}) = \sqrt{(\Delta\vartheta_{ij})^2 - \Delta\beta_{ij} \ln \frac{\alpha_i}{\alpha_j} + \frac{1}{2} \Delta\beta_{ij} \ln \frac{p_{k,i}}{p_{k,j}}}, \tag{4.37}$$

   where $\lambda_{ij} = \frac{\beta_i^2 \vartheta_j - \beta_j^2 \vartheta_i}{\Delta\beta_{ij}}$, $b_{ij} = \frac{\beta_i \beta_j}{\Delta\beta_{ij}}$, $\Delta\beta_{ij} = \beta_i^2 - \beta_j^2$, and $\Delta\vartheta_{ij} = \vartheta_i - \vartheta_j$. TSLS chooses either one of the solutions in (4.36) by taking estimates of the RSS into account. Similarly to (4.33), RSS estimates can be obtained for each solution $\hat{\varphi}_{k,ij}^{[l]}$, $l = 1, 2$ and each sector i, j as

$$\hat{\gamma}_{k,ij,m}^{[l]} = \frac{p_{k,m}}{[\alpha_m \exp(-[\mathcal{M}(\hat{\varphi}_{k,ij}^{[l]} - \vartheta_m)]^2 / \beta_m^2)]^2}. \tag{4.38}$$

   For $N \to \infty$, the RSS estimates $\hat{\gamma}_{k,ij,i}^{[l]}$ and $\hat{\gamma}_{k,ij,j}^{[l]}$ are equal if $\hat{\varphi}_{k,ij}^{[l]} = \varphi_k$. Thus, TSLS chooses the solution in (4.36) that minimizes $|\hat{\gamma}_{k,ij,i}^{[l]} - \hat{\gamma}_{k,ij,j}^{[l]}|$. In cases where (4.37) is imaginary, the respective sector-pair DoA is discarded.

DoA Fusion (DFU)

In the SDE stage, TSLS estimates P sector-pair DoAs $\hat{\varphi}_{k,ij} = \varphi_k + \delta\varphi_{k,ij}$ that are fused together into the final DoA estimate $\hat{\varphi}_k$ in the DFU stage. Obviously, when fusing the size of the errors $\delta\varphi_{k,ij}$ should be taken into account. However, conventional weighted

averaging does not perform well for DoA estimates due to their circular nature. Thus, in TSLS we use the weighted averaging for circular random variables proposed in [35]

$$\frac{\sin\hat{\varphi}_k}{\cos\hat{\varphi}_k} = \frac{\sum w_{k,ij}\sin\hat{\varphi}_{k,ij}}{\sum w_{k,ij}\cos\hat{\varphi}_{k,ij}}, \tag{4.39}$$

where $w_{k,ij}$ are the weights for the sector-pair DoA estimate $\hat{\varphi}_{k,ij}$. In this thesis, we consider the following three weighting schemes.

1. *Equal weighting (EW)*: In the simplest form of weighting we set all weights equal to one, i.e.,

$$w_{k,ij}^{\mathrm{EW}} = 1. \tag{4.40}$$

2. *Power weighting (PW)*: Sector-powers are an indication for the TN signal SNR within the corresponding sectors. Hence, a simple and robust weighting scheme is given by

$$w_{k,ij}^{\mathrm{PW}} = p_{k,i}p_{k,j}, \tag{4.41}$$

   where we use the noise-centered sector-powers $p_{k,m}$ in order to mitigate the influence of sectors dominated by the noise variance σ_{w}^2.

3. *Variance weighting (VW)*: Intuitively, the overall best performance is achieved with a weighting $w_{k,ij} = 1/\sigma_{ij}^2$ where $\sigma_{ij}^2 = \mathrm{var}[\delta\hat{\varphi}_{k,ij}]$ is the variance of the individual sector-pair DoA estimates. Now, in practice σ_{ij}^2 is generally not known. However, in Section 4.2.3.3 we derive an approximation $v_{k,ij}^{(1)} \approx \sigma_{ij}^2$ of the SP-DoA error variance in free space. This approximated variance can be estimated as $\hat{v}_{k,ij}^{(1)}$ if we set $\mu_{k,i} \approx p_{k,i}$ in $a_{k,i}$ of (4.55). This leads to a variance-based weighting scheme equal to

$$w_{k,ij}^{\mathrm{VW}} = \left(\hat{v}_{k,ij}^{(1)}\right)^{-1}. \tag{4.42}$$

Once the final DoA estimate is available, the RSS can be estimated following the same principle as in SLS. Much like in SLS, we also apply a validity check in TSLS [P2].

4.2.3 Analytical Error Models

4.2.3.1 Max-E

It is easy to see that MaxE DoA estimates are biased, even in the asymptotic case $N \to \infty$. For $N \to \infty$, MaxE will always find the sector i such that $|\mathcal{M}(\vartheta_{k,i} - \varphi_k)| \leq |\mathcal{M}(\vartheta_{k,m} - \varphi_k)|$, $m = 1 \ldots M$. Thus, in the asymptotic case the bias of MaxE is given

as $\text{bias}[\hat{\varphi}_{\text{m},k}] = \mathcal{M}(\vartheta_{k,i} - \varphi_k)$. At the same time, the bias completely determines the RMSE via (2.4). Assuming a uniformly distributed DoA and $N \to \infty$, MaxE therefore results in an average DoA estimation RMSE equal to [P4]

$$\overline{\text{RMSE}}^{N}_{\text{DoA,m}} = \sqrt{\frac{2}{\Delta\vartheta}\int_{0}^{\frac{1}{2}\Delta\vartheta} \varphi^2 d\varphi} = \frac{\Delta\vartheta}{\sqrt{12}} = \frac{\pi}{M\sqrt{3}}. \tag{4.43}$$

Similarly to DoA estimation, MaxE also produces biased RSS estimates. For $N \to \infty$, the RSS estimation bias becomes $\text{bias}[\hat{\gamma}_{k,\text{m}}] = \gamma_k[\rho_{k,m} - 1]$. Again, the bias completely determines the asymptotic RMSE. For uniformly distributed DoA, the average asymptotic RRMSE of RSS estimation is calculated as [P4]

$$\overline{\text{RRMSE}}^{N}_{\text{RSS,m}} = \sqrt{\frac{2}{\Delta\vartheta}\int_{0}^{\frac{1}{2}\Delta\vartheta} [\rho_{k,m} - 1]^2 d\varphi}. \tag{4.44}$$

where the sector m is arbitrarily chosen such that $\vartheta_m = 0$. This expression depends on the radiation pattern. For the Gaussian pattern (4.1), the RRMSE becomes [P4]

$$\overline{\text{RRMSE}}^{N}_{\text{RSS,m}} = \left[1 + \frac{1}{2}\sqrt{\frac{\pi}{|\ln a_{\text{s}}|}}\text{erf}\Big(\sqrt{|\ln a_{\text{s}}|}\Big) - \sqrt{\frac{2\pi}{|\ln a_{\text{s}}|}}\text{erf}\left(\sqrt{\frac{|\ln a_{\text{s}}|}{2}}\right)\right]^{\frac{1}{2}}. \tag{4.45}$$

4.2.3.2 SLS

In [P1], we derived an analytical expression for the bias and RMSE of SLS DoA estimation by means of approximating (4.32) with a first-order Taylor series around the means of $p_{k,i}$ and $p_{k,j}$. In short, this means that we approximated $\ln p_{k,m}$, $m = i, j$ in (4.32) as $\ln p_{k,m} \approx \ln \bar{\mu}_{k,m} + \frac{p_{k,m} - \bar{\mu}_{k,m}}{\bar{\mu}_{k,m}}$. In order to obtain the expressions for bias and RMSE, we furthermore made the following two assumptions:

1. SLS selects the two sectors i and j such that $\vartheta_i \geq \varphi_k \geq \vartheta_j$ as discussed in Section 4.2.2.2.

2. The variances of the powers $p_{k,m} \sim \mathcal{N}(\bar{\mu}_{k,l}, \bar{\sigma}^2_{k,m})$ are much smaller than their corresponding means, i.e., $\bar{\sigma}^2_{k,l} \ll \bar{\mu}_{k,l}$, where mean and variance are given by $\bar{\mu}_{k,l} = \rho_{k,l}\gamma_k$ and $\bar{\sigma}^2_{k,l} = \sigma^2_{k,l}$, respectively.

Intuitively, the above assumptions hold for large N and SNR. These assumptions in combination with the first-order Taylor series approximation lead to the following

expressions for bias and variance of SLS DoA estimation [P1]

$$\text{bias}[\hat{\varphi}_k] \approx 0 \tag{4.46}$$

$$\text{RMSE}_{\text{SLS}} \approx \frac{\kappa}{\sqrt{N}} \sqrt{a_{k,i}^{-1} + a_{k,j}^{-1}} \tag{4.47}$$

where $a_{k,m}$ is given in (4.17). Assuming again a uniform distribution of DoAs and a Gaussian radiation pattern, we obtain the average DoA estimation RMSE by integrating over (4.47) as [P1]

$$\overline{\text{RMSE}}_{\text{SLS}} \approx \kappa \sqrt{\frac{2\sqrt{\pi}}{N\sqrt{\ln a_{\text{s}}^{-1}}} \left[\frac{f(a_{\text{s}})}{4\,\text{SNR}^2} + \frac{g(a_{\text{s}})}{\sqrt{2}\,\text{SNR}} \right] + \frac{2}{N}} \tag{4.48}$$

with

$$f(a_{\text{s}}) = \text{erfi}\left(2\sqrt{\ln\left(a_{\text{s}}^{-1}\right)} \right) \tag{4.49}$$

$$\text{and} \quad g(a_{\text{s}}) = \text{erfi}\left(\sqrt{2\ln\left(a_{\text{s}}^{-1}\right)} \right). \tag{4.50}$$

Both (4.49) and (4.50) depend on the imaginary error function (1.2) via the SSP a_{s}. As discussed in more detail in Section 4.2.4, we recommend to design sectorized antennas with a fixed SSP of around $a_{\text{s}} = 0.2 - 0.4$ for good performance. In general the imaginary error functions in (4.48) can thus be treated as constants with a few example values listed in Table 4.1. If it is nevertheless necessary to evaluate (4.49) and (4.50) explicitly, it is possible to calculate the imaginary error function using, e.g., MATLAB's symbolic toolbox [3]. From (4.47), we also obtain the SLS DoA estimation RMSE for asymptotically large SNR as

$$\text{RMSE}_{\text{SLS}}^{\text{SNR}} = \overline{\text{RMSE}}_{\text{SLS}}^{\text{SNR}} = \frac{\pi}{\sqrt{2N}M|\ln a_{\text{s}}|}. \tag{4.51}$$

As already indicated above $\text{RMSE}_{\text{SLS}}^{\text{SNR}}$ is equal to the asymptotic RMSE for a uniformly distributed DoA since (4.51) is independent of the DoA. As discussed in more detail in [P1], the above expression is equal to the asymptotic RMSE derived in [110] when N is sufficiently large. For asymptotically large N, the DoA estimation RMSE becomes

$$\text{RMSE}_{\text{SLS}}^{N} = \overline{\text{RMSE}}_{\text{SLS}}^{N} = 0. \tag{4.52}$$

Tab. 4.1. Example values of (4.49) and (4.50)

a_s	0.2	0.3	0.4	0.5	0.6	0.7	0.8	0.9
$f(a_\mathrm{s})$	154.4	37.0	14.1	6.9	3.9	2.4	1.5	0.8
$g(a_\mathrm{s})$	9.8	5.2	3.3	2.3	1.7	1.2	0.9	0.6

4.2.3.3 TSLS

In [P2] we derived approximations for bias and variance of individual sector-pair DoA estimates obtained with TSLS. Towards that end, we have approximated the TSLS sector-pair DoA estimators (4.35) and (4.36) through their Taylor series. This approach is of course similar to the derivation of SLS DoA estimation bias and RMSE discussed in the previous section. However, SLS DoA estimation can be approximated as a sum of two separate Taylor series in a single variable, while TSLS sector-pair DoA estimation according to (4.36) has to be approximated as a Taylor series in two variables. Moreover, in the derivation in [P2] we have chosen a slightly different approach than in the derivations discussed in the previous section. Instead of first approximating the estimator through its first-order Taylor series and thereafter calculating the bias and RMSE, we have in [P2] first calculated the mean and variance of first-order and second-order Taylor series approximations of any function $f : \mathbb{R}^{L\times 1} \to \mathbb{R}$ ([P2, Lemma 1]). Only thereafter, we have calculated the bias and RMSE of TSLS sector-pair DoA estimation by using the generic approximations for mean and variance with $f = \hat{\varphi}_{k,ij}$. For DBS, i.e., the estimator (4.36), this leads to first-order and second-order Taylor approximations of the bias given by

$$b_{k,ij}^{(1)} = 0 \tag{4.53}$$

$$b_{k,ij}^{(2)} = \pm\frac{\beta_i\beta_j}{8Ng(\boldsymbol{\mu})}\left[a_{k,j} - a_{k,i} - \frac{\Delta\beta_{ij}}{4[g(\boldsymbol{\mu})]^2}(a_{k,i} + a_{k,j})\right] \tag{4.54}$$

and first-order and second-order Taylor approximations of the variance equal to

$$v_{k,ij}^{(1)} = \frac{\beta_i^2\beta_j^2}{16N[g(\boldsymbol{\mu})]^2}(a_{k,i} + a_{k,j}) \tag{4.55}$$

$$v_{k,ij}^{(2)} = \frac{\beta_i^2\beta_j^2}{16N[g(\boldsymbol{\mu})]^2}\left[a_{k,i} + a_{k,j} + \frac{1}{2N}(a_{k,i}^2 + a_{k,j}^2) + \right.$$
$$\left. \frac{\Delta\beta_{ij}}{4N[g(\boldsymbol{\mu})]^2}(a_{k,i}^2 - a_{k,j}^2) + \frac{\Delta^2\beta_{ij}}{32N[g(\boldsymbol{\mu})]^4}(a_{k,i} + a_{k,j})^2\right]. \tag{4.56}$$

where $g(\boldsymbol{\mu}) = g(\mu_{k,i}, \mu_{k,j})$. From (4.53)-(4.56), we obtain the respective expressions for EBS, i.e., the estimator (4.35) by replacing β_i and β_j with β leading to $\Delta\beta_{ij} = 0$.

In general, we assume the signal model (4.3), where the LoS path dominates the received signal. However, in [P2] we have derived similar expressions to (4.53)–(4.56)

Tab. 4.2. Expressions used in the evaluation of DoA estimation performance.

Expression	Alg./CRB	Type	References
$\mathrm{RMSE}_{\mathrm{DoA}}$	CRB	numerical average over DoA	(4.18), [P1]
$\mathrm{RMSE}^{\mathrm{a}}_{\mathrm{DoA}}$	CRB	approximation, numerical average over DoA	(4.20), [P1]
$\overline{\mathrm{RMSE}}^{\mathrm{SNR}}_{\mathrm{DoA}}$	CRB	asymptotical SNR $\to \infty$, analytical	(4.24), [P1]
$\overline{\mathrm{RMSE}}^{N}_{\mathrm{DoA,m}}$	MaxE	asymptotical $N \to \infty$, analytical	(4.43), [P4]
$\overline{\mathrm{RMSE}}_{\mathrm{SLS}}$	SLS	approximation, analytical	(4.48), [P1]
$\overline{\mathrm{RMSE}}^{\mathrm{SNR}}_{\mathrm{SLS}}$	SLS	asymptotical SNR $\to \infty$, analytical	(4.48), [P1]
SLS	SLS	numerical algorithm evaluation	Sec. 4.2.2.2, [P5]
TSLS	TSLS	numerical algorithm evaluation	Sec. 4.2.2.3, [P2]

also for a signal model with strong multipath components. The resulting expressions along with a detailed evaluation of (4.53)–(4.56) for both models can be found in [P2]. Our main observation in [P2] is that strong multipath components result in an increased sector-pair DoA estimation bias compared to an estimation in conditions where the LoS path is dominating.

4.2.4 Numerical Evaluation and Comparison

In the evaluation of the estimators and CRBs discussed in the previous sections, we will be considering two different antenna models. On the one hand, we assume an ESA with $M = 6$ sectors and, on the other hand, we use the LWA model from [P2]. This model was obtained by approximating the measured radiation patterns of the LWA [81] according to the procedure described later in Section 4.4. The resulting model consists of $M = 12$ sectors each approximated by a Gaussian radiation pattern (4.1) with the parameters listed in [P2, Tab. III]. The ESA can be used in combination with any of the discussed estimators, whereas the LWA consists of sectors where the main beam is different in all sectors meaning that it can be used with TSLS only (see [P2]). For the ESA, we use TSLS with $L = 3$ and variance weighting, which results in the overall best performance [P2]. The influence of L and the weighting scheme on the performance of TSLS is then studied using the LWA.

All results presented in the following were obtained assuming a DoA uniformly distributed over the whole angular coverage area of the respective antennas. This means that the DoA is distributed as $\varphi_k \sim \mathcal{U}(-180°; 180°)$ for the ESA and as $\varphi_k \sim \mathcal{U}(-60°; 60°)$ for the LWA. An overview of the expressions used in the figures can be found in Tables 4.2 and 4.3. For a detailed description of the simulation setup please refer to the references in those tables.

Figures 4.6 and 4.7 depict the performance of DoA estimation and RSS estimation with the ESA as a function of the SSP a_{s}, respectively. We notice that, in certain conditions, both SLS and TSLS result in an RMSE that is lower than the respective

Tab. 4.3. Expressions used in the evaluation of RSS estimation performance.

Expression	Alg./CRB	Type	References
$\mathrm{RRMSE}_{\mathrm{RSS}}$	CRB	numerical average over DoA	(4.19), [P1]
$\mathrm{RRMSE}^{\mathrm{a}}_{\mathrm{RSS}}$	CRB	approximation, numerical average over DoA	(4.21), [P1]
$\overline{\mathrm{RRMSE}}^{\mathrm{SNR}}_{\mathrm{RSS}}$	CRB	asymptotical SNR $\to \infty$, analytical	(4.25), [P1]
$\overline{\mathrm{RRMSE}}^{N}_{\mathrm{RSS,m}}$	MaxE	asymptotical $N \to \infty$, analytical	(4.45), [P4]
SLS	SLS	numerical algorithm evaluation	Sec. 4.2.2.2, [P5]

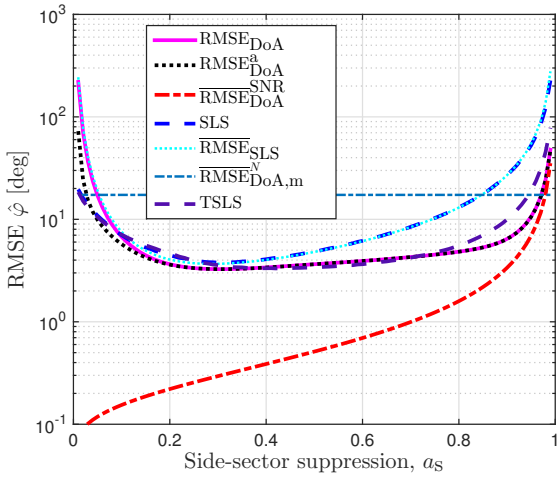

Fig. 4.6. DoA estimation performance as a function of the side-sector suppression. Parameters: ESA with $M = 6$, $N = 100$, and SNR $= 5\,\mathrm{dB}$.

CRB. Clearly, this indicates that both algorithms are not entirely unbiased. As shown and discussed in [P2] and [P5], a significant non-zero bias in SLS and TSLS occurs in adverse operation conditions, such as for a low SNR, for strong multipath or for antennas with disadvantageous values for the SSP. Now the choice of the SSP is a compromise. As can be seen from the asymptotic CRB in Figure 4.6, the SSP should be as small as possible for SNR $\to \infty$. However, for moderate to large SNR, the lowest CRB is attained for a SSP around $a_{\mathrm{s}} \in [0.2; 0.4]$. This is in line with the SSP interval where the DoA estimators SLS and TSLS result in the lowest RMSE. However, as evident from Figure 4.6 TSLS is much less susceptible to the choice of a_{s} than SLS. For RSS estimation and SNR $\to \infty$, the asymptotic CRB is entirely independent of a_{s}. However, for finite SNR, the trend in the RSS estimation CRB is opposite to the trend in $\overline{\mathrm{RMSE}}^{\mathrm{SNR}}_{\mathrm{DoA}}$ as an omnidirectional antenna ($a_{\mathrm{s}} = 1$) results in the lowest CRB. Overall, a SSP $a_{\mathrm{s}} \in [0.2; 0.4]$ is thus a good compromise. Consequently, the approximations $\overline{\mathrm{RMSE}}^{\mathrm{a}}_{\mathrm{DoA}}$ and $\overline{\mathrm{RMSE}}^{\mathrm{a}}_{\mathrm{RSS}}$ are very accurate for well-tuned antennas since the respective curves in Figures 4.6 and 4.7 match perfectly with the CRBs for $a_{\mathrm{s}} > 0.1$.

Figures 4.6 and 4.7 also include the asymptotic RMSEs $N \to \infty$ of MaxE DoA and RSS estimation. Even in the asymptotic case, the performance of MaxE is far from the

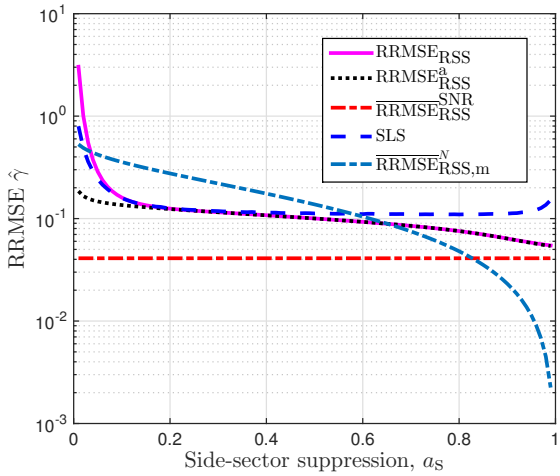

Fig. 4.7. RSS estimation performance as a function of the side-sector suppression. Parameters: ESA with $M = 6$, $N = 100$, and SNR $= 5\,\text{dB}$.

CRBs and the performance of SLS and TSLS with finite N. Note that for the asymptotic case $N \to \infty$, the other estimators as well as the CRB result in an RMSE $= 0$. Due to this significant difference in performance, we will, in the following, not discuss MaxE anymore. For a detailed performance discussion of MaxE refer to [P4] and [P5] instead.

Figure 4.8 depicts the performance of DoA estimation with an ESA as a function of the SNR. As can be seen, $\text{RMSE}^{\text{a}}_{\text{DoA}}$ is a perfect approximation for the CRB RMSE_{DoA} and the analytical expression for the RMSE of SLS is also very accurate for SNR $> 2\,\text{dB}$. Moreover, for moderate SNRs around 5 dB both SLS and TSLS perform quite close to the CRB. For increasing SNRs, TSLS approaches the CRB even closer. The performance of SLS, in contrast, saturates at a much higher level ($\overline{\text{RMSE}}^{\text{SNR}}_{\text{SLS}}$) than the CRB for SNR $> 15\,\text{dB}$. As discussed in more detail in [P1], this is due to SLS excluding all but two sectors from the DoA estimation. For increasing SNRs, our assumption that all but two sectors are too noisy to exploit the TN signal component becomes increasingly worse. For low SNRs, on the other hand, the performance of TSLS and SLS is in fact equal. This is due to the weighting in TSLS, which practically excludes all other but the two sectors that are also used in SLS.

In TSLS the number of sectors L that results in the best performance depends on the type of antenna, as well as on the SNR. This is illustrated in Figure 4.9 using the LWA as an example. For large SNRs, the best performance is achieved with $L = 11$, i.e., with significantly more sectors compared to the ESA. While the ESA has $M = 6$ sectors with a beam-width $\beta \approx 0.22\,\text{rad}$ distributed over 360°, the LWA has $M = 12$ sectors with beam-widths between 0.5 rad and 0.7 rad distributed over 120° [P1]. This means that the number of sectors that receive the TN signal with a significant signal strength is much larger in the LWA than in the ESA. Consequently, L should also be

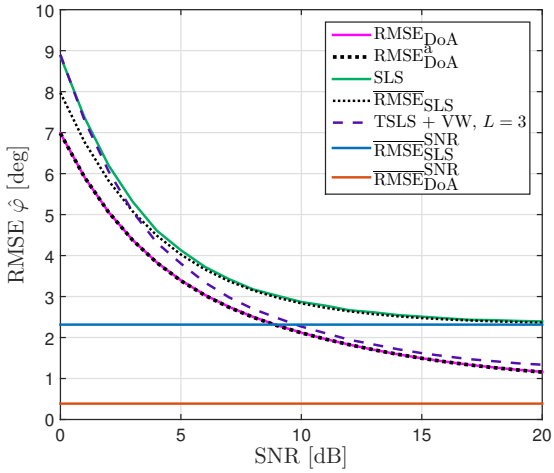

Fig. 4.8. DoA estimation performance as a function of the SNR. Parameters: ESA with $a_{\text{s}} = 0.4$, $M = 6$, and $N = 100$.

larger for the LWA than for the ESA. However, Figure 4.9 also shows that using too many sectors can degrade the performance in TSLS. For SNR $< 5\,\text{dB}$, the performance of TSLS with EW and VW is in fact better with $L = 4$ than with $L = 11$. Only TSLS with PW results in the best performance with $L = 11$ over the whole observed SNR range. However, for larger SNR the PW scheme saturates at a RMSE level larger than that of VW and EW. In fact, for large SNRs TSLS with VW performs very close to the respective CRB also for the LWA.

4.3 Localization Using Sectorized Antennas

4.3.1 Cramer-Rao Bound

As discussed in Section 4.1.2, the localization CRB will be stated for a given channel that is modeled as constant during the observation period. We moreover assume that the TN is uncooperative, meaning that the TN signal as well as the TN ACF are unknown. Finally, the CRB is valid for estimators that do not attempt to extract any TN location information from the RSS, but merely estimate the TN location from the location-dependent attenuation of the sectorized antennas [P1]. This leads to a $(\mathcal{N} + K + 2) \times 1$ parameter vector $\mathbf{q} = \left[x, y, \boldsymbol{\gamma}^{\text{T}}, \mathbf{c}^{\text{T}}\right]^{\text{T}}$, where $\mathbf{c}$ is the vector composed of the $\mathcal{N} = \frac{1}{2}K(K-1)(2M-1)$ unique elements of the matrix $\mathbf{C}$ [P1]. Overall, the parameter vector $\mathbf{q}$ is therefore composed of $\mathcal{N} + K$ nuisance parameters and only two parameters (x and y) that are of actual interest for the localization. Overall, this leads

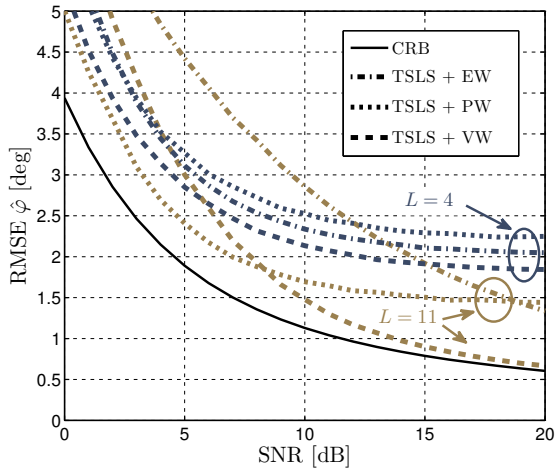

Fig. 4.9. DoA estimation performance as a function of the SNR. Parameters: LWA approximated by Gaussian radiation pattern [P2], $M = 12$, $N = 100$.

to the following FIM elements [P1]

$$\boldsymbol{\Lambda}_{ij} = [\mathbf{g}]^{\mathrm{T}}_{(\boldsymbol{\ell}_{\mathrm{P}})_i} \mathbf{Q}^{-1} [\mathbf{g}]_{(\boldsymbol{\ell}_{\mathrm{P}})_j} + \frac{1}{2} \operatorname{tr}\Big\{ \mathbf{Q}^{-1} [\mathbf{Q}]_{(\boldsymbol{\ell}_{\mathrm{P}})_i} \mathbf{Q}^{-1} [\mathbf{Q}]_{(\boldsymbol{\ell}_{\mathrm{P}})_j} \Big\} \tag{4.57}$$

$$\boldsymbol{\Lambda}_{i,2+k} = [\mathbf{g}]^{\mathrm{T}}_{(\boldsymbol{\ell}_{\mathrm{P}})_i} \mathbf{Q}^{-1} [\mathbf{g}]_{\gamma_k} + \frac{1}{2} \operatorname{tr}\Big\{ \mathbf{Q}^{-1} [\mathbf{Q}]_{(\boldsymbol{\ell}_{\mathrm{P}})_i} \mathbf{Q}^{-1} [\mathbf{Q}]_{\gamma_k} \Big\} \tag{4.58}$$

$$\boldsymbol{\Lambda}_{i,(2+K+m)} = \frac{1}{2} \operatorname{tr}\Big\{ \mathbf{Q}^{-1} [\mathbf{Q}]_{(\boldsymbol{\ell}_{\mathrm{P}})_i} \mathbf{Q}^{-1} [\mathbf{Q}]_{\mathbf{c}_m} \Big\} \tag{4.59}$$

$$\boldsymbol{\Lambda}_{(2+k),(2+l)} = [\mathbf{g}]^{\mathrm{T}}_{\gamma_k} \mathbf{Q}^{-1} [\mathbf{g}]_{\gamma_l} + \frac{1}{2} \operatorname{tr}\Big\{ \mathbf{Q}^{-1} [\mathbf{Q}]_{\gamma_k} \mathbf{Q}^{-1} [\mathbf{Q}]_{\gamma_l} \Big\} \tag{4.60}$$

$$\boldsymbol{\Lambda}_{(2+k),(2+K+m)} = \frac{1}{2} \operatorname{tr}\Big\{ \mathbf{Q}^{-1} [\mathbf{Q}]_{\gamma_k} \mathbf{Q}^{-1} [\mathbf{Q}]_{\mathbf{c}_m} \Big\} \tag{4.61}$$

$$\boldsymbol{\Lambda}_{(2+K+m),(2+K+n)} = \frac{1}{2} \operatorname{tr}\{ \mathbf{Q}^{-1} [\mathbf{Q}]_{\mathbf{c}_m} \mathbf{Q}^{-1} [\mathbf{Q}]_{\mathbf{c}_n} \} \tag{4.62}$$

with $i = 1, 2$, $j = 1, 2$, $k = 1 \ldots K$, $l = 1 \ldots K$, $m = 1 \ldots \mathcal{N}$, $n = 1 \ldots \mathcal{N}$ and derivatives equal to

$$[\mathbf{Q}]_{(\boldsymbol{\ell}_{\mathrm{P}})_i} = \Big([\boldsymbol{\rho}]_{(\boldsymbol{\ell}_{\mathrm{P}})_i} \boldsymbol{\rho}^{\mathrm{T}} + \boldsymbol{\rho} [\boldsymbol{\rho}]^{\mathrm{T}}_{(\boldsymbol{\ell}_{\mathrm{P}})_i} \Big) \circ \bar{\boldsymbol{\gamma}} \bar{\boldsymbol{\gamma}}^{\mathrm{T}} \circ \mathbf{C} + 2 \frac{\sigma_{\mathrm{w}}^2}{N} \operatorname{diag}\Big([\boldsymbol{\rho}]_{(\boldsymbol{\ell}_{\mathrm{P}})_i} \circ \bar{\boldsymbol{\gamma}} \Big) \tag{4.63}$$

$$[\mathbf{Q}]_{\gamma_k} = \boldsymbol{\rho} \boldsymbol{\rho}^{\mathrm{T}} \circ \big[\bar{\boldsymbol{\gamma}} \bar{\boldsymbol{\gamma}}^{\mathrm{T}} \big]_{\gamma_k} \circ \mathbf{C} + 2 \frac{\sigma_{\mathrm{w}}^2}{N} \operatorname{diag}\Big(\boldsymbol{\rho} \circ [\bar{\boldsymbol{\gamma}}]_{\gamma_k} \Big) \tag{4.64}$$

$$[\mathbf{Q}]_{\mathbf{c}_m} = \boldsymbol{\rho} \boldsymbol{\rho}^{\mathrm{T}} \circ \bar{\boldsymbol{\gamma}} \bar{\boldsymbol{\gamma}}^{\mathrm{T}} \circ [\mathbf{C}]_{\mathbf{c}_m} \tag{4.65}$$

$$[\mathbf{g}]_{(\boldsymbol{\ell}_{\mathrm{P}})_i} = [\boldsymbol{\rho}]_{(\boldsymbol{\ell}_{\mathrm{P}})_i} \circ \bar{\boldsymbol{\gamma}}, \quad [\mathbf{g}]_{\gamma_k} = \boldsymbol{\rho} \circ [\bar{\boldsymbol{\gamma}}]_{\gamma_k}, \quad [\mathbf{g}]_{\mathbf{c}_m} = 0 \tag{4.66}$$

which in turn depend on the trivial derivative $[\mathbf{C}]_{\mathbf{c}_m}$ and $[\rho_{k,m}]_{(\boldsymbol{\ell}_{\mathrm{P}})_i} = [\rho_{k,m}]_{\varphi_k} [\varphi_k]_{(\boldsymbol{\ell}_{\mathrm{P}})_i}$. Using the above FIM, the CRB on the RMSE of localization with sectorized antennas is

given by

$$\mathrm{RMSE} = \sqrt{\left(\mathbf{\Lambda}^{-1}\right)_{11} + \left(\mathbf{\Lambda}^{-1}\right)_{22}} > \mathrm{RMSE_R} > \mathrm{RMSE_L} \tag{4.67}$$

$$\mathrm{RMSE_R} = \sqrt{\left(\mathbf{\Lambda}_\mathrm{R}^{-1}\right)_{11} + \left(\mathbf{\Lambda}_\mathrm{R}^{-1}\right)_{22}} \tag{4.68}$$

$$\mathrm{RMSE_L} = \sqrt{\left(\mathbf{\Lambda}_\mathrm{L}^{-1}\right)_{11} + \left(\mathbf{\Lambda}_\mathrm{L}^{-1}\right)_{22}} = \frac{\sqrt{\mathbf{\Lambda}_{11} + \mathbf{\Lambda}_{22}}}{\sqrt{\mathbf{\Lambda}_{11}\mathbf{\Lambda}_{22} - \mathbf{\Lambda}_{12}^2}}. \tag{4.69}$$

Both $\mathrm{RMSE_R}$ and $\mathrm{RMSE_L}$ in (4.68) and (4.69) are approximations of the CRB that assume the knowledge of some of the nuisance parameters. $\mathrm{RMSE_R}$ assumes the knowledge of the matrix $\mathbf{C}$, i.e., $\mathbf{\Lambda}_\mathrm{R} \in \mathbb{R}^{(2+K)\times(2+K)}$, $(\mathbf{\Lambda}_\mathrm{R})_{ij} = (\mathbf{\Lambda})_{ij}, i, j = 1 \ldots 2+K$ and $\mathrm{RMSE_L}$ assumes the knowledge of all nuisance parameters, i.e., $\mathbf{\Lambda}_\mathrm{L} \in \mathbb{R}^{2\times 2}$, $(\mathbf{\Lambda}_\mathrm{L})_{ij} = (\mathbf{\Lambda})_{ij}$, $i, j = 1, 2$. As shown in Section 4.3.2, $\mathrm{RMSE_R}$ approximates RMSE almost perfectly, whereas $\mathrm{RMSE_L}$ is not quite as good an approximation but still fairly close to RMSE.

4.3.2 Numerical Evaluation and Comparison

Localization with sectorized antennas is studied assuming a uniform distribution of ONs on a ring centered around the TN with inner and outer radii given by 5 m and 150 m, respectively. The TN signal is modeled as Gaussian with a bandwidth $B = 20\,\mathrm{MHz}$ (see Section 4.1.2) and a transmit power of 20 dBm. This signal propagates through a channel given by (3.6) with $\alpha = 4$ and $\sigma_\mathrm{f} = 0$, i.e., without any shadow fading. For an analysis of the impact of non-zero σ_f on the localization performance the reader may refer to [P1]. Within the ONs, the TN signal is received with an ESA with $M = 6$ sectors and a SSP, $a_\mathrm{s} = 0.4$. The sampling frequency and noise variance are equal to $f_\mathrm{s} = \frac{1}{B}$ and $\sigma_\mathrm{w}^2 = -70\,\mathrm{dBm}$, respectively. A more detailed description of the simulation setup can be found in [P1] and [P2].

Figure 4.10 shows the performance of localization as a function of the number of ONs, K. The figure includes curves for the CRB (4.67), the two approximations of the CRB (4.68), (4.69) as well as a numerical evaluation of SLS and TSLS in combination with Stansfield-based DoA fusion, denoted as here as SLS-S and TSLS-S, respectively. TSLS is again configured as in Section 4.2.4, i.e., with VW and $L = 3$. As discussed in Section 3.3, the classical Stansfield algorithm requires the knowledge of both the TN-ON distances as well as the covariance of DoA estimates. However, we neither assume the knowledge of TN-ON distances nor of the DoA estimation covariance. Thus, in this evaluation, we use the modified Stansfield algorithm proposed in [P4], where the weighting matrix $\mathbf{D}^{-1}\mathbf{Q}_\varphi^{-1}$ is replaced with a diagonal matrix $\mathrm{diag}[\hat{\gamma}_1, \ldots, \hat{\gamma}_K]$ with RSS estimates $\hat{\gamma}_k$ obtained according to (4.33). From Figure 4.10, we can see that the approximation $\mathrm{RMSE_R}$ matches the CRB perfectly, whereas $\mathrm{RMSE_L}$ is only slightly smaller than the CRB. As expected, the increased DoA estimation performance of TSLS compared to

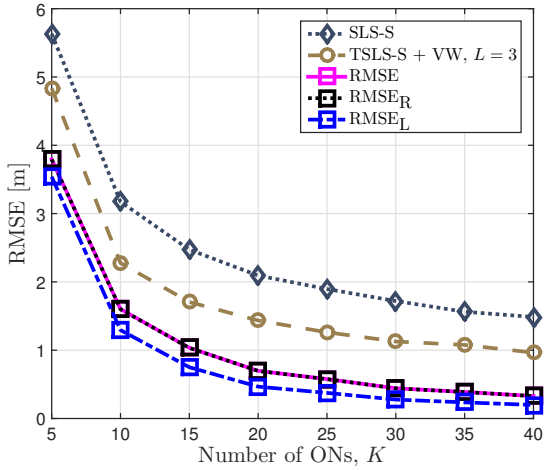

Fig. 4.10. Localization performance as a function of the number of ONs. Parameters: ESA with $a_\text{s} = 0.4$, $M = 6$, and $N = 100$.

SLS also results in an improved localization performance of TSLS-S compared to SLS-S. However, TSLS-S still does not attain the CRB. As we have discussed in [P1], this indicates that the intermediate step of DoA estimation employed in TSLS-S and SLS-S may be harmful for the localization. Thus, for optimal performance it may be necessary to estimate the TN location directly from the sector-powers obtained at all ONs.

4.4 Measurement Example

In [P2] we have evaluated the performance of TSLS DoA estimation with subsequent Stansfield location estimation on the basis of practical indoor measurements. Towards that end, we have placed six ONs equipped with the LWA from [81] and three TNs equipped with omnidirectional antennas in a lobby at Drexel University as depicted in Figure 4.11. The system was set to operate with a bandwidth of 20 MHz and at a center frequency of 2.462 GHz. As described in greater detail in [P2], we have then measured the sector-powers of all $M = 12$ sectors at all $K = 6$ ONs and for every one of the three TNs. Thereby, we have activated the TN-ON pairs one at a time. However, interference was introduced from nearby WiFi hotspots that were active at the time of our measurements.

Before the TSLS estimator can be used with a sectorized antenna in practice, the radiation pattern of the antenna has to be approximated by the Gaussian radiation pattern (4.1) in every sector m, $m = 1, \ldots, M$. In the following, we will sketch the approximation procedure that we have used in [P2] to obtain a fit $\hat{\rho}_m(\vartheta) = [\hat{\zeta}_m(\vartheta)]^2$ for the LWA from [81]. Essentially, the approximation was obtained as an LS fit to the measured radiation pattern $\tilde{\rho}_m(k\,\delta\vartheta) = [\tilde{\zeta}_m(k\,\delta\vartheta)]^2$. In [P2], we have measured

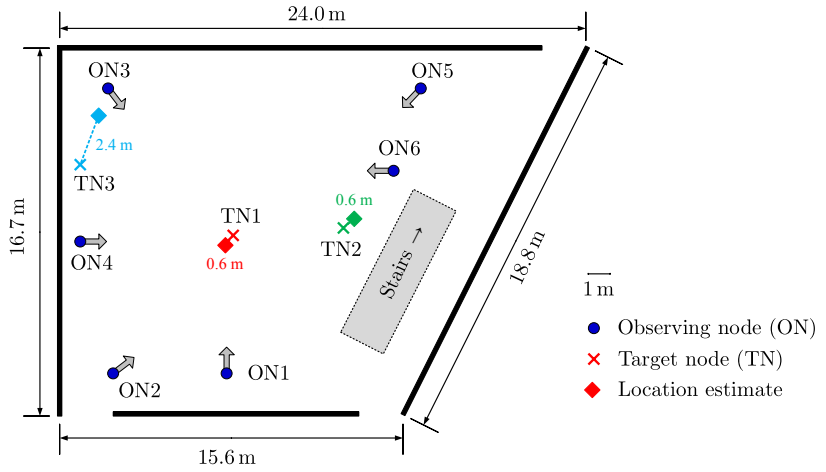

Fig. 4.11. Measurement example: localization with TSLS and subsequent Stansfield DoA fusion in a lobby in Drexel University. The arrows at the ONs illustrate the orientation of the LWAs.

the radiation pattern of each sector m with a resolution of $\delta\vartheta = 1°$ meaning that $k = 1, \ldots, 360$. However, the Gaussian radiation pattern models only the main beam of each sectors. Thus, the LS fit should be calculated using only measurement points around the maximum gain, i.e., $\tilde{\vartheta}_m = \mu\Delta\vartheta$, $\mu = \arg\max_k \tilde{\rho}_m(k\,\Delta\vartheta)$. In [P2], we have used an interval of $\Omega = 20°$ on both sides of $\tilde{\vartheta}_m$. The parameters of the Gaussian radiation pattern approximation are then obtained as

$$(\hat{\alpha}_m, \hat{\beta}_m, \hat{\vartheta}_m) = \underset{\alpha_m,\beta_m,\vartheta_m}{\arg\min} \sum_{k=-\Omega/\Delta\vartheta}^{\Omega/\Delta\vartheta} [\rho_m(\tilde{\vartheta}_m + k\,\Delta\vartheta) - \tilde{\rho}_m(\tilde{\vartheta}_m + k\,\Delta\vartheta)]^2 \qquad (4.70)$$

with the result listed in [P2, Table III] and an example of the approximation for two sectors depicted in Figure 4.12.

In the measurement processing, we have used TSLS in a configuration with $L = 3$ and PW. This particular TSLS configuration is motivated by the indoor environment that results in strong multipath components at the ONs. Now strong multipath, in turn, results in dominating NLoS paths for sectors far from the DoA of the LoS path. Thus, in an indoor environment L cannot be too large in order to avoid biased sector-pair DoA estimates. Finally, PW was chosen as the weighting scheme since it results in a better performance than EW and is also more robust than VW, which was derived assuming free space propagation. A location estimate for each TN was then obtained using the Stansfield algorithm with an RSS-based weighting of the individual DoA estimates $\hat{\varphi}_k$, $k = 1 \ldots K$ (see Section 4.3.2). For simplicity, we have estimated the RSS at each ON k as $\hat{\gamma}_k = \max(p_{k,q}, p_{k,q+1})$, where q and $q+1$ are the neighboring sectors determined in the SSL stage (see Section 4.2.2.3).

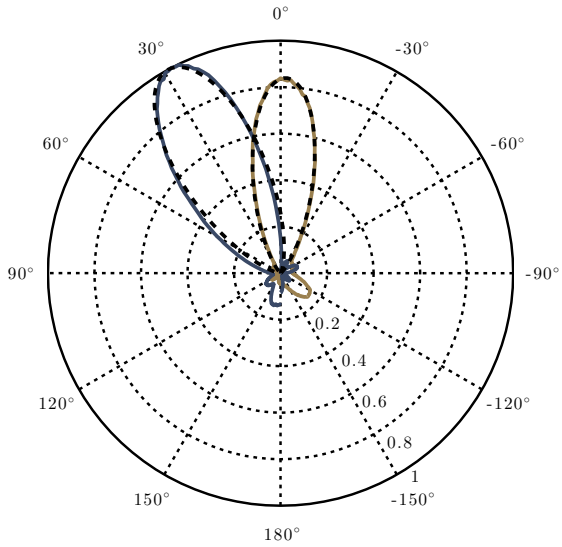

Fig. 4.12. Approximation of the LWA from [81] through the Gaussian radiation pattern (4.1).

Figure 4.11 shows the estimated TN locations along with the estimation RMSE. As expected, the TNs in the center of the observation area (TN1 and TN2) were localized with a higher accuracy than the TN at the border of the observation area (TN3). The RMSE of location estimates are 0.6 m for TN1, 0.6 m for TN2, and 2.4 m for TN3.

4.5 Chapter Summary

In this chapter, three DoA/RSS estimators for sectorized antennas have been proposed and analyzed. The estimators MaxE and SLS are applicable to ESAs only, whereas the third estimator TSLS can also be used with sectorized antennas where the shape of the main beam varies throughout the sectors. Thus, in a practical application, the type of sectorized antennas available at the ONs might already dictate the choice of the DoA/RSS estimator. Apart from the available sectorized antennas, the choice of the proper estimator is also influenced by the available computational resources as well as the targeted estimation accuracy. A numerical comparison of the DoA estimation as well as localization performance can be found in Table 4.4. The table moreover includes the results of a complexity analysis that is a contribution of [P2], but not discussed in great detail here. In this complexity analysis, we count the number of basic operations, i.e., additions (ADD) and multiplications (MUL), and the number of calls to standard functions such as the natural logarithm or trigonometric functions (LUT). The analysis reveals that the difference in complexity between the estimators is mainly due to the number of calls to standard functions, which is zero for MaxE, two for SLS and ten for TSLS. In contrast, the number of basic operations is dominated by the

Tab. 4.4. DoA estimation and localization (loc.) with sectorized antennas: comparison of performance and computational complexity. Parameters: ESA with $a_s = 0.4$, $M = 6$, $N = 100$, TSLS DoA estimation with VW and $L = 3$.

Algorithm	Complexity per DoA estimate (in basic operations)	RMSE DoA (SNR = 20 dB)	RMSE loc. ($K = 20$)
MaxE	1194 ADD +1206 MUL	17.3°	12 m
SLS	1198 ADD +1213 MUL +2 LUT	2.4°	2.1 m
TSLS	1213 ADD +1234 MUL +10 LUT	1.3°	1.4 m

sector-power calculation (4.2) as shown in [P2]. In practice, the standard function could be implemented as a look-up table. Thus, the difference in the computational complexity between the three estimators is not very significant. Moreover, the estimators with the larger complexity also result in the better DoA estimation and localization performance. Finally, TSLS has the advantage that the performance and computational complexity are scalable by changing L or the weighting scheme. In fact, TSLS can be parameterized to be nearly efficient as revealed in our CRB analysis.

CHAPTER 5

Localization and Tracking Using Heterogeneous Measurements

It is well known that localization based on heterogeneous measurements results in an increased performance compared to a localization based on homogeneous measurements. In [21], as an example, it has been shown that hybrid ToA/RSS and TDoA/RSS based localization outperforms ToA-only and TDoA-only based localization, respectively. In this chapter, we thus focus on localization and tracking using DoA estimates along with either RSS or ToA estimates. As discussed in Section 3.2, both RSS and ToA estimates are a measurement for the TN-ON distance. As such, they form a very compelling counterpart to DoA estimation since DoAs are measurements for the angles between TN and ONs. In this chapter, we study the fusion of DoA and RSS estimates as an example for the localization and tracking of an uncooperative TN. In contrast, the fusion of DoA and ToA estimates is studied as an example for the tracking of a cooperative TN. While we discuss the former fusion process in general terms, we focus our discussions of the latter fusion process specifically on 5G ultra-dense networks.

This chapter is organized as follows. Section 5.1 is devoted to DoA/RSS-based localization and tracking. Thereafter, in Section 5.2, we focus on DoA/ToA-based tracking.

5.1 Hybrid RSS/DoA-based Localization and Tracking of an Uncooperative TN

Practically parallel in time to the work presented in this thesis, hybrid RSS/DoA-based localization has also been studied in [107, 111]. The authors of [111] propose a linear LS estimator and a ML estimator for DoA/RSS-based localization. Similarly, to [P6] the article [107] is dedicated to a CRB analysis for DoA/RSS-based localization. Although [107] deals with PU localization, i.e., non-cooperative TN localization, the assumptions in [107] imply that the ONs know the parameter P in (3.6). This is a somewhat unrealistic assumption and the first major difference to the work in [P6]. Moreover, the authors of [107] do not study the geometric reasons for the increased performance of DoA/RSS-based localization compared to a localization based on DoA-only or RSS-only. This is the second major difference to [P6]. Apart from the DoA/RSS CRB, presented in the following section, we will also study a hybrid DoA/RSS-EKF in Section 5.1.2.

5.1.1 Cramer-Rao Bound

In this section we will first develop the FIM for hybrid DoA/RSS-based localization in Section 5.1.1.1. Thereafter, in Section 5.1.1.2, we derive a closed-form expression for the hybrid DoA/RSS CRB using an informative example geometry and discuss how the localization geometry influences the localization performance. Finally, in Section 5.1.1.3 we present and discuss numerical evaluations of the CRB for the example geometry as well as arbitrary geometries.

5.1.1.1 Fisher Information Matrix

In order to derive the hybrid DoA/RSS FIM, we model the DoA and RSS estimates according to (3.2) and (3.6), respectively. Now, in general, the parameter P in (3.6) is unknown to the localization system and needs to be included as a nuisance parameter in the estimation problem. Thus, the complete parameter vector is given as $\mathbf{p} = [x, y, P]^T$. Assume next that the DoA and RSS estimation errors are independent. Then, the FIM is given by

$$\mathbf{J}_{\mathrm{H,u}} = \mathbf{J}_{\mathrm{RSS,u}} + \begin{bmatrix} \mathbf{J}_{\mathrm{DoA}} & \mathbf{0}_2 \\ \mathbf{0}_2^T & 0 \end{bmatrix} \tag{5.1}$$

where $\mathbf{J}_{\mathrm{DoA,u}}$ and $\mathbf{J}_{\mathrm{RSS,u}}$ are given by (3.3) and (3.8), respectively. In theory, it may be possible that a cooperative TN knows the value of P and communicates it to the

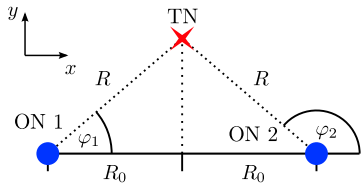

Fig. 5.1. Illustration of the special case used to study geometries that are disadvantageous for DoA-only and RSS-only localization.

localization system. In such a case the FIM is given as the upper-leftmost 2×2 matrix of $\mathbf{J}_{\mathrm{H,u}}$.

5.1.1.2 Closed-Form CRB for Disadvantageous Geometry

In theory, obtaining the CRB in closed-form by inverting the FIM (5.1) is possible. However, the result is not very informative. In [P6] we have therefore considered a special case of localization with $K = 2$ ONs as illustrated in Figure 5.1. As will be seen, this special case helps us to model ONs-TN geometries that cause DoA-only and RSS-only localization to fail. In order to obtain simple and meaningful expressions, we assume the two ONs are at equal distance R_0 from the TN and at a distance $2R_0$ apart from one another. It is then also reasonable to model the STD of DoA estimation equal at both ONs leading to a covariance $\mathbf{Q}_{\varphi} = \sigma_{\varphi}^2 \mathbf{I}_2$. Assume moreover that $R_0 \gg d_{\mathrm{c}}$, such that we can neglect the shadowing correlation and obtain $\mathbf{Q}_{\gamma} = \sigma_{\mathrm{f}}^2 \mathbf{I}_2$. Define, without loss of generality, the DoAs in Figure 5.1 as $\varphi_1 = \varphi$ and $\varphi_2 = \pi - \varphi$. Then, we can express the TN-ON distance as

$$R = \frac{R_0}{\cos \varphi}. \tag{5.2}$$

For the interval $\varphi \in [0°; 90°]$, the distance R is therefore increasing with φ. Based on this special case, we obtain the following CRBs for the estimation of the x/y coordinates and P (where applicable). The localization CRB using DoA as well as RSS estimates without knowing P is given as

$$\mathrm{CRB}[\hat{x}_{\mathrm{H,u}}] = \frac{\sigma_{\varphi}^2 \sigma_{\mathrm{f}}^2 R_0^2}{2 \cos \varphi \left(\sigma_{\varphi}^2 \alpha_{\mathrm{s}}^2 \cos^2 \varphi + \sigma_{\mathrm{f}}^2 \sin^2 \varphi \right)} \tag{5.3}$$

$$\mathrm{CRB}[\hat{y}_{\mathrm{H,u}}] = \frac{\sigma_{\varphi}^2 R_0^2}{2 \cos^3 \varphi} \tag{5.4}$$

$$\mathrm{CRB}[\hat{P}_{\mathrm{H,u}}] = \frac{\sigma_{\mathrm{f}}^2}{2} + \frac{\sigma_{\varphi}^2 \alpha_{\mathrm{s}}^2}{2} \tan^2 \varphi \tag{5.5}$$

with $\alpha_\mathrm{s} = \frac{10\alpha}{\ln 10}$. When P is known this CRB becomes

$$\mathrm{CRB}[\hat{x}_\mathrm{H,k}] = \frac{\sigma_\varphi^2 \sigma_\mathrm{f}^2 R_0^2}{2\cos\varphi\big(\sigma_\varphi^2 \alpha_\mathrm{s}^2 \cos^2\varphi + \sigma_\mathrm{f}^2 \sin^2\varphi\big)} \tag{5.6}$$

$$\mathrm{CRB}[\hat{y}_\mathrm{H,k}] = \frac{\sigma_\varphi^2 \sigma_\mathrm{f}^2 R_0^2}{2\cos\varphi\big(\sigma_\varphi^2 \alpha_\mathrm{s}^2 \sin^2\varphi + \sigma_\mathrm{f}^2 \cos^2\varphi\big)}. \tag{5.7}$$

For DoA-only localization, the CRB becomes

$$\mathrm{CRB}[\hat{x}_\mathrm{DoA}] = \frac{\sigma_\varphi^2 R_0^2}{2\cos\varphi\sin^2\varphi} \tag{5.8}$$

$$\mathrm{CRB}[\hat{y}_\mathrm{DoA}] = \frac{\sigma_\varphi^2 R_0^2}{2\cos^3\varphi}. \tag{5.9}$$

Finally, the CRB for RSS-only localization is given by

$$\mathrm{CRB}[\hat{x}_\mathrm{RSS}] = \frac{\sigma_\mathrm{f}^2 R_0^2}{2\alpha_\mathrm{s}\cos^3\varphi} \tag{5.10}$$

$$\mathrm{CRB}[\hat{y}_\mathrm{RSS}] = \frac{\sigma_\mathrm{f}^2 R_0^2}{2\alpha_\mathrm{s}\cos\varphi\sin^2\varphi}. \tag{5.11}$$

Note that (5.10) and (5.11) assume that P is known, which is indeed required for RSS-only based localization with only two ONs.

Intuitively, DoA-only localization will fail when the ONs and the TN are located on a straight line, i.e., for $\varphi = 0$. From (5.8) and (5.9), we obtain the following CRB

$$\lim_{\varphi\to 0} \mathrm{CRB}[\hat{x}_\mathrm{DoA}] = \infty \tag{5.12}$$

$$\mathrm{CRB}[\hat{y}_\mathrm{DoA}]|_{\varphi=0} = \frac{\sigma_\mathrm{a}^2 R_0^2}{2}. \tag{5.13}$$

This result is, of course, very intuitive as it means that DoA-only localization, is able to determine that the TN is located somewhere on the line between the two ONs (y coordinate), but not exactly where (x coordinate). Interestingly, RSS-only localization also fails to properly localize the TN for $\varphi = 0$. From (5.10) and (5.11) follows that

$$\mathrm{CRB}[\hat{x}_\mathrm{RSS}]|_{\varphi=0} = \frac{\sigma_\mathrm{f}^2 R_0^2}{2\beta^2} \tag{5.14}$$

$$\lim_{\varphi\to 0} \mathrm{CRB}[\hat{y}_\mathrm{RSS}] = \infty. \tag{5.15}$$

Obviously, DoA-only and RSS-only localization fail in orthogonal coordinates, which indicates that hybrid DoA/RSS localization should be able to determine the TN coordinates.

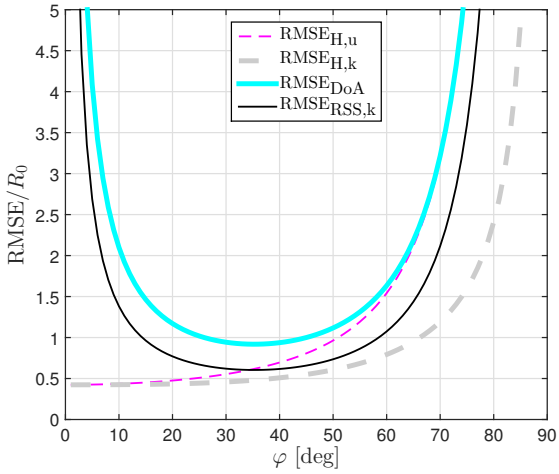

Fig. 5.2. Evaluation of the hybrid DoA/RSS CRBs for the special case in Figure 5.1. Parameters: $\alpha = 3.5$, $\sigma_\varphi = 0.5\,\mathrm{rad}$, and $\sigma_\mathrm{f} = 5\,\mathrm{dB}$.

Indeed, from (5.3) and (5.3) follows that

$$\mathrm{CRB}[\hat{x}_{\mathrm{H,u}}]|_{\varphi=0} = \mathrm{CRB}[\hat{x}_{\mathrm{H,k}}]|_{\varphi=0} = \mathrm{CRB}[\hat{x}_{\mathrm{RSS}}]|_{\varphi=0} \tag{5.16}$$

$$\mathrm{CRB}[\hat{y}_{\mathrm{H,u}}]|_{\varphi=0} = \mathrm{CRB}[\hat{y}_{\mathrm{H,k}}]|_{\varphi=0} = \mathrm{CRB}[\hat{y}_{\mathrm{DoA}}]|_{\varphi=0}. \tag{5.17}$$

Thus, for hybrid DoA/RSS localization and $\varphi = 0$ the x coordinate is determined by RSS-based localization, whereas the y coordinate is determined by DoA-based localization.

5.1.1.3 Numerical Evaluation

For the following evaluation, define $\mathrm{RMSE}_{\mathrm{H,u}} = \sqrt{\mathrm{CRB}[\hat{x}_{\mathrm{H,u}}] + \mathrm{CRB}[\hat{y}_{\mathrm{H,u}}]}$, $\mathrm{RMSE}_{\mathrm{H,k}} = \sqrt{\mathrm{CRB}[\hat{x}_{\mathrm{H,k}}] + \mathrm{CRB}[\hat{y}_{\mathrm{H,k}}]}$, $\mathrm{RMSE}_{\mathrm{DoA}} = \sqrt{\mathrm{CRB}[\hat{x}_{\mathrm{DoA}}] + \mathrm{CRB}[\hat{y}_{\mathrm{DoA}}]}$, $\mathrm{RMSE}_{\mathrm{RSS,k}} = \sqrt{\mathrm{CRB}[\hat{x}_{\mathrm{RSS}}] + \mathrm{CRB}[\hat{y}_{\mathrm{RSS}}]}$, and $\mathrm{RMSE}_{\mathrm{RSS,u}} = \sqrt{\mathrm{CRB}[\hat{x}_{\mathrm{RSS,u}}] + \mathrm{CRB}[\hat{y}_{\mathrm{RSS,u}}]}$, where $\mathrm{CRB}[\hat{x}_{\mathrm{RSS,u}}]$ and $\mathrm{CRB}[\hat{y}_{\mathrm{RSS,u}}]$ denote the CRBs on TN x and y coordinate estimation for RSS-only localization with unknown parameter P.

First, we evaluate the CRBs for the special case using the closed-form expressions stated in the previous section. Figure 5.2 depicts the bounds on the RMSE (normed to R_0) as a function of the DoA. As noted before, increasing DoAs in Figure 5.2 also imply an increase in the ON-TN distance R. It is thus not surprising that all CRBs increase with DoA φ (for $\varphi > 40°$). However, the figure also confirms our observation that for small DoA φ/distance R, the performance of DoA-only and RSS-only localization is getting increasingly worse. The hybrid DoA/RSS CRB, on the other hand, monotonically increases with the DoA φ/distance R.

Next, we evaluate the CRBs for arbitrary geometries. Towards that end, we randomly place the TN and ONs in an area of $100 \times 100\,\mathrm{m}^2$, numerically invert the FIMs, and

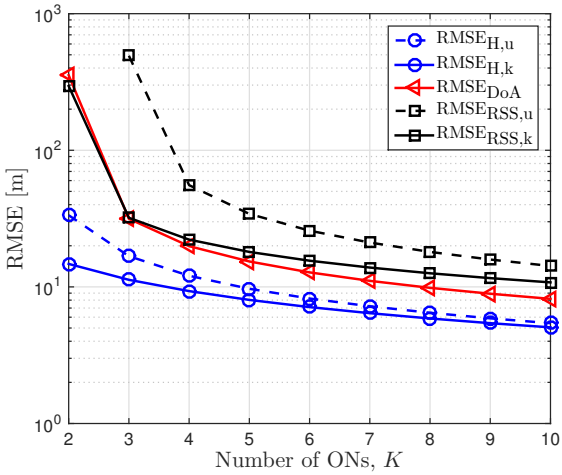

Fig. 5.3. Evaluation of the hybrid DoA/RSS CRBs for arbitrary geometries. Note that RSS-based localization with unknown parameter P ($\mathrm{RMSE}_{\mathrm{RSS,u}}$) requires at least three ONs. Parameters: $\alpha = 3.5$, $d_{\mathrm{c}} = 30\,\mathrm{m}$, $\sigma_{\varphi} = 0.5\,\mathrm{rad}$, and $\sigma_{\mathrm{f}} = 5\,\mathrm{dB}$.

average over the resulting RMSEs as described in more detail in [P6]. The final RMSEs as a function of the number of ONs K is shown in Figure 5.3. Unsurprisingly, the CRBs decrease with K. Interestingly, the largest decrease of the DoA-only and RSS-only CRBs occurs in the step from $K = 2$ to $K = 3$, while the decrease in the hybrid DoA/RSS CRBs from $K = 2$ to $K = 3$ is not that significant. Note also that the gap between the hybrid DoA/RSS CRBs and the DoA-only and RSS-only CRBs is largest for $K = 2$. This can be explained by the probability of disadvantageous geometries that decreases with K. While it is possible that $K > 3$ ONs are located on a straight line with the TN, such a situation is of course most likely for $K = 2$. In general, when checking placements that resulted in very large CRBs for DoA-only and RSS-only localization, we noticed that they were almost exclusively caused by geometries where ONs and the TN were located on a straight line.

5.1.2 Extended Kalman Filter

In [P3], we have studied DoA/RSS-based tracking using an EKF as an example algorithm. In contrast to DoA-only tracking (e.g. [8]), the hybrid DoA/RSS-EKF has to track parameter P in (3.6) as well, resulting in a state equal to

$$\mathbf{s}[n] = [x[n], y[n], v_x[n], v_y[n], P]^T \tag{5.18}$$

where $v_x[n]$ and $v_y[n]$ are the velocities in x and y direction, respectively. Assuming, for simplicity, that P remains constant, we then obtain a state transition matrix given by

$$\mathbf{F} = \begin{bmatrix} \mathbf{I}_2 & T\,\mathbf{I}_2 & 0 \\ \mathbf{0}_{2\times 2} & \mathbf{I}_2 & 0 \\ \mathbf{0}_2^T & \mathbf{0}_2^T & 1 \end{bmatrix}, \tag{5.19}$$

where the upper leftmost 4×4 submatrix originates from a conventional movement model (e.g. [56, p. 459]). In practice, it may not be justified to assume a constant parameter P. In order to address divergence due to modeling P as constant, the EKF could then be modified by implementing a fading memory [91, p. 208] or by adding fictitious process noise [50], [91, p. 140]. Both of these approaches essentially result in the filter emphasizing the measurements more, while placing less emphasis on the model.

At each time instant n, the input of the hybrid DoA/RSS-EKF is composed of the DoA and RSS estimates from all K ONs. Thus, the measurement vector can be expressed as

$$\mathbf{y}[n] = [\hat{\boldsymbol{\varphi}}^T[n], \hat{\boldsymbol{\gamma}}^T[n]]^T = [\hat{\varphi}_1[n], \ldots, \hat{\varphi}_K[n], \hat{\gamma}_1[n], \ldots, \hat{\gamma}_K[n]]^T. \tag{5.20}$$

With the estimation models (3.2) and (3.6), the Jacobian matrix in (2.25)–(2.27) becomes

$$\mathbf{H} = \begin{bmatrix} [\hat{\boldsymbol{\varphi}}[n]]_x & [\hat{\boldsymbol{\varphi}}[n]]_y & \mathbf{0}_K & \mathbf{0}_K & \mathbf{0}_K \\ [\hat{\boldsymbol{\gamma}}[n]]_x & [\hat{\boldsymbol{\gamma}}[n]]_y & \mathbf{0}_K & \mathbf{0}_K & \mathbf{1}_K \end{bmatrix} \tag{5.21}$$

where the elements of $[\hat{\boldsymbol{\varphi}}[n]]_x$, $[\hat{\boldsymbol{\varphi}}[n]]_y$, $[\hat{\boldsymbol{\gamma}}[n]]_x$, and $[\hat{\boldsymbol{\gamma}}[n]]_y$ are given by (3.4), (3.5), (3.9), and (3.10), evaluated at $\hat{\mathbf{s}}^-[n]$.

Note that, with this formulation of the state and measurement equation, we implicitly assume uncorrelated shadow fading since successive measurement noise samples $\mathbf{u}[n]$ in (2.22) are assumed to be independent. However, with (3.7) the correlation of successive samples is given by

$$\mathrm{cov}[\mathbf{u}[n], \mathbf{u}[n+1]] = \sigma_{\mathrm{f}}^2 \exp\left(-\frac{v[n]\,T}{d_{\mathrm{c}}}\right) \tag{5.22}$$

where

$$v[n] = \sqrt{v_x^2[n] + v_y^2[n]}. \tag{5.23}$$

Obviously, for good performance the correlation of shadow fading should not be ignored. Two methods to account for correlated measurement noise are discussed in [91, p. 188], namely state augmentation and measurement differencing. In state augmentation, the

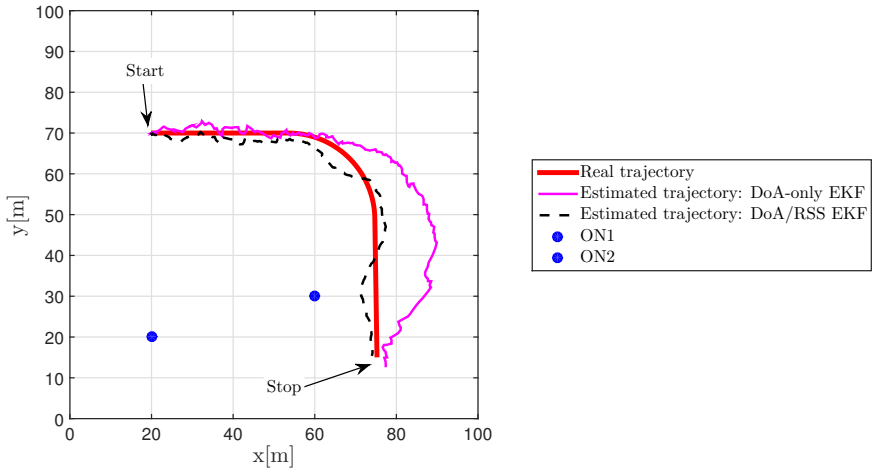

Fig. 5.4. Example trajectory and illustration of temporary tracking divergence of the DoA-only EKF due to disadvantageous geometry.

state (5.18) is extended to also include an estimate for the current shadow fading at all ONs. In measurement differencing, the measurement vector at time step n is transformed into an auxiliary signal taking the measurement vector at time step $n-1$ into account. However, in this thesis we will only investigate the hybrid DoA/RSS-EKF that does not take correlated shadow fading into account as we are mainly interested in studying the influence of disadvantageous geometries. Towards that end, we consider a TN moving with constant velocity $v = \sqrt{v_x^2 + v_y^2}$ on a trajectory as depicted in Figure 5.4. Moreover, we place two ONs randomly on an area of $100 \times 100\,\mathrm{m}^2$ and estimate DoA and RSS for every $\Delta d = vT = 0.5\,\mathrm{m}$ that the TN is moving. For simplicity, we assume that σ_φ is constant and that the shadowing at the two ONs is mutually uncorrelated. Finally, we also initialize the EKFs with the true states in order to avoid divergence due to poor initialization. A more detailed description of the simulation setup can be found in [P3].

Figure 5.5 shows the tracking RMSE of the DoA-only EKF and the hybrid DoA/RSS-EKF as a function of the correlation distance, d_c, and for different DoA STDs, σ_φ. For $d_\mathrm{c} = 0$, the hybrid DoA/RSS-EKF outperforms the DoA-only EKF for all considered σ_φ. Now for $d_\mathrm{c} = 0$, shadowing is uncorrelated in time meaning that the underlying shadowing model in the hybrid DoA/RSS-EKF is in fact correct. However, for increasing d_c the shadowing model within the hybrid DoA/RSS-EKF is becoming increasingly more inaccurate resulting, in turn, in an increasing RMSE with d_c. Whether the hybrid DoA/RSS-EKF is in the end beneficial depends moreover also on σ_φ and σ_f as shown in Figure 5.6. The RMSE of hybrid DoA/RSS-EKF tracking increases with the shadowing STD, σ_f. And as also visible from Figure 5.6, the hybrid DoA/RSS-EKF results in a worse performance than the DoA-only EKF if σ_f is large in relation to σ_φ. Again, this is due to ignoring the correlation of shadow fading within the hybrid DoA/RSS-EKF.

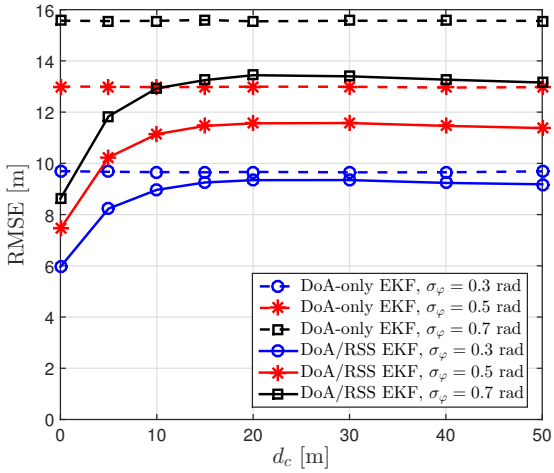

Fig. 5.5. Tracking RMSE as a function of the correlation distance, d_c. Parameters: $\Delta d = vT = 0.5\,\mathrm{m}$ and $\sigma_\mathrm{f} = 4\,\mathrm{dB}$.

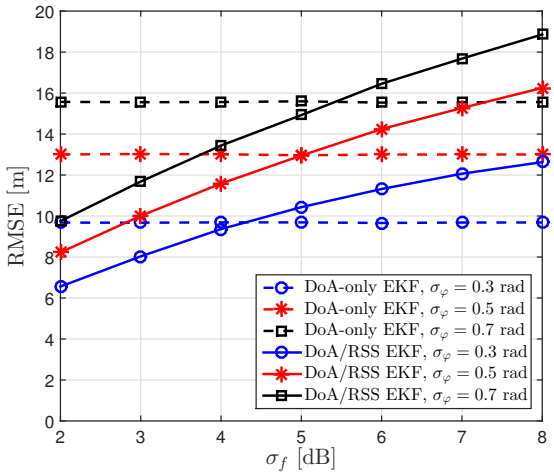

Fig. 5.6. Tracking RMSE as a function of the shadowing STD, σ_φ. Parameters: $\Delta d = vT = 0.5\,\mathrm{m}$ and $d_\mathrm{c} = 20\,\mathrm{m}$.

Finally, the ON-TN geometry also determines whether the hybrid DoA/RSS-EKF outperforms the DoA-only EKF. The example ON placement in Figure 5.4 clearly shows that the DoA-only EKF diverges when the ON-TN geometry resembles a straight line. In fact for the DoA-only EKF, an ON placement as depicted in Figure 5.4 results in a significantly worse tracking performance than a uniform placement [P3]. In contrast, the performance of the hybrid DoA/RSS-EKF is not as susceptible to the ONs placement [P3]. We therefore conclude that the insights gained from the CRB analysis in Section 5.1.1 should be taken into consideration when developing practical DoA-based fusion algorithms.

5.2 Joint Clock Offset and Location Tracking in Ultra Dense Networks

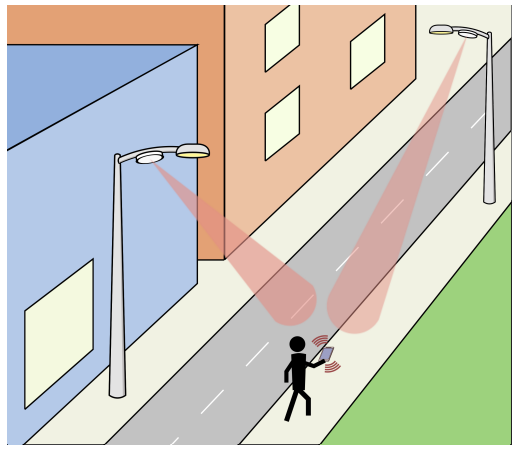

Fig. 5.7. Localization in 5G ultra-dense networks.

It is commonly expected that network densification, as depicted in Figure 5.7, will play an important role in achieving the communication throughputs targeted for 5G mobile networks [9,13,33,48,72,74]. As we will elaborate in the following, the envisioned ultra-dense 5G networks have an enormous potential for highly accurate UN localization. First, the high density of ANs means that UNs in 5G networks are most likely in LoS with one or multiple ANs for most of the time. Provided that the ANs implement LoS detection schemes, this means that localization can be based on LoS DoA/ToA estimates that are much easier to process than estimates obtained from NLoS links. Second, the envisioned radio frames for 5G small cells typically include some form of uplink pilots for channel estimation. At the same time, the radio frames are also very short (0.1 ms – 0.5 ms [57,60,68]) in order to guarantee a commonly targeted latency below 1 ms in the networks [34,74,116]. Now, the availability of these frequent uplink pilots enables nearly continuous DoA/ToA estimation at the ANs and UN location tracking in the network as a whole. Third, it is commonly agreed that 5G networks require high bandwidths in order to satisfy the large capacity demands [57]. As discussed in Section 3.2.3, this enables ToA estimation with very high accuracy, which obviously also results in an increased localization performance.

As a consequence, joint DoA/ToA-based approaches are promising candidates for UN localization and location tracking in 5G ultra-dense networks. In the past, joint DoA/ToA-based localization and tracking have been addressed in [36] and [69, 70], respectively. However, these approaches assume that the ONs (here ANs) and the TN (here UN) clocks are synchronized (see discussion in Section 3.2). When recalling that

the error of a ToA estimate subject to an ON-AN clock offset of 1 µs is equal to a range error of about 300 m, it is clear that the level of ON-AN clock synchronization within wireless networks does not justify such an assumption. In [P7], we have addressed this problem by tracking both the UN location as well as the UN device clock offset using an EKF. The resulting joint DoA/ToA-EKF will be described in detail in the following section.

5.2.1 Extended Kalman Filter

The joint DoA/ToA-EKF was developed for networks where the ANs are synchronized in time. Such an AN clock synchronization is more feasible than a UN-AN clock synchronization since ANs are generally not subject to the same stringent resource constraints as UNs. Moreover, the AN synchronization does not have to be perfect but should not exceed the range of ToA estimation errors, which are around 1 ns – 4 ns with the setup considered in [P7]. Note that we might be able to relax this requirement by including the AN synchronization into the localization process, similarly to what was proposed for E-OTD in [32]. However, for now let us assume that the ANs are synchronized. Assume next that the ANs have detected whether they are in LoS with the UN. In practice LoS detection could be implemented based on the Rice factor of the RSS [12] or on the kurtosis of the estimated channel impulse response [121]. Denote $K[n]$ as the number of ANs that are in LoS with the UN at time step n and let

$$\mathbf{y} = [\hat{\varphi}_1[n], \hat{\tau}_1[n], \ldots, \hat{\varphi}_{K[n]}[n], \hat{\tau}_{K[n]}[n]]^T \tag{5.24}$$

be the vector of DoA/ToA estimates from all those LoS ANs. Note that (5.24) could be obtained by either estimating DoA and ToA at each time step n using, e.g., the RIMAX algorithm [99] or by implementing another EKF that tracks the DoA and ToA based on channel estimates [87]. While the DoA estimates can again be modeled according to (3.2), (3.12) is not sufficient to model the ToA estimates due to the assumed lack of synchronization between the ANs and the UN. Instead, ToA estimates should be modeled as

$$\tau_k[n] = \frac{d_k[n]}{c} + \rho[n] \tag{5.25}$$

where $k = 1 \ldots K[n]$ and $\rho[n]$ is the clock offset between the ANs and the UN. Stemming from the imperfect oscillators built into commercial UN devices, the clock offset is a time-varying quantity [58, 115]. In discrete time, the clock offset can be modeled as [58]

$$\rho[n] = \rho[n-1] + \alpha[n]T \tag{5.26}$$

where T is the measurement period and $\alpha[n]$ is known as the clock skew. Often it is assumed that the clock skew is constant [115]. However, supported by measurements obtained from real world low-precision clocks, the authors of [58] propose to model the clock skew as an auto-regressive (AR) process. Based on their measurement results, the best tradeoff between accuracy and model complexity is achieved with an AR process of first order. We therefore adopt the following clock skew model

$$\alpha[n] = \beta\alpha[n-1] + \eta[n] \tag{5.27}$$

where β is a (constant) parameter and $\eta[n] \sim \mathcal{N}(0, \sigma_\eta^2)$ is AWGN. Modeling the UN movement using a conventional movement model as in Section 5.1.2, our overall state for tracking UN location and clock offset is given as

$$\mathbf{s}[n] = [x[n], y[n], v_x[n], v_y[n], \rho[n], \alpha[n]]^T \tag{5.28}$$

with a state transition matrix given by

$$\mathbf{F} = \begin{bmatrix} \mathbf{I}_2 & T \cdot \mathbf{I}_2 & \mathbf{0}_{2\times 2} \\ \mathbf{0}_{2\times 2} & \mathbf{I}_2 & \mathbf{0}_{2\times 2} \\ \mathbf{0}_{2\times 2} & \mathbf{0}_{2\times 2} & \mathbf{F}_\mathrm{c} \end{bmatrix}, \quad \mathbf{F}_\mathrm{c} = \begin{bmatrix} 1 & T \\ 0 & \beta \end{bmatrix}. \tag{5.29}$$

For the state (5.28) and the measurement vector (5.24), we have

$$\mathbf{h}[n] = [\varphi_1[n], \tau_1[n], \ldots, \varphi_{K[n]}[n], \tau_{K[n]}[n]]^T \tag{5.30}$$

in (2.22) and a Jacobian matrix given by

$$\mathbf{H} = \Big[[\mathbf{h}[n]]_x \quad [\mathbf{h}[n]]_y \quad \mathbf{0}_{2K[n]} \quad \mathbf{0}_{2K[n]} \quad [\mathbf{h}[n]]_\rho \quad \mathbf{0}_{2K[n]} \Big]. \tag{5.31}$$

The vectors $[\mathbf{h}[n]]_x$ and $[\mathbf{h}[n]]_y$ in (5.31) are composed of the derivatives $[\varphi_k[n]]_x$ and $[\varphi_k[n]]_y$, $k = 1 \ldots K[n]$ that are given by (3.4) and (3.5), respectively, as well as $[\tau_k[n]]_x$ and $[\tau_k[n]]_y$, $k = 1 \ldots K[n]$ equal to

$$[\tau_k[n]]_x = \frac{\Delta x_k[n]}{c\, d_k[n]} \tag{5.32}$$

$$[\tau_k[n]]_y = \frac{\Delta y_k[n]}{c\, d_k[n]}. \tag{5.33}$$

Finally, the vector $[\mathbf{h}[n]]_\rho$ in (5.31) is given by

$$[\mathbf{h}[n]]_\rho = [0, 1, \ldots, 0, 1]^T. \tag{5.34}$$

Using (5.29), (5.30), and (5.31), we are then able to execute the EKF iterations (2.23)–(2.27) and obtain the location estimate at time step n as $\hat{\boldsymbol{\ell}}[n] = [\hat{s}_1^+[n], \hat{s}_2^+[n]]^T$ and an estimated clock offset given by $\hat{s}_5^+[n]$. Note that for executing the joint DoA/ToA-EKF iterations, we have to assume a value for the parameter β contained in the state transition (5.29). Since β is a device specific parameter, this value might have to be estimated. Methods for the estimation of β were proposed in [58]. Unfortunately, these methods may be impractical in real-world wireless networks. However, according to our observations in [P7], the joint DoA/ToA-EKF is not very sensitive to mismatches between the real value of β and the value $\tilde{\beta}$ used in the implementation of the EKF. We therefore generally set $\tilde{\beta} = 1$ within the EKF. Similarly, the STD σ_η of the parameter η in (5.27) may be unknown to the network as well. However, in [P7] we have observed that very small values of σ_η within the joint DoA/ToA-EKF can lead to divergence in the initial tracking phase. We therefore have proposed to use a value σ'_η within the EKF that is much larger than the actual value of σ_η. In our simulations in [P7], as an example, the actual value was set to $\sigma_\eta = 6.3 \cdot 10^{-8}$ in accordance with [58], whereas the joint DoA/ToA-EKF was executed with $\sigma'_\eta = 10^{-4}$.

In [P7] we have also shortly discussed how to initialize the joint DoA/ToA-EKF in order to avoid divergence. Generally, divergence of the joint DoA/ToA-EKF in ultra-dense networks is detected relatively fast when checking if the current location estimate matches the locations of the ANs that can hear the UN. Nevertheless, initialization is crucial for good tracking performance. In [P7], we assume that an initial estimate for the UN location and velocity are available via, e.g., GNSS. In our future work we are planing to also study solutions where the initial location estimate is directly obtained through fusion of the DoA/ToA estimates using, e.g., the Stansfield estimator (see Section 3.3). However, of greater interest for this work is the initialization of the clock offset and clock skew. A very rough initial clock offset estimate may be obtained by communicating the current time of the UN device to the network. In this way, the clock offset is known with an accuracy up to the UN-AN signal propagation time and transmission/reception delays within the UN/AN devices. Manufactures typically specify the maximum clock skew of their oscillators in parts per million (ppm). As an example, if an oscillator is specified to have a maximum clock skew of 20 ppm, we can expect the clock offset to grow by a maximum of 20 µs per 1 s of runtime. However, taking the results in [26, 58, 59] into account, it seems that the clock skew is more often negative than positive. Thus, in [P7] we concluded that $\hat{\alpha}[0] = 25$ ppm with a STD of a few 10 ppm could be a good initialization for the clock skew. Of course, in practice it would make sense to obtain more detailed statistics for the clock skew of different kind of oscillators and initialize the joint DoA/ToA-EKF accordingly. Interestingly, the results in [26, 59] indicate that the *average* clock skew is a device-specific constant. This is also in line with the results depicted in [58], where the clock skew seems to fluctuate around a constant average value. Thus, once an estimate for the average clock skew of a device is available, it

could serve as a good initial value whenever the device is reconnecting with the network. However, neither of the articles [26, 58, 59] investigates the influence of the temperature on the average clock skew. Therefore, additional research may be required in order to enable an initialization with pre-saved and device-specific average clock skews in a practical tracking system.

5.2.2 Numerical Evaluation

In order to study the performance of the joint DoA/ToA-EKF, we simulated the UN-AN channel according to the METIS geometry-based stochastic channel model (MGSCM) [67]. The MGSCM was developed specifically for the simulation of 5G networks and is an advancement of the WINNER+ channel model [23]. In [P7], we have first evaluated the CRBs for DoA/ToA estimation using the MGSCM. Thereafter, we have used the statistics obtained from the CRB analysis for testing the joint DoA/ToA-EKF. The results of the CRB evaluation are presented in Section 5.2.2.1 and the overall performance of the joint DoA/ToA-EKF is discussed in Section 5.2.2.2.

5.2.2.1 DoA and ToA estimation CRB for the Stochastic METIS Channel Model

From the available options of the MGSCM, we chose the 3D urban micro propagation scenario. Since it is assumed that only LoS ANs estimate the DoA/ToA, we simulate LoS links only. The CRB that we use to evaluate the DoA/ToA estimation performance in 5G ultra-dense networks can be found in [83]. In our evaluation, we realized that some of the channel realizations result in a DoA estimation CRB much larger than $(180°)^2$. This is a result of the CRB that was derived assuming non-circular statistics (see Section 3.2.1). In order to address this problem, we decided to drop channel realizations that result in a DoA estimation CRB larger than $(180°)^2$ altogether. From a practical point of view, this is justified since we would anyways recommend to fuse only those DoAs estimates that are in line with our earlier estimated trajectory.

The ANs are assumed to be mounted at a height of 10 m, whereas the UN is assumed to be located at a height of 1.5 m above the ground. Moreover, we assume that ANs are equipped with a concentric circular antenna array consisting of nine cross dipoles arranged in a horizontal plane. In accordance with [57], the UN is transmitting uplink pilots with an OFDM waveform consisting of 640 subcarriers, spread over a bandwidth of 200 MHz. However, for localization purposes we exploit only every 10th subcarrier at the ANs. Finally, the UN transmit power is set to a fixed value such that an AN at a distance of 60 m receives the uplink pilots with a signal-to-interference-plus-noise ratio (SINR) of SINR = 15 dB. For a more detailed discussion of the simulation setup refer to [P7].

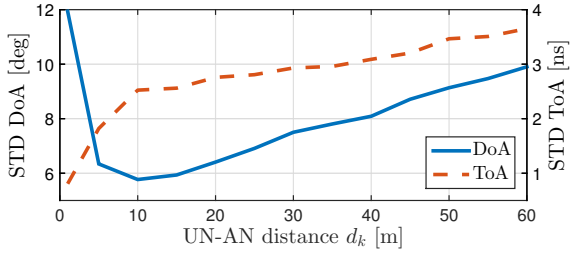

Fig. 5.8. CRB on the STD of DoA and ToA estimation as a function of the AN-UN distance using the stochastic Mobile and wireless communications enablers for the twenty-twenty information society (METIS) channel model [67].

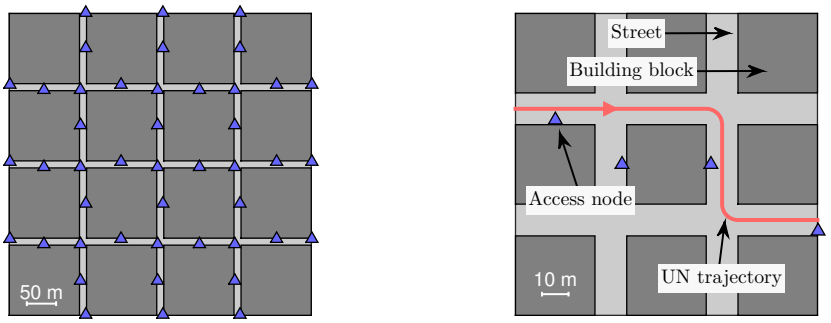

(a) Multiple LoS-AN map. **(b)** Single LoS-AN map.

Fig. 5.9. Example maps used for testing the tracking performance of the proposed joint DoA/ToA-EKF.

Figure 5.8 depicts the CRBs on the STD of DoA/ToA estimation for AN-UN distances d_k ranging from 0 m – 60 m. Interestingly, the CRB for DoA estimation decreases with distances from 0 m to 10 m. As discussed in more detail in [P7], this is explained by the estimation geometry and the assumed antenna array. For $d_k > 10$ m, the DoA estimation CRB increases monotonically with the distance, whereas the ToA estimation CRB increases monotonically with the distance for all d_k. This, of course, is a result of the SINR monotonically decreasing with the distance. Overall, the CRB on the STD of DoA estimation is below 10 m for $5\,\text{m} < d_k < 60\,\text{m}$, whereas the CRB on the STD of ToA estimation is below 4 ns for all considered d_k.

5.2.2.2 Tracking Performance

To test the joint DoA/ToA-EKF, we assume that a UN is moving with a constant velocity $v = \sqrt{v_x^2 + v_y^2} = 15\,\text{km/h}$ on the map depicted in Figure 5.9a. This map has parameters that are very similar to those of the Madrid model proposed in the METIS simulation guidelines [66]. On the map, ANs are placed with a density of 60 m, which is a value similar to the densities assumed in, e.g., [9, 57]. The EKF updating period T is chosen to be an integer multiple of the radio frame length $T_\text{f} = 167.3\,\mu\text{s}$ from [57],

Tab. 5.1. Tracking RMSE of UN location (Loc.) and clock offset (Clk.).

	DoA-only EKF [8]		proposed joint DoA/ToA-EKF	
N_T	Loc.	Clk.	Loc.	Clk.
100	5.3 m	–	0.4 m	4 ns
500	8.2 m	–	0.6 m	4 ns
1000	10.3 m	–	1.0 m	4 ns

i.e., $T = N_\mathrm{T} T_\mathrm{f}$. For each time step nT, $n = 1, 2, \ldots$, we assume that the closest two ANs not obscured by buildings are in LoS with the UN. Those LoS-ANs then produce normally distributed DoA/ToA estimates with a STD according to the CRB results from the previous section. For a more detailed description of the simulation setup and the values chosen to initialize the joint DoA/ToA-EKF refer to [P7].

Table 5.1 lists the RMSE for UN location and clock offset tracking. As a comparison, we have also included the RMSE for the DoA-only EKF (e.g. [8]). Unsurprisingly, the location tracking RMSE can be reduced by updating the EKFs more frequently, i.e., with lower N_T. Overall, the results also show that the joint DoA/ToA-EKF greatly outperforms the DoA-only EKF. The tracking RMSE of the DoA-only EKF is more than ten times larger compared to the joint DoA/ToA-EKF, which is able to track the UN location with an RMSE below 1 m. In addition and in contrast to the DoA-only EKF, the joint DoA/ToA-EKF is also able to estimate the clock offset with a RMSE of 4 ns. Upon detailed inspection of the location tracking behavior, we noticed that the joint DoA/ToA-EKF outperforms the DoA-only EKF in particular when the tracking geometry resembles a straight line. This is expected, when taking the results in Section 5.1.2 into account. Similarly to the RSS, the ToA is a measurement for the AN-UN distance. Thus, similar arguments as discussed for DoA/RSS-based localization in Section 5.1.2 apply also for DoA/ToA-based localization. However, in practice such geometries are unavoidable. In fact, even the assumption that the UN is in LoS with two ANs at any given moment may not be realistic. Therefore, we have tested the tracking performance of the joint DoA/ToA-EKF also with a second map depicted in Figure 5.9b. In this scenario, the UN is in LoS with a single AN only for most of the time. Nevertheless, the joint DoA/ToA-EKF is capable of tracking UN location and clock offset with a RMSE of 3.0 m and 10.3 ns, respectively, for $N_\mathrm{T} = 100$. Tracking the UN location with the DoA-only EKF, on the other hand, is only possible when the number of LoS-ANs is larger than one. For the map depicted in Figure 5.9b, the DoA-only EKF is therefore unable to provide location estimates for most of the time.

The tracking behavior of the joint DoA/ToA-EKF is also illustrated in videos that we have uploaded to: `http://www.tut.fi/5G/GLOBECOM15`.

CHAPTER 6

Summary

In this thesis, we have studied methods to utilize directional antennas for DoA/RSS estimation, localization and location tracking in future generation wireless networks. The contributions of this thesis consist of the derivation of performance bounds, algorithm development, as well as analytical, numerical, and experimental performance evaluation. Topically, we have focused mainly on low complexity DoA/RSS estimation and localization with sectorized antennas, on the one hand, and on the fusion of DoA estimates with other types of measurements for localization and location tracking, on the other hand. The main outcomes of this thesis are summarized below.

Chapter 4 and the articles [P1],[P2],[P4],[P5] deal with DoA/RSS estimation and localization in a network where the ONs are equipped with sectorized antennas. We introduced the sectorized antenna model first in [P4]. This model enables us to study DoA/RSS estimation with a broad range of single RF front-end directional antennas in a generic framework. In [P4] we have moreover introduced the MaxE DoA/RSS estimator, studied its performance both numerically and analytically, and demonstrated its application in localization with a modified Stansfield fusion algorithm. While MaxE is very low in computational complexity, its estimation performance may not be sufficient in certain application areas. In [P5], we have thus introduced and studied the more advanced SLS DoA/RSS estimator for sectorized antennas. While still low in computational complexity, SLS has a significantly improved performance compared to MaxE. Following a numerical performance study in [P5], we have then derived accurate analytical expressions for the performance of SLS in [P1]. In addition, [P1] includes an extensive CRB analysis for DoA/RSS estimation and localization with sectorized antennas. This analysis revealed that SLS performs close to the CRB for moderate SNRs. However, for large SNRs the performance of SLS saturates at a much higher level than the CRB. Motivated by that and by the fact that both MaxE and SLS are limited to sectorized antennas where the

main beams are of equal shape in all sectors, we have proposed the TSLS DoA estimator in [P2]. TSLS does not require equally-shaped main beams in all sectors and practically achieves the CRB for moderate to large SNRs. [P2] also includes an analytical and numerical performance evaluation for TSLS as well as a complexity analysis for MaxE, SLS, and TSLS. Finally, in [P2] we have also studied the application of TSLS in a localization system by means of using LWAs in a measurement example.

Chapter 5 and the articles [P3],[P6],[P7] deal with the fusion of heterogeneous measurements. In [P3] and [P6] we have studied the fusion of DoA and RSS estimates. More specifically, in [P6] we have first derived the FIM on hybrid DoA/RSS-based localization of a non-cooperative TN. Thereafter, we have considered an important TN-ON geometry that helps us to understand one of the main benefits of hybrid DoA/RSS-based localization and derived the CRB for this special case. Finally, we have evaluated the CRB also for arbitrary geometries using numerical methods. As a practical example of hybrid DoA/RSS-based fusion, we have then studied a hybrid DoA/RSS-EKF in [P3]. Next, in [P7], we have considered DoA/ToA-based tracking in the framework of 5G ultra-dense networks. More specifically, we have proposed the joint DoA/ToA-EKF that tracks both the UN location as well as the clock offset of the UN device. The performance of this algorithm was verified to significantly outperform the DoA-only EKF using a numerical evaluation of the METIS stochastic channel model. This numerical evaluation moreover revealed that UN localization with the often prescribed accuracy in the sub-meter range may be possible in ultra-dense 5G networks, in general, and with the proposed joint DoA/ToA-EKF in particular.

Overall, this thesis highlights the benefits of directional antenna-based localization and location tracking and moreover provides specific guidelines and algorithm proposals for the implementation of such systems in future generation wireless networks. The contributions are expected to be especially useful when considering an implementation based on directional antennas from the group herein denoted as sectorized antennas. Apart from that, the contributions in Chapter 5 are independent of a specific antenna architecture and are expected to be useful when designing and implementing directional antenna-based systems in future generation wireless networks in general.

References

[1] *Revision of the commission's rules to ensure compatibility with enhanced 911 emergency calling systems.* Federal Communications Commission (FCC), Oct. 1999. [Online]. Available: https://apps.fcc.gov/edocs_public/attachmatch/FCC-15-9A1.pdf

[2] *Evolved universal terrestrical radio access (E-UTRA).* The 3rd Generation Partnership Project (3GPP) TR 25.814 V. 7.10, 2011.

[3] "Imaginary error function - MATLAB," 2014. [Online]. Available: http://www.mathworks.com/help/symbolic/mupad_ref/erfi.html

[4] "Indoor location market by solution (tag-based, RF-based, sensor-based), by application (indoor maps & navigation, indoor location-based analytics, tracking & tracing, monitoring & emergency management), by service, by vertical, & by region - global forecast up to 2019," MarketsandMarkets, Tech. Rep., Nov. 2014. [Online]. Available: http://www.marketsandmarkets.com/Market-Reports/indoor-positioning-navigation-ipin-market-989.html

[5] *Observed time difference of arrival (OTDOA) positioning in 3GPP LTE.* Qualcomm Technologies, Inc., Jun. 2014.

[6] 5G Forum, "5G white paper: New wave towards future societies in the 2020s," Mar. 2015. [Online]. Available: http://www.5gforum.org/5GWhitePaper/5G_Forum_White_Paper_Service.pdf

[7] S. Abielmona, H. Nguyen, and C. Caloz, "Analog direction of arrival estimation using an electronically-scanned CRLH leaky-wave antenna," *IEEE Trans. Antennas Propag.*, vol. 59, no. 4, pp. 1408 –1412, Apr. 2011.

[8] V. Aidala, "Kalman filter behavior in bearings-only tracking applications," *IEEE Trans. Aerosp. Electron. Syst.*, vol. AES-15, no. 1, pp. 29 –39, 1979.

[9] R. Baldemair, T. Irnich, K. Balachandran, E. Dahlman, G. Mildh, Y. Selen, S. Parkvall, M. Meyer, and A. Osseiran, "Ultra-dense networks in millimeter-wave frequencies," *IEEE Commun. Mag.*, vol. 53, no. 1, pp. 202–208, Jan. 2015.

[10] Y. Bar-Shalom, F. Daum, and J. Huang, "The probabilistic data association filter," *IEEE Control Syst. Mag.*, vol. 29, no. 6, pp. 82 –100, Dec. 2009.

[11] J. Becker, M.-B. A. Colas, S. Nordbruch, and M. Fausten, "Bosch's vision and roadmap toward fully autonomous driving," in *Road Vehicle Automation*, ser. Lecture Notes in Mobility, G. Meyer and S. Beiker, Eds. Springer International Publishing, 2014, pp. 49–59.

[12] F. Benedetto, G. Giunta, A. Toscano, and L. Vegni, "Dynamic LOS/NLOS statistical discrimination of wireless mobile channels," in *Proc. IEEE 65th Vehicular Technology Conference (VTC spring)*, Apr. 2007, pp. 3071–3075.

[13] N. Bhushan, J. Li, D. Malladi, R. Gilmore, D. Brenner, A. Damnjanovic, R. Sukhavasi, C. Patel, and S. Geirhofer, "Network densification: The dominant theme for wireless evolution into 5G," *IEEE Commun. Mag.*, vol. 52, no. 2, pp. 82–89, Feb. 2014.

[14] J. Blumenthal, R. Grossmann, F. Golatowski, and D. Timmermann, "Weighted centroid localization in ZigBee-based sensor networks," in *Proc. IEEE Int. Symp. on Intelligent Signal Processing (WISP)*, Oct. 2007, pp. 1–6.

[15] F. Boccardi, R. Heath, A. Lozano, T. Marzetta, and P. Popovski, "Five disruptive technology directions for 5G," *IEEE Commun. Mag.*, vol. 52, no. 2, pp. 74–80, Feb. 2014.

[16] J. Boerman and J. Bernhard, "Performance study of pattern reconfigurable antennas in MIMO communication systems," *IEEE Trans. Antennas Propag.*, vol. 56, no. 1, pp. 231–236, Jan. 2008.

[17] M. Bolic, M. Rostamian, and P. Djuric, "Proximity detection with RFID: A step toward the internet of things," *IEEE Pervasive Comput.*, vol. 14, no. 2, pp. 70–76, Apr. 2015.

[18] N. Bulusu, J. Heidemann, and D. Estrin, "GPS-less low-cost outdoor localization for very small devices," *IEEE Pers. Commun.*, vol. 7, no. 5, pp. 28–34, Oct. 2000.

[19] D. Cabric, S. Mishra, and R. Brodersen, "Implementation issues in spectrum sensing for cognitive radios," in *Proc. 38th Asilomar Conf. Signals, Systems and Computers*, vol. 1, Nov. 2004, pp. 772 – 776 Vol.1.

[20] A. B. Carlson and P. B. Crilly, *Communication Systems: An Introduction to Signals and Noise in Electrical Communication*. Boston: McGraw-Hill Higher Education, 2010.

[21] A. Catovic and Z. Sahinoglu, "The Cramer-Rao bounds of hybrid TOA/RSS and TDOA/RSS location estimation schemes," *IEEE Commun. Lett.*, vol. 8, no. 10, pp. 626 – 628, Oct. 2004.

[22] H. Celebi and H. Arslan, "Utilization of location information in cognitive wireless networks," *IEEE Wireless Commun. Mag.*, vol. 14, no. 4, pp. 6–13, Aug. 2007.

[23] CELTIC, *D5.3: WINNER+ final channel models*, Jun. 2010.

[24] C. Chang and A. Sahai, "Estimation bounds for localization," in *Proc. 1st Annu. IEEE Communications Society Conf. Sensor and Ad Hoc Communications Networks (SECON)*, Oct. 2004, pp. 415–424.

[25] X. Chen, Y. Chen, M. Dong, and C. Zhang, "Demystifying energy usage in smartphones," in *Proc. 51st Design Automation Conference*, Jun. 2014, pp. 1–5.

[26] M. Cristea and B. Groza, "Fingerprinting smartphones remotely via ICMP timestamps," *IEEE Commun. Lett.*, vol. 17, no. 6, pp. 1081–1083, Jun. 2013.

[27] A. Dammann, R. Raulefs, and S. Zhang, "On prospects of positioning in 5G," in *Proc. IEEE Int. Conf. Communications (ICC)*, Jun. 2015.

[28] D. Dardari, P. Closas, and P. Djuric, "Indoor tracking: Theory, methods, and technologies," *IEEE Trans. Veh. Technol.*, vol. PP, no. 99, pp. 1–1, 2015.

[29] D. Dardari, A. Conti, U. Ferner, A. Giorgetti, and M. Win, "Ranging with ultrawide bandwidth signals in multipath environments," *Proc. IEEE*, vol. 97, no. 2, pp. 404–426, Feb. 2009.

[30] S. Deb, M. Yeddanapudi, K. Pattipati, and Y. Bar-Shalom, "A generalized S-D assignment algorithm for multisensor-multitarget state estimation," *IEEE Trans. Aerosp. Electron. Syst.*, vol. 33, no. 2, pp. 523–538, Apr. 1997.

[31] R. Di Taranto, S. Muppirisetty, R. Raulefs, D. Slock, T. Svensson, and H. Wymeersch, "Location-aware communications for 5G networks: How location information can improve scalability, latency, and robustness of 5G," *IEEE Signal Process. Mag.*, vol. 31, no. 6, pp. 102–112, Nov. 2014.

[32] C. R. Drane, P. Duffett-Smith, S. Hern, and J. Brice, "Mobile location without network-based synchronization or how to do E-OTD without LMUs," in *Proc. SPIE.*, vol. 5084, 2003, pp. 59–66.

[33] Ericsson, *5G radio access research and vision (White Paper)*, Jun. 2013. [Online]. Available: http://www.ericsson.com/res/docs/whitepapers/wp-5g.pdf

[34] G. Fettweis and S. Alamouti, "5G: Personal mobile internet beyond what cellular did to telephony," *IEEE Commun. Mag.*, vol. 52, no. 2, pp. 140–145, Feb. 2014.

[35] N. I. Fisher and T. Lewis, "Estimating the common mean direction of several circular or spherical distributions with differing dispersions," *Biometrika*, vol. 70, no. 2, pp. 333–341, Aug. 1983.

[36] Y. Fu and Z. Tian, "Cramer Rao Bounds for Hybrid TOA/DOA-Based Location Estimation in Sensor Networks," *IEEE Signal Process. Lett.*, vol. 16, no. 8, pp. 655–658, Aug. 2009.

[37] M. Gavish and A. Weiss, "Performance analysis of bearing-only target location algorithms," *IEEE Trans. Aerosp. Electron. Syst.*, vol. 28, no. 3, pp. 817–828, 1992.

[38] K. Gotsis, K. Siakavara, and J. Sahalos, "On the direction of arrival (DoA) estimation for a switched-beam antenna system using neural networks," *IEEE Trans. Antennas Propag.*, vol. 57, no. 5, pp. 1399–1411, May 2009.

[39] M. Gudmundson, "Correlation model for shadow fading in mobile radio systems," *IET Electronics Lett.*, vol. 27, no. 23, pp. 2145 –2146, Nov. 1991.

[40] N. Gulati and K. Dandekar, "Learning state selection for reconfigurable antennas: A multi-armed bandit approach," *IEEE Trans. Antennas Propag.*, vol. 62, no. 3, pp. 1027–1038, Mar. 2014.

[41] F. Gunnarsson, M. Johansson, A. Furuskar, M. Lundevall, A. Simonsson, C. Tidestav, and M. Blomgren, "Downtilted base station antennas - a simulation model proposal and impact on HSPA and LTE performance," in *Proc. IEEE 68th Vehicular Technology Conf., VTC Fall*, Sep. 2008, pp. 1–5.

[42] F. Gustafsson and F. Gunnarsson, "Mobile positioning using wireless networks: possibilities and fundamental limitations based on available wireless network measurements," *IEEE Signal Process. Mag.*, vol. 22, no. 4, pp. 41–53, Jul. 2005.

[43] A. Hakkarainen, J. Werner, M. Costa, K. Leppanen, and M. Valkama, "High-efficiency device localization in 5G ultra-dense networks: Prospects and enabling technologies," in *Proc. IEEE 82nd Vehicular Technology Conference (VTC fall)*, Sep. 2015.

[44] Y. Hamdy and S. Mawjoud, "Performance assessment of U-TDOA and A-GPS positioning methods," in *Proc. Int. Conf. Future Communication Networks (ICFCN)*, Apr. 2012, pp. 99–104.

[45] K. Heurtefeux and F. Valois, "Is RSSI a good choice for localization in wireless sensor network?" in *Proc. IEEE 26th Int. Conf. Advanced Information Networking Applications (AINA)*, Mar. 2012, pp. 732–739.

[46] K. Ho and Y. Chan, "Solution and performance analysis of geolocation by TDOA," *IEEE Trans. Aerosp. Electron. Syst.*, vol. 29, no. 4, pp. 1311–1322, Oct. 1993.

[47] V. Honkavirta, T. Perala, S. Ali-Loytty, and R. Piche, "A comparative survey of WLAN location fingerprinting methods," in *Proc. 6th Workshop Positioning, Navigation Communication (WPNC)*, Mar. 2009, pp. 243–251.

[48] Huawei, *5G: A technology vision (white paper)*, 2013. [Online]. Available: http://www.huawei.com/5gwhitepaper/

[49] ITU-R, *Propagation data and prediction methods for the planning of indoor radiocommunication systems and radio local area networks in the frequency range 900 MHz to 100 GHz*. ITU-R P.1238-7, Feb. 2012.

[50] A. H. Jazwinski, "Adaptive filtering," *Automatica*, vol. 5, no. 4, pp. 475–485, Jul. 1969.

[51] T. Jia and R. Buehrer, "A new Cramer-Rao lower bound for TOA-based localization," in *Proc. IEEE Military Communications Conf. (MILCOM)*, Nov. 2008, pp. 1–5.

[52] Y. Jung, "Dual-band reconfigurable antenna for base-station applications," *Electron. Lett.*, vol. 46, no. 3, pp. 195–196, Feb. 2010.

[53] I. Kadar, "Optimum geometry selection for sensor fusion," *Proc. Signal Processing, Sensor Fusion, and Target Recognition*, vol. 3374, no. 1, pp. 96–107, Jul. 1998.

[54] K. Kaemarungsi and P. Krishnamurthy, "Modeling of indoor positioning systems based on location fingerprinting," in *Proc. IEEE 23rd Annu. Joint Conf. Computer Communications Societies (INFOCOM)*, vol. 2, Mar. 2004, pp. 1012–1022 vol.2.

[55] L. Kaplan, "Global node selection for localization in a distributed sensor network," *IEEE Trans. Aerosp. Electron. Syst.*, vol. 42, no. 1, pp. 113–135, Jan. 2006.

[56] S. M. Kay, *Fundamentals of Statistical Signal Processing, Volume I: Estimation Theory*, 1st ed. Prentice Hall, Apr. 1993.

[57] P. Kela, M. Costa, J. Salmi, K. Leppanen, J. Turkka, T. Hiltunen, and M. Hronec, "A novel radio frame structure for 5G dense outdoor radio access networks," in *Proc. IEEE 81st Vehicular Technology Conference (VTC spring)*, 2015.

[58] H. Kim, X. Ma, and B. Hamilton, "Tracking low-precision clocks with time-varying drifts using Kalman filtering," *IEEE/ACM Trans. Netw.*, vol. 20, no. 1, pp. 257–270, Feb. 2012.

[59] T. Kohno, A. Broido, and K. Claffy, "Remote physical device fingerprinting," *IEEE Trans. on Dependable Secure Comput.*, vol. 2, no. 2, pp. 93–108, Apr. 2005.

[60] T. Levanen, J. Pirskanen, T. Koskela, J. Talvitie, and M. Valkama, "Radio interface evolution towards 5G and enhanced local area communications," *IEEE Access*, vol. 2, pp. 1005–1029, 2014.

[61] H. Liu, Y. Gan, J. Yang, S. Sidhom, Y. Wang, Y. Chen, and F. Ye, "Push the limit of WiFi based localization for smartphones," in *Proc. 18th Annu. Int. Conf. Mobile Computing and Networking (MobiCom)*. New York, NY, USA: ACM, 2012, pp. 305–316.

[62] V. Lottici, A. D'Andrea, and U. Mengali, "Channel estimation for ultra-wideband communications," *IEEE J. Sel. Areas Commun.*, vol. 20, no. 9, pp. 1638–1645, Dec. 2002.

[63] K. V. Mardia and P. E. Jupp, *Directional Statistics*, 1st ed. Chichester ; New York: Wiley, Jan. 1999.

[64] R. Martin and R. Thomas, "Algorithms and bounds for estimating location, directionality, and environmental parameters of primary spectrum users," *IEEE Trans. Wireless Commun.*, vol. 8, no. 11, pp. 5692 –5701, Nov. 2009.

[65] J. Medbo, I. Siomina, A. Kangas, and J. Furuskog, "Propagation channel impact on LTE positioning accuracy: A study based on real measurements of observed time difference of arrival," in *Proc. IEEE 20th Int. Symp. Personal, Indoor and Mobile Radio Communications*, Sep. 2009, pp. 2213–2217.

[66] METIS, *D6.1 simulation guidelines*. ICT-317669-METIS/D6.1, Oct. 2013.

[67] METIS, *D1.4 channel models*, Feb. 2015.

[68] P. Mogensen, K. Pajukoski, E. Tiirola, J. Vihriala, E. Lahetkangas, G. Berardinelli, F. Tavares, N. Mahmood, M. Lauridsen, D. Catania, and A. Cattoni, "Centimeter-wave concept for 5G ultra-dense small cells," in *Proc. IEEE 79th Vehicular Technology Conf. (VTC spring)*, May 2014, pp. 1–6.

[69] M. Navarro and M. Najar, "TOA and DOA Estimation for Positioning and Tracking in IR-UWB," in *Proc. IEEE Int. Conf. Ultra-Wideband (ICUWB)*, Sep. 2007, pp. 574–579.

[70] M. Navarro and M. Najar, "Frequency Domain Joint TOA and DOA Estimation in IR-UWB," *IEEE Trans. Wireless Commun.*, vol. 10, no. 10, pp. 1–11, Oct. 2011.

[71] NGMN Alliance, "5G white paper," Dec. 2014. [Online]. Available: http://www.ngmn.org/uploads/media/141222_NGMN-Executive_Version_of_the_5G_White_Paper_v1_0.pdf

[72] Nokia, *Looking ahead to 5G (white paper)*, Dec. 2013. [Online]. Available: http://networks.nokia.com/sites/default/files/document/5g_white_paper_0.pdf

[73] T. Ohira and K. Gyoda, "Hand-held microwave direction-of-arrival finder based on varactor-tuned analog aerial beamforming," in *Proc. 2001 Asia-Pacific Microwave Conf.*, 2001, pp. 585–588.

[74] A. Osseiran, F. Boccardi, V. Braun, K. Kusume, P. Marsch, M. Maternia, O. Queseth, M. Schellmann, H. Schotten, H. Taoka, H. Tullberg, M. Uusitalo, B. Timus, and M. Fallgren, "Scenarios for 5G mobile and wireless communications: the vision of the METIS project," *IEEE Commun. Mag.*, vol. 52, no. 5, pp. 26–35, May 2014.

[75] H. Paaso, A. Mammela, D. Patron, and K. R. Dandekar, "DoA estimation through modified unitary MUSIC algorithm for CRLH leaky-wave antennas," in *Proc. IEEE 24th Int. Symp. Personal Indoor and Mobile Radio Communications (PIMRC)*, 2013, pp. 311–315.

[76] A. T. Parameswaran, M. I. Husain, and S. Upadhyaya, "Is RSSI a reliable parameter in sensor localization algorithms - an experimental study," in *Proc. Field Failure Data Analysis Workshop (F2DA)*, New York, 2009.

[77] M. Patzold, *Mobile Radio Channels*. Chichester, West Sussex, U.K.; Hoboken, N.J.: Wiley, 2012.

[78] R. Paucher and M. Turk, "Location-based augmented reality on mobile phones," in *2010 IEEE Computer Society Conference on Computer Vision and Pattern Recognition Workshops (CVPRW)*, Jun. 2010, pp. 9–16.

[79] F. Penna and D. Cabric, "Bounds and tradeoffs for cooperative DoA-only localization of primary users," in *Proc. IEEE Global Telecommunications Conf. (GLOBECOM)*, 2011, pp. 1–5.

[80] D. Piazza, N. Kirsch, A. Forenza, R. Heath, and K. Dandekar, "Design and evaluation of a reconfigurable antenna array for MIMO systems," *IEEE Trans. Antennas Propag.*, vol. 56, no. 3, pp. 869–881, Mar. 2008.

[81] D. Piazza, D. Michele, and K. Dandekar, "Two port reconfigurable CRLH leaky wave antenna with improved impedance matching and beam tuning," in *Proc. 3rd European Conf. Antennas and Propagation (EuCAP)*, 2009, pp. 2046–2049.

[82] B. Rao and H. Durrant-Whyte, "Fully decentralised algorithm for multisensor Kalman filtering," *IEE Proc. D Control Theory Applicat.*, vol. 138, no. 5, pp. 413–420, Sep. 1991.

[83] A. Richter, "Estimation of radio channel parameters: Models and algorithms," Ph.D. dissertation, Dept. Elektr. Messtechnik, Ilmenau Univ. Techn., Ilmenau, 2005.

[84] T. Roos, P. Myllymaki, H. Tirri, P. Misikangas, and J. Sievanen, "A probabilistic approach to WLAN user location estimation," *Int. J. Wireless Inform. Networks*, vol. 9, no. 3, pp. 155–164, Jul. 2002.

[85] A. Roxin, J. Gaber, M. Wack, and A. Nait-Sidi-Moh, "Survey of wireless geolocation techniques," in *Proc. IEEE Global Communications Conf. (GLOBECOM)*, Nov. 2007, pp. 1–9.

[86] R. Roy and T. Kailath, "ESPRIT-estimation of signal parameters via rotational invariance techniques," *IEEE Trans. Acoust., Speech, Signal Process.*, vol. 37, no. 7, pp. 984–995, Jul. 1989.

[87] J. Salmi, A. Richter, and V. Koivunen, "Detection and tracking of MIMO propagation path parameters using state-space approach," *IEEE Trans. Signal Process.*, vol. 57, no. 4, pp. 1538–1550, Apr. 2009.

[88] R. Schmidt, "Multiple emitter location and signal parameter estimation," *IEEE Trans. Antennas Propag.*, vol. 34, no. 3, pp. 276 – 280, Mar. 1986.

[89] C. K. Seow and S. Y. Tan, "Non-line-of-sight localization in multipath environments," *IEEE Trans. Mobile Comput.*, vol. 7, no. 5, pp. 647–660, May 2008.

[90] Y. Shen and M. Win, "On the accuracy of localization systems using wideband antenna arrays," *IEEE Trans. Commun.*, vol. 58, no. 1, pp. 270–280, Jan. 2010.

[91] D. Simon, *Optimal State Estimation: Kalman, H Infinity, and Nonlinear Approaches*, 1st ed. Hoboken, N.J: Wiley-Interscience, Jun. 2006.

[92] R. Stansfield, "Statistical theory of d.f. fixing," *J. Institution Elect. Engineers - Part IIIA: Radiocommunication*, vol. 94, no. 15, pp. 762–770, Mar. 1947.

[93] P. Stoica and N. Arye, "MUSIC, maximum likelihood, and Cramer-Rao bound," *IEEE Trans. Acoust., Speech, Signal Process.*, vol. 37, no. 5, pp. 720–741, 1989.

[94] P. Stoica, E. Larsson, and A. Gershman, "The stochastic CRB for array processing: a textbook derivation," *IEEE Signal Process. Lett.*, vol. 8, no. 5, pp. 148–150, May 2001.

[95] C. Sukumar, H. Eslami, A. Eltawil, and B. Cetiner, "Link performance improvement using reconfigurable multiantenna systems," *IEEE Antennas Wireless Propag. Lett.*, vol. 8, pp. 873–876, 2009.

[96] C. Sun and N. C. Karmakar, "Direction of arrival estimation with a novel single-port smart antenna," *EURASIP J. Advances in Signal Process.*, vol. 2004, no. 9, pp. 1364–1375, Aug. 2004.

[97] G. Sun, J. Chen, W. Guo, and K. Liu, "Signal processing techniques in network-aided positioning: a survey of state-of-the-art positioning designs," *IEEE Signal Process. Mag.*, vol. 22, no. 4, pp. 12–23, Jul. 2005.

[98] R. Tandra and A. Sahai, "SNR walls for signal detection," *IEEE J. Sel. Topics Signal Process.*, vol. 2, no. 1, pp. 4–17, Feb. 2008.

[99] R. Thoma, M. Landmann, and A. Richter, "RIMAX - a maximum likelihood framework for parameter estimation in multidimensional channel sounding measurement," in *Proc. Int. Symp. Antennas and Propagation*, Sendai, Japan, Aug. 2004, pp. 53–56.

[100] S. Thrun, W. Burgard, and D. Fox, *Probabilistic Robotics*. Cambridge, Mass: The MIT Press, Aug. 2005.

[101] P. Tichavsky, C. Muravchik, and A. Nehorai, "Posterior Cramer-Rao bounds for discrete-time nonlinear filtering," *IEEE Trans. Signal Process.*, vol. 46, no. 5, pp. 1386–1396, May 1998.

[102] H. L. V. Trees, K. L. Bell, and Z. Tian, *Detection Estimation and Modulation Theory, Detection, Estimation, and Filtering Theory*, 1st ed. Hoboken, N.J: Wiley, 2003.

[103] V. Vakilian, J.-F. Frigon, and S. Roy, "Direction-of-arrival estimation in a clustered channel model," in *Proc. IEEE 10th Int. New Circuits and Systems Conf. (NEWCAS)*, 2012, pp. 313–316.

[104] C.-X. Wang, F. Haider, X. Gao, X.-H. You, Y. Yang, D. Yuan, H. Aggoune, H. Haas, S. Fletcher, and E. Hepsaydir, "Cellular architecture and key technologies for 5G wireless communication networks," *IEEE Commun. Mag.*, vol. 52, no. 2, pp. 122–130, Feb. 2014.

[105] J. Wang and D. Cabric, "A cooperative DoA-based algorithm for localization of multiple primary-users in cognitive radio networks," in *Proc. IEEE Global Communications Conference (GLOBECOM)*, Dec. 2012, pp. 1266–1270.

[106] J. Wang, J. Chen, and D. Cabric, "Stansfield localization algorithm: Theoretical analysis and distributed implementation," *IEEE Wireless Commun. Lett.*, vol. 2, no. 3, pp. 327–330, 2013.

[107] J. Wang, J. Chen, and D. Cabric, "Cramer-Rao bounds for joint RSS/DoA-based primary-user localization in cognitive radio networks," *IEEE Trans. Wireless Commun.*, vol. 12, no. 3, pp. 1363–1375, Mar. 2013.

[108] J. Wang, J. Chen, Y. Lu, M. Gerla, and D. Cabric, "Robust power control under location and channel uncertainty in cognitive radio networks," *IEEE Wireless Commun. Lett.*, vol. 4, no. 2, pp. 113–116, Apr. 2015.

[109] J. Wang, P. Urriza, Y. Han, and D. Cabric, "Weighted centroid localization algorithm: Theoretical analysis and distributed implementation," *IEEE Trans. Wireless Commun.*, vol. 10, no. 10, pp. 3403–3413, Oct. 2011.

[110] J. Wang, J. Werner, M. Valkama, and D. Cabric, "Performance analysis of primary user RSS/DoA estimation and localization in cognitive radio networks using sectorized antennas," *IEEE Wireless Commun. Lett.*, vol. 3, no. 2, pp. 237–240, Apr. 2014.

[111] S. Wang, B. Jackson, and R. Inkol, "Hybrid RSS/AOA emitter location estimation based on least squares and maximum likelihood criteria," in *Proc. 26th Biennial Symp. Communications (QBSC)*, May 2012, pp. 24 –29.

[112] S. Wang, B. Jackson, and R. Inkol, "Performance characterization of AOA geolocation systems using the von Mises distribution," in *Proc. IEEE 76th Vehicular Technology Conf. (VTC fall)*, Sep. 2012, pp. 1–5.

[113] A. Weiss, "On the accuracy of a cellular location system based on RSS measurements," *IEEE Trans. Veh. Technol.*, vol. 52, no. 6, pp. 1508–1518, Nov. 2003.

[114] J. Winters, J. Salz, and R. Gitlin, "The impact of antenna diversity on the capacity of wireless communication systems," *IEEE Trans. Commun.*, vol. 42, no. 234, pp. 1740–1751, Feb. 1994.

[115] Y.-C. Wu, Q. Chaudhari, and E. Serpedin, "Clock synchronization of wireless sensor networks," *IEEE Signal Process. Mag.*, vol. 28, no. 1, pp. 124–138, Jan. 2011.

[116] G. Wunder, P. Jung, M. Kasparick, T. Wild, F. Schaich, Y. Chen, S. Brink, I. Gaspar, N. Michailow, A. Festag, L. Mendes, N. Cassiau, D. Ktenas, M. Dryjanski, S. Pietrzyk, B. Eged, P. Vago, and F. Wiedmann, "5GNOW: Non-orthogonal, asynchronous waveforms for future mobile applications," *IEEE Commun. Mag.*, vol. 52, no. 2, pp. 97–105, Feb. 2014.

[117] H. Wymeersch, J. Lien, and M. Win, "Cooperative localization in wireless networks," *Proc. IEEE*, vol. 97, no. 2, pp. 427–450, Feb. 2009.

[118] X. Yu and H. Xin, "Direction of arrival estimation utilizing incident angle dependent spectra," in *Proc. IEEE MTT-S Int. Microwave Symp. Dig.*, 2012, pp. 1–3.

[119] D. Zachariah and P. Stoica, "Cramer-Rao bound analog of Bayes' rule," *IEEE Signal Process. Mag.*, vol. 32, no. 2, pp. 164–168, Mar. 2015.

[120] P. A. Zandbergen, "Accuracy of iPhone locations: A comparison of assisted GPS, WiFi and cellular positioning," *Transactions in GIS*, vol. 13, pp. 5–25, Jun. 2009.

[121] J. Zhang, J. Salmi, and E. S. Lohan, "Analysis of kurtosis based LOS/NLOS identification using indoor MIMO channel measurement," *IEEE Trans. Vehicular Tech.*, vol. 62, no. 6, pp. 2871–2874, Jul. 2013.

[122] K. Zickuhr, "Location-based services," Pew Research Center, Tech. Rep., Sep. 2013. [Online]. Available: http://www.pewinternet.org/files/old-media/Files/Reports/2013/PIP_Location-based%20services%202013.pdf

Publications

Publication 1

J. Werner, A. Hakkarainen, J. Wang, D. Cabric, and M. Valkama, "Performance and Cramer-Rao bounds for DoA/RSS estimation and transmitter localization using sectorized antennas," accepted for publication in *IEEE Transactions on Vehicular Technology*, 2015.

Performance and Cramer-Rao Bounds for DoA/RSS Estimation and Transmitter Localization Using Sectorized Antennas

Janis Werner, Jun Wang, Aki Hakkarainen, Danijela Cabric, and Mikko Valkama

***Abstract*—Using collaborative sensors or other observing devices equipped with sectorized antennas provides a practical and low-cost solution to direction of arrival (DoA) and received signal strength (RSS) estimation, as well as non-cooperative transmitter localization. In this paper, we study the performance and theoretical bounds of DoA/RSS estimation and localization using sectorized antennas. We first show that the sector-power measurements at an individual sensor form a sufficient statistic for DoA/RSS estimation and transmitter localization. Motivated by that, we then derive the Cramer-Rao bound (CRB) on DoA/RSS estimation based on sector-powers and study its asymptotic behavior. Moreover, we derive an analytical expression for the mean squared error of a practical sectorized-antenna based DoA estimator, compare its performance to the derived CRB and study its asymptotic properties. Next, we derive the CRB for localization based on sector-powers. The resulting CRB is a lower bound for a localization system where the DoA/RSS estimates, obtained from sector-powers at individual sensors, are fused together into a location estimate. Moreover, the CRB also covers the more general case of a localization system where sector-powers from individual nodes are directly fused together, without an intermediate DoA/RSS estimation step. We compare the obtained CRB to a localization approach employing an intermediate DoA/RSS estimation step, and observe that skipping this intermediate processing step may result in a substantially improved localization performance. Finally, we study the influence of various important system parameters, like the number of sensors, sectors and measurement samples, on the achievable estimation and localization performance. Overall, this paper demonstrates and quantifies the achievable DoA/RSS estimation and localization performance of sectorized antennas, and provides comprehensive design guidelines for sector-power based low-complexity localization systems.**

***Index Terms*—Angle-of-arrival, cognitive radio, Cramer-Rao bounds, directional antennas, direction-of-arrival estimation, leaky-wave antennas, localization, received signal strength, reconfigurable antennas, sectorized antennas, single RF front-end**

J. Werner, A. Hakkarainen and M. Valkama are with the Department of Electronics and Communications Engineering, Tampere University of Technology, FI-33101 Tampere, Finland (email: {janis.werner, aki.hakkarainen, mikko.e.valkama}@tut.fi).

J. Wang and D. Cabric are with the Department of Electrical Engineering, University of California Los Angeles, CA 90095, USA (email: eejunwang@ucla.edu, danijela@ee.ucla.edu).

This work is supported by the Doctoral Program of the President of Tampere University of Technology, the Tuula and Yrjö Neuvo Fund, the Nokia Foundation, and the Finnish Funding Agency for Technology and Innovation (Tekes, under the projects "Reconfigurable Antenna-based Enhancement of Dynamic Spectrum Access Algorithms", "5G Networks and Device Positioning", and "Future Small-Cell Networks using Reconfigurable Antennas"). This work is also supported by the National Science Foundation under Grant No.1117600.

I. Introduction

LOCALIZATION of a non-cooperative transmitter (TX), i.e. a TX that does not directly communicate with the localization network, using multiple cooperating receivers (RXs), is an important task in several application areas [1], [2]. For example, knowledge about primary user location can enable several advanced functionalities in cognitive radio (CR) networks, such as improved spatio-temporal sensing, intelligent location-aware power control and routing, as well as spectrum policy enforcement [2]. However, both the complexity and energy constraints of the RXs as well as the wireless communication among the RXs require efficient use of the available resources, namely the available energy of the RX devices [1] and the radio frequency spectrum [2]. Moreover, it is desirable to distribute the computational complexity among the participating RXs [1]. As a consequence, it is prohibitive that the RXs communicate their measurement samples directly. Instead, every RX should preprocess the samples into compressed measurements that are useful for localization. These compressed measurements are then communicated to a fusion center (FC), which may also be one of the sensors, where the compressed measurements from all RXs are combined into a location estimate [3].

Traditionally, three different types of measurements are used in the localization of a non-cooperative TX, i.e. the received signal strength (RSS), direction of arrival (DoA) and time difference of arrival (TDoA) [4]. However, TDoA-based algorithms require perfect synchronization among the RXs, which is generally infeasible in many application areas [4]. Therefore, related research has focused on RSS [5], [6] and DoA [7] as well as joint DoA/RSS-based localization, which has been shown to significantly outperform RSS-only and DoA-only schemes [4], [8]. However, traditional DoA estimation techniques such as MUSIC [9] require digitally controlled antenna arrays (DCAAs) with a high number of antenna units and associated RF chains, and thus may not be suitable for RX devices in many applications due to size and cost limits.

Stemming from the above, we have recently proposed to use sectorized antennas for DoA and RSS estimation [10], [11]. A sectorized antenna is an antenna structure that can selectively receive energy from different sectors. A sector denotes a continuous range of angles and selectivity means that signals arriving from outside of the activated sector are strongly attenuated. We further assume that only a single sector can be activated at a time. Thus, the class of sectorized-antennas encompasses all directional antennas with a single RF front-end.

Examples of antenna structures that can be used as sectorized antennas are switched-beam systems (SBSs) [12] and leaky-wave antennas (LWAs) [13]. Using sectorized antennas as opposed to DCAAs can result in a great reduction of hardware complexity as illustrated in Fig. 1. An LWA, for example, is operated with a single RF front-end and one analog-to-digital converter (ADC) only, while a DCAA requires a receiver chain and a separate ADC for each of its antennas [14].

The DoA/RSS estimators for sectorized antennas proposed in [10], [11] first calculate the power in every sector and successively estimate the DoA and RSS based on these sector-powers. From a practical point of view, this way of processing attenuates the influence of channel fluctuations. In this paper, we will furthermore show that, at an individual RX, the sector-powers are a sufficient statistic for DoA/RSS estimation if successively received samples are independent. Thus, a RX that is equipped with a sectorized antenna can estimate the DoA/RSS based on sector-powers without loss in performance compared to estimation based on raw samples. Therefore, in this paper we derive the Cramer-Rao bounds (CRBs) on DoA/RSS estimation based on sector-powers. These DoA/RSS CRBs for sectorized antennas differ significantly from the respective CRBs [15], [16] for DCAAs since different samples in a sectorized antenna are received sequentially in time instead of being received in parallel. In [11] we already used the DoA/RSS estimation CRBs as a reference when evaluating the performance of a practical DoA/RSS estimator. However, both a detailed evaluation as well as the derivation of the CRBs were not part of [11]. Moreover and in contrast to [11], this article also presents an analytical analysis of the asymptotic behavior of the CRBs as well as a novel and highly accurate approximation of the DoA/RSS CRBs that relates the bounds to the RX parameters in a very simple form.

Since the DoA is a function of the TX location, sector-powers at individual RXs are also a sufficient statistic for TX location estimation. However, the TX location cannot be estimated based on the sector-powers from an individual RX alone. Therefore, in this paper we propose a system where multiple collaborating RXs localize a non-cooperative TX based on sector-powers instead of RSSs or DoAs. More specifically, we derive the CRB on sector-power based collaborative localization of a non-cooperative TX, as well as two approximations of the obtained bound. In related works, the CRB has been derived for localization based on RSSs only [5], [6], DoAs only [7] or for joint DoA/RSS based approaches using DCAAs [4], [8]. However, to the best of our knowledge, no prior work considers localization based on sector-powers nor the localization CRB for sectorized antennas in general.

The derived DoA/RSS CRBs are compared to the performance of the simplified least squares (SLS) algorithm, which is one of the earlier proposed [10] practical sector-power based DoA/RSS estimators. Towards that end, we derive an accurate analytical expression for the root mean squared error (RMSE) of SLS DoA estimation, which is valid also for low signal-to-noise ratio (SNR) regions in contrast to the asymptotic high SNR expression in [17]. Overall, the comparison between SLS and the derived DoA/RSS CRBs gives valuable insights into performance and mechanisms of the algorithm that are useful for further improvements. Since currently no algorithm exists that calculates TX location estimates directly from sector-powers, we compare the localization CRB to a combination of SLS DoA/RSS estimation and a modified version of the Stansfield DoA fusion algorithm [3], [10]. Although this combined algorithm, referred to as SLS-ST, computes DoA estimates from the sector-powers in an intermediate step, it is overall lower bounded by the localization CRB as will be discussed in Section III-A. Moreover, SLS performs fairly close to the CRB on DoA/RSS estimation and the Stansfield algorithm is known to very efficiently compute location estimates from DoA/RSS estimates [4]. Therefore, the comparison of SLS-ST to the sector-power localization CRB is a good indication for the potential benefit of sector-power based localization without an intermediate DoA/RSS estimation step. In summary, the contributions of this article are the following:

- Introduction of a sector-power based localization system and its statistical model.
- Analysis showing that sector-powers at individual RXs are a sufficient statistic for DoA/RSS estimation as well as TX location.
- Derivation of CRBs for DoA/RSS estimation based on sector-powers.
- Analytical study of the asymptotic behavior of the DoA/RSS CRBs.
- Derivation of an accurate analytical expression for the RMSE of SLS DoA estimation.
- Derivation of the CRB for localization based on sector-powers.
- Providing simple and accurate approximations of the derived CRBs.
- Extensive evaluation of the derived CRBs with respect to important system parameters.
- Comparison of the CRBs to the performance of existing algorithms and identification of weaknesses in the algorithms.

This paper is organized as follows. Section II introduces the localization system under consideration. A more detailed description of sector-powers and the motivation for using them in the localization system is presented in Section III. The CRBs for both DoA/RSS estimation and TX localization are derived in Section IV. In Section V, we briefly summarize the algorithms that we compare to the CRBs. We then derive an analytical expression for the error of the selected DoA estimation algorithm in Section VI. A comparison of the algorithms to the CRBs along with a detailed evaluation and analysis can be found in Section VII. Finally, the work is concluded in Section VIII. Details of derivations and proofs are reported in Appendices A, B, and C.

Notation: Throughout this paper, vectors and matrices are written as bold letters. We will be handling signals with continuous time nature as well as samples of the same signals. We indicate a signal with continuous time as $\tilde{x}(t)$, $t \in \mathbb{R}$, and the respective signal samples as $x(n)$, $n \in \mathbb{N}$, with the convention that $\tilde{x}(nT_\mathrm{s}) = x(n)$, where T_s is the sampling period. For $z \in \mathbb{C}$, $\Re(z)$ and $\Im(z)$ denote the real and imaginary

TABLE I: Most commonly used symbols.

Symbol	Description
$a_{k,m}$	$a_{k,m} = (\mathrm{SNR}_{k,m}^{-1}+1)^{-2}$
a_s	Side-sector suppression (Fig. 4)
M	Number of sectors
N	Number of samples
K	Number of RXs
SNR_k	SNR at RX k, $\mathrm{SNR}_k = \frac{\gamma_k}{\sigma_\mathrm{w}^2}$
$\mathrm{SNR}_{k,m}$	$\mathrm{SNR}_{k,m} = \rho_{k,m}\,\mathrm{SNR}_k$
β	Beamwidth, $\beta = 2\pi/[M\sqrt{\ln(1/a_\mathrm{s})}]$
γ_k	RSS at RX k
$\Delta\vartheta$	Sector spacing, $\Delta\vartheta = \frac{2\pi}{M}$
$\epsilon_{k,m}$	Sector power (8)
$\zeta(\varphi)$	Gaussian radiation pattern (1)
ϑ_m	Orientation of sector m
$\rho_{k,m}$	$\rho_{k,m} = [\zeta(\varphi_k - \vartheta_m)]^2$
σ_w^2	Noise variance
$\mathcal{M}(x)$	$\mathcal{M}(x) = \mathrm{mod}_{2\pi}(x+\pi) - \pi$
$\boldsymbol{\ell}_k$	Location of RX k, $\boldsymbol{\ell}_k = [x_k, y_k]^T$
$\boldsymbol{\ell}_\mathrm{P}$	Location of TX, $\boldsymbol{\ell}_\mathrm{P} = [x_\mathrm{P}, y_\mathrm{P}]^T$

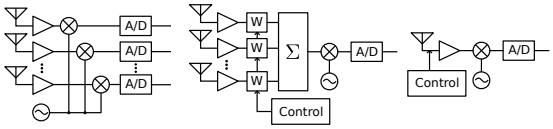

Fig. 1: Required hardware for different directional antennas: left - digitally controlled antenna array (DCAA), middle - switched beam system (SBS), right - leaky wave antenna (LWA) [14].

part of z, and z^* its complex conjugate. $\mathrm{E}[X]$ and $\mathrm{var}[X]$ denote expected value and variance of the random variable X, while $\mathrm{bias}[\hat{y}] = \mathrm{E}[\hat{y}] - y$ denotes the bias of estimator $\hat{y}$ for a deterministic quantity y. $\mathrm{mod}_y(x)$ expresses the remainder of the division x/y. For a vector $\mathbf{x}$ and a matrix $\mathbf{M}$, we denote an individual element as $\mathbf{x}_i$ and $\mathbf{M}_{ij}$ or alternatively $(\mathbf{x})_i$ and $(\mathbf{M})_{ij}$. The transpose of a matrix $\mathbf{M}$ is written as $\mathbf{M}^\mathrm{T}$ and its conjugate transpose as $\mathbf{M}^\mathrm{H}$. $|\mathbf{M}|$ denotes the determinant of matrix $\mathbf{M}$, while $\mathbf{M} = \mathrm{diag}(\mathbf{x})$ denotes the diagonal matrix that is composed of all the elements of vector $\mathbf{x}$, i.e. $[\mathrm{diag}(\mathbf{M})]_{ii} = \mathbf{x}_i$. $\mathbf{A}\circ\mathbf{B}$ denotes the Hadamard product of two $M\times N$ matrices $\mathbf{A}$ and $\mathbf{B}$. Derivatives are written in short as $\frac{df}{dx} = [f]_x$ and matrix derivatives are always element-wise, i.e. $([\mathbf{M}]_x)_{ij} = [\mathbf{M}_{ij}]_x$.

For the readers' convenience, we have collected the most commonly used symbols in Table I.

II. Preliminaries and System Model

In this paper, we consider a localization system illustrated in Fig. 2. In this system, K RXs with given locations $\boldsymbol{\ell}_k = [x_k, y_k]^\mathrm{T}$, $k = 1\ldots K$ collaborate to estimate the location, $\boldsymbol{\ell}_\mathrm{P} = [x_\mathrm{P}, y_\mathrm{P}]^\mathrm{T}$, of a non-cooperative TX. Towards that end, each of the RXs is equipped with a sectorized antenna, as will be further discussed in Section II-A. During the localization, RX k receives N samples of the incoming TX signal $\tilde{s}_{k,m}(t)$ at antenna sector m, $m = 1\ldots M$. The respective transmission model is described in detail in Section II-B. Since we are targeting low network overhead, it is prohibitive that the RXs communicate raw samples to the FC. Instead, the raw samples are preprocessed into a compressed measurement Ψ_k at each

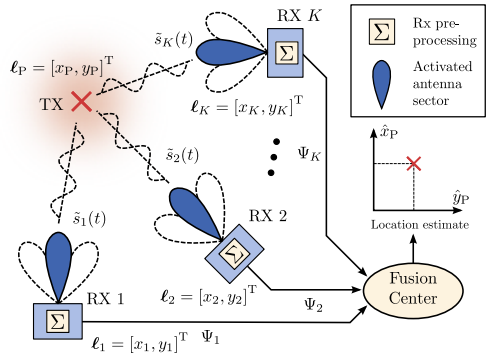

Fig. 2: The studied localization system. Every RX is equipped with a sectorized-antenna and preprocesses the received samples into a compressed measurement Ψ_k that is then send to the FC for the final location estimation. The derived CRBs are for compressed measurements that contain the sector-powers, while the algorithm that we use as a comparison, employs an intermediate step that turns sector-powers into DoA/RSS estimates and could, consequently, communicate DoA/RSSs instead of sector-powers.

RX k, which is then communicated to the FC. Using these compressed measurement from all RXs, the FC finally estimates the TX location. In addition to limiting the network overhead, RX preprocessing has a further advantage that computations are distributed and less data has to be handled within the FC. This also makes it possible to use one of the RXs as the FC, even if using resource constrained devices.

For the derivation of the localization CRB, we assume compressed measurements that contain sector-powers as will be motivated in Section III. However, so far no algorithm exists that turns sector-powers directly into TX location estimates. Therefore, we compare the CRB to a localization algorithm that obtains the location estimate via an intermediate step (see Section V). In this step the DoAs are estimated based on the sector-powers and only the DoAs and RSSs are finally used in TX location estimation. Consequently, if the DoA estimation takes place in every individual RX, the compressed measurements can consist of the RSSs and DoAs only.

A. Sectorized Antenna Model

A sector is characterized by its radiation pattern, which describes the attenuation of the received signal as a function of its DoA. In this paper we first develop the CRBs in a general form such that they are applicable to any sectorized antenna. However, in order to identify some general trends, we then assume that the radiation pattern, $\zeta_{k,m} = \zeta(\varphi_k - \vartheta_m)$, depends only on the angular distance between the incoming signal's DoA, $\varphi_k = \arctan\frac{y_\mathrm{P}-y_k}{x_\mathrm{P}-x_k}$, at RX k and orientation ϑ_m of sector m, $m = 1\ldots M$. Thereby, we assume equal sector orientations for all RXs for simplicity and without loss of generality. In addition, for analysis purposes, we further simplify the model of the radiation pattern by approximating only the antenna's main beam using a Gaussian-like shape as in [10], [11]. Then, the radiation pattern can be expressed as

$$\zeta(\varphi) = \exp\left(-\left[\mathcal{M}(\varphi)\right]^2/\beta^2\right) \tag{1}$$

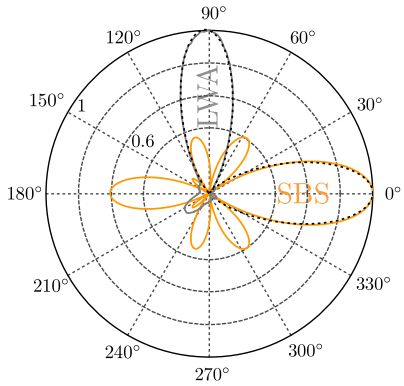

Fig. 3: Example for the approximation (dotted line) of an antennas's main beam through a Gaussian radiation pattern (1). Depicted is a) the measured radiation pattern of a sector with $\vartheta = 90°$ from a leaky wave antenna (LWA) [13] and b) the theoretical radiation pattern of a sector with $\vartheta = 0°$ from a switched beam system (SBS) with an underlying uniform circular antenna array consisting of 8 antenna elements.

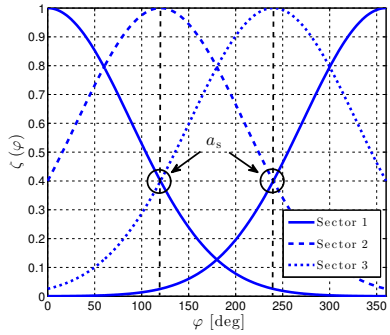

Fig. 4: Illustration of the side-sector suppression of a sectorized antenna with Gaussian radiation pattern, $M = 3$ sectors and $a_\mathrm{s} = 0.4$.

with $\mathcal{M}(\varphi) = \mathrm{mod}_{2\pi}(\varphi + \pi) - \pi$ and beamwidth β. This approximation is very accurate for e.g. the measured radiation pattern of the LWA [13], [18] or the radiation pattern of an SBS based on a circular array, as can be seen in Fig. 3. In this paper, we assume a spacing between the sectors that is $\Delta\vartheta = \frac{2\pi}{M}$, resulting in an orientation of sector m equal to

$$\vartheta_m = \begin{cases} \mathcal{M}\left[(m - \frac{1}{2})\Delta\vartheta\right] & \text{if } M \text{ is even} \\ \mathcal{M}\left[(m-1)\Delta\vartheta\right] & \text{if } M \text{ is odd} \end{cases}, \tag{2}$$

where we define the angles such that the sector-orientations are symmetric around 0° for convenience and without loss of generality. We parameterize the radiation pattern via the side-sector suppression, a_s. The side-sector suppression is defined as the attenuation that a signal, arriving at the orientation ϑ_m of the m^{th} sector, experiences in the neighboring sectors $m-1$ and $m+1$, i.e. $a_\mathrm{s} = \zeta(\Delta\vartheta)$ [10]. Therefore, the side-sector suppression determines the amount of overlap between neighboring sectors, independent of the number of sectors. The beamwidth can be derived from the above assumptions as $\beta = 2\pi/[M\sqrt{\ln(1/a_\mathrm{s})}]$. An illustration of the side-sector suppression can be found in Fig. 4.

B. Channel and Receiver Model

We denote the complex baseband equivalent signal emitted by the non-cooperative TX as $\tilde{s}(t)$, and make the common assumption that its distribution can be well approximated as circular symmetric complex Gaussian, $\tilde{s}(t) \sim \mathcal{CN}(0, \sigma_\mathrm{s}^2)$, an approximation that fits well for a range of practical relevant signals, such as OFDM with a reasonable number of subcarriers. In our derivations, we do not assume any specific autocorrelation function (ACF) of the TX signal $u_{\tilde{s}}(\tau) = \mathrm{E}[\tilde{s}(t)\tilde{s}^*(t-\tau)]$. For simplicity, we only require the ACF to satisfy $u_{\tilde{s}}(nT_\mathrm{s}) = 0$, where T_s is the sampling period at the RXs and $n = \pm 1, \pm 2, \ldots$. However, in our evaluations of the localization CRBs, we need to assume a specific ACF. In Section VII-B, we therefore model the TX signal as bandlimited to the frequencies $-B/2 < f < B/2$, where B denotes the physical bandwidth of the actual RF signal. Then, the TX signal has an ACF [19, pp. 416-418]

$$u_{\tilde{s}}(\tau) = \mathrm{E}[\tilde{s}(t)\tilde{s}^*(t-\tau)] = \sigma_\mathrm{s}^2 \,\mathrm{sinc}(B\tau). \tag{3}$$

For the ACF (3), our earlier assumption $u_{n\tilde{s}}(T_\mathrm{s}) = 0$ holds if $T_\mathrm{s} = 1/B$, which means in practice we do not oversample at the RXs. In general, we assume that the ACF is unknown to the localizing network since the TX is non-cooperative.

The incoming signal in sector m at RX k is next written as

$$\tilde{s}_{k,m}(t) = h_k \tilde{s}_k(t - (m-1)T_\mathrm{a}) \tag{4}$$
$$= h_k \tilde{s}(t - \eta_k - (m-1)T_\mathrm{a}), \tag{5}$$

where the delay at RX k is dependent on $\eta_k = \frac{d_k}{c}$, i.e. the fraction of RX-TX distance $d_k = \|\boldsymbol{\ell}_k - \boldsymbol{\ell}_\mathrm{P}\|$ and the speed of light c, as well as on the sector-switching period $T_\mathrm{a} = NT_\mathrm{s}$. The incoming signal is furthermore experiencing propagation loss by the TX-RX channel modeled here with the channel coefficients h_k. In this work we do not consider fast varying channels explicitly. Instead, we generally assume that the channel coefficients are constant during the relatively short localization phase $T_\mathrm{L} = T_\mathrm{a}M$ (e.g. $M = 6$ sectors, $N = 100$ samples, $f_\mathrm{s} = 1/T_\mathrm{s} = 20$ MHz: $T_\mathrm{L} = 30$ µs). For simplicity, we moreover consider scenarios where the energy of the line of sight (LoS) path is dominating. At the RX, the incoming signal is then attenuated by the DoA-dependent antenna attenuation and corrupted by additive circular symmetric complex white Gaussian noise $\tilde{w}_{k,m}(t) \sim \mathcal{CN}(0, \sigma_\mathrm{w}^2)$, so that the received signal in sector m at RX k becomes

$$\tilde{r}_{k,m}(t) = \zeta_{k,m}\tilde{s}_{k,m}(t) + \tilde{w}_{k,m}(t) \tag{6}$$

or

$$r_{k,m}(n) = \zeta_{k,m}s_{k,m}(n) + w_{k,m}(n) \tag{7}$$

in sample notation. Hence, at every RX k we obtain a sample vector $\mathbf{r}_k = [\mathbf{r}_{k,1}^\mathrm{T}, \mathbf{r}_{k,2}^\mathrm{T}, \ldots, \mathbf{r}_{k,M}^\mathrm{T}]^\mathrm{T} \in \mathbb{C}^{MN\times 1}$ composed of the N samples, $\mathbf{r}_{k,m} = [r_{k,m}(0), r_{k,m}(1), \ldots, r_{k,m}(N-1)]^\mathrm{T} \in \mathbb{C}^{N\times 1}$, by the M sectors.

The CRBs for DoA/RSS estimation, as well as the RMSE for the SLS algorithm, will be derived for a given channel

realization. Similarly, we will derive the localization CRB for given channel realizations at all RXs as well as given RX locations. Given these assumptions, the RSS at RX k can be expressed as $\gamma_k = \mathrm{E}\left[|s_k(n)|^2\right] = |h_k|^2\sigma_\mathrm{s}^2$ and the received signal samples are Gaussian distributed according to $r_{k,m}(n) \sim \mathcal{CN}(0, \rho_{k,m}\gamma_k + \sigma_\mathrm{w}^2)$ with $\rho_{k,m} = \zeta_{k,m}^2$. Consequently, we obtain a Gaussian distributed sample vector $\mathbf{r}_k \sim \mathcal{CN}(0, \mathbf{\Sigma}_k)$ with covariance matrix $\mathbf{\Sigma}_k = \mathrm{E}[(\mathbf{r}_k - \mathrm{E}[\mathbf{r}_k])(\mathbf{r}_k - \mathrm{E}[\mathbf{r}_k])^\mathrm{H}] = \mathrm{diag}(\rho_{k,1}\gamma_k + \sigma_\mathrm{w}^2, \rho_{k,2}\gamma_k + \sigma_\mathrm{w}^2, \ldots, \rho_{k,M}\gamma_k + \sigma_\mathrm{w}^2)$, which is diagonal due to our assumption of uncorrelated samples in (7). Overall, our sample model is very similar to the models in related works such as e.g. [16], where the DoA estimation CRB is derived for digitally controlled antenna arrays and a given RSS under the assumption that the received samples are temporarily uncorrelated.

In order to establish this sample model, we have made two assumptions that simplify our analysis significantly. In the following, we will motivate these assumptions further and also shortly sketch how they could be relaxed. First we assumed that $u_{\tilde{s}}(\tau) = 0$ if $\tau = nT_\mathrm{s}$, $n = \pm 1, 2, \ldots$ holds for the TX signal ACF. As will be seen in the following section, this helps us to approximate the sector powers as Gaussian distributed and uncorrelated at an individual RX. Now for signals with a non-zero ACF at $\tau = nT_\mathrm{s}$, it might still be possible to approximate sector-powers as Gaussian distributed depending of course on the structure of the ACF (see, e.g., [20] and references therein). Similarly, modeling sector-powers at individual RXs as uncorrelated is still a fairly good approximation, e.g., for ACFs that strongly decay with τ. Note also that the derivation of the localization CRB does not assume uncorrelated sector-powers. We could thus also obtain the RSS/DoA CRBs for correlated sector-powers by simply following the derivation of the localization CRB.

The second assumption that we have made is that the energy of the LoS path is dominating. In order to consider strong non line of sight (NLoS) components explicitly, we would have to sum up over all NLoS paths and the LoS path in (7). The resulting distribution of the received samples $r_{k,m}$ is, in general, again dependent on the TX signal ACF. In order to obtain results that are independent of a specific ACF, we could, however, approximate the contributions from different paths as independent and Gaussian distributed. The resulting $r_{k,m}(n)$ is then still Gaussian distributed, but with a mean and variance determined by all the paths. From there on the results for scenarios with strong NLoS paths are obtained in a similar manner as those that we derive in this article. Thus, this approach would significantly simplify the analysis, while at the same time making it possible to study the influence of NLoS paths arriving from angles other than the DoA of the LoS path.

However, the above discussed relaxations are beyond the scope of this article and we will, in the following, assume that the two assumptions hold.

III. Sector-Powers and Their Statistics

As discussed above, the communication of raw sensor measurements is impractical in a network where the communication between the collaborating RXs is wireless. Therefore, we consider a localization system, where the received samples of all sectors $m = 1 \ldots M$ at every RX k are preprocessed into sector-powers according to

$$\epsilon_{k,m} = \frac{1}{N}\sum_{n=0}^{N-1} |r_{k,m}(n)|^2. \tag{8}$$

The motivation for this particular preprocessing is discussed in detail in Section III-A below, while the model for the sector-powers is described in Section III-B.

A. Sector-Powers as Compressed Measurements and Sufficient Statistics

In this section we will establish the use of sector-powers as compressed measurements by means of Neyman-Fisher factorization [21, pp. 116-117]. Towards that end we will first identify the part of the measurements that is relevant for the localization. The received sample vector $\mathbf{r}_k$ at RX k depends on the TX location $\boldsymbol{\ell}_\mathrm{P}$ via the following variables: time delay η_k between TX and RX, RSS γ_k and antenna attenuations $\rho_{k,m}$, $m = 1 \ldots M$. While the time delay is dependent on the TX-RX distance via a very simple relationship, it is not very useful for the localization due to the assumed lack of synchronization among the RXs, as well as due to the assumption that the TX is non-cooperative and its signal ACF unknown. In case of the RSS, the exact dependence on the location is strongly influenced by the environment and is thus hard to describe with a model that is both simple and accurate. Therefore, we do not consider localization algorithms that extract the TX location from the delay η_k or the RSS γ_k. Instead we focus solely on algorithms that extract the TX location from the antenna attenuation $\rho_{k,m}$. Note that it nevertheless makes sense to estimate the RSS at every RX, if an intermediate step with DoA estimation is targeted, as the RSS is an indicator for the quality of the DoA estimates and can therefore be used for e.g. weighting the DoA estimates (see Section V-B). Having established the above, we are now ready to state the following theorem.

Theorem 1: Sector powers are a sufficient statistic for the estimation of $\boldsymbol{\ell}_\mathrm{P}$ and consequently an ideal compressed message for the localization system. Moreover, DoA/RSS estimation at an RX can, equally and without loss of performance, be based on the received samples or the sector-powers.

Proof: Since the preprocessing of samples into compressed message takes place in every individual RX, we will consider only the samples, $\mathbf{r}_k$, originating from an arbitrary RX k. For a given TX location, $\mathbf{r}_k$ has the PDF $f(\mathbf{r}_k|\boldsymbol{\ell}_\mathrm{P}) = \frac{1}{\pi^{MN}|\mathbf{\Sigma}_k|}\exp\left(-\mathbf{r}_k^H\mathbf{\Sigma}_k^{-1}\mathbf{r}_k\right)$. Given the assumption that the RXs do not oversample, the PDF can also be written as

$$f(\mathbf{r}_k|\boldsymbol{\ell}_\mathrm{P}) = \frac{1}{(\pi)^{MN}|\mathbf{\Sigma}_k|} \cdot \exp\left(-\sum_{m=1}^{M}\frac{1}{\rho_{k,m}\gamma_k + \sigma_\mathrm{w}^2}\sum_{n=0}^{N-1}|r_{k,m}(n)|^2\right). \tag{9}$$

The Neyman-Fisher factorization theorem states that, if a PDF can be factorized as $f(\mathbf{r}_k|\boldsymbol{\ell}_\mathrm{P}) = u(\mathbf{T}(\mathbf{r}_k), \boldsymbol{\ell}_\mathrm{P})h(\mathbf{r}_k)$, where

$h(\mathbf{r}_k)$ is a factor independent of the parameter $\boldsymbol{\ell}_\mathrm{P}$ that we want to estimate and $u(\mathbf{T}(\mathbf{r}_k), \boldsymbol{\ell}_\mathrm{P})$ is a factor that depends on the measured data $\mathbf{r}_k$ only through a function $\mathbf{T}(\mathbf{r}_k)$, then $\mathbf{T}(\mathbf{r}_k)$ is a sufficient statistic for the estimation of $\boldsymbol{\ell}_\mathrm{P}$ [21]. For PDF (9) we can choose the factors $h(\mathbf{r}_k) = 1$ and $u(\mathbf{T}(\mathbf{r}_k), \boldsymbol{\ell}_\mathrm{P}) = f(\mathbf{r}_k|\boldsymbol{\ell}_\mathrm{P})$ with $\mathbf{T}(\mathbf{r}_k) = \boldsymbol{\epsilon}_k(\mathbf{r}_k)$ which denotes the $M \times 1$ vector composed of the M sector-powers in (8). Thus, we have shown that the sector powers are a sufficient statistic for the estimation of $\boldsymbol{\ell}_\mathrm{P}$. Now, the antenna attenuation depends on the TX location only via the DoA. Hence, $\boldsymbol{\ell}_\mathrm{P}$ can be replaced with φ_k in (9) and, in case of sectorized antennas, DoA estimation based on sector-powers is equal to the estimation based on samples. A similar argument can be made for RSS estimation based on sector-powers. ■

A consequence of the above theorem is that the CRB for DoA/RSS estimation based on sectors-powers is equal to the sample-based DoA/RSS CRB. Moreover, the localization CRB for sector-powers also encompasses all localization algorithms that employ an intermediate DoA/RSS estimation step such as the one discussed in Section V.

B. Sector-Power Model

Since consecutively received samples in a single receiver are independent, sector-powers for a given and slowly varying channel are chi-squared distributed. It is well known (e.g. [22]) that such a distribution can be well approximated as Gaussian if the number of samples is large enough. Using this approximation, we model the sector-powers as $\epsilon_{k,m} \sim \mathcal{N}(g_{k,m}, \sigma^2_{k,m})$ with mean $g_{k,m} = \mathrm{E}[\epsilon_{k,m}] = \rho_{k,m}\gamma_k + \sigma^2_\mathrm{w}$ and variance $\sigma^2_{k,m} = \mathrm{E}[(\epsilon_{k,m} - g_{k,m})^2]$. Overall, this results in a model at a single RX that is very similar to the commonly used one, e.g., in the energy detection literature [22]. In the following we will discuss this model in more detail for the two cases of DoA/RSS estimation and localization.

1) DoA/RSS Estimation: Since DoA/RSS estimation is carried out within a single RX, it suffices to model the sector-powers at a single RX alone. At RX k, the $M \times 1$ vector of all sector-powers $\boldsymbol{\epsilon}_k = [\epsilon_{k,1}, \epsilon_{k,2}, \dots \epsilon_{k,M}]^\mathrm{T} \sim \mathcal{N}(\mathbf{g}_k, \mathbf{Q}_k)$, has a mean vector $\mathbf{g}_k = \mathrm{E}[\boldsymbol{\epsilon}_k]$ and covariance $\mathbf{Q}_k = \mathrm{E}[(\boldsymbol{\epsilon}_k - \mathbf{g}_k)(\boldsymbol{\epsilon}_k - \mathbf{g}_k)^\mathrm{T}]$ equal to

$$\mathbf{g}_k = [g_{k,1}, g_{k,2}, \dots g_{k,M}]^\mathrm{T} \tag{10}$$

$$\mathbf{Q}_k = \mathrm{diag}(\sigma^2_{k,1}, \sigma^2_{k,2}, \dots, \sigma^2_{k,M}) \tag{11}$$

with $\sigma^2_{k,m} = \frac{1}{N}(\rho_{k,m}\gamma_k + \sigma^2_\mathrm{w})^2$. We note that, due to the assumption of independent samples, we also obtain independent sector-powers and, as a consequence, a diagonal covariance matrix $\mathbf{Q}_k$.

2) Localization: In contrast to DoA/RSS estimation, the model for localization has to be a global one, meaning that it involves the sector-powers from all RXs. This leads to a $KM \times 1$ vector of sector-powers $\boldsymbol{\epsilon} = [\boldsymbol{\epsilon}_1^\mathrm{T}, \boldsymbol{\epsilon}_2^\mathrm{T}, \dots, \boldsymbol{\epsilon}_K^\mathrm{T}]^\mathrm{T} \sim \mathcal{N}(\mathbf{g}, \mathbf{Q})$, with a mean vector, $\mathbf{g} = \mathrm{E}[\boldsymbol{\epsilon}] = [\mathbf{g}_1, \mathbf{g}_2, \dots, \mathbf{g}_K]^\mathrm{T}$, that is composed of the means, $\mathbf{g}_k$, from all RXs $k = 1 \dots K$ as in (10). However, in contrast to the sector-power covariance at an individual RX, the covariance for the sector-powers from all RXs, $\mathbf{Q} = \mathrm{E}[(\boldsymbol{\epsilon} - \mathbf{g})(\boldsymbol{\epsilon} - \mathbf{g})^\mathrm{T}]$, cannot be modeled as a diagonal matrix. A diagonal covariance matrix $\mathbf{Q}_k$ at RX k implies an incoming signal with ACF $u_{\tilde{s}_i\tilde{s}_i}(nT_\mathrm{s}) = \mathrm{E}[\tilde{s}_i(t)\tilde{s}_i^*(t - nT_\mathrm{s})] = 0$ for $n = \pm 1, \pm 2, \dots$, which is true for the bandlimited Gaussian TX signal without oversampling at the RX. However, considering the incoming signals $\tilde{s}_i$ and $\tilde{s}_j$, at two RXs i and j, the ACF $u_{\tilde{s}_i\tilde{s}_j}(\Delta\eta_{ij}) = \mathrm{E}\left[\tilde{s}_i(t)\tilde{s}_j^*(t - \Delta\eta_{ij})\right]$ depends on the difference of delays, i.e. $\Delta\eta_{ij} = \eta_i - \eta_j$, for which practically always holds that $\Delta\eta_{ij} \neq mT_\mathrm{s}$. In particular, if $d_i \approx d_j$, then $\Delta\eta_{ij} \ll mT_\mathrm{s}$ such that the respective ACF $u_{\tilde{s}_i,\tilde{s}_j}(\Delta\eta_{ij}) \neq 0$.

As shown in Appendix A, the sector-powers covariance can then be written as

$$\mathbf{Q} = \boldsymbol{\rho}\boldsymbol{\rho}^\mathrm{T} \circ \bar{\boldsymbol{\gamma}}\bar{\boldsymbol{\gamma}}^\mathrm{T} \circ \mathbf{C} + \mathbf{D} \tag{12}$$

$$\mathbf{D} = \frac{\sigma^2_\mathrm{w}}{N}\left(2\,\mathrm{diag}(\boldsymbol{\rho} \circ \bar{\boldsymbol{\gamma}}) + \sigma^2_\mathrm{w}\mathbf{I}\right) \tag{13}$$

with

$$\boldsymbol{\rho} = \left[\boldsymbol{\rho}_1^\mathrm{T}, \boldsymbol{\rho}_2^\mathrm{T}, \dots, \boldsymbol{\rho}_K^\mathrm{T}\right]^\mathrm{T} \tag{14}$$

$$\boldsymbol{\rho}_k = [\rho_{k,1}, \rho_{k,2}, \dots, \rho_{k,M}]^\mathrm{T} \tag{15}$$

$$\bar{\boldsymbol{\gamma}} = \left[\gamma_1\mathbf{1}^{1\times M}, \gamma_2\mathbf{1}^{1\times M}, \dots \gamma_K\mathbf{1}^{1\times M}\right]^\mathrm{T} \tag{16}$$

and the $KM \times KM$ matrix $\mathbf{C}$ composed of the $M \times M$ submatrices

$$\boldsymbol{\Omega}_{ij} = \begin{pmatrix} c_{ij}(0) & c_{ij}(-1) & \dots & c_{ij}(-(M-1)) \\ c_{ij}(1) & c_{ij}(0) & \dots & c_{ij}(-(M-2)) \\ \vdots & \vdots & \ddots & \vdots \\ c_{ij}(M-1) & c_{ij}(M-2) & \dots & c_{ij}(0) \end{pmatrix} \tag{17}$$

with elements

$$\begin{aligned} c_{ij}(m) = \frac{1}{N}\mathcal{R}_{\tilde{\mathrm{s}}}(\Delta\eta_{ij} + mT_\mathrm{a}) - 1 \\ + \frac{1}{N^2}\sum_{p=1}^{N-1}(N-p)[\mathcal{R}_{\tilde{\mathrm{s}}}(\Delta\eta_{ij} + mT_\mathrm{a} + pT_\mathrm{s}) \\ + \mathcal{R}_{\tilde{\mathrm{s}}}(\Delta\eta_{ij} + mT_\mathrm{a} - pT_\mathrm{s})] \end{aligned} \tag{18}$$

that are dependent on the normalized ACF of the squared envelope $\mathcal{R}_{\tilde{\mathrm{s}}}(\tau) = \frac{1}{\sigma^4_\mathrm{s}}\mathrm{E}[|\tilde{s}(t)|^2\,|\tilde{s}(t-\tau)|^2]$. For a zero-mean complex Gaussian signal, $\mathcal{R}_{\tilde{\mathrm{s}}}(\tau)$ can be expressed in terms of its ACF as [23, pp. 67-68]

$$\mathcal{R}_{\tilde{\mathrm{s}}}(\tau) = 1 + \frac{1}{\sigma^4_\mathrm{s}}|u_{\tilde{s}}(\tau)|^2. \tag{19}$$

Hence, for the example case of a bandlimited Gaussian signal that we use in our evaluations in Section VII, we obtain $\mathcal{R}_{\tilde{\mathrm{s}}}(\tau) = 1 + \mathrm{sinc}^2(B\tau)$ and a matrix $\mathbf{C}$ with elements

$$\begin{aligned} c_{ij}(m) = \frac{1}{N}\mathrm{sinc}^2(t_{ij}(m)) + \frac{1}{N}\sum_{p=1}^{N-1}(N-p) \\ \cdot\left[\mathrm{sinc}^2(t_{ij}(m) + pBT_\mathrm{s}) + \mathrm{sinc}^2(t_{ij}(m) - pBT_\mathrm{s})\right] \end{aligned} \tag{20}$$

where $t_{ij}(m) = B\Delta\eta_{ij} + mBT_\mathrm{a}$. However, neither our sector-power model nor the CRB that we will derive in the next section is limited to the bandlimited Gaussian signal assumption.

IV. Cramer-Rao Bounds

The CRB is a lower bound on the covariance matrix of any unbiased estimator [21]. For the estimation of a $P \times 1$ parameter vector $\mathbf{q}$, given an $R \times 1$ vector $\boldsymbol{\epsilon}$ composed of the observations, the CRB is obtained as the inverse of the Fisher information matrix (FIM) (e.g. [15], [21]). The FIM is element-wise defined as

$$\mathbf{F}_{ij} = -\mathrm{E}\left(\frac{\partial^2}{\partial \mathbf{q}_i \partial \mathbf{q}_j} \ln\left[f\left(\boldsymbol{\epsilon}|\mathbf{q}\right)\right]\right) \tag{21}$$

with $i,j = 1 \dots P$. For the estimation problems considered in this paper, the observation vector $\boldsymbol{\epsilon} \sim \mathcal{N}(\mathbf{g},\mathbf{Q})$ is approximately Gaussian distributed, as discussed earlier, and both the mean $\mathbf{g}$ and covariance $\mathbf{Q}$ depend on the parameter vector, i.e. $\mathbf{g} = \boldsymbol{\xi}(\mathbf{q}), \boldsymbol{\xi} : \mathbb{R}^{P\times 1} \mapsto \mathbb{R}^{R\times 1}$ and $\mathbf{Q} = \boldsymbol{\Lambda}(\mathbf{q}), \boldsymbol{\Lambda} : \mathbb{R}^{P\times 1} \mapsto \mathbb{R}^{R\times R}$. As shown in [21, p. 47], the FIM in (21) can then be calculated as

$$\mathbf{F}_{ij} = \left[\mathbf{g}\right]_{\mathbf{q}_i}^{\mathrm{T}} \mathbf{Q}^{-1} \left[\mathbf{g}\right]_{\mathbf{q}_j} + \frac{1}{2}\,\mathrm{tr}\left\{\mathbf{Q}^{-1}\left[\mathbf{Q}\right]_{\mathbf{q}_i}\mathbf{Q}^{-1}\left[\mathbf{Q}\right]_{\mathbf{q}_j}\right\}. \tag{22}$$

A. CRBs for DoA/RSS Estimation

As discussed in Section III-A, the CRBs on DoA/RSS estimation can be computed using either samples or sector-powers. However, since the algorithms under consideration are based on sector-powers, we will also derive the respective CRBs assuming a pre-processing of samples into sector-powers. The model for the sector-powers (10)-(11) involves the DoA as well as the RSS. Hence, theoretically the estimation of DoA and RSS cannot be considered independently. Instead the respective parameter vector consists of both DoA and RSS, i.e. $\mathbf{q} = [\varphi_k, \gamma_k]^{\mathrm{T}}$, which results in a 2×2 FIM $\boldsymbol{\Gamma}$. Given the diagonal matrix (11) and using (22) it follows that

$$\boldsymbol{\Gamma}_{11} = (N+2)\sum_{m=1}^{M} a_{k,m}\tilde{\rho}_{k,m}^2 \tag{23}$$

$$\boldsymbol{\Gamma}_{12} = \boldsymbol{\Gamma}_{21} = \frac{N+2}{\gamma_k}\sum_{m=1}^{M} a_{k,m}\tilde{\rho}_{k,m} \tag{24}$$

$$\boldsymbol{\Gamma}_{22} = \frac{N+2}{\gamma_k^2}\sum_{m=1}^{M} a_{k,m} \tag{25}$$

where $a_{k,m} = (\mathrm{SNR}_{k,m}^{-1}+1)^{-2}$ is a weight for the contribution from sector m depending on the signal-to-noise ratio (SNR) in sector m at RX k, $\mathrm{SNR}_{k,m} = \rho_{k,m}\frac{\gamma_k}{\sigma_{\mathrm{w}}^2}$. Furthermore, $\tilde{\rho}_{k,m} = \frac{[\rho_{k,m}]_\varphi}{\rho_{k,m}}$ which becomes $\tilde{\rho}_{k,m} = -4\mathcal{M}(\varphi_k - \vartheta_m)/\beta^2$ for the Gaussian radiation pattern. Using the FIM elements (23)-(25), the CRBs on the RMSE of DoA estimation, $\mathrm{RMSE}_{\mathrm{DoA}}$, and the relative RMSE (RRMSE) on RSS estimation, $\mathrm{RRMSE}_{\mathrm{RSS}} = \mathrm{RMSE}_{\mathrm{RSS}}/\gamma_k$, are finally obtained as

$$\mathrm{RMSE}_{\mathrm{DoA}} = \sqrt{\left(\boldsymbol{\Gamma}^{-1}\right)_{11}} > \mathrm{RMSE}_{\mathrm{DoA}}^{\mathrm{a}} \tag{26}$$

$$\mathrm{RMSE}_{\mathrm{DoA}}^{\mathrm{a}} = \sqrt{\boldsymbol{\Gamma}_{11}^{-1}} = \sqrt{\frac{1}{N+2}\left(\sum_{m=1}^{M} a_{k,m}\tilde{\rho}_{k,m}^2\right)^{-1}} \tag{27}$$

$$\mathrm{RRMSE}_{\mathrm{RSS}} = \frac{1}{\gamma_k}\sqrt{\left(\boldsymbol{\Gamma}^{-1}\right)_{22}} > \mathrm{RRMSE}_{\mathrm{RSS}}^{\mathrm{a}} \tag{28}$$

$$\mathrm{RRMSE}_{\mathrm{RSS}}^{\mathrm{a}} = \frac{1}{\gamma_k}\sqrt{\boldsymbol{\Gamma}_{22}^{-1}} = \sqrt{\frac{1}{N+2}\left(\sum_{m=1}^{M} a_{k,m}\right)^{-1}}. \tag{29}$$

Thereby, $\mathrm{RMSE}_{\mathrm{DoA}}^{\mathrm{a}}$ is the CRB on the RMSE of DoA estimation when the RSS is known and accordingly $\mathrm{RRMSE}_{\mathrm{RSS}}^{\mathrm{a}}$ is the CRB on the RRMSE of RSS estimation when the DoA is known. Thus, these quantities are also lower bounds for the complete estimation problem where both RSS and DoA are unknown. Moreover, as will be seen in Section VII, the bounds $\mathrm{RMSE}_{\mathrm{DoA}}^{\mathrm{a}}$ and $\mathrm{RRMSE}_{\mathrm{RSS}}^{\mathrm{a}}$ are indeed very good approximations for the CRB of the complete estimation problem, i.e. $\mathrm{RMSE}_{\mathrm{DoA}} \approx \mathrm{RMSE}_{\mathrm{DoA}}^{\mathrm{a}}$ and $\mathrm{RRMSE}_{\mathrm{RSS}} \approx \mathrm{RRMSE}_{\mathrm{RSS}}^{\mathrm{a}}$. This means that $\boldsymbol{\Gamma}_{12}^2 \ll \boldsymbol{\Gamma}_{11}\boldsymbol{\Gamma}_{22}$ and therefore indicates that the DoA can be estimated independently of the RSS and vice versa. In fact, this observation is also confirmed by the SLS DoA estimator (see Section V-A). In SLS the measured sector-powers, which depend on both RSS and DoA, are transformed into a ratio, $J_{\mathrm{SLS}} \approx \rho_{k,i}/\rho_{k,j}$, that depends only on the DoA but not anymore on the RSS.

In the following sections, we will study the asymptotic behavior of the CRBs (27)-(29).

1) Asymptotic CRBs for Large SNR: In the derivation of the asymptotic bounds for large SNR, we will be using the following lemma:

Lemma 1: The function $\kappa_p(\varphi) = \sum_{m=1}^{M}\mathcal{M}(\varphi - \vartheta_m)^p$, $p \in \mathbb{N}$ is periodic with period $\Delta\vartheta$.

Proof: The periodicity is easily proven by substituting the index m of the sector-orientation with $m' = \mathrm{mod}_M(m)+1$ such that $\kappa_p(\varphi) = \sum_{m'=1}^{M}\mathcal{M}(\varphi+\Delta\vartheta-\vartheta_{m'})^p = \kappa_p(\varphi+\Delta\vartheta)$ since $\vartheta_m = \vartheta_{m'} - \Delta\vartheta$. ∎

Based on Lemma 1 and following the steps in Appendix B, we obtain the asymptotic (large SNR) RMSE of DoA estimation and the asymptotic RRMSE of RSS estimation as

$$\mathrm{RMSE}_{\mathrm{DoA}}^{\mathrm{SNR}} = \frac{\sqrt{3}\pi}{|\ln(a_{\mathrm{s}})|\sqrt{(M^5-M^3)(N+2)}} \tag{30}$$

$$\mathrm{RRMSE}_{\mathrm{RSS}}^{\mathrm{SNR}} = \frac{1}{\sqrt{M(N+2)}}\sqrt{1+\frac{3\,M^2\left[\mathcal{P}(\varphi_k)\right]^2}{\pi^2\left(M^2-1\right)}}, \tag{31}$$

where $\mathcal{P}(\varphi) = \mathrm{mod}_{\Delta\vartheta}(\varphi + \Delta\vartheta/2) - \Delta\vartheta/2$. The asymptotic bounds (30)-(31) were derived for a given DoA. Interestingly, $\mathrm{RMSE}_{\mathrm{DoA}}^{\mathrm{SNR}}$ is independent of the DoA, while $\mathrm{RRMSE}_{\mathrm{RSS}}^{\mathrm{SNR}}$ is a function of the DoA. If we assume a uniformly distributed DoA, i.e. $\varphi_k \sim \mathcal{U}(-\pi,\pi)$, we obtain the following bounds

$$\overline{\mathrm{RMSE}}_{\mathrm{DoA}}^{\mathrm{SNR}} = \mathrm{RMSE}_{\mathrm{DoA}}^{\mathrm{SNR}} \tag{32}$$

$$\overline{\mathrm{RRMSE}}_{\mathrm{RSS}}^{\mathrm{SNR}} = \frac{1}{\sqrt{(M-\frac{1}{M})(N+2)}} \tag{33}$$

as shown in detail in Appendix B.

2) Asymptotic CRBs for large N: As evident from (23)-(29), the FIM for DoA/RSS estimation can be written as $\boldsymbol{\Gamma} = (N+2)\boldsymbol{\Gamma}'$, where $\boldsymbol{\Gamma}'$ is the part of the FIM that is independent of N. Consequently, the CRB on the RMSE of DoA as well as RSS estimation is proportional to $\sqrt{N+2}^{-1}$ since $\boldsymbol{\Gamma}^{-1} =$

$(N+1)^{-1}\left(\mathbf{\Gamma}'\right)^{-1}$. Therefore, for $N \to \infty$, the bounds on DoA and RSS estimation are equal to

$$\mathrm{RMSE}_{\mathrm{DoA}}^{N} = 0 \tag{34}$$

$$\mathrm{RRMSE}_{\mathrm{RSS}}^{N} = 0. \tag{35}$$

Clearly, (35) and (34) are independent of the DoA and consequently the bounds for uniformly distributed DoAs become $\overline{\mathrm{RMSE}}_{\mathrm{DoA}}^{N} = 0$ and $\overline{\mathrm{RRMSE}}_{\mathrm{RSS}}^{N} = 0$ as well. According to the law of large numbers, $N \to \infty$ means that the measured sector-powers attain their expected values, which are completely determined by DoA and RSS. Inversely, this also makes it possible to estimate both RSS and DoA without error as reflected by the CRBs in (34) and (35).

B. CRBs for Localization

As discussed in Section III-B2, the sector-power model for localization includes the unknown RSSs from all RXs along with the TX location. Moreover, the model includes the covariance matrix (12) that depends on the TX location via the ACF, which is unknown to the RXs according to our assumptions. Therefore the covariance matrix is treated as an unknown that is part of the overall estimation problem. As a consequence, the Fisher information of the RSSs, $\gamma_1, \gamma_2, \ldots, \gamma_K$ as well as the Fisher information of the covariance matrix have to be included in the localization FIM as so-called nuisance parameters (see e.g. [9], [24]), although they are not of direct interest for the localization. With respect to the covariance matrix, it can be seen from (12) that it is sufficient to estimate the unique elements of the matrix $\mathbf{C}$. Thereby, we notice that each submatrix $\mathbf{\Omega}_{ij}$ given in (17) has a maximum number of $2M-1$ unique elements $c_{ij}(m)$ as $m = -(M-1), -(M-2), \ldots, M-1$. Furthermore, $\mathbf{\Omega}_{ij} = \mathbf{\Omega}_{ij}^{\mathrm{T}}$ since $c_{ij}(m) = c_{ji}(-m)$. In addition $c_{ii}(m) = c_{jj}(m)$, so that there are only M unique elements for all the submatrices on the diagonal. The overall number of unique elements $c_{ij}(m)$ is therefore $\frac{1}{2}K(K-1)(2M-1)+M$. However, the M elements on the main diagonal submatrices do not depend on the actual ACF since $c_{ii}(0) = \frac{1}{N}$ and $c_{ii}(m) = 0$ for $m \neq 0$ due to our assumption that $u_{\tilde{s}}(nT_{\mathrm{s}}) = 0$ for $n = \pm 1, \pm 2, \ldots$.. Therefore, the number of unknown elements $c_{ij}(m)$ that have to be estimated is $\mathcal{N} = \frac{1}{2}K(K-1)(2M-1)$. Now define $\mathbf{c}$ as the $\mathcal{N} \times 1$ vector composed of all elements of $c_{ij}(m)$. Then, the parameter vector for localization may be expressed as $\mathbf{q} = \left[x_{\mathrm{P}}, y_{\mathrm{P}}, \boldsymbol{\gamma}^{\mathrm{T}}, \mathbf{c}^{\mathrm{T}}\right]^{\mathrm{T}}$. Using again (22), we can then calculate the following FIM elements

$$\mathbf{\Lambda}_{ij} = [\mathbf{g}]_{(\boldsymbol{\ell}_{\mathrm{P}})_i}^{\mathrm{T}} \mathbf{Q}^{-1} [\mathbf{g}]_{(\boldsymbol{\ell}_{\mathrm{P}})_j} + \frac{1}{2}\,\mathrm{tr}\left\{\mathbf{Q}^{-1}[\mathbf{Q}]_{(\boldsymbol{\ell}_{\mathrm{P}})_i}\mathbf{Q}^{-1}[\mathbf{Q}]_{(\boldsymbol{\ell}_{\mathrm{P}})_j}\right\} \tag{36}$$

$$\mathbf{\Lambda}_{i,2+k} = [\mathbf{g}]_{(\boldsymbol{\ell}_{\mathrm{P}})_i}^{\mathrm{T}} \mathbf{Q}^{-1} [\mathbf{g}]_{\gamma_k} + \frac{1}{2}\,\mathrm{tr}\left\{\mathbf{Q}^{-1}[\mathbf{Q}]_{(\boldsymbol{\ell}_{\mathrm{P}})_i}\mathbf{Q}^{-1}[\mathbf{Q}]_{\gamma_k}\right\} \tag{37}$$

$$\mathbf{\Lambda}_{i,(2+K+m)} = \frac{1}{2}\,\mathrm{tr}\left\{\mathbf{Q}^{-1}[\mathbf{Q}]_{(\boldsymbol{\ell}_{\mathrm{P}})_i}\mathbf{Q}^{-1}[\mathbf{Q}]_{\mathbf{c}_m}\right\} \tag{38}$$

$$\mathbf{\Lambda}_{(2+k),(2+l)} = [\mathbf{g}]_{\gamma_k}^{\mathrm{T}} \mathbf{Q}^{-1} [\mathbf{g}]_{\gamma_l} + \frac{1}{2}\,\mathrm{tr}\left\{\mathbf{Q}^{-1}[\mathbf{Q}]_{\gamma_k}\mathbf{Q}^{-1}[\mathbf{Q}]_{\gamma_l}\right\} \tag{39}$$

$$\mathbf{\Lambda}_{(2+k),(2+K+m)} = \frac{1}{2}\,\mathrm{tr}\left\{\mathbf{Q}^{-1}[\mathbf{Q}]_{\gamma_k}\mathbf{Q}^{-1}[\mathbf{Q}]_{\mathbf{c}_m}\right\} \tag{40}$$

$$\mathbf{\Lambda}_{(2+K+m),(2+K+n)} = \frac{1}{2}\,\mathrm{tr}\left\{\mathbf{Q}^{-1}[\mathbf{Q}]_{\mathbf{c}_m}\mathbf{Q}^{-1}[\mathbf{Q}]_{\mathbf{c}_n}\right\} \tag{41}$$

where $i = 1,2$, $j = 1,2$, $k = 1 \ldots K$, $l = 1 \ldots K$, $m = 1 \ldots \mathcal{N}$, $n = 1 \ldots \mathcal{N}$ and derivatives equal to

$$[\mathbf{Q}]_{(\boldsymbol{\ell}_{\mathrm{P}})_i} = \left([\boldsymbol{\rho}]_{(\boldsymbol{\ell}_{\mathrm{P}})_i}\boldsymbol{\rho}^{\mathrm{T}} + \boldsymbol{\rho}\,[\boldsymbol{\rho}]_{(\boldsymbol{\ell}_{\mathrm{P}})_i}^{\mathrm{T}}\right) \circ \bar{\boldsymbol{\gamma}}\bar{\boldsymbol{\gamma}}^{\mathrm{T}} \circ \mathbf{C} + 2\frac{\sigma_{\mathrm{w}}^2}{N}\,\mathrm{diag}\left([\boldsymbol{\rho}]_{(\boldsymbol{\ell}_{\mathrm{P}})_i} \circ \bar{\boldsymbol{\gamma}}\right) \tag{42}$$

$$[\mathbf{Q}]_{\gamma_k} = \boldsymbol{\rho}\boldsymbol{\rho}^{\mathrm{T}} \circ \left[\bar{\boldsymbol{\gamma}}\bar{\boldsymbol{\gamma}}^{\mathrm{T}}\right]_{\gamma_k} \circ \mathbf{C} + 2\frac{\sigma_{\mathrm{w}}^2}{N}\,\mathrm{diag}\left(\boldsymbol{\rho} \circ [\bar{\boldsymbol{\gamma}}]_{\gamma_k}\right) \tag{43}$$

$$[\mathbf{Q}]_{\mathbf{c}_m} = \boldsymbol{\rho}\boldsymbol{\rho}^{\mathrm{T}} \circ \bar{\boldsymbol{\gamma}}\bar{\boldsymbol{\gamma}}^{\mathrm{T}} \circ [\mathbf{C}]_{\mathbf{c}_m} \tag{44}$$

$$[\mathbf{g}]_{(\boldsymbol{\ell}_{\mathrm{P}})_i} = [\boldsymbol{\rho}]_{(\boldsymbol{\ell}_{\mathrm{P}})_i} \circ \bar{\boldsymbol{\gamma}},\ [\mathbf{g}]_{\gamma_k} = \boldsymbol{\rho} \circ [\bar{\boldsymbol{\gamma}}]_{\gamma_k},\ [\mathbf{g}]_{\mathbf{c}_m} = 0 \tag{45}$$

which in turn depend on the trivial derivative $[\mathbf{C}]_{\mathbf{c}_m}$ and $[\rho_{k,m}]_{(\boldsymbol{\ell}_{\mathrm{P}})_i} = [\rho_{k,m}]_{\varphi_k}[\varphi_k]_{(\boldsymbol{\ell}_{\mathrm{P}})_i}$ with $[\varphi_k]_x = -\frac{y_{\mathrm{P}}-y_k}{d_k^2}$ and $[\varphi_k]_y = \frac{x_{\mathrm{P}}-x_k}{d_k^2}$. Hence, the CRB on the RMSE of location estimation can be stated as

$$\mathrm{RMSE} = \sqrt{\left(\mathbf{\Lambda}^{-1}\right)_{11} + \left(\mathbf{\Lambda}^{-1}\right)_{22}} \tag{46}$$

$$\mathrm{RMSE} > \mathrm{RMSE}_{\mathrm{R}} = \sqrt{\left(\mathbf{\Lambda}_{\mathrm{R}}^{-1}\right)_{11} + \left(\mathbf{\Lambda}_{\mathrm{R}}^{-1}\right)_{22}} \tag{47}$$

$$\mathrm{RMSE} > \mathrm{RMSE}_{\mathrm{L}} = \sqrt{\left(\mathbf{\Lambda}_{\mathrm{L}}^{-1}\right)_{11} + \left(\mathbf{\Lambda}_{\mathrm{L}}^{-1}\right)_{22}} = \frac{\sqrt{\mathbf{\Lambda}_{11} + \mathbf{\Lambda}_{22}}}{\sqrt{\mathbf{\Lambda}_{11}\mathbf{\Lambda}_{22} - \mathbf{\Lambda}_{12}^2}} \tag{48}$$

The latter RMSEs, $\mathrm{RMSE}_{\mathrm{R}}$ and $\mathrm{RMSE}_{\mathrm{L}}$, are again CRBs that assume the knowledge of some of the nuisance parameters. (47) assumes the knowledge of the covariance, i.e. $\mathbf{\Lambda}_{\mathrm{R}} \in \mathbb{R}^{(2+K)\times(2+K)}$, $(\mathbf{\Lambda}_{\mathrm{R}})_{ij} = (\mathbf{\Lambda})_{ij}, i,j = 1 \ldots 2+K$ and (48) assumes the knowledge of both the covariance and RSSs, i.e. $\mathbf{\Lambda}_{\mathrm{L}} \in \mathbb{R}^{2\times 2}$, $(\mathbf{\Lambda}_{\mathrm{L}})_{ij} = (\mathbf{\Lambda})_{ij}, i,j = 1,2$. Note that we could interrelate RMSE, $\mathrm{RMSE}_{\mathrm{R}}$ and $\mathrm{RMSE}_{\mathrm{RL}}$ also through the work in [25] as alternative expressions to (46)-(48). As will be seen in Section VII, the approximation $\mathrm{RMSE} \approx \mathrm{RMSE}_{\mathrm{R}}$ is almost a perfect match and greatly reduces the size of the FIM. For an even more compact FIM (and faster computations), it is also possible to apply the latter approximation $\mathrm{RMSE} \approx \mathrm{RMSE}_{\mathrm{L}}$ which is likewise a lower bound on the performance, yet not quite as tight as the CRB (46). Illustrations will be given in Section VII.

V. Algorithms

In the following, we shortly describe the SLS algorithm, a sector-power based DoA/RSS estimator that was proposed in [11], as well as a modified Stansfield estimator [10], that computes a TX location estimate using DoA/RSS estimates from multiple RXs. We will be referring to SLS DoA/RSS estimation with successive Stansfield location estimation as SLS-ST. SLS as well as SLS-ST will be used to compare the derived CRBs to practical DoA/RSS and localization algorithms.

A. SLS DoA/RSS Estimator

Due to the nonlinear dependence of the sector-powers on the DoA and RSS, classical estimation approaches such as least-squares and maximum likelihood would require iterative solutions. In order to overcome associated problems such as divergence, the SLS DoA/RSS estimator was therefore proposed in [11]. SLS finds the two neighboring sectors $i, j \in 1 \dots M, |i-j| = 1$ at RX k, such that $\epsilon_{k,i} + \epsilon_{k,j} > \epsilon_{k,m} + \epsilon_{k,n}$ for all other neighboring sectors $n, m = 1 \dots M$, $n, m \neq i, j$, $|n-m| = 1$. The DoA φ_k is then, with high probability, in-between the orientations ϑ_i and ϑ_j of the two sectors i and j. Given an adequate tuning of the antenna and practical working conditions [11], the incoming signal at the RX is of meaningful strength only in very few sectors, while the remaining measurements are likely to be very noisy. Hence, SLS discards the sector-powers from all sectors except $\epsilon_{k,i}$ and $\epsilon_{k,j}$ and finds the DoA $\hat{\varphi}_k$ that minimizes the norm $J_{\text{SLS}} = \left(p_{k,i}/p_{k,j} - \rho_{k,i}/\rho_{k,j}\right)^2$ where $p_{k,m} = \epsilon_{k,m} - \sigma_{\text{w}}^2$, $m = i, j$. Using an approximation of the antenna's main beam as in Section II-A, the DoA at RX k is obtained in closed-form as

$$\hat{\varphi}_k = \bar{\vartheta}_{ij} + \kappa \left(\ln p_{k,i} - \ln p_{k,j}\right) \tag{49}$$

where $\bar{\vartheta}_{ij} = \frac{1}{2}(\vartheta_i + \vartheta_j)$ and $\kappa = -\frac{\pi}{2M \ln a_{\text{s}}}$ assuming $\vartheta_i > \vartheta_j$ for simplicity and without loss of generality. Exploiting the direct mapping between the DoA estimate $\hat{\varphi}_k$ and its corresponding RSS estimate $\hat{\gamma}_k$ via the antenna's radiation pattern, $\hat{\rho}_{k,m} = \left[\zeta\left(\hat{\varphi}_k - \vartheta_m\right)\right]^2$, SLS consequently estimates the RSS at RX k as

$$\hat{\gamma}_k = \frac{1}{2}\left[\left(\epsilon_{k,i} - \sigma_{\text{w}}^2\right)/\hat{\rho}_{k,i} + \left(\epsilon_{k,j} - \sigma_{\text{w}}^2\right)/\hat{\rho}_{k,j}\right]. \tag{50}$$

In order to prevent large estimation errors when the signal is severely attenuated, we have also added a validation check as discussed in detail in [11].

B. Stansfield Location Estimator

The Stansfield estimator was first introduced in [3]. It is closely related to the maximum likelihood (ML) DoA fusion algorithm. The ML DoA fusion scheme is a nonlinear least square function that has to be solved by iterative algorithms such as the Gauss-Newton method. The iterative algorithms suffer from divergence which makes the ML DoA fusion scheme not reliable in practical scenarios [26]. The Stansfield algorithm is a linear approximation of the ML fusion scheme resulting in the following closed-form TX location estimate

$$\hat{\boldsymbol{\ell}}_P = (\mathbf{A}^{\text{T}}\mathbf{W}\mathbf{A})^{-1}\mathbf{A}^{\text{T}}\mathbf{W}\mathbf{b}, \tag{51}$$

where

$$\mathbf{A} = \begin{bmatrix} \sin(\hat{\varphi}_1) & -\cos(\hat{\varphi}_1) \\ \vdots & \vdots \\ \sin(\hat{\varphi}_K) & -\cos(\hat{\varphi}_K) \end{bmatrix}, \tag{52}$$

$$\mathbf{b} = \begin{bmatrix} x_1 \sin(\hat{\varphi}_1) - y_1 \cos(\hat{\varphi}_1) \\ \vdots \\ x_K \sin(\hat{\varphi}_K) - y_K \cos(\hat{\varphi}_K) \end{bmatrix} \tag{53}$$

and the weighting matrix is defined as $\mathbf{W} = \text{diag}[w_1, \dots, w_K]$. In here we use the modified Stansfield algorithm [10], where the contribution of each RX is weighted with the corresponding RSS by setting $\mathbf{W} = \text{diag}[\hat{\gamma}_1, \dots, \hat{\gamma}_K]$, which is equivalent to weighting the DoA estimates with the SNRs, given that the noise variance σ_{w}^2 is the same at every RX. Consequently, each RX communicates the estimated DoA as well as the estimated RSS to the FC. However, at the FC the RSS is only used to indicate the quality of the DoA estimates, while TX location information is not extracted from the RSS. Therefore, the SLS-ST algorithm is lower bounded by the localization CRB that we derived earlier in this paper. This will be illustrated in Section VII.

VI. Analytical Error Models for SLS DoA Estimation

A. Bias and RMSE for a Given DoA

In order to derive the bias and RMSE of SLS DoA estimation we will make the following two simplifying assumptions. First, we assume that SLS always picks the two sectors i and j, such that $\vartheta_j < \varphi_k < \vartheta_i$. Second, we assume that the variances of the powers $p_{k,l} \sim \mathcal{N}(\bar{\mu}_{k,l}, \bar{\sigma}_{k,l}^2)$, $\bar{\mu}_{k,l} = \rho_{k,l}\gamma_k$, $\bar{\sigma}_{k,l}^2 = \sigma_{k,l}^2$, $l = i, j$ are much smaller than their respective means, i.e. $\bar{\sigma}_{k,l}^2 \ll \bar{\mu}_{k,l}$. Intuitively, both of these assumptions are valid if the number of samples N and the SNR are sufficiently large. As will be seen in Section VII, these assumptions lead to a very good approximation of the RMSE in most of the relevant cases. In the derivation, the first assumption allows us to disregard the sector-selection process, which is difficult to model analytically. Due to the second assumption, we can well approximate the logarithms $\ln p_l$, $l = i, j$ in (49) with a first order Taylor series around the mean of $p_{k,l}$, i.e. $\ln p_{k,l} \approx \ln \bar{\mu}_{k,l} + \frac{p_{k,l} - \bar{\mu}_{k,l}}{\bar{\mu}_{k,l}}$. This leads to an approximation of the DoA estimation (49) that is equal to

$$\tilde{\varphi}_k = \bar{\vartheta}_{ij} + \kappa \left(\ln \frac{\bar{\mu}_{k,i}}{\bar{\mu}_{k,j}} + \frac{p_{k,i} - \bar{\mu}_{k,i}}{\bar{\mu}_{k,i}} - \frac{p_{k,j} - \bar{\mu}_{k,j}}{\bar{\mu}_{k,j}}\right). \tag{54}$$

The expected value of $\tilde{\varphi}_k$ can be calculated as $\text{E}[\tilde{\varphi}_k] = \bar{\vartheta}_{ij} + \kappa \ln \frac{\bar{\mu}_{k,i}}{\bar{\mu}_{k,j}}$. We then obtain an approximation for the bias of SLS DoA estimation as (see Appendix C)

$$\text{bias}[\hat{\varphi}_k] \approx \text{bias}[\tilde{\varphi}_k] = \text{E}[\tilde{\varphi}_k] - \varphi_k = 0. \tag{55}$$

Therefore, SLS is unbiased for large SNR, which was already verified by numerical results in [11]. Similarly, we calculate the variance of $\tilde{\varphi}_k$ as $\text{var}[\tilde{\varphi}_k] = \kappa^2(\frac{\bar{\sigma}_{k,i}^2}{\bar{\mu}_{k,i}^2} + \frac{\bar{\sigma}_{k,j}^2}{\bar{\mu}_{k,j}^2})$, and approximate the mean squared error of SLS DoA estimation for given DoA using first order Taylor series, i.e. $\text{MSE}[\hat{\varphi}_k] \approx \text{MSE}[\tilde{\varphi}_k] = \text{var}[\tilde{\varphi}_k] + \left[\text{bias}[\hat{\varphi}_k]\right]^2$ such that the RMSE becomes

$$\text{RMSE}_{\text{SLS}}[\hat{\varphi}_k] \approx \frac{\kappa}{\sqrt{N}}\sqrt{a_{k,i}^{-1} + a_{k,j}^{-1}}. \tag{56}$$

B. RMSE for Uniformly Distributed DoA

For a uniformly distributed DoA $\varphi_k \sim \mathcal{U}(-\pi, \pi)$, we can approximate the average RMSE of SLS DoA estimation as

$$\overline{\text{RMSE}}_{\text{SLS}} \approx \sqrt{\frac{1}{\Delta\theta}\int_0^{\Delta\vartheta} \text{MSE}[\tilde{\varphi}_k + \vartheta_j] d\tilde{\varphi}}, \tag{57}$$

TABLE II: Example values of (60) and (61)

a_s	0.2	0.3	0.4	0.5	0.6	0.7	0.8	0.9
$f(a_\mathrm{s})$	154.4	37.0	14.1	6.9	3.9	2.4	1.5	0.8
$g(a_\mathrm{s})$	9.8	5.2	3.3	2.3	1.7	1.2	0.9	0.6

where we use the assumption of equal sectors and integrate only over one sector instead of over all DoAs from $-\pi$ to π. The solution of (57) involves integrals of the form $\int_0^x e^{t^2}dt$, which can be expressed using, among others, imaginary error functions [27], defined as

$$\mathrm{erfi}(x) = -i\,\mathrm{erf}(ix) = \frac{2}{\sqrt{\pi}}\int_0^x e^{t^2}\,dt. \tag{58}$$

An implementation of the imaginary error function can be found in e.g. MATLAB's symbolic toolbox. Using (58) in (57), we then obtain an approximation of the average RMSE of SLS DoA estimation equal to

$$\overline{\mathrm{RMSE}}_\mathrm{SLS} \approx \kappa\sqrt{\frac{2\sqrt{\pi}}{N\sqrt{\ln a_\mathrm{s}^{-1}}}\left[\frac{f(a_\mathrm{s})}{4\,\mathrm{SNR}^2}+\frac{g(a_\mathrm{s})}{\sqrt{2}\,\mathrm{SNR}}\right]+\frac{2}{N}} \tag{59}$$

with

$$f(a_\mathrm{s}) = \mathrm{erfi}\left(2\sqrt{\ln\left(a_\mathrm{s}^{-1}\right)}\right), \tag{60}$$

$$g(a_\mathrm{s}) = \mathrm{erfi}\left(\sqrt{2\ln\left(a_\mathrm{s}^{-1}\right)}\right) \tag{61}$$

where we have highlighted explicitly that $f(a_\mathrm{s})$ and $g(a_\mathrm{s})$ depend only on the side-sector suppression, a_s. As will be discussed in Section VII, a_s should be set to a fixed value in the interval $[0.2, 0.4]$ for good performance. Therefore, it is not necessary to evaluate the imaginary error functions contained in (59). Instead, the functions (60) and (61) can be treated as constants with a few exemplary values for practically relevant cases of a_s shown in Table II.

C. Asymptotic RMSE

As can be seen from (56) and (59), the asymptotic RMSEs for large SNR are equal to

$$\mathrm{RMSE}_\mathrm{SLS}^\mathrm{SNR} = \overline{\mathrm{RMSE}}_\mathrm{SLS}^\mathrm{SNR} = \frac{\pi}{\sqrt{2N}M|\ln a_\mathrm{s}|}, \tag{62}$$

while the asymptotic RMSEs for large N are equal to

$$\mathrm{RMSE}_\mathrm{SLS}^N = \overline{\mathrm{RMSE}}_\mathrm{SLS}^N = 0. \tag{63}$$

We notice that (62) is slightly different from the result in [17], where $\mathrm{RMSE}_{\mathrm{SLS,\,[17]}}^\mathrm{SNR} = \frac{\pi\sqrt{\ln(1+1/N)}}{\sqrt{2M|\ln a_\mathrm{s}|}}$ due to a different approximation of the sector-power distribution. However, $\ln(1+x) = \sum_{n=1}^\infty \frac{(-1)^{n+1}x^n}{n}$ for $-1 < x \leq 1$, such that $\mathrm{RMSE}_{\mathrm{SLS,\,[17]}}^\mathrm{SNR} \approx \mathrm{RMSE}_\mathrm{SLS}^\mathrm{SNR}$ for sufficiently large N (say $N > 10$). Moreover, when comparing (30) to (62) and (34) to (63) we see that SLS is an asymptotically efficient estimator in the number of samples N, but not in the SNR. We will discuss this in more detail in the next section.

VII. Evaluation, Illustrations and Analysis

A. DoA/RSS Estimation

DoA and RSS estimation performance is studied assuming a uniform distribution of incoming DoAs, i.e. $\varphi \sim \mathcal{U}(-\pi;\pi)$ in an individual arbitrary RX. We limit our simulation to 100 steps in the interval $\varphi_k \in [-\frac{\Delta\vartheta}{2};\frac{\Delta\vartheta}{2}]$ due to the periodicity of the radiation pattern. For each DoA-step we average over 1000 realizations to obtain numerical results for the CRBs and RMSE of SLS for uniformly distributed DoA. The CRBs (27) and (29) as well as the RMSE of DoA/RSS estimation with SLS depend on the RSS only via the $\mathrm{SNR} = \frac{\gamma}{\sigma_\mathrm{w}^2}$. Therefore, we set the RSS to an arbitrary fixed value and adjust the noise power σ_w^2 in order to control the SNR.

Fig. 5 and Fig. 6 depict the dependence of DoA/RSS estimation performance on the side-sector suppression a_s. For values $a_\mathrm{s} > 0.2$ the CRBs on DoA/RSS estimation can be perfectly approximated by the other lower bounds in (27)-(29), i.e. $\mathrm{RMSE}_\mathrm{DoA} \approx \mathrm{RMSE}_\mathrm{DoA}^\mathrm{a}$ and $\mathrm{RRMSE}_\mathrm{RSS} \approx \mathrm{RRMSE}_\mathrm{RSS}^\mathrm{a}$. Similarly, the analytical expression for the RMSE (59) of SLS, i.e. $\overline{\mathrm{RMSE}}_\mathrm{SLS}$, is also very accurate for $a_\mathrm{s} > 0.2$. This coincides with the region where SLS is unbiased and thus lower bounded by the CRBs [11]. As a guideline for sectorized antenna design, we are interested in finding the value $a_\mathrm{s} = a_\mathrm{s,o}$ that results in the lowest RMSE of DoA and RSS estimation. Unfortunately, $a_\mathrm{s,o}$ is a function of the SNR, while a_s is a value that is fixed during the design process for most sectorized antennas. In the case of asymptotically large SNR, $\overline{\mathrm{RMSE}}_\mathrm{DoA}^\mathrm{SNR}$ increases monotonically with a_s, while $\overline{\mathrm{RRMSE}}_\mathrm{RSS}^\mathrm{SNR}$ is independent of a_s. In other words, if the noise is neglectable, the sectors in a sectorized antenna should be as selective as possible in order to obtain the most accurate DoA and RSS estimates. However, for finite SNR a reduction of a_s results in a decrease of the effective SNR, i.e. $\mathrm{SNR}_{k,m} = \rho_{k,m}\,\mathrm{SNR}_k$, for all DoAs $\varphi \neq \vartheta_m$. This of course affects the performance adversely such that the choice of a_s is a compromise. We have found that a side-sector suppression a_s in the interval $[0.2, 0.4]$ results in a good trade-off between low and high SNR values. Therefore, we can conclude that the derived approximation of the CRBs is valid for adequately tuned antennas.

As can be seen from (23)-(29), the dependence of the DoA and RSS estimation CRBs on the SNR are similar. Therefore, we only show the performance of DoA estimation as a function of the SNR in Fig. 7. Again, the approximations of the CRBs in (27)-(29) are highly accurate. Generally, SLS performs close to the CRB, with the smallest gap to the CRBs in the interval $0\ \mathrm{dB} < \mathrm{SNR} < 15\ \mathrm{dB}$. In contrast to the earlier asymptotic expression for the RMSE [17] (not explicitly shown in Fig. 7 for clarity), $\overline{\mathrm{RMSE}}_\mathrm{SLS}$ describes the performance of SLS very well already for low $\mathrm{SNR} > 5$ dB instead of only for the saturated region $\mathrm{SNR} > 15$ dB.

In the saturated region, SLS starts to diverge slightly from the CRB. This is due to the fact that SLS discards the sector-powers from all sectors, except for the two neighboring sectors i and j (see Section V-A). Thus, for SLS the CRB approximation in (27) becomes $\mathrm{RMSE}_\mathrm{DoA}^\mathrm{SLS,b} = \sqrt{(N+2)^{-1}(a_{k,i}\tilde{\rho}_{k,i} + a_{k,j}^2\tilde{\rho}_{k,j})^{-1}}$. For high SNR, $a_{k,i}$ and $a_{k,j}$ attain their maximum with $a_{k,i} \approx a_{k,j} \approx 1$ such

that $\mathrm{RMSE}_{\mathrm{DoA}}^{\mathrm{SLS,b}} = \sqrt{(N+2)^{-1}(\tilde{\rho}_{k,i}^2+\tilde{\rho}_{k,j}^2)^{-1}}$, which is independent of the SNR and ultimately limits the performance of SLS. Naturally, we can make a similar argument for the CRB in general and conclude that the RMSE saturates at $\mathrm{RMSE}_{\mathrm{DoA}}^{\mathrm{SNR}} \approx \sqrt{(N+2)^{-1}(\sum_{m=1}^{M}\tilde{\rho}_{k,m})^{-1}}$ for very large SNR. However, for increasingly high SNR, those sectors that were discarded by SLS are responsible for the performance increase in the CRB as the respective weighting $a_{k,m}$, $m=1\dots M, m\neq i,j$ will attain its maximum significantly later than $a_{k,i}$ and $a_{k,j}$. This manifests itself also in the ratio of the asymptotic RMSEs (62) and (32). For $N+2\approx N$, we can write $\overline{\mathrm{RMSE}}_{\mathrm{SLS}}^{\mathrm{SNR}}/\overline{\mathrm{RMSE}}_{\mathrm{DoA}}^{\mathrm{SNR}} \approx \sqrt{(M^3-M)/6}$, which is an increasing function with M due to the fact that the number of sectors that SLS discards also grows with M. For the case of $M=6$, SLS saturates at an almost six-fold larger RMSE compared to the CRB.

For comparison, we have also added a curve for the CRB of DoA estimation with DCAAs and parallel processing of all antenna branches in Fig. 7. As an example DCAA, we have chosen a uniform circular array (UCA) with $N_{\mathrm{a}}=8$ antennas. Assuming next that the signal bandwidth is significantly smaller than the carrier frequency, we can then approximate the $N_{\mathrm{a}}\times 1$ steering vector $\mathbf{b}(\varphi)$ of the UCA as $\mathbf{b}_i(\varphi) = 1/N_{\mathrm{a}}\exp(-j2\pi r/\lambda\cos(\varphi-\varphi_i))$, $i=1\dots N_{\mathrm{a}}$ where the antennas are arranged on a circle with radius r and angles φ_i, and λ is the wavelength. Now we can obtain the respective DoA CRB for parallel processing, $\mathrm{CRB}_{\mathrm{PL}}$, using [16, eq. 5]. In accordance with our signal model for sectorized antennas (see Section II-B), we moreover set the array output covariance [16, eq. 1] to $\mathbf{R}=\gamma_k\mathbf{b}\mathbf{b}^{\mathrm{H}}+\sigma_{\mathrm{w}}^2\mathbf{I}$. Through straightforward calculations we then notice that the CRB is inversely proportional to the SNR, i.e., $\mathrm{CRB}_{\mathrm{PL}}\sim\mathrm{SNR}^{-1}$. Therefore, asymptotically for large SNR we have $\mathrm{CRB}_{\mathrm{PL}}^{\mathrm{SNR}}=0$. This is different compared to the CRB for sectorized antennas, which is non-zero even in the asymptotic case as discussed above. This behavior is also visible in the respective $\mathrm{RMSE}_{\mathrm{PL}}$ curve in Fig. 7. Furthermore, one can observe that under the made assumptions, sequential processing with sectorized antennas actually outperforms parallel processing with the UCA for low SNRs. This result is, however, strongly dependent on the assumed antenna characteristics, namely the number of antenna units N_{a} and steering vector characteristics in the UCA as well as the exact radiation pattern in the sectorized antenna deployed in the sequential processing. At low SNRs, in general, it is evident that the levels of the side-lobes in the spatial processing characteristics play an important role since the sector powers are strongly influenced by noise. Thus drawing universal and generally-applicable conclusions between the relative performances of parallel and sequential processing approaches is difficult, and is always subject to made assumptions related to the radiation patterns.

A detailed illustration of the influence of M on the performance of DoA estimation is shown in Fig. 8. As before, the approximation for the CRB and the RMSE of SLS are very accurate for all considered values of M. From (27), (29) and (59), we observe that $\mathrm{RMSE}_{\mathrm{DoA}}$, $\mathrm{RMSE}_{\mathrm{RSS}}$ and $\overline{\mathrm{RMSE}}_{\mathrm{SLS}}$ behave approximately proportional to $1/\sqrt{N}$ (for $N\gg 2$). Due to space limitations, we have not included a separate plot for the dependence of the estimation performance on N.

B. Localization

Localization performance is analyzed by numerically averaging the derived CRBs in (46)-(48) over 1000 randomly drawn TX and RX locations. For each set of RX locations we also draw a separate channel realization with channel coefficients that we model according to $|h_k|^2 = c_0 d_k^{-\alpha}10^{-F_k/10}$, where c_0 is the (constant) average multiplicative gain at reference distance, α is the path loss exponent, and $10^{-F_k/10}$ is the i.i.d. log-normal shadowing with $F_k\sim\mathcal{N}(0,\sigma_{\mathrm{f}}^2)$. Similarly, we obtain the RMSE of SLS-ST location estimation by numerically averaging over 500 randomly drawn RX locations, each with 100 random sector-power realizations. Thereby, we assume the following basic parameter settings. The RXs are uniformly placed inside a circle of radius $R=150$ m with a protective region $R_0=5$ m, centered around the TX with location $\boldsymbol{\ell}_{\mathrm{P}}=[0,0]^{\mathrm{T}}$ for simplicity and without loss of generality. The Tx transmit power σ_{s}^2 is $+20$ dBm (100 mW) and the signal occupies a bandwidth of $B=20$ MHz. On the RX side, the measurement noise power σ_{w}^2 is -70 dBm (100 pW), the sampling frequency is assumed to be $f_{\mathrm{s}}=\frac{1}{B}$, the RX antennas have $M=6$ sectors and a side sector suppression of $a_{\mathrm{s}}=0.4$. The path-loss exponent is $\alpha=4$ and for now the shadowing standard deviation is $\sigma_{\mathrm{f}}=0$ dB. Later in this section, we will also analyze the impact of shadowing on the localization performance. Based on these parameters, the average SNR can easily be shown to be $\overline{\mathrm{SNR}}=10\log_{10}\left(\frac{2}{\alpha-2}\frac{\sigma_{\mathrm{s}}^2}{\sigma_{\mathrm{w}}^2}\frac{R_0^{2-\alpha}-R^{2-\alpha}}{R^2-R_0^2}\right)=33$ dB.

Fig. 9 depicts the localization performance as a function of the number of RXs, K. Increasing K leads to a better performance, however, the biggest gain is achieved in the range $K<20$. In general, the CRB on localization is practically identical with the approximation (47), i.e. $\mathrm{RMSE}\approx\mathrm{RMSE}_{\mathrm{R}}$. This means that the knowledge of the sector-power covariance (12) is essentially not significant for the localization. In contrast to DoA estimation, the knowledge of the RSSs, however, is actually beneficial for localization, i.e. $\mathrm{RMSE}_{\mathrm{L}}<\mathrm{RMSE}$. Nevertheless, the difference between the bounds (46) and (48) is not very significant such that, besides $\mathrm{RMSE}_{\mathrm{R}}$, $\mathrm{RMSE}_{\mathrm{L}}$ also serves as an approximation of the localization CRB with reasonable accuracy. From Fig. 9, we furthermore observe that the performance of SLS-ST seems to saturate at a higher level than the CRBs. This can in part be explained by the fact that SLS does not efficiently utilize large SNRs (see Section VII-A). As a consequence, SLS-ST also does not fully benefit from RXs with high SNR that become increasingly likely with increasing K. Additionally, the gap between the CRBs and SLS-ST indicates that the intermediate step of turning the sector-powers into DoA estimates, and communicating those to the FC, limits the performance of localization. This is supported by the fact that, for a given set of DoAs and RSSs, Stansfield is known to achieve the respective CRB asymptotically in K [4]. Furthermore, as we have seen earlier, the performance of SLS is quite close to the DoA/RSS CRB. Hence, the combination of SLS and Stansfield should yield close-to-optimal results in a localization system where estimated DoAs and RSSs are

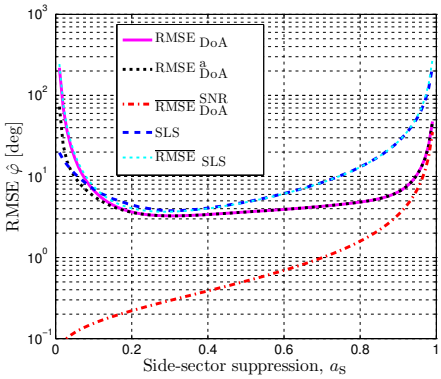

Fig. 5: Performance of DoA estimation as a function of the side-sector suppression a_s for a uniform distribution of DoAs. Parameters: $M = 6$, $N = 100$, SNR $= 5$ dB.

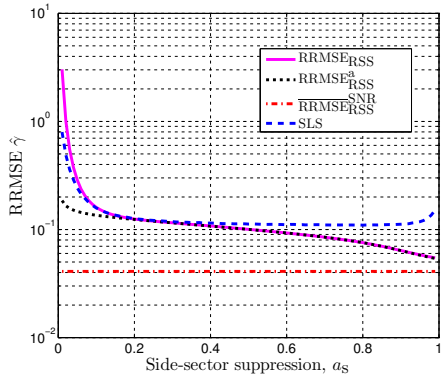

Fig. 6: Performance of RSS estimation as a function of the side-sector suppression a_s for a uniform distribution of DoAs. Parameters: $M = 6$, $N = 100$, SNR $= 5$ dB.

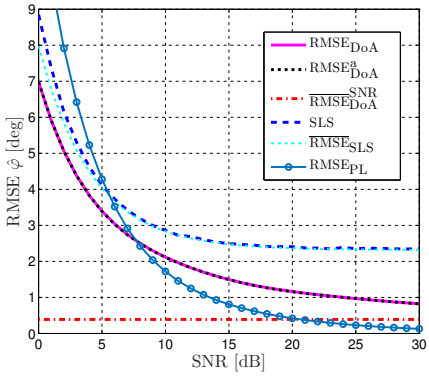

Fig. 7: Performance of DoA estimation as a function of the SNR for a uniform distribution of DoAs. Parameters: $a_\mathrm{s} = 0.4$, $M = 6$, $N = 100$.

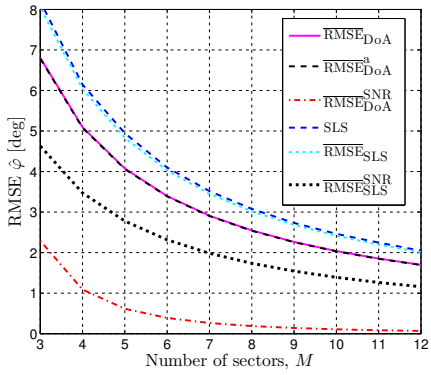

Fig. 8: Performance of DoA estimation as a function of the number of sectors M for a uniform distribution of DoAs. Parameters: $a_\mathrm{s} = 0.4$, $N = 100$, SNR $= 5$ dB.

communicated instead of sector-powers. In Section III, we have shown, by means of Neyman-Fisher factorization, that sector-powers at individual RXs are a sufficient statistic for localization. However, to the best of our knowledge, such a factorization is not possible for DoA/RSS estimates. Thus, the observed gap in performance between SLS-ST and the CRB can also be understood as a consequence of sector-powers being a sufficient statistic for localization (at individual RXs) while DoA/RSS estimates are not.

Fig. 10 shows the relationship between the number of samples and the localization performance. Up to $N = 200$ samples, the performance of the localization system increases significantly with increasing N, for both the CRB and SLS-ST. However, for $N > 200$, the increase in performance flattens out. We hence conclude that a localization system with $N < 200$ provides a good performance/complexity trade-off. Fig. 11 depicts the performance of localization as a function of the number of sectors, M. As expected, the performance improves with increasing M. Similarly, to what we have observed for N, the improvement in localization performance flattens out for larger M such that, e.g., antennas with $M = 10$ sectors seem like a good performance/complexity trade-off.

Fig. 12 illustrates the influence of shadowing on the localization performance. Since shadowing results in additional randomness in the simulations, we have increased the number of randomly drawn TX locations, RX locations and channel realizations from 1000 to 5000. Note that for a shorter run time of the simulations, we have not calculated the exact CRB, but only the two approximations $\mathrm{RMSE_R}$ and $\mathrm{RMSE_L}$. As discussed earlier, $\mathrm{RMSE} \approx \mathrm{RMSE_R}$, which we confirmed also for $\sigma_\mathrm{f} \neq 0$ by simulations with less realizations than the ones depicted in Fig. 12. A channel with shadowing standard deviation $\sigma_\mathrm{f} \neq 0$ results in a spread of the SNRs such that it becomes more probable for the RXs to observe larger as well as smaller SNRs. As can be seen in Fig. 12, this SNR spread does not affect the localization CRB significantly. While this might seem surprising at first it is well in line with [4], where the localization CRB for digitally controlled antenna arrays was observed to even decrease with increasing σ_f. For the SLS-ST estimator, on the contrary, an increase of σ_f results in a decreased performance. This is explained by the nonlinear relationship between SNR and DoA estimation performance,

which we have observed in Fig. 7. As a consequence of this nonlinearity, the spread of the SNR results in worse DoA estimates due to lower SNRs that, on average, cannot be compensated by the better DoAs due to higher SNRs.

VIII. Conclusion

In this article we have thoroughly investigated the performance of DoA/RSS estimation and TX localization using RX devices that are equipped with sectorized antennas. Towards that end, we first derived the CRBs on DoA/RSS estimation with sectorized antennas and studied their asymptotic behavior. We then developed an accurate expression for the mean squared error of a practical DoA estimation algorithm, the SLS algorithm, compared its performance to the bound and determined the algorithm's asymptotic properties. Finally, we derived the localization CRB in a general form that encompasses scenarios where the location is directly estimated from the so-called sector-powers as well as two-step scenarios where each RX device individually estimates the DoA/RSS, which are then centrally fused into a location estimate. A comparison of a two-step localization algorithm to the CRB reveals that skipping the intermediate DoA/RSS estimation step may improve the overall localization performance. Moreover, we provided simple and accurate approximations for all CRBs. Overall, we believe that the insights gained in this paper and the derived performance bounds will help to understand, design and improve the performance of sectorized antenna based localization algorithms and systems.

Appendix A
Derivation of Sector-Power Covariance

The covariance of sector-powers originating from sector j at RX i and sector l at RX k is equal to

$$\begin{aligned}\mathrm{E}\left[(\epsilon_{i,j}-g_{i,j})(\epsilon_{k,l}-g_{k,l})\right] &= \mathrm{E}\left[\epsilon_{i,j}\epsilon_{k,l}\right]-g_{i,j}g_{k,l}\\ &= 2R_{ijkl}+2M_{ijkl}-g_{i,j}g_{k,l} \end{aligned} \tag{64}$$

with the terms

$$\begin{aligned}R_{ijkl} &= \frac{1}{N^2}\sum_{m=0}^{N-1}\sum_{n=0}^{N-1}\mathrm{E}\left[\Re\left\{\tilde{r}_{i,j}(nT_\mathrm{s})\right\}^2\Re\left\{\tilde{r}_{k,l}(mT_\mathrm{s})\right\}^2\right]\\ &= \frac{1}{N^2}\sum_{m=0}^{N-1}\sum_{n=0}^{N-1}\mathrm{E}\left[\Im\left\{\tilde{r}_{i,j}(nT_\mathrm{s})\right\}^2\Im\left\{\tilde{r}_{k,l}(mT_\mathrm{s})\right\}^2\right]\end{aligned} \tag{65}$$

$$\begin{aligned}M_{ijkl} &= \frac{1}{N^2}\sum_{m=0}^{N-1}\sum_{n=0}^{N-1}\mathrm{E}\left[\Re\left\{\tilde{r}_{i,j}(nT_\mathrm{s})\right\}^2\Im\left\{\tilde{r}_{k,l}(mT_\mathrm{s})\right\}^2\right]\\ &= \frac{1}{N^2}\sum_{m=0}^{N-1}\sum_{n=0}^{N-1}\mathrm{E}\left[\Im\left\{\tilde{r}_{i,j}(nT_\mathrm{s})\right\}^2\Re\left\{\tilde{r}_{k,l}(mT_\mathrm{s})\right\}^2\right]\end{aligned} \tag{66}$$

where the interchangeability of real and imaginary signal parts is due to the assumption of a circularly symmetric signal. We then obtain for $i\neq k\vee j\neq l$

$$\begin{aligned}R_{ijkl} = \frac{\rho_{i,j}\rho_{k,l}}{N^2}\sum_{m=0}^{N-1}\sum_{n=0}^{N-1}\mathrm{E}\left[\Re\left\{\tilde{s}_{i,j}(nT_\mathrm{s})\right\}^2\Re\left\{\tilde{s}_{k,l}(mT_\mathrm{s})\right\}^2\right]\\ +\frac{1}{4}\left(\rho_{i,j}\gamma_i+\rho_{k,l}\gamma_k\right)\sigma_\mathrm{w}^2+\frac{1}{4}\sigma_\mathrm{w}^4\end{aligned} \tag{67}$$

$$M_{ijkl} = \frac{1}{4}\rho_{i,j}\gamma_i\rho_{k,l}\gamma_k+\frac{1}{4}\left(\rho_{i,j}\gamma_i+\rho_{k,l}\gamma_k\right)\sigma_\mathrm{w}^2+\frac{1}{4}\sigma_\mathrm{w}^4 \tag{68}$$

and for $i=k\wedge j=l$

$$\begin{aligned}R_{ijij} = \frac{\rho_{i,j}^2\gamma_k^2}{N^2}\sum_{m=0}^{N-1}\sum_{n=0}^{N-1}\mathrm{E}\left[\Re\left\{\tilde{s}_{i,j}^2(nT_\mathrm{s})\right\}\Re\left\{\tilde{s}_{i,j}^2(mT_\mathrm{s})\right\}\right]\\ +\rho_{i,j}\gamma_i\frac{N+2}{2N}\sigma_\mathrm{w}^2+\frac{N+2}{4N}\sigma_\mathrm{w}^4\end{aligned} \tag{69}$$

$$M_{ijij} = \frac{1}{4}\rho_{i,j}^2\gamma_i^2+\frac{N+2}{2N}\rho_{i,j}\gamma_i\sigma_\mathrm{w}^2+\frac{N+2}{4N}\sigma_\mathrm{w}.^4 \tag{70}$$

Given our stationary signals and noting the easily verified identity

$$\sum_{m=0}^{N-1}\sum_{n=0}^{N-1}f(n-m) = Nf(0)+\sum_{p=1}^{N-1}(N-p)\left[f(p)+f(-p)\right] \tag{71}$$

that holds for any function $f:\mathbb{N}\to\mathbb{R}$, we can then obtain equations (12)-(18) by using (67)-(70) in (64). ■

Appendix B
Derivation of Asymptotic Bounds

First we derive the DoA estimation CRB for asymptotic SNR. With $\lim_{\mathrm{SNR}_k\to\infty}a_{k,m}=1$ we get

$$\lim_{\mathrm{SNR}_k\to\infty}\left(\mathbf{\Gamma}^{-1}\right)_{11} = \frac{\beta^4}{16(N+2)\left[\kappa_2(\varphi_k)-\frac{1}{M}\left[\kappa_1(\varphi_k)\right]^2\right]} \tag{72}$$

Due to the periodicity of $\kappa_p(\varphi_k)$, we can equally write $\kappa_p(\varphi_k)=\sum_{m=1}^{M}\left[\mathcal{P}(\varphi_k)-\vartheta_m\right]^p$, which is easier to handle mathematically than the earlier expression in Lemma 1. We then obtain

$$\lim_{\mathrm{SNR}_k\to\infty}\left(\mathbf{\Gamma}^{-1}\right)_{11} = \frac{\beta^4}{16(N+2)\sum_{m=1}^{M}\vartheta_m^2} \tag{73}$$

since $\sum_{m=1}^{M}\vartheta_m=0$. For both even and odd M, we obtain $\sum_{m=1}^{M}\vartheta_m^2=\frac{\Delta^2\vartheta M}{12}(M^2-1)$, where we have used the well-known identities $\sum_{m=1}^{M}m=\frac{1}{2}M(M+1)$ and $\sum_{m=1}^{M}m^2=\frac{1}{6}M(M+1)(2M+1)$. Finally, we can solve (72) and are then able to obtain the RMSE (31). In a similar fashion, we can derive the RSS estimation CRB for asymptotic SNR as

$$\lim_{\mathrm{SNR}_k\to\infty}\left(\mathbf{\Gamma}^{-1}\right)_{22} = \frac{\gamma_k^2}{N+2}\left[\frac{1}{\sum_{m=1}^{M}\vartheta_m^2}\left[\mathcal{P}(\varphi_k)\right]^2+\frac{1}{M}\right]. \tag{74}$$

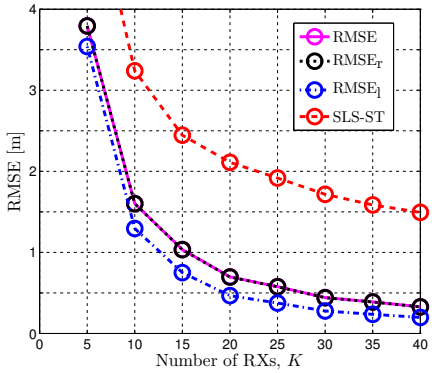

Fig. 9: Performance of localization as a function of the number of RXs for a uniform distribution of RXs. Parameters: $a_\mathrm{s} = 0.4$, $M = 6$, $N = 100$, $\sigma_\mathrm{f} = 0$ dB.

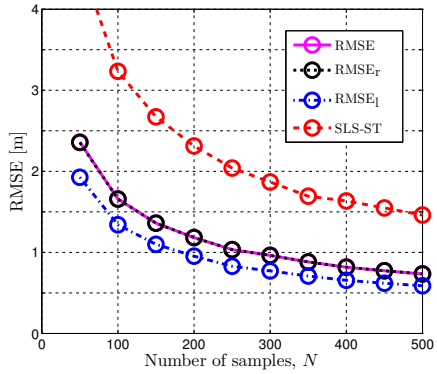

Fig. 10: Performance of localization as a function of the number of samples N for a uniform distribution of RXs. Parameters: $a_\mathrm{s} = 0.4$, $K = 10$, $M = 6$, $\sigma_\mathrm{f} = 0$ dB.

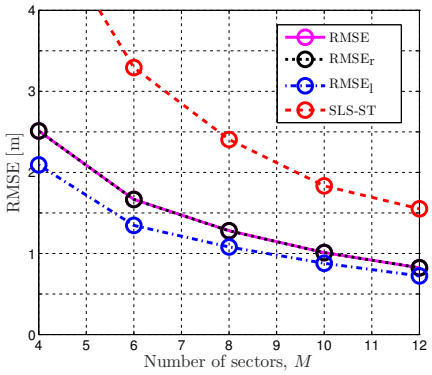

Fig. 11: Performance of localization as a function of the number of sectors M for a uniform distribution of RXs. Parameters: $a_\mathrm{s} = 0.4$, $K = 10$, $\sigma_\mathrm{f} = 0$ dB.

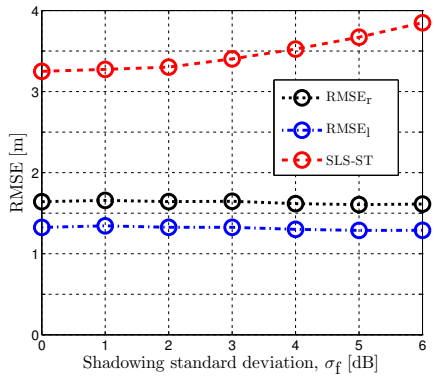

Fig. 12: Performance of localization as a function of the shadowing standard deviation σ_f for a uniform distribution of RXs. Parameters: $a_\mathrm{s} = 0.4$, $K = 10$, $M = 6$, $N = 100$.

In contrast to (72), (74) depends on the DoA. The average RSS CRB for asymptotic SNR is calculated through integration over the period of $\kappa_p(\varphi_k)$, i.e.

$$\frac{1}{\Delta\vartheta}\int_{-\Delta\vartheta/2}^{\Delta\vartheta/2}\lim_{\mathrm{SNR}_k\to\infty}\left(\mathbf{\Gamma}^{-1}\right)_{22}d\varphi_k, \tag{75}$$

which finally yields the RRMSE (33). ■

Appendix C
Derivation of SLS DoA Estimation Bias

It is easy to show that $\mathrm{E}[\tilde{\varphi}_k]$ can be written as

$$\mathrm{E}[\tilde{\varphi}_k] = \bar{\vartheta}_{ij} + \frac{2\kappa}{\beta^2}\left[\mathcal{M}(\varphi-\vartheta_j)^2 - \mathcal{M}(\varphi-\vartheta_i)^2\right]. \tag{76}$$

Next we choose $\vartheta_j = 0$ and $\vartheta_i = \Delta\vartheta$. Since our antenna was assumed to have equal sectors and since the mapping of angles is arbitrary, this choice does not result in a loss of generality but simplifies the handling of $\mathcal{M}(\varphi-\vartheta_m)$, $m = i, j$. Recalling our earlier assumption that $\vartheta_j < \varphi_k < \vartheta_i$ we can now write $\mathcal{M}(\varphi-\vartheta_m)^2 = (\varphi-\vartheta_m)^2$. Therefore, we obtain

$$\mathrm{E}[\tilde{\varphi}_k] = \frac{\Delta\vartheta}{2}\frac{2\kappa}{\beta^2}\left[2\Delta\vartheta\varphi - \Delta^2\vartheta\right] \tag{77}$$

from where we arrive at (55) through straightforward calculations. ■

References

[1] L. Kaplan, "Global node selection for localization in a distributed sensor network," *IEEE Trans. Aerosp. Electron. Syst.*, vol. 42, no. 1, pp. 113–135, Jan. 2006.

[2] H. Celebi and H. Arslan, "Utilization of location information in cognitive wireless networks," *IEEE Wireless Commun. Mag.*, vol. 14, no. 4, pp. 6–13, Aug. 2007.

[3] R. Stansfield, "Statistical theory of d.f. fixing," *J. Institution Elect. Engineers - Part IIIA: Radiocommunication*, vol. 94, no. 15, pp. 762–770, Mar. 1947.

[4] J. Wang, J. Chen, and D. Cabric, "Cramer-Rao bounds for joint RSS/DoA-based primary-user localization in cognitive radio networks," *IEEE Trans. Wireless Commun.*, vol. 12, no. 3, pp. 1363–1375, Mar. 2013.

[5] A. Weiss, "On the accuracy of a cellular location system based on RSS measurements," *IEEE Trans. Veh. Technol.*, vol. 52, no. 6, pp. 1508–1518, Nov. 2003.

[6] R. Martin and R. Thomas, "Algorithms and bounds for estimating location, directionality, and environmental parameters of primary spectrum users," *IEEE Trans. Wireless Commun.*, vol. 8, no. 11, pp. 5692 –5701, Nov. 2009.
[7] F. Penna and D. Cabric, "Bounds and tradeoffs for cooperative DoA-only localization of primary users," in *Proc. IEEE Global Telecommunications Conf., GLOBECOM*, 2011, pp. 1–5.
[8] J. Werner, A. Hakkarainen, and M. Valkama, "Cramer-Rao bounds for hybrid RSS-DOA based location and transmit power estimation in cognitive radio systems," in *Proc. IEEE 78th Vehicular Technology Conf., VTC Fall*, 2013.
[9] R. Schmidt, "Multiple emitter location and signal parameter estimation," *IEEE Trans. Antennas Propag.*, vol. 34, no. 3, pp. 276 – 280, Mar. 1986.
[10] J. Werner, J. Wang, A. Hakkarainen, M. Valkama, and D. Cabric, "Primary user localization in cognitive radio networks using sectorized antennas," in *Proc. 10th Annu. Conf. on Wireless On-demand Network Systems and Services, WONS*, 2013, pp. 155–161.
[11] ——, "Primary user DoA and RSS estimation in cognitive radio networks using sectorized antennas," in *Proc. 8th Int. Conf. on Cognitive Radio Oriented Wireless Networks, CROWNCOM*, 2013, pp. 43–48.
[12] K. Gotsis, K. Siakavara, and J. Sahalos, "On the direction of arrival (DoA) estimation for a switched-beam antenna system using neural networks," *IEEE Trans. Antennas Propag.*, vol. 57, no. 5, pp. 1399–1411, May 2009.
[13] D. Piazza, D. Michele, and K. Dandekar, "Two port reconfigurable CRLH leaky wave antenna with improved impedance matching and beam tuning," in *Proc. 3rd European Conf. Antennas and Propagation, EuCAP*, 2009, pp. 2046–2049.
[14] T. Ohira, "Adaptive array antenna beamforming architectures as viewed by a microwave circuit designer," in *Proc. 2000 Asia-Pacific Microwave Conf.*, 2000, pp. 828 –833.
[15] P. Stoica and N. Arye, "MUSIC, maximum likelihood, and Cramer-Rao bound," *IEEE Trans. Acoust., Speech, Signal Process.*, vol. 37, no. 5, pp. 720–741, 1989.
[16] P. Stoica, E. Larsson, and A. Gershman, "The stochastic CRB for array processing: a textbook derivation," *IEEE Signal Process. Lett.*, vol. 8, no. 5, pp. 148–150, May 2001.
[17] J. Wang, J. Werner, M. Valkama, and D. Cabric, "Performance analysis of primary user RSS/DoA estimation and localization in cognitive radio networks using sectorized antennas," *IEEE Wireless Commun. Lett.*, vol. 3, no. 2, pp. 237–240, Apr. 2014.
[18] A. Hakkarainen, J. Werner, N. Gulati, D. Patron, D. Pfeil, H. Paaso, A. Mammela, K. Dandekar, and M. Valkama, "Reconfigurable antenna based DoA estimation and localization in cognitive radios: Low complexity algorithms and practical measurements," in *Proc. 9th Int. Conf. on Cognitive Radio Oriented Wireless Networks, CROWNCOM*, 2014.
[19] A. B. Carlson and P. B. Crilly, *Communication systems: an introduction to signals and noise in electrical communication*. Boston: McGraw-Hill Higher Education, 2010.
[20] L.-L. Chuang and Y.-S. Shih, "Approximated distributions of the weighted sum of correlated chi-squared random variables," *Journal of Statistical Planning and Inference*, vol. 142, no. 2, pp. 457–472, Feb. 2012.
[21] S. M. Kay, *Fundamentals of Statistical Signal Processing, Volume I: Estimation Theory*, 1st ed. Prentice Hall, Apr. 1993.
[22] R. Tandra and A. Sahai, "SNR walls for signal detection," *IEEE J. Sel. Areas Commun.*, vol. 2, no. 1, pp. 4–17, 2008.
[23] M. Pätzold, *Mobile radio channels*. Chichester, West Sussex, U.K.; Hoboken, N.J.: Wiley, 2012.
[24] E. Dilaveroglu, "Simple general expression for Cramer-Rao bound in presence of nuisance parameters," *Electronics Letters*, vol. 38, no. 25, pp. 1750–1751, 2002.
[25] D. Zachariah and P. Stoica, "Cramer-Rao Bound Analog of Bayes' Rule," *IEEE Signal Process. Mag.*, vol. 32, no. 2, pp. 164–168, Mar. 2015.
[26] M. Gavish and A. Weiss, "Performance analysis of bearing-only target location algorithms," *IEEE Trans. Aerosp. Electron. Syst.*, vol. 28, no. 3, pp. 817–828, 1992.
[27] "Imaginary error function - MATLAB," 2014. [Online]. Available: http://www.mathworks.com/help/symbolic/mupad_ref/erfi.html

Janis Werner was born in Berlin, Germany, in 1986. He received the Dipl. Ing. degree in electrical engineering from Dresden University of Technology (TUD), Germany in 2011. Currently he is working towards a Ph.D. degree at Tampere University of Technology (TUT), Finland, where he is a researcher at the Department of Electronics and Communications Engineering. His main research interests are localization with an emphasis on directional antenna-based systems as well as the utilization and further processing of location information in future generation mobile networks.

Jun Wang received his B.Eng. degree in electronic information engineering from Beijing University of Technology and M.Phil. degree in electrical engineering from City University of Hong Kong, in 2006 and 2009, respectively. He received his Ph.D. degree in electrical engineering from University of California Los Angeles in 2014, advised by Prof. Danijela Cabric. He joined Broadcom Corporation as a research scientist in wireless communication systems design in 2014. His research interests include acquisition and utilization of primary-user location information and various issues related to spectrum sensing in cognitive radio networks.

Aki Hakkarainen received the M.Sc. (with honors) in Communication Electronics from Tampere University of Technology (TUT), Finland in 2007. From 2007 to 2009, he was working as a RF Design Engineer with Nokia, Salo. From 2009 to 2011, he was working as a Radio System Specialist with Elisa, Tampere. Currently, he is working towards a Ph.D. degree at TUT. He is a Researcher and Doctoral Student at the Department of Electronics and Communications Engineering, TUT. His research interests include digital signal processing methods for RF impairment mitigation and digital signal processing for localization.

Danijela Cabric received the Dipl. Ing. degree from the University of Belgrade, Serbia, in 1998, and the M.Sc. degree in electrical engineering from the University of California, Los Angeles, in 2001. She received her Ph.D. degree in electrical engineering from the University of California, Berkeley, in 2007, where she was a member of the Berkeley Wireless Research Center. In 2008, she joined the faculty of the Electrical Engineering Department at the University of California, Los Angeles, where she is now Associate Professor. Dr. Cabric received the Samueli Fellowship in 2008, the Okawa Foundation Research Grant in 2009, Hellman Fellowship in 2012 and the National Science Foundation Faculty Early Career Development (CAREER) Award in 2012. She serves as an Associate Editor in IEEE Journal on Selected Areas in Communications (Cognitive Radio series) and IEEE Communications Letters, and TPC Co-Chair of 8th International Conference on Cognitive Radio Oriented Wireless Networks (CROWNCOM) 2013. Her research interests include novel radio architecture, signal processing, and networking techniques to implement spectrum sensing functionality in cognitive radios.

Mikko Valkama was born in Pirkkala, Finland, on November 27, 1975. He received the M.Sc. and Ph.D. Degrees (both with honors) in electrical engineering (EE) from Tampere University of Technology (TUT), Finland, in 2000 and 2001, respectively. In 2002, he received the Best Ph.D. Thesis–award by the Finnish Academy of Science and Letters for his dissertation entitled "Advanced I/Q signal processing for wideband receivers: Models and algorithms". In 2003, he was working as a visiting researcher with the Communications Systems and Signal Processing Institute at SDSU, San Diego, CA. Currently, he is a Full Professor and Department Vice-Head at the Department of Electronics and Communications Engineering at TUT, Finland. He has been involved in organizing conferences, like the IEEE SPAWC'07 (Publications Chair) held in Helsinki, Finland. His general research interests include communications signal processing, estimation and detection techniques, signal processing algorithms for software defined flexible radios, cognitive radio, full-duplex radio, radio localization, 5G mobile cellular radio, digital transmission techniques such as different variants of multicarrier modulation methods and OFDM, and radio resource management for ad-hoc and mobile networks.

Publication 2

J. Werner, A. Hakkarainen, J. Wang, N. Gulati, D. Patron, D. Pfeil, K. Dandekar, D. Cabric, and M. Valkama, "Sectorized antenna-based DoA estimation and localization: Advanced algorithms and measurements," in *IEEE Journal on Selected Areas in Communications*, vol. 33, pp. 2272–2286, Nov. 2015.

Sectorized Antenna-based DoA Estimation and Localization: Advanced Algorithms and Measurements

Janis Werner, *Student Member, IEEE*, Jun Wang, Aki Hakkarainen, *Student Member, IEEE*, Nikhil Gulati, *Member, IEEE*, Damiano Patron, *Student Member, IEEE*, Doug Pfeil, Kapil Dandekar, *Senior Member, IEEE*, Danijela Cabric, *Member, IEEE*, and Mikko Valkama, *Member, IEEE*

***Abstract*—Sectorized antennas are a promising class of antennas for enabling direction-of-arrival (DoA) estimation and successive transmitter localization. In contrast to antenna arrays, sectorized antennas do not require multiple transceiver branches and can be implemented using a single RF front-end only, thus reducing the overall size and cost of the devices. However, for good localization performance the underlying DoA estimator is of uttermost importance. In this paper, we therefore propose a novel high performance DoA estimator for sectorized antennas that does not require cooperation between the transmitter and the localizing network. The proposed DoA estimator is broadly applicable with different sectorized antenna types and signal waveforms, and has low computational complexity. Using computer simulations, we show that our algorithm approaches the respective Cramer-Rao lower bound for DoA estimation variance if the signal-to-noise ratio (SNR) is moderate to large and also outperforms the existing estimators. Moreover, we also derive analytical error models for the underlying DoA estimation principle considering both free space as well as multipath propagation scenarios. Furthermore, we also address the fusion of the individual DoA estimates into a location estimate using the Stansfield algorithm and study the corresponding localization performance in detail. Finally, we show how to implement the localization in practical systems and demonstrate the achievable performance using indoor RF measurements obtained with practical sectorized antenna units.**

***Index Terms*—Angle-of-arrival, cognitive radio, directional antennas, direction-of-arrival estimation, leaky-wave antennas, localization, location-awareness, measurements, reconfigurable antennas, sectorized antennas, Stansfield algorithm**

I. Introduction

Transmitter (TX) localization has many application areas [1], [2]. In many of those areas, it is desired that the TX location is estimated based on observing or measuring the transmission alone, without any direct collaboration or feedback signaling between the TX and localization network. In cognitive radio networks, as an example, the primary user (PU) cannot be expected to cooperate with the secondary network. Nevertheless, PU location information has been identified as one of the key requirements to enable several advanced functionalities in cognitive radio networks [2]. Other good examples of TX localization are spectrum enforcement, surveillance, first responder operations as well as transportation and navigation.

The location of a non-cooperative TX can generally be estimated by measuring time-difference-of-arrival (TDoA) [3], received-signal-strength (RSS) [4], [5], direction-of-arrival (DoA) [6] or combinations thereof [7], [8]. However, TDoA measurements require accurate timing synchronization in the localizing network itself [7]. In order to avoid the increased complexity associated with synchronization, most recent research has therefore focused on RSS [4], [5] and DoA-based localization [6]–[8]. Intuitively and as shown also in, e.g., [6]–[8], the accuracy of DoA-based localization systems is strongly determined by the quality of DoA estimates. Therefore, this paper will thoroughly investigate advanced DoA estimation algorithms and their application and performance in localization systems.

Traditional approaches of DoA estimation such as the popular MUSIC algorithm [9] require digitally controlled antenna arrays (DCAA). For accurate DoA estimation, the DCAAs must be equipped with a large number of antennas, each with a complete receiver branch [10]. However, the associated hardware complexity of such an implementation might be infeasible in handheld devices. We have therefore recently proposed to use so-called sectorized antennas for DoA estimation [11]–[13]. A sectorized antenna is an abstraction that encompasses all types of antennas that can receive energy selectively within an angular sector. Thereby, it is not required that different sectors can receive the signal in a time-parallel manner. Sectorized antennas can, consequently, be implemented with a single RF front-end only and are therefore generally much less hardware-intensive than DCAAs. Practical examples of sectorized antennas are reconfigurable antennas such as leaky-wave antennas (LWAs) [14] or electronically steerable parasitic array radiators (ESPARs) [15] as well as switched-beam systems (SBSs) [16] or antenna arrays with a single RF front-end [17], [18].

Manuscript received August 15, 2014; revised December 7, 2014. This work was supported by the Doctoral Program of the President of Tampere University of Technology, the Tuula and Yrjö Neuvo Fund, the Nokia Foundation, the Academy of Finland under the project 251138 "Digitally-Enhanced RF for Cognitive Radio Devices" and the Finnish Funding Agency for Technology and Innovation (Tekes, under the project "Reconfigurable Antenna-based Enhancement of Dynamic Spectrum Access Algorithms"). This work was also supported by the National Science Foundation under Grant No. 1117600 and Grant No. 1147838.

J. Werner, A. Hakkarainen and M. Valkama are with the Department of Electronics and Communications Engineering, Tampere University of Technology, FI-33101 Tampere, Finland (email: {janis.werner, aki.hakkarainen, mikko.e.valkama}@tut.fi).

J. Wang and D. Cabric are with the Department of Electrical Engineering, University of California Los Angeles, CA 90095, USA (email: eejunwang@ucla.edu, danijela@ee.ucla.edu).

N. Gulati, D. Patron, D. Pfeil and K. Dandekar are with the Department of Electrical and Computer Engineering, Drexel University, Philadelphia, PA 19104, USA (email: {ng54, dp578, dsp36, krd26}@drexel.edu)

In the literature, various DoA estimators for sectorized antennas have been proposed. However, most of these estimators were developed for a specific type of sectorized antenna and some are moreover restricted to specific signal types or require a cooperating TX. In [19] the angle-dependent frequency response of an LWA is exploited to estimate the DoA of a wideband pulsed signal. The algorithms in [15], [20], [21] require a cooperating TX that sends the same signal repeatedly, such that the signal is received in all sectors of an ESPAR [15] or an LWA [20], [21]. In that way, the antennas can be used to emulate a DCAA and subsequent MUSIC DoA estimation becomes possible. DoA estimation of multiple DS-CDMA signals impinging on a base station equipped with an SBS is considered in [16]. However, the estimator in [16] requires either the RSS to be known or an additional omnidirectional antenna at the receiver in order to normalize the received signals properly. In [22], [23] different DoA estimators for antenna arrays with a single RF front-end are compared based on simulations with advanced propagation modeling [22], [23] and open field measurements [23]. Analog DoA estimation with an LWA is proposed in [24]. Since the estimation is performed by continuously changing the antenna's beam, the algorithm is not applicable to all sectorized antennas. In addition, the associated measurement process takes longer time than a measurement in sectors (i.e. in discrete steps). In [11], [22], [25] an estimator is considered that estimates the DoA as the orientation of the sector with the maximum power measurement. In accordance with [11], we refer to this algorithm as the maxE estimator. While maxE has very low computational complexity, its performance is ultimately limited by the number of sectors and is far from the performance bounds as discussed in detail in [11] and [12].

Another DoA estimator for sectorized antennas, namely the simplified least squares (SLS) estimator, was proposed in [12]. SLS builds on the assumption that only a few sectors receive the TX signal at a sufficiently high SNR, while the attenuation in the other sectors is too high to exploit the TX signal component. Based on this assumption, SLS measures the powers in all sectors and discards all sector-powers except for the maximum two. The ratio of the two remaining sector-powers is then used in a least-squares formulation to estimate the DoA. SLS has been shown to outperform the estimators in [11], [25], and also closely approaches the Cramer-Rao bound (CRB) for moderate SNRs [12]. However, for high SNRs the performance of SLS saturates and does not achieve the CRB. In addition, our analysis in [12] assumes a somewhat optimal beamwidth for the antenna's main beam. This optimal beamwidth decreases with the number of sectors. However, in practice it is often impossible to change the beamwidth, which is determined by the underlying antenna technology. Instead, the only way to improve DoA estimation performance is to increase the number of sectors while keeping the beamwidth constant. Consequently, the assumption that all but two sectors can be discarded in DoA estimation does not apply for a number of practical scenarios, which severely degrades the performance of SLS DoA estimation for all SNRs. Moreover, the estimators in [11], [12], [25] require a sectorized antenna where the main beam is equally shaped in all sectors. In practice this is not necessarily the case as is evident, e.g., from the LWA in [14].

In this paper, we therefore propose, analyze and test the three-stage SLS (TSLS) DoA estimator for sectorized antennas. TSLS does not make any assumptions about the TX signal, nor does it require sectors with equally shaped radiation patterns. We only require that the main beam of the radiation pattern can be roughly approximated by a Gaussian-shaped curve, an approximation that has been shown feasible for a large number of antennas [11], [26], [27]. For the proposed estimator, we then shown that its performance closely approaches the respective CRB for moderate to large SNR. Finally, this paper demonstrates the application of TSLS in a practical localization system that computes a TX location estimate from TSLS DoA estimates obtained at multiple sensors.

In detail, our contributions in this paper are the following:

- Generalization of the model for sectorized antennas in [11] such that it is also applicable to sectorized antennas where the shape of the main beam varies throughout the sectors.
- We propose and analyze the universal and high-performance TSLS DoA estimator for sectorized antennas. TSLS computes the DoA in three stages. First, TSLS selects the sectors suitable for DoA estimation. Using pairs of these sectors, TSLS subsequently estimates sector-pair DoAs (SP-DoAs) that are then fused together to obtain the final DoA estimate.
- We develop different methods for SP-DoA fusion.
- We derive analytical error models for bias and variance of SP-DoA estimates.
- We analyze the effects of multipath on the underlying DoA estimation principle both analytically and through simulations.
- We study in detail the performance of a complete localization system where TSLS DoA estimates from multiple sensors are combined into a TX location estimate by means of the modified Stansfield algorithm.
- We apply TSLS DoA estimation in practice and demonstrate the achievable localization performance with real-world RF measurements that were obtained in an indoor environment.

This paper is organized as follows. Section II describes the localization system and the sectorized antenna model. The TSLS estimator is introduced in Section III, while the analytical error models for SP-DoA estimation are derived in Section IV. The Stansfield localization algorithm is briefly reviewed in Section V. A thorough performance and complexity evaluation of DoA estimation and localization with TSLS through computer simulations and practical measurements can be found in Section VI and Section VII, respectively. The work is concluded in Section VIII. Details of derivations and proofs can be found in the Appendices A, B and C.

Notation: Throughout this paper, vectors and matrices are written as bold letters. The absolute value of a complex number x is represented as $|x|$, the maximum of two real values x_1 and x_2 is written as $\max(x_1, x_2)$, and $\mathrm{mod}_y(x)$ expresses the remainder of the division x/y. $\mathrm{E}[X]$ and $\mathrm{var}[X]$ denote expected value and variance of the random variable X, while $\mathrm{bias}[\hat{y}] = \mathrm{E}[\hat{y}] - y$ denotes the bias of estimator $\hat{y}$ for a

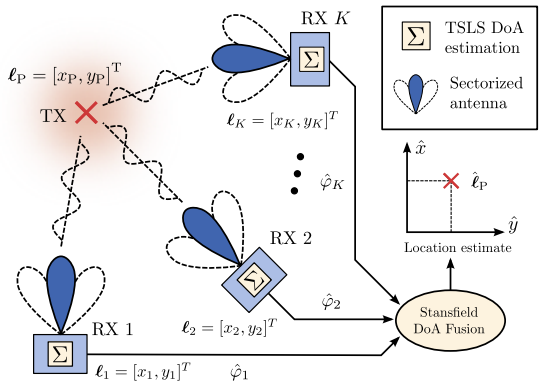

Fig. 1. Considered localization system with K RX units and a single TX.

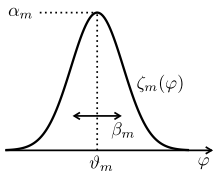

Fig. 2. An illustration of the antenna model (1) for sector m.

deterministic quantity y. $\mathrm{RMSE} = \sqrt{\mathrm{E}[\|\hat{\mathbf{y}} - \mathbf{y}\|^2]}$ denotes the root-mean squared error of an estimator $\hat{\mathbf{y}}$ for a deterministic vector (or scalar) $\mathbf{y}$, where $\|\mathbf{y}\|$ refers to the L^2 norm. We use $|A|$ to denote the cardinality of a set A. The superscripts $(\cdot)^T$ and $(\cdot)^{-1}$ represent transpose and matrix inverse, respectively. The trace of a matrix is expressed as $\mathrm{trace}(\mathbf{M})$, while $\mathrm{diag}(\mathbf{x})$ denotes the diagonal matrix with the elements of vector $\mathbf{x}$ on its diagonal. The symbol $\mathbf{e}_n$ is used to express a vector with 1 in the n-th coordinate and 0s otherwise. Finally, $X \sim \mathcal{N}(\mu_x, \sigma_x^2)$ denotes a Gaussian distributed real random variable with mean μ_x and variance σ_x^2 and $Z \sim \mathcal{CN}(\mu_z, \sigma_z^2)$ denotes a circular symmetric complex Gaussian distributed random variable with mean μ_z and variance σ_z^2.

For the readers' convenience, we have collected the most commonly used abbreviations in Table I.

II. System Model

In this paper, we consider a localization system illustrated in Fig. 1. In this system, K receivers (RXs) with known locations $\boldsymbol{\ell}_k = [x_k, y_k]^\mathrm{T}$, $k = 1, \ldots, K$ collaborate in order to estimate the location, $\boldsymbol{\ell}_\mathrm{P} = [x_\mathrm{P}, y_\mathrm{P}]^\mathrm{T}$, of a non-cooperative TX. With the help of a sectorized antenna, each RX k estimates the TX signal DoA φ_k using the algorithm we propose in Section III. Thereafter, the DoA estimates from all RXs are communicated to a central fusion center, where they are combined into a TX location estimate $\hat{\boldsymbol{\ell}}_\mathrm{P} = [\hat{x}_\mathrm{P}, \hat{x}_\mathrm{P}]^T$ using a modified version of the Stansfield algorithm [11], [28] (see Section V).

As discussed in [11], [26], [27], the main beam of many directional antennas can be well approximated through a Gaussian-like shape. Here, we consider a generalized radiation pattern model that has more degrees of freedom compared to our earlier model (e.g. [11]). Consequently, this new model is well suited for a broader range of practical antennas.

Assume that each sensor is capable of taking measurements in M different sectors. The radiation pattern of sector m, $m = 1, \ldots, M$ is then modeled as

$$\zeta_m(\varphi) = \alpha_m \exp\left(-\left[\mathcal{M}(\varphi - \vartheta_m)\right]^2 / \beta_m^2\right) \tag{1}$$

where β_m is the beamwidth of the main beam, ϑ_m is the orientation and α_m is the attenuation of the antenna in sector m, and $\mathcal{M}(\varphi) = \mathrm{mod}_{2\pi}(\varphi + \pi) - \pi$. An illustration of (1) can be found in Fig. 2. The TSLS DoA estimator, proposed in Section III, estimates SP-DoAs using measurements from two sectors. Hence, for a given sector pair (i, j), $i, j = 1, \ldots, M$, we distinguish between two cases: 1) equal beamwidth sectors (EBS): $\beta_i = \beta_j$ and 2) different beamwidth sectors (DBS): $\beta_i \neq \beta_j$. This distinction is necessary since EBS and DBS require different SP-DoA estimators as will be shown in Section III-B. From (1), the earlier model in [11] is obtained when $\alpha_i = \alpha_j = 1$, $\beta_i = \beta_j$ and $|\Delta\vartheta_{ij}| = |\vartheta_i - \vartheta_j| = \frac{2\pi}{M}$ for all sectors $i, j = 1, \ldots, M$. We will refer to this special class of antennas as equal-sector antennas (ESAs) and parameterize them via the side-sector suppression a_s that determines the beamwidth as $\beta = 2\pi/[M\sqrt{\ln(1/a_\mathrm{s})}]$ [11]. In practice, antennas such as the LWA [14] that we use in our measurements (see Section VII) cannot be modeled as ESAs since the beamwidth as well as the attenuation vary for different sectors. An SBS composed of a circular antenna array, in contrast, has approximately constant α_m and β_m and can hence be modeled as an ESA.

Initially, every RX k computes so-called sector-powers from the N received samples $r_{k,m}(n)$ in sector m according to

$$\epsilon_{k,m} = \frac{1}{N} \sum_{n=0}^{N-1} |r_{k,m}(n)|^2 . \tag{2}$$

In free space, the received signal samples can be modeled as [12]

$$r_{k,m}(n) = \zeta_m(\varphi_k) s_{k,m}(n) + w_{k,m}(n) \tag{3}$$

where $s_{k,m} \sim \mathcal{CN}(0, \gamma_k)$ is the incoming signal impinging with DoA φ_k on RX k in sector m with RSS γ_k, and $w_{k,m}(n) \sim \mathcal{CN}(0, \sigma_\mathrm{w}^2)$ is additive noise. As shown in [12], we can then approximate the distribution of the sector-powers as $\epsilon_{k,m} \sim \mathcal{N}(\tilde{\mu}_{k,m}, \tilde{\sigma}_{k,m}^2)$ with $\tilde{\mu}_{k,m} = \mathrm{E}[\epsilon_{k,m}] = \rho_{k,m}\gamma_k + \sigma_\mathrm{w}^2$ and $\tilde{\sigma}_{k,m}^2 = \mathrm{var}[\epsilon_{k,m}] = \frac{1}{N}\left(\rho_{k,m}\gamma_k + \sigma_\mathrm{w}^2\right)^2$ where $\rho_{k,m} = [\zeta_m(\varphi_k)]^2$.

In multipath scenarios, in contrast, we use the following model for the received signal samples

$$r_{k,m}(n) = \sum_{g=1}^{G} \zeta_{k,m,g} \psi_{k,g} s_{k,m}(n) + w_{k,m}(n) \tag{4}$$

where G is the number of paths, $\zeta_{k,m,g} = \zeta_m(\varphi_{k,g})$ is the attenuation from the mth sector of the kth RX on the DoA of the gth path $\varphi_{k,g}$, and $\psi_{k,g}$ is the power scaling of the gth path. We assume $g = 1$ is the path with the greatest power (e.g. line-of-sight path), so that $\psi_{k,1} > \psi_{k,g}, \forall g > 1$. We further assume path powers sum to unity, i.e., $\sum_{g=1}^{G} \psi_{k,g}^2 = 1$. Note that in (4) we assume the sample time delays among multiple paths are

TABLE I. Most commonly used abbreviations.

CRB	Cramer-Rao bound	PW	power weighting	RSS	received-signal-strength
DBS	different beamwidth sectors	VW	variance weighting	RX/TX	receiver/transmitter
DCAA	digitally controlled antenna arrays	LS	least squares	SBS	switched beam system
		LWA	leaky-wave antenna	SDE	sector-pair DoA estimation
DFU	DoA fusion	MASP	maximum adjacent sector-pair	SLS	simplified least squares
DoA	direction-of-arrival			SNR	signal-to-noise ratio
EBS	equal beamwidth sectors	NCSP	noise-centered sector-powers	SSL	sector selection
ESA	equal sector antenna			SP-DoA	sector-pair DoAs
EW	equal weighting	RMSE	root mean squared error	TSLS	three-stage SLS

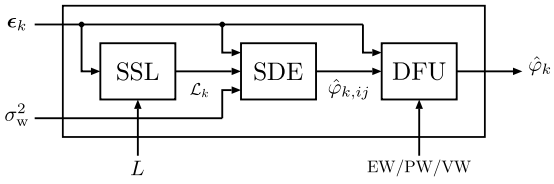

Fig. 3. The three stages of TSLS DoA estimation: sector selection (SSL), SP-DoA estimation (SDE) and DoA fusion (DFU) with the weighting methods equal weighting (EW), power weighting (PW), and variance weighting (VW).

negligible. This assumption is valid when the signal bandwidth is significantly smaller than the channel coherence bandwidth, or all paths with delays greater than the sample period obtain small energies. More complicated multipath signal models with significant delays among paths will be included in our future work. Notice, however, that the above model anyway takes into account the different arriving angles of different multipath components. Similar to the free space scenario, we can approximate the sector-powers as $\epsilon_{k,m} \sim \mathcal{N}(\bar{\mu}_{k,m}, \bar{\sigma}^2_{k,m})$, with $\bar{\mu}_{k,m} = \eta^2_{k,m}\gamma_k + \sigma^2_{\mathrm{w}}$ and $\bar{\sigma}^2_{k,m} = \frac{1}{N}(\eta^2_{k,m}\gamma_k + \sigma^2_{\mathrm{w}})^2$, where $\eta_{k,m} = \sum_{g=1}^{G} \zeta_{k,m,g}\psi_{k,g}$.

For ease of presentation and without loss of generality, we moreover make the following simplifying assumptions in this paper:

- All RXs are equipped with a similar kind of antenna.
- Sector-orientations ϑ_m, $m = 1, \ldots, M$ are the same at all RXs.
- Sectors are numbered in ascending order of their orientation, i.e., $\vartheta_m < \vartheta_{m+1}$, $m = 1, \ldots, M$.

III. Three-Stage SLS DoA Estimation

The underlying principle of TSLS DoA estimation is similar to that of our earlier proposed SLS DoA estimator. In fact, for ESAs and $L = 2$, TSLS results in the same DoA estimates as SLS. However, in contrast to SLS, TSLS DoA estimation can be based on $L > 2$ sectors. As depicted in Figure 3, TSLS first selects a subset $\mathcal{L}_k$, $|\mathcal{L}_k| = L$ of all sectors, subsequently estimates a SP-DoA, $\hat{\varphi}_{k,ij}$, for all sector pairs (i, j), $i, j \in \mathcal{L}_k$, $i \neq j$, and finally obtains the DoA estimate, $\hat{\varphi}_k$, through weighted fusion of the SP-DoAs. The three stages of TSLS DoA estimation are discussed in detail in the following sections.

A. Sector Selection (SSL)

The purpose of SSL is to find the subset $\mathcal{L}_k$ containing the L sectors that are best suited to extract the DoA from their respective sector-powers. Towards that end, SSL first finds the maximum adjacent sector-pair (MASP), i.e., the sector-pair $(q, q+1)$ such that $\epsilon_{k,q}\,\epsilon_{k,q+1} > \epsilon_{k,l}\,\epsilon_{k,l+1}$ for all other sector-pairs $(l, l+1)$, $l = 1, \ldots, M$, $l \neq q$. Thus, when α_m does not vary too strongly with m, $\vartheta_q < \varphi_k < \vartheta_{q+1}$ with high probability. For even L, SSL then returns the sector subset $\mathcal{L}_k = \{q - L/2 + 1, \ldots, q + L/2\}$. For odd L, SSL next estimates whether φ_k is closer to ϑ_q or ϑ_{q+1}. This is achieved by comparing $\epsilon_{k,q}$ and $\epsilon_{k,q+1}$. If $\epsilon_{k,q} > \epsilon_{k,q+1}$ then SSL estimates that $|\varphi_k - \vartheta_q| < |\varphi_k - \vartheta_{q+1}|$ and returns $\mathcal{L}_k = \{q - (L+1)/2 + 1, \ldots, q + (L-1)/2\}$. Otherwise, $\mathcal{L}_k = \{q - (L-1)/2 + 1, \ldots, q + (L+1)/2\}$ is returned. Note that for clarity we have not considered that the sector indices are circular for antennas spanning the whole 360° range, i.e., sector 1 is also adjacent to sector M. However, the extension of the above to the circular case is trivial.

We have compared this SSL method to other methods such as picking the L sectors with the L maximum sector-powers. For the ESA and LWA that we discuss in more detail in Section VI-B, we found that the above described method works best. It is important to note though that the best SSL method for one antenna type might not necessarily be the best for another antenna type. For example, if α_m varies strongly with the sectors m, then another SSL might perform better. On the other hand, if α_l is particularly small in a sector l, then sector l is not suitable for DoA estimation anyways, as the TX signal is severely attenuated in that sector.

B. Sector-Pair DoA Estimation (SDE)

In TSLS a SP-DoA is estimated for all sector-pairs (i, j), $i, j \in \mathcal{L}_k$, $i \neq j$. Towards that end, the noise-centered sector-powers (NCSP) are first calculated as

$$p_{k,i} = \epsilon_{k,i} - \sigma^2_{\mathrm{w}}. \tag{5}$$

Thereafter, NCSPs with $p_{k,i} < 0$ are discarded and the respective sectors are removed from $\mathcal{L}_k$. The SP-DoAs are then obtained as the DoA $\hat{\varphi}_{k,ij}$ that minimizes the squared error of the ratio of NCSPs from sector i and j, i.e.,

$$\hat{\varphi}_{k,ij} = \arg\min_{\varphi} \left(\frac{p_{k,i}}{p_{k,j}} - \frac{\rho_{k,i}(\varphi)}{\rho_{k,j}(\varphi)} \right)^2. \tag{6}$$

In that way, we can estimate the DoA without estimating the RSS, which is also contained in $p_{k,m}$, $m = i, j$ but with good approximation not anymore in the ratio $p_{k,i}/p_{k,j}$. In order to obtain a closed-form solution to (6), we assume that the main beam of the antenna can be approximated through a Gaussian curve, which is possible for many practical antennas [26], [29]. This closed-form solution is different for EBS and DBS as derived in Appendix A.

1) Equal Beamwidth Sectors: The solution of (6) for EBS is straight-forward and is given by

$$\hat{\varphi}_{k,ij} = \bar{\vartheta}_{ij} + \kappa_{ij}\left(\ln\frac{p_{k,i}}{p_{k,j}} - 2\ln\frac{\alpha_i}{\alpha_j}\right) \tag{7}$$

with $\bar{\vartheta}_{k,ij} = \frac{1}{2}(\vartheta_i + \vartheta_j)$ and $\kappa_{ij} = \frac{\beta^2}{4(\vartheta_i - \vartheta_j)}$. For the special case of $\alpha_i = \alpha_j$ we obtain the equation for classical SLS that we have already derived in [11].

2) Different Beamwidth Sectors: For DBS the minimization in (6) results in a quadratic equation and has, hence, two solutions of the form

$$\hat{\varphi}_{k,ij}^{[1/2]} = \lambda_{ij} \pm b_{ij} g(p_{k,i}, p_{k,j}) \tag{8}$$

with

$$g(\mathbf{p}) = \sqrt{(\Delta\vartheta_{ij})^2 - \Delta\beta_{ij}\ln\frac{\alpha_i}{\alpha_j} + \frac{1}{2}\Delta\beta_{ij}\ln\frac{p_{k,i}}{p_{k,j}}}, \tag{9}$$

where $\mathbf{p} = (p_{k,i}, p_{k,j})^T$, $\lambda_{ij} = \frac{\beta_i^2\vartheta_j - \beta_j^2\vartheta_i}{\Delta\beta_{ij}}$, $b_{ij} = \frac{\beta_i\beta_j}{\Delta\beta_{ij}}$, $\Delta\beta_{ij} = \beta_i^2 - \beta_j^2$, and $\Delta\vartheta_{ij} = \vartheta_i - \vartheta_j$. The ambiguity in (8) can be resolved by taking the NCSPs into account. For each of the solutions $\hat{\varphi}_{k,ij}^{[l]}$ $l = 1, 2$, we can estimate two RSSs as $\hat{\gamma}_{k,ij,m}^{[l]} = \frac{p_{k,m}}{\hat{\rho}_{k,ij,m}^{[l]}}$, where $m = i, j$ and $\hat{\rho}_{k,ij,m}^{[l]} = [\alpha_m \exp(-[\mathcal{M}(\hat{\varphi}_{k,ij}^{[l]} - \vartheta_m)]^2/\beta_m^2)]^2$ is the estimated attenuation in sector m given that the DoA is $\hat{\varphi}_{k,ij}^{[l]}$. In the case $N \to \infty$, the two RSS estimates per DoA solution $\hat{\varphi}_{k,ij}^{[l]}$, $l = 1, 2$ are equal, i.e., $\hat{\gamma}_{k,ij,i}^{[l]} = \hat{\gamma}_{k,ij,j}^{[l]}$, if $\hat{\varphi}_{k,ij}^{[l]} = \varphi_k$. Therefore, we choose the solution l in (8) such as to minimize $|\hat{\gamma}_{k,ij,i}^{[l]} - \hat{\gamma}_{k,ij,j}^{[l]}|$. If $g(\mathbf{p})$ becomes imaginary, the respective SP-DoA estimate is discarded.

C. DoA Fusion (DFU)

SDE results in P SP-DoA estimates $\hat{\varphi}_{k,ij} = \varphi_k + \delta\hat{\varphi}_{k,ij}$ that have to be fused together in order to obtain the final DoA estimate. Obviously, it is desirable to give larger weight to those SP-DoA estimates that have a smaller error $\delta\hat{\varphi}_{k,ij}$. However, $\hat{\varphi}_{k,ij}$ are circular random variables such that conventional weighted averaging is not applicable. Instead, we use a weighted fusion method for circular random variables as discussed in [30]:

$$\frac{\sin\hat{\varphi}_k}{\cos\hat{\varphi}_k} = \frac{\sum w_{k,ij}\sin\hat{\varphi}_{k,ij}}{\sum w_{k,ij}\cos\hat{\varphi}_{k,ij}}, \tag{10}$$

where we denote the weights for DoA $\varphi_{k,ij}$ as $w_{k,ij}$. Geometrically, (10) can be interpreted as the summation of P vectors with magnitude $w_{k,ij}$ and angle $\hat{\varphi}_{k,ij}$ in a two-dimensional plane. The resulting vector then has an angle that is equal to the final DoA estimate $\hat{\varphi}_k$. Our simulations have shown that (10) has identical performance to conventional weighted averaging if the error $\delta\hat{\varphi}_{k,ij}$ is very small. However, for large $\delta\hat{\varphi}_{k,ij}$ (10) outperforms conventional weighted averaging significantly. Different choices for the weights $w_{k,ij}$ are discussed next.

1) Equal Weighting (EW): For equal weighting of the SP-DoAs, the weights can simply be set to $w_{k,ij}^{\mathrm{EW}} = 1$.

2) Sector-Power Weighting (PW): Based on the discussion in Section III-A, sector-powers are a good indication for the potential contribution of different sectors in DoA estimation. Consequently, an intuitive and robust weighting scheme for SP-DoA $\hat{\varphi}_{k,ij}$ is the product of NCSPs i and j

$$w_{k,ij}^{\mathrm{PW}} = p_{k,i}p_{k,j}. \tag{11}$$

3) Variance Weighting (VW): If the variance $\sigma_{ij}^2 = \mathrm{var}[\delta\hat{\varphi}_{k,ij}]$ of individual SP-DoA errors is known, a weighting scheme $w_{k,ij} = 1/\sigma_{ij}^2$ can be applied. However, in practice the knowledge of σ_{ij}^2 is not a realistic assumption. In Section IV-A we derive an approximation $v_{k,ij}^{(1)} \approx \sigma_{ij}^2$ of the SP-DoA error variance in free space. This variance can be estimated as $\hat{v}_{k,ij}^{(1)}$, simply by approximating the $\mu_{k,i}$ that is contained in (19) via $a_{k,i}$ as $p_{k,i}$. Thus, a variance-based weighting scheme can be achieved by setting

$$w_{k,ij}^{\mathrm{VW}} = \left(\hat{v}_{k,ij}^{(1)}\right)^{-1}. \tag{12}$$

D. Validity check

In particular for low SNR it is possible that $p_{k,i} < 0\,\forall\, i = 1, \ldots, M$ or that all SP-DoAs are discarded, as discussed in Section III-B2. Then $P = 0$ and DFU stage cannot be executed. In that case, TSLS estimates the DoA using the modified maxE estimator introduced in [31].

IV. Analytical Models for the Error of SP-DoA Estimation

In this section we derive analytical models for the error of the SP-DoA estimates obtained in SDE. Towards that end, we first notice that $p_{k,m}$ is distributed as $p_{k,m} \sim \mathcal{N}(\mu_{k,m}, \sigma_{k,m}^2)$ with $\mu_{k,m} = \mathrm{E}[p_{k,m}] = \rho_{k,m}\gamma_k$ and $\sigma_{k,m}^2 = \mathrm{var}[p_{k,m}] = \frac{1}{N}(\rho_{k,m}\gamma_k + \sigma_{\mathrm{w}}^2)^2$. We then assume that $\sigma_{k,m}^2 \ll \mu_{k,m}$, which holds for sufficiently high SNR and a moderate to large number of samples. Given this assumption, we can approximate the SP-DoA estimate $\hat{\varphi}_{k,ij}$ through its n-th order Taylor series expansion developed around the means $p_{k,i} = \mu_{k,i}$ and $p_{k,j} = \mu_{k,j}$. In our derivation we will be using the following lemma:

Lemma 1: Given an $L \times 1$ random vector $\mathbf{X} \sim \mathcal{N}(\boldsymbol{\mu}, \mathbf{Q})$ with mean vector $\boldsymbol{\mu} = \mathrm{E}[\mathbf{X}]$ and diagonal covariance $\mathbf{Q} = \mathrm{E}[(\mathbf{X} - \boldsymbol{\mu})(\mathbf{X} - \boldsymbol{\mu})^T] = \mathrm{diag}[\sigma_1^2, \ldots \sigma_L^2]$, and the random variable $Y = f(\mathbf{X})$, where $f : \mathbb{R}^{L\times 1} \to \mathbb{R}$. Denote $Y^{(n)}(\boldsymbol{\mu})$ as the n-th order Taylor series of Y around $\boldsymbol{\mu}$, the gradient of Y as $\mathbf{j} = \frac{\partial f}{\partial \mathbf{X}_1}\mathbf{e}_1 + \cdots + \frac{\partial f}{\partial \mathbf{X}_L}\mathbf{e}_L$ and the Hessian matrix of Y as $\mathbf{H}$. Then, we obtain the expected values of the first and second order Taylor series of Y developed around its mean as

$$\mathrm{E}[Y^{(1)}(\boldsymbol{\mu})] = f(\boldsymbol{\mu}) \tag{13}$$

$$\mathrm{E}[Y^{(2)}(\boldsymbol{\mu})] = f(\boldsymbol{\mu}) + \frac{1}{2}\,\mathrm{trace}\,\{\mathbf{H}(\boldsymbol{\mu})\mathbf{Q}\} \tag{14}$$

and the respective variances as

$$\mathrm{var}[Y^{(1)}(\boldsymbol{\mu})] = \sum_l \mathbf{j}_l^2(\boldsymbol{\mu})\sigma_l^2 \tag{15}$$

$$\mathrm{var}[Y^{(2)}(\boldsymbol{\mu})] = \sum_l \mathbf{j}_l^2(\boldsymbol{\mu})\sigma_l^2 + \frac{1}{2}\,\mathrm{trace}\left\{(\mathbf{H}(\boldsymbol{\mu})\mathbf{Q})^2\right\}. \tag{16}$$

A detailed derivation of this lemma can be found in Appendix B.

A. Free Space Propagation

The approximations for bias and variance of SP-DoA estimation that we present in the following are derived for DBS, i.e., the SP-DoA estimator (8). Following similar steps, we can also obtain bias and variance approximations for EBS, i.e., the SP-DoA estimator (7). However, the resulting EBS approximations are in fact equal to the DBSs approximations when noting that $\beta_i = \beta_j$ and therefore replacing $\Delta\beta_{ij} = 0$ in (17)-(20) in the EBS case.

For the derivations, we first assume that the SP-DoA estimated in the SDE stage is the correct one out of the two possibilities in (8), which is a very reasonable assumption as discussed later in Section VI-B. Next, we approximate the SP-DoA through its n-th order Taylor series as $\hat{\varphi}_{k,ij} \approx \hat{\varphi}^{(n)}_{k,ij}$. Using Lemma 1 and following the derivations in Appendix C, we then obtain an approximation of the bias $\mathrm{E}[\hat{\varphi}_{k,ij}] - \varphi_k \approx b^{(n)}_{k,ij} = \mathrm{E}[\hat{\varphi}^{(n)}_{k,ij}] - \varphi_k$ through first and second-order Taylor series as

$$b^{(1)}_{k,ij} = 0 \tag{17}$$

$$b^{(2)}_{k,ij} = \pm\frac{\beta_i\beta_j}{8g(\boldsymbol{\mu})}\left[a_{k,j} - a_{k,i} - \frac{\Delta\beta_{ij}}{4g^2(\boldsymbol{\mu})}(a_{k,i} + a_{k,j})\right] \tag{18}$$

where $a_{k,m} = \frac{1}{N}\left(\mathrm{SNR}^{-1}_{k,m} + 1\right)^2$, $\mathrm{SNR}_{k,m} = \frac{\mu_{k,m}}{\sigma^2_w} = \rho_{k,m}\,\mathrm{SNR}_k$. Using the same approach, we can also approximate the variance of the SP-DoA estimation error through its n-th order Taylor series, i.e., $\mathrm{var}[\hat{\varphi}_{k,ij}] \approx v^{(n)}_{k,ij} = \mathrm{var}\left[\hat{\varphi}^{(n)}_{k,ij}\right]$. For the first and second order Taylor approximations, the variances are then equal to

$$v^{(1)}_{k,ij} = \frac{\beta_i^2\beta_j^2}{16\left[g(\boldsymbol{\mu})\right]^2}(a_{k,i} + a_{k,j}) \tag{19}$$

$$v^{(2)}_{k,ij} = \frac{\beta_i^2\beta_j^2}{16g^2(\boldsymbol{\mu})}\Bigg[a_{k,i} + a_{k,j} + \frac{1}{2}(a^2_{k,i} + a^2_{k,j}) + \frac{\Delta\beta_{ij}}{4g^2(\boldsymbol{\mu})}(a^2_{k,i} - a^2_{k,j}) + \frac{\Delta^2\beta_{ij}}{32g^4(\boldsymbol{\mu})}(a_{k,i} + a_{k,j})^2\Bigg]. \tag{20}$$

The derivation of (19)-(20) is again based on Lemma 1 with the details given in Appendix C.

B. Multipath Propagation

In this subsection we present the bias and variance of SP-DoA estimation when multipath is considered. We present only results for EBS due to their mathematical conciseness. It is straightforward to extend the derivation to DBS. Following Lemma 1, the bias of the SP-DoA using first and second order Taylor approximations are given by

$$\bar{b}^{(1)}_{k,ij} = \bar{\vartheta}_{k,ij} + \kappa_{ij}\left(2\ln\frac{\eta_{k,i}}{\eta_{k,j}} - \ln\frac{\alpha_i}{\alpha_j}\right) - \varphi_{k,1} \tag{21}$$

$$\bar{b}^{(2)}_{k,ij} = \bar{b}^{(1)}_{k,ij} - \frac{1}{2}\left(\frac{\kappa_{ij}\bar{\sigma}^2_{k,i}}{\gamma_k^2\eta^4_{k,i}} - \frac{\kappa_{ij}\bar{\sigma}^2_{k,j}}{\gamma_k^2\eta^4_{k,j}}\right), \tag{22}$$

respectively, where $\varphi_{k,1}$ is the DoA of the strongest path, i.e., the "true" DoA. The variances are equal to

$$\bar{v}^{(1)}_{k,ij} = \frac{\kappa^2_{ij}\bar{\sigma}^2_{k,i}}{\gamma_k^2\eta^4_{k,i}} + \frac{\kappa^2_{ij}\bar{\sigma}^2_{k,j}}{\gamma_k^2\eta^4_{k,j}} \tag{23}$$

$$\bar{v}^{(2)}_{k,ij} = \bar{v}^{(1)}_{k,ij} + \frac{1}{2}\left(\frac{\kappa^2_{ij}\bar{\sigma}^4_{k,i}}{\gamma_k^4\eta^8_{k,i}} + \frac{\kappa^2_{ij}\bar{\sigma}^4_{k,j}}{\gamma_k^4\eta^8_{k,j}}\right). \tag{24}$$

The derivations of (21)-(24) are very similar to Section IV-A and Appendix C, and are thus omitted due to space limitation.

V. Localization

DoA estimates $\hat{\varphi}_k$ from individual sensors k, $k = 1, \ldots, K$, are fused together into a location estimate using a modified version of the Stansfield algorithm [11]. The original Stansfield algorithm was proposed in [28] as an approximation to the maximum likelihood estimator. Its location estimate $\hat{\boldsymbol{\ell}} = (\hat{x}_\mathrm{P}, \hat{y}_\mathrm{P})^T$ is obtained as

$$\hat{\boldsymbol{\ell}} = \left(\mathbf{A}^T\mathbf{W}\mathbf{A}\right)^{-1}\mathbf{A}^T\mathbf{W}\mathbf{b}, \tag{25}$$

with

$$\mathbf{A} = \begin{bmatrix}\sin(\hat{\varphi}_1) & -\cos(\hat{\varphi}_1)\\ \vdots & \vdots\\ \sin(\hat{\varphi}_K) & -\cos(\hat{\varphi}_K)\end{bmatrix}, \tag{26}$$

$$\mathbf{b} = \begin{bmatrix}x_1\sin(\hat{\varphi}_1) - y_1\cos(\hat{\varphi}_1)\\ \vdots\\ x_K\sin(\hat{\varphi}_K) - y_K\cos(\hat{\varphi}_K)\end{bmatrix} \tag{27}$$

and a weighting matrix $\mathbf{W}$. In the original Stansfield algorithm, the weighting matrix is dependent on both the individual TX-RX distances as well as the quality of the DoA estimates. In practice this information is not available for the DoA fusion. Therefore, we use the modified version [11] where the contribution of each sensor k is weighted with an estimate of the sensor's RSS, $\hat{\gamma}_k$. This results in a diagonal weighting matrix $\mathbf{W} = \mathrm{diag}\,(\hat{\gamma}_1, \hat{\gamma}_2, \ldots, \hat{\gamma}_K)$.

VI. Numerical Evaluations and Analysis

As the following presentation builds heavily on previously-defined abbreviations, the reader may refer to Table I for a summary of the most commonly used ones.

A. Error of SP-DoA Estimation

We analyze the error of SP-DoA estimation in free space using two sectors with $\alpha_i = 1$, $\alpha_j = 0.9$, $\beta_i = 1/2$ rad, $\beta_j = 1/3$ rad, $\vartheta_i = 0°$, $\vartheta_j = 20°$ and an incoming signal DoA of $\varphi_k = 10°$. These numbers reflect a realistic example scenario, though any other numerical values could be used as well. Fig. 4 depicts the bias and standard deviation of the SP-DoA estimator proposed in Section III-B. The simulated curves are obtained empirically over 10^6 realizations per SNR-step while the analytical curves are obtained by calculating the first and second order Taylor approximation models derived in Section IV-A.

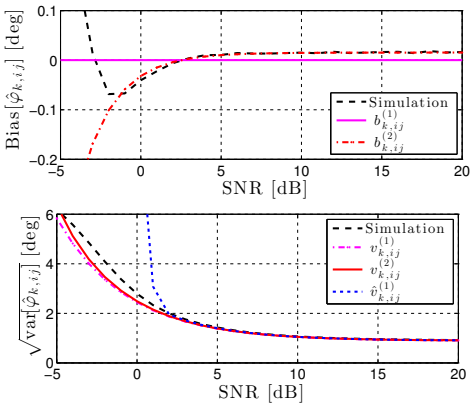

Fig. 4. Analytical and empirical bias and standard deviation of sector-pair DoA estimation in free space.

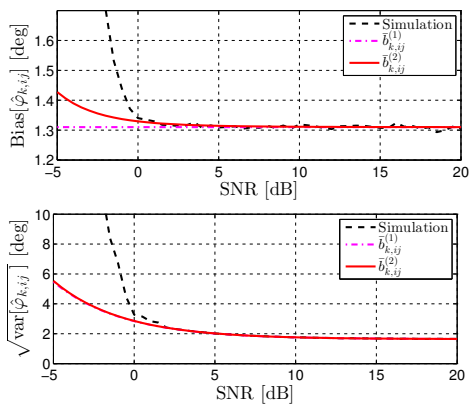

Fig. 5. Analytical and empirical bias and standard deviation of sector-pair DoA estimation with multipath.

We first notice that the SP-DoA estimates are slightly biased, even for large SNR. This bias is nicely described by the 2nd-order Taylor approximation from SNR ≈ -2 dB onwards. The 1st-order approximation, in contrast, fails to model the bias adequately. However, the sectors considered in here are DBS. For EBS, we have $\beta_i = \beta_j$ in (18) such that $b^{(2)}_{k,ij} \to 0$ for SNR $\to \infty$ since $a_{k,i} \to a_{k,j} \to \frac{1}{N}$. Hence, SP-DoA estimation with EBS is asymptotically unbiased for large SNR as we have confirmed already for SLS in [12], [13].

With respect to the variance, both 1st- and 2nd-order Taylor approximations model the behavior very well for low to high SNR. Only for very low SNR < 0 dB, we observe that $v^{(2)}_{k,ij}$ approximates the variance slightly more accurately. For comparison, we have also included the estimate of the 1st-order Taylor variance approximation, $\hat{v}^{(1)}_{k,ij}$ that is calculated according to the discussion in Section III-C3. This estimate is very accurate for SNR > 2 dB. However, for SNRs below 2 dB, the slope of the variance estimates is very steep, resulting in overly pessimistic estimates in the low SNR range. This is a consequence of $a_{k,m}$, $m = i, j$ in the estimation of (19) behaving proportional to $1/p^2_{k,m}$ for low SNRs. Since $p_{k,m}$ is symmetrically distributed around its mean, $a_{k,m}$ is hence on average estimated larger than it actually is. For TSLS DoA estimation this means that a DFU weighting with an estimated 2nd order Taylor approximation variance (20) cannot be beneficial, as $v^{(2)}_{k,ij}$ is only slightly more accurate than $v^{(1)}_{k,ij}$ for SNRs that are anyways already too low to estimate the variance properly.

We next proceed to analyze the error of SP-DoA estimation in multipath scenarios, using two sectors with $\alpha_i = 1$, $\alpha_j = 0.9$, $\vartheta_i = 0°$, $\vartheta_j = 20°$. Since our results for multipath in Section IV-B are for EBS, we calculate the common β of the two sectors from a setting of $M = 6$ and $a_s = 0.4$. We include two paths in our simulations: a line-of-sight path with power scaling $\psi^2_{k,1} = 0.9$ and DoA $\varphi_{k,1} = 10°$, and a reflected path with power scaling $\psi^2_{k,2} = 0.1$ and DoA $\varphi_{k,2} = 15°$. Similarly to our example of free space propagation, these numbers reflect a realistic example scenario. Naturally, other numerical values could be used for multipath propagation as well. Our results of simulated bias and standard deviation, as well as theoretical results using the 1st- and 2nd-order Taylor approximations derived in Section IV-B, are shown in Fig. 5.

We observe that the SP-DoA estimates are more strongly biased in a multipath scenario than in free space, as the bias increased from $0.02°$ in Fig. 4 to $1.3°$ in Fig. 5 for SNR greater than 5 dB. The bias increase is primarily because of the reflected path that is $5°$ away from the main path. Both theoretical bias using the 1st- and 2nd-order Taylor approximations match the empirical simulations for SNR greater than 0 dB. The gap between theoretical and simulation results is smaller for the 2nd-order curve compared to the 1st-order curve. The standard deviation of the SP-DoA estimations under multipath is also greatly increased compared with the free space scenario, e.g., for 10 dB the standard deviation is $1°$ in free space and $2°$ with multipath. Theoretical results using 1st- and 2nd-order Taylor approximations behave similarly, i.e., they match simulations accurately for SNR greater than 0 dB.

Note that the root-mean squared error (RMSE) of SP-DoA estimation will increase in multipath scenarios due to the increased bias and variance. This fact will further affect the TSLS DoA estimation and transmitter localization performance. However, due to space limitation, the following sections only contain simulation results without multipath. In Section VII, the impact of severe multipath on DoA estimation and localization accuracy will be further discussed and elaborated with practical RF measurements.

B. TSLS DoA Estimation Performance

The performance of TSLS DoA estimation is evaluated next using two different antenna models. On the one hand, we study the performance using an ESA with $M = 6$ sectors, each with a radiation pattern as in (1) and $a_s = 0.4$. On the other hand, we consider a model of an actual LWA that we use in the practical measurements in Section VII. The LWA is modeled using the radiation patterns according to (1) with the parameters $\alpha_m = \hat{\alpha}_m$, $\beta_m = \hat{\beta}_m$ and $\vartheta_m = \hat{\vartheta}_m$ shown in Table III. These

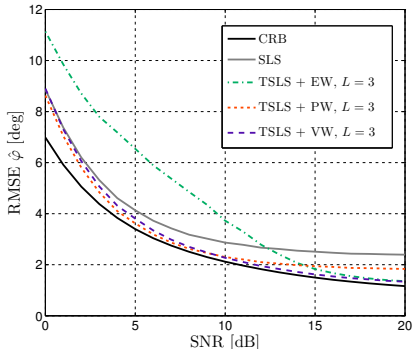

Fig. 6. DoA estimation performance with equal-sector antenna and different algorithms. Parameters: $a_s = 0.4$, $M = 6$, and $N = 100$.

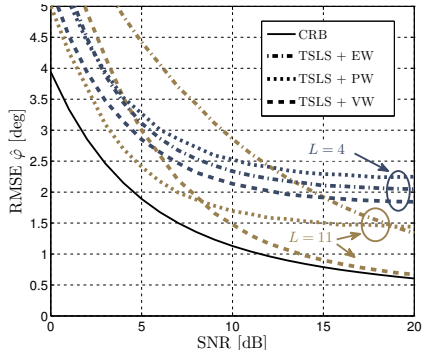

Fig. 7. DoA estimation performance with leaky-wave antenna approximated by Gaussian radiation pattern (1). Parameters: $M = 12$, $N = 100$, and antenna parameters in Table III.

parameters were obtained from a least-squares (LS) fit of the actual radiation pattern as discussed in more detail in Section VII-B. In total, the LWA has $M = 12$ sectors with orientations ranging from roughly $-50°$ to $50°$, making the antenna suitable for DoAs from around $-60°$ to $60°$. In contrast, the ESA covers the entire angular range from $-180°$ to $180°$. However, with respect to TSLS DoA estimation, the main difference between the two models is that the ESA consists entirely of EBS, while the LWA model has only DBS. Therefore, TSLS is run with the SP-DoA estimation as described in Section III-B1 for the former, while the latter uses SP-DoA estimation as discussed in Section III-B2. It is assumed that the DoA is uniformly distributed over the whole angular coverage area of the antennas. We emulate this distribution via 100 equidistant steps in the interval $\varphi_k \in \left[0; \frac{180°}{M}\right)$ for the ESA [12] and 120 equidistant steps in the interval $\varphi_k \in [-60°; 60°)$ for the LWA model. For each DoA-step we then simulate 2000 realizations, and average over the results at each step in order to obtain the RMSE. In the following, we will be using different configurations of TSLS, such as TSLS+EW. Please refer to Fig. 3 for an overview of the configurations and to Section III for detailed descriptions.

Fig. 6 depicts the RMSE of DoA estimation as a function of the SNR when using the ESA. For reference, we have also included the CRB on DoA estimation with sectorized antennas [12], along with the SLS DoA estimator [12]. For TSLS, we have determined that $L = 3$ provides the best performance for moderate to high SNRs in separate simulations that are not explicitly shown due to space limitations. Note that this value is specific to the antenna and in particular its beamwidth as will be discussed later in this section. From the results in [12] it can be concluded that SLS is not making efficient use of high SNRs. In contrast, TSLS with EW in the DFU stage is approaching the CRB for large $\mathrm{SNR} \approx 20$ dB. However, the performance of TSLS+EW degrades rapidly for lower SNRs such that SLS outperforms TSLS+EW already for $\mathrm{SNR} \approx 12$ dB. The combination of TSLS and PW performs best of all algorithms for the low SNR region, while its performance saturates at a higher RMSE than the CRB and the other TSLS configurations, starting from $\mathrm{SNR} \approx 10$ dB. Nevertheless, it outperforms SLS for all SNRs. The overall best performance is achieved with TSLS+VW. For low SNR, TSLS+VW behaves like SLS and performs therefore only slightly worse than TSLS+PW. This is explained by the earlier made observation that the variance is estimated much larger than it actually is when the sector $\mathrm{SNR}_{k,m}$ is low. In the DFU stage and for overall low SNR this therefore leads to an implicit exclusion of all SP-DoAs other than the one used in SLS. For high SNR, on the other hand, TSLS+VW performs like TSLS+EW. This, in turn, is explained by the variance of the SP-DoA estimates that become independent of the sector for very large SNRs and ESAs since $a_{k,m} \to \frac{1}{N}$ for $\mathrm{SNR} \to \infty$ in (19).

The performance of the LWA model as a function of the SNR is shown in Fig. 7. Although the CRB was only discussed for ESAs in [12], it was derived in a generic format such that it is also applicable for our LWA model. Therefore, we have included the CRB as a reference also in this figure. Besides the sector parameters, α_m and β_m varying for different sectors m, the LWA model also has a much bigger overlap between the sectors than the ESA. As an example, the sectors 3 and 4 (Table III) have $\alpha_4 \approx \alpha_3 = 1$ and $\Delta\vartheta_{43} \approx 12°$. With these parameters an ESA would have $M = 30$ sectors, resulting in $\beta \approx 0.22$ rad if we assume the same side-sector suppression $a_s = 0.4$ as for the above described ESA. The LWA antenna, in contrast, has an almost 8-fold larger beamwidth in the sectors 3 and 4. Compared to the ESA, much more sectors of the LWA therefore receive the TX signal at a high SNR. This, in turn, implies that L, i.e., the number of sectors used for SP-DoA estimation, should be increased for the LWA. We have found that parameterizing TSLS with $L = 11$ results in the overall best performance. However, this is not the case over the whole SNR range. Using, e.g., only $L = 4$ sectors, yields a bit better performance for low SNRs if EW or VW is used in the DFU stage of TSLS. When using PW, on the other hand, it seems that the performance is best with $L = 11$ sectors for all SNRs. Otherwise, the behavior of TSLS and its DFU configurations is very similar to what we have observed already for the ESA. Most notably, TSLS+VW approaches the CRB for high SNR

also for LWAs.

The SP-DoA estimator (8) yields two solutions. To verify that our selection mechanism described in Section III-B2 works properly, we have run the same simulations with the actual DoA as an input to TSLS. Out of the two possible solutions in (8), this TSLS test version then picks the one that is closer to the actual DoA. Naturally, this test version yields better performance than the practical implementation. However, the increase in performance is only marginal. Therefore, we can conclude that the selection mechanism based on the RSS works well. For clarity of presentation, we have not included these test curves in Fig. 7.

C. Localization Performance

In this section, we evaluate the performance of localization with TSLS+VW DoA estimation and subsequent Stansfield fusion (TSLS-S). For comparison, we also include the combination of SLS and Stansfield (SLS-S) as well as the CRB on non-cooperative TX localization using sectorized antennas [29]. In our simulation, we assume that the RXs are uniformly distributed on a circle with radius $R = 150$ m centered around the TX. However, no RX is placed in a protective inner circle with radius $R_0 = 5$ m. The TX transmit power is $P_\mathrm{T} = 20$ dBm, while the measurement noise power at the RXs is $\sigma_\mathrm{w}^2 = -70$ dBm. For the propagation, we assume a log-distance path loss model with path loss exponent $\alpha = 4$. Overall, these settings result in an average $\overline{\mathrm{SNR}} = 10\log_{10}\left(\frac{2}{\alpha-2}\frac{P_\mathrm{T}}{\sigma_\mathrm{w}^2}\frac{R_0^{2-\alpha}-R^{2-\alpha}}{R^2-R_0^2}\right) = 33$ dB. The TX signal is modeled as bandlimited Gaussian with a bandwidth $B = 20$ MHz and without oversampling at the RXs. This leads to a correlation of sector-powers at different RXs that we have derived in detail in [29]. As we have seen in Section VI-B, the behavior of the ESA and the LWA in TSLS DoA estimation is qualitatively similar. To keep the simulations simple, we therefore assume that all RXs are equipped with an ESA, parameterized as in Section VI-B. In the simulations we obtain the RSS estimates for weighting in the modified Stansfield algorithm using the principle discussed in Section III-B2. Based on the sector-powers of the MASP and the estimated DoA at every RX k, we obtain two RSS estimates $\hat{\gamma}_{k,i}$ and $\hat{\gamma}_{k,j}$, and estimate the final RSS as $\hat{\gamma}_k = \frac{1}{2}(\hat{\gamma}_{k,i} + \hat{\gamma}_{k,j})$.

Fig. 8 depicts the RMSE of location estimation as a function of the number of RXs, K. Overall, the biggest gain in performance for increasing K is achieved for $K < 20$ RXs as reflected by the CRB as well as the algorithms. When estimating the DoA with TSLS instead of SLS, we observe a localization performance improvement of $0.5 - 0.8$ m. This is mainly explained by the fact that the modified Stansfield algorithm is dominated by RXs with a large SNRs as we have concluded in [13]. Since TSLS is outperforming SLS in particular for moderate to large SNR, we consequently also observe a strong localization performance improvement. Nevertheless, TSLS-S is not able to approach the CRB. In this context it is, however, important to note that the CRB in [29] is derived for a more general case where the TX location is estimated directly from the KM sector-powers in (2). In SLS-S/TSLS-S, on the other hand, we first estimate K DoAs from the KM sector-powers and only thereafter we estimate the location using the DoA estimates. As we have already suggested in [29], this intermediate step might deteriorate the performance and hence it might be impossible for algorithms such as TSLS-S to exactly reach the CRB.

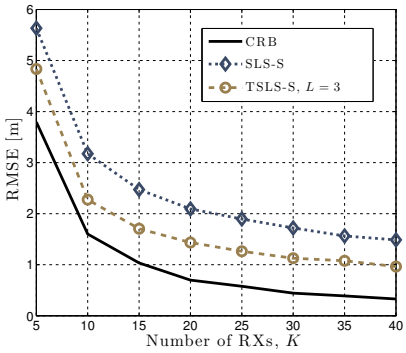

Fig. 8. Localization performance with an equal-sector antenna and a uniform distribution of RXs. Parameters: $a_\mathrm{s} = 0.4$, $M = 6$ and $N = 100$.

D. Performance and Complexity in Comparison to Related Algorithms

In this section, we compare the proposed TSLS algorithm to related works. First, we quantify the complexity of the proposed TSLS DoA estimation in terms of the number of basic operations. As such, we define additions/subtractions and multiplications/divisions and refer to them as ADD and MUL, respectively. In addition to such basic operations, SLS [12] as well as TSLS rely on some standard functions that cannot be expressed directly in terms of the basic operations. For fast processing in a digital signal processor these standard functions could be implemented in form of a look-up table, which makes them neglectable in the overall processing time. Nevertheless, we include them in our considerations and refer to the natural logarithm as LOG, the exponential function as EXP, the square-root as SQR, sine/cosine as SIN/COS and finally as AT2 to the function that calculates the final DoA estimate from the left side of (10), which is often referred to as the *atan2* function in the literature.

Obviously, the maxE algorithm [11], [22], [25] that estimates the DoA as the sector with the maximum power has the lowest complexity since it only calculates the sector-powers according to (2) and finds the smallest of those sector-powers. The sector-power calculation is in fact also part of SLS as well as TSLS and has a complexity of $M(2N-1)\,\mathrm{ADD} + M(2N+1)\,\mathrm{MUL}$. Next, we derive the complexity of TSLS and obtain the complexity of SLS [12] as a by-product by setting $L = 2$ and not counting the DFU stage. In the derivation, we assume an implementation of TSLS that relies on pre-calculated values as much as possible. In (7), as an example, $\bar{\vartheta}_{ij}$, κ_{ij} and $2\ln\frac{\alpha_i}{\alpha_j}$ depend only on the approximation of the radiation pattern and can therefore be loaded as constants during runtime. Overall, this approach is very feasible for a

practically reasonable number of sectors and avoids lots of computations. In the SSL stage we compute M products of sector-powers and find the maximum of those M products. The latter is comparable to finding the maximum of the M sector-powers in maxE, which we do not include in our complexity analysis since the compare operation is normally neglectable in comparison to ADD and MUL. The complexity in the SSL stage is thus equal to M MUL. In the SDE stage, we then calculate metrics $\tilde{p}_{k,i} = \ln p_{k,i}, \forall i \in \mathcal{L}_k$ with complexity $L(\text{ADD} + \text{LOG})$. Thereafter, the calculation of $\ln \frac{p_{k,i}}{p_{k,j}}$ in (7) and (8) is reduced to a single subtraction. Let us now define N_{SP} as the number of sector-pairs used in the SDE stage, for which it holds that $N_{\text{SP}} \leq \binom{L}{2}$. For EBS we then obtain an overall complexity in the SDE stage equal to $(2N_{\text{SP}} + L)\,\text{ADD} + N_{\text{SP}}\,\text{MUL} + L\,\text{LOG}\,[+N_{\text{SP}}\,\text{ADD}]$, where the square brackets indicate operations that are only needed for antennas, where $\alpha_i \neq \alpha_j$, $i, j = 1, \ldots, M$. And for DBS we obtain an overall complexity of $(10N_{\text{SP}} + L)\,\text{ADD} + 17N_{\text{SP}}\,\text{MUL} + N_{\text{SP}}\,\text{SQR} + 4N_{\text{SP}}\,\text{EXP} + L\,\text{LOG}$ in the SDE stage. Finally, the DFU stage has a complexity of $2(N_{\text{SP}} - 1)\,\text{ADD} + \text{MUL} + N_{\text{SP}}(\text{COS} + \text{SIN}) + \text{AT2}$, with an additional complexity of $3N_{\text{SP}}\,\text{MUL}$ and $(N_{\text{SP}} + L)\,\text{ADD} + (4N_{\text{SP}} + 2L)\,\text{MUL}$ for PW and VW, respectively.

The complexity and DoA estimation performance as well as localization performance of TSLS in comparison to maxE and SLS can be found in Table II. Since SLS and maxE are estimators targeted at ESAs, we use an ESA as described in Section VI-B as the sectorized antenna, along with simulation setups as described in Section VI-B and Section VI-C for DoA estimation and localization, respectively. For simplicity, we do not separate between the aforementioned standard functions in the complexity metric. Instead, we count a call to one of the standard function as a call to a look-up table (LUT). Based on the results in Table II, we conclude that the proposed estimator has the best performance of all three, while its additional complexity is very low and mainly due to calls to standard functions, which could be handled with LUTs for fast processing.

VII. Practical RF Measurements

A. Measurement Setup

The practical performance of the proposed TSLS DoA estimation with subsequent Stansfield localization was evaluated with the help of an extensive indoor measurement campaign at the 2.4 GHz ISM band, carried out at Drexel University. In our measurements, we used LWAs as an example of a sectorized antenna. However, other sectorized antennas such as antenna arrays with a single front-end [17], [18] would also have been a good alternative. During the measurements, several uncontrolled WiFi hotspots in the surroundings were active, causing substantial in-band interference. In addition, passers-by generated spatial and temporal variations in the measurement conditions. Both these aspects imply that the measurement environment was far from ideal, thus enhancing further the practical impact of the measurements.

As illustrated in Fig. 9, we placed a TX at three different locations and measured the signal at six RXs. The TX and RX

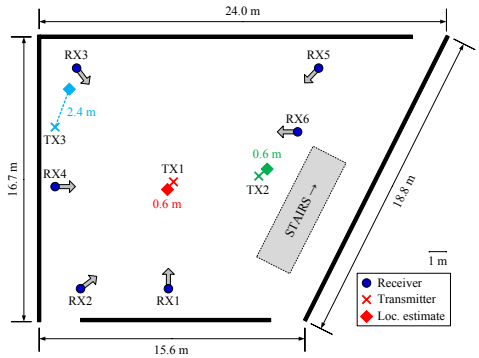

Fig. 9. Illustration of the measurement setup and the localization capabilities of the proposed algorithms in a lobby at Drexel University.

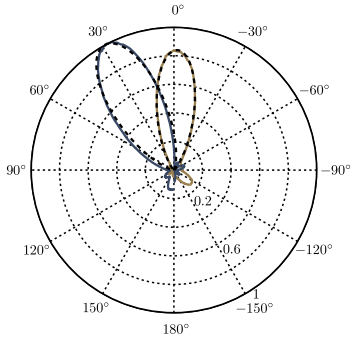

Fig. 10. Radiation pattern for two sectors (solid lines) of the leaky-wave antenna [14] used in our measurements. The main beams are well approximated by a Gaussian curve (dotted lines).

locations were selected such that the performance could be tested in different challenging estimation scenarios. The RX antennas were oriented in such a way that they can hear the TXs within their directivity ranges in most of the cases.

Each transceiver consisted of a software defined radio platform, called Wireless Open-Access Research Platform (WARP) v3 [32]. Each WARP board was connected to its own antenna(s) and to a centralized controlling system. The TXs were equipped with omni-directional antennas whereas each RX had a single two-port LWA [21] with two antenna ports enabling simultaneous measurements in two sectors. The composite right/left-handed (CRLH) LWAs [14] were tuned to operate within the entire 2.4 GHz WiFi band. The physical size of the antenna is 156 mm $\times$ 38 mm and the antenna consists of a cascade of 12 metamaterial unit cells for obtaining good directivity and a small size simultaneously. The main beam of the antenna can be steered from broadside to backward and forward direction by changing two control voltages. Due to the practically symmetric antenna structure, antenna ports have symmetric radiation properties with respect to the broadside direction. As a trade-off between estimation complexity and estimation accuracy, we have used 6 control voltage values for a total of 12 antenna sectors.

TABLE II. Proposed DoA estimator in comparison to other algorithms

Algorithm	Complexity per DoA estimate (in basic operations)	RMSE DoA (SNR = 20 dB)	RMSE loc. ($K = 20$)
maxE [11], [22], [25]	1194 ADD +1206 MUL	17.3°	12 m
SLS [12]	1198 ADD +1213 MUL +2 LUT	2.4°	2.1 m
TSLS + VW, $L = 3$	1213 ADD +1234 MUL +10 LUT	1.3°	1.4 m

The system was operating with a 20 MHz channel bandwidth and a carrier frequency of 2.462 GHz. This combination is heavily overlapping with the WiFi channel no. 11 which was measured to have active traffic during the measurements, acting as direct cochannel interference. The TX power was set to +15 dBm and since our algorithms rely on the received signal powers, automatic gain controls (RF and baseband) were deactivated in the RXs and the gains were set to constant values. As a practical example, we used orthogonal frequency division multiplexing (OFDM) waveforms. Only one of the transmission links, i.e., TX-RX antenna pair, was active at a time and thus we needed to ensure fairness between different transmission links by transmitting the same data over all links. Note that realistically all RXs could receive the same transmitted data only propagated through different channels. Therefore, the measurement arrangement matches the real world scenario well. For testing each link, we transmitted in total 300 packets, each containing 5420 binary phase shift keying (BPSK) symbols. Finally, for each antenna sector, we calculated the received signal power from the baseband signal snapshots by averaging over the powers of all received packets observed through the considered sector. These sector powers are then processed further using the proposed algorithms, as described in the previous sections.

B. Localization System Settings

The TSLS DoA estimator requires an approximation $\hat{\rho}_m(\varphi) = [\hat{\zeta}_m(\varphi)]^2$ of the antenna's main beam through a Gaussian curve (1) in all sectors m, $m = 1, \ldots, M$. In order to obtain the approximation, we first measured the LWA's radiation pattern in each sector m as $\tilde{\rho}_m(k\,\Delta\varphi) = [\tilde{\zeta}_m(k\,\Delta\varphi)]^2$, $k = 1, \ldots, 360$ with a step-size $\Delta\varphi = 1°$. We then found an approximation through a LS fit of (1) to $\tilde{\rho}_m(k\,\Delta\varphi)$. However, only the main beam of the antenna can be well approximated through (1). More importantly, due to the SSL process TSLS will make use of the approximated radiation patterns only around the main beam. In order to obtain a good approximation, the LS fit was consequently calculated only around $\tilde{\vartheta}_m = \mu\Delta\varphi$, $\mu = \arg\max_k \tilde{\rho}_m(k\,\Delta\varphi)$, i.e., the initial estimate for the orientation of the main beam in sector m. We used an interval of $\Omega = 20°$ on both sides of $\tilde{\vartheta}_m$ and obtain $\hat{\rho}_m$ with the parameters $\hat{\alpha}_m$, $\hat{\beta}_m$ and $\hat{\vartheta}_m$ that minimize $\sum_{k=-\Omega/\Delta\varphi}^{\Omega/\Delta\varphi}[\rho_m(\tilde{\vartheta}_m + k\,\Delta\varphi) - \tilde{\rho}_m(\tilde{\vartheta}_m + k\,\Delta\varphi)]^2$. For the LWA used in our measurements, this results in the values shown in Table III. The radiation patterns of two sectors along with their approximation are shown in Fig. 10. As evident, the approximation fits very well for the main beam.

TSLS is furthermore parameterized to take into account the strong multipath environment. For heavy multipath, sectors far from the line-of-sight direction to the TX can be expected to be dominated by multipath components. Hence, we chose to use only $L = 3$ sectors in TSLS DoA estimation. Moreover, PW is chosen as the DoA fusion method since it is more robust than VW, which has been derived for a free space propagation, while generally having better performance than EW. For simplicity, we estimate the RSSs for Stansfield weighting simply as the maximum NCSP of the MASP (see Sections III-B and III-A) at RX k, $k = 1, \ldots, K$, i.e., $\hat{\gamma}_k = \max(p_{k,q}, p_{k,q+1})$.

TABLE III. LS fit for leaky-wave antenna. The LWA has symmetric sectors around 0°. Therefore, this table depicts only 6 out of the 12 sectors. Furthermore, we have normalized the attenuation to $\alpha_m \leq 1$, $\max(\alpha_m) = 1$, $m = 1, \ldots, M$.

Sector	1	2	3	4	5	6
$\hat{\alpha}_m$	0.77	0.90	1.00	0.98	0.93	0.92
$\hat{\beta}_m$ [rad]	0.64	0.61	0.62	0.58	0.52	0.53
$\hat{\theta}_m$ [deg]	-47.9	-40.6	-29.0	-17.6	-9.5	-1.5

C. Measured Performance

Table IVa presents the DoA estimation errors stemming from the processing of the measurements with the above described TSLS configuration. Based on these results, we recognize clear differences in the DoA estimation accuracy at different RXs. RX3 performs very well with all TXs and reaches the lowest RMSE due to its good coverage and interference-free location. In contrast to that, RX2 yields a relatively high DoA estimation RMSE. There is no obvious geometrical reason for that. However, one of the active WiFi hotspots was located right behind the wall close to RX2 and may thus have negatively influenced the estimation performance. The highest individual estimation error of 30.2° was obtained for the TX3-RX6 combination, which might have been caused by the rich scattering conditions due to the stairs (made of metal, concrete and glass) in proximity of RX6.

When analyzing the results in Table IVa row-wise, we see that the DoA of TX3 is the most difficult to estimate, as expected due to TX3's relatively isolated location. Moreover, TX3 was the node closest to the walls with metal doors on either side. We suspect that this caused strong multipath, contributing further to the large DoA estimation error. Surprisingly, TX2 turns out to have the most accurate DoA estimates even though it is located close to the stairs which might act as local scatterers. Actually, only two out of six DoA estimation errors of TX2 are in excess of 10°, meaning that TSLS provides very accurate estimates in this case. Overall, these results reveal that the TSLS algorithm is capable of estimating DoAs with fairly high accuracy even in a challenging indoor environment with severe multipath.

Fig. 9 depicts the TX location estimates resulting from the above described combination of TSLS DoA estimation

TABLE IV. Practical measurement results.

(a) Absolute error of DoA estimation.

	RX1	RX2	RX3	RX4	RX5	RX6	RMSE
TX1	18.5°	29.6°	5.3°	17.0°	21.9°	3.3°	18.4°
TX2	16.3°	21.3°	9.5°	0.6°	6.3°	2.2°	11.9°
TX3	23.1°	14.5°	8.0°	24.1°	26.6°	30.2°	22.4°
RMSE	19.5°	22.6°	7.8°	17.0°	20.2°	17.6°	

(b) Localization error after Stansfield fusion of DoA estimates.

	TX1 (TSLS)	TX2 (TSLS)	TX3 (TSLS)	RMSE (TSLS)	RMSE (maxE [31])
Absolute error	0.6 m	0.6 m	2.4 m	1.5 m	2.8 m

with subsequent Stansfield localization. A detailed summary of the localization results is shown in Table IVb. Based on these results, TX1 and TX2 can be localized very precisely as the location error is around 60 cm for both. This is an expected result due to their central locations with respect to the RXs. Although some of the individual DoA estimates have a comparably large error, location estimation is fairly accurate, which is mainly explained by the Stansfield weighting scheme that gives larger weight to the DoA estimates of those RXs that have large sector-powers. In case of TX3, the majority of the DoA estimates are relatively inaccurate with four out of six estimation errors being larger than 20°. Consequently, the location estimate is also more inaccurate (2.4 m). However, this is explained by the location of TX3 which was on purpose placed at the boarder of the localization system's coverage area.

The total localization RMSE is 1.5 m, which corresponds to a circle with an area of 2.1 % of the whole measurement area. In our earlier work [31], we have used the same measurement data to test the performance of the modified maxE DoA estimator [31]. Using the same Stansfield fusion algorithm, but in combination with simple maxE DoA estimates resulted in a RMSE of 2.8 m, which is an almost two-fold RMSE compared to the localization based on TSLS DoA estimates. Hence the algorithms proposed in this article are clearly outperforming the existing state-of-the-art.

VIII. Conclusion

In this paper, we have substantially extended our earlier work on DoA estimation and TX localization using sectorized antennas. We have introduced a modified antenna model with more degrees of freedom and have shown that it can be used to model a broader range of practical antennas. Based on the new model we have proposed the novel TSLS DoA estimator. In contrast to existing DoA estimators, TSLS is applicable to all antennas that can be described by our modified antenna model, independent of the TX signal type and without the requirement for cooperation between the TX and the localizing network. Besides being more universal, we have shown that TSLS has also better performance than existing algorithms and that it approaches the CRB on signal DoA estimation of a non-cooperative TX if the SNR is moderate to large. In order to better understand the performance of TSLS, we have furthermore derived analytical error models for the underlying DoA estimation principle of TSLS DoA estimation considering free space as well as multipath propagation. We have then analyzed the performance of localization with the Stansfield estimator that estimates the TX location by fusing the TSLS DoA estimates. As expected, the improved DoA estimation performance of TSLS also results in a localization performance improvement compared to the localization using previously published DoA estimators. Finally, we have shown how to configure the TSLS DoA estimator to work with a practical sectorized antenna, namely a leaky-wave antenna. Based on that configuration we have then demonstrated the achievable performance of a sectorized antenna-based localization system using real-world measurements obtained in an indoor environment. Overall, we believe that the results in this paper are crucial for the practical implementation of low complexity DoA estimation and TX localization using sectorized antenna systems. In particular this is the case when the TX is non-cooperative or when dedicated signaling between TX and localization network is otherwise unfeasible.

Appendix A
Derivation of DoA Estimators

The criterion (6) is clearly minimized for $p_{k,i}/p_{k,j} - \rho_{k,i}/\rho_{k,i} = 0$. Recalling the Gaussian approximation $\rho_{k,m} = [\zeta_m(\varphi_k)]^2$, $m = i, j$ in (1), we can write

$$0 = \ln\frac{p_{k,i}}{p_{k,j}} - 2\ln\frac{\alpha_i}{\alpha_j} + \frac{2\left[\mathcal{M}\left(\hat{\varphi}_{k,ij} - \vartheta_i\right)\right]^2}{\beta_i^2} - \frac{2\left[\mathcal{M}\left(\hat{\varphi}_{k,ij} - \vartheta_j\right)\right]^2}{\beta_j^2}. \quad (28)$$

The above equation contains the function $\mathcal{M}(\varphi)$, which is difficult to handle mathematically. However, the mapping of the angles to $[-\pi; \pi)$ is arbitrary. Hence, for practically relevant cases we can always find a mapping for the angles ϑ_i and ϑ_j such that we can write $\mathcal{M}(\hat{\varphi}_k - \vartheta_m) = \tilde{\varphi}_{k,ij} - \tilde{\vartheta}_m$, where $m = i, j$ and $\tilde{\varphi}_{k,ij}$ is the mapped SP-DoA estimate. One such mapping could be $\tilde{\vartheta}_i = 0$ and $\tilde{\vartheta}_j = \vartheta_j - \vartheta_i$. We can then solve (28) to obtain (7) and (8). For presentation simplicity, we have not included the mapping in (7) and (8).

Appendix B
Proof of Lemma 1

In the following we will derive the mean (14) and variance (16) for the 2nd order Taylor series expansion. The 2nd order Taylor series of Y in Lemma 1 around its mean $\boldsymbol{\mu}$ can be written as

$$Y^{(2)} = f + \mathbf{j}^T(\mathbf{X} - \boldsymbol{\mu}) + \frac{1}{2}(\mathbf{X} - \boldsymbol{\mu})^T\mathbf{H}(\mathbf{X} - \boldsymbol{\mu}) \quad (29)$$

where we have omitted the dependence of f, $\mathbf{j}$ and $\mathbf{H}$ on $\boldsymbol{\mu}$ for notational simplicity. According to [33, p. 53], the moments of a quadratic form $V' = \mathbf{X}^T\mathbf{A}\mathbf{X}$ for normally distributed

random vector $\mathbf{X} \sim \mathcal{N}(\boldsymbol{\mu}, \mathbf{Q})$ with symmetric matrix $\mathbf{A}$ are given as

$$\mathrm{E}[V'] = \mathrm{trace}(\mathbf{AQ}) + \boldsymbol{\mu}^T\mathbf{A}\boldsymbol{\mu} \quad (30)$$

$$\mathrm{E}[V'^2] = 2[\mathrm{trace}(\mathbf{AQ})^2 + 2\boldsymbol{\mu}^T\mathbf{AQA}\boldsymbol{\mu}] \quad (31)$$

$$+ [\mathrm{trace}(\mathbf{AQ}) + \boldsymbol{\mu}^T\mathbf{A}\boldsymbol{\mu}]^2. \quad (32)$$

In (29), we have $V = \Delta\mathbf{X}^T\mathbf{H}\Delta\mathbf{X}$ with $\Delta\mathbf{X} = \mathbf{X} - \boldsymbol{\mu} \sim \mathcal{N}(\mathbf{0}, \mathbf{Q})$ and the Hermitian matrix $\mathbf{H}$ that is consequently symmetric. We can therefore write the moments of V as

$$\mathrm{E}[V] = \mathrm{trace}(\mathbf{HQ}) \quad (33)$$

$$\mathrm{E}[V^2] = 2\,\mathrm{trace}(\mathbf{HQ})^2 + [\mathrm{trace}(\mathbf{HQ})]^2. \quad (34)$$

Hence, the first moment of Y is obtained as in (14). The variance of Y can be written as

$$\begin{aligned}\mathrm{var}[Y^{(2)}] &= \mathrm{E}\left[\left(Y^{(2)}\right)^2\right] - \mathrm{E}[Y^{(2)}]^2 \\ &= \mathrm{E}\left[f^2\right] + \mathrm{E}\left[\left(\mathbf{j}^T\Delta\mathbf{X}\right)^2\right] + \frac{1}{4}\mathrm{E}\left[V^2\right] \\ &\quad + 2f\mathbf{j}^T\mathrm{E}\left[\Delta\mathbf{X}\right] + f\,\mathrm{E}\left[V\right] + \mathbf{j}^T\mathrm{E}\left[\Delta\mathbf{X}\,V\right] \\ &\quad - f^2 - f\,\mathrm{trace}\left\{\mathbf{HQ}\right\} - \frac{1}{4}\left[\mathrm{trace}(\mathbf{HQ})\right]^2. \quad (35)\end{aligned}$$

We notice that $\Delta\mathbf{X}\,V$ is a vector with elements composed of products $\Delta\mathbf{X}_k^p\,\Delta\mathbf{X}_l^q\,\Delta\mathbf{X}_m^r$, where $\Delta\mathbf{X}_k$, $\Delta\mathbf{X}_l$ and $\Delta\mathbf{X}_m$ are independent and at least one of the powers p, q or r is uneven. Therefore, we have $\mathrm{E}\left[\Delta\mathbf{X}\,V\right] = 0$ and obtain (16) by using (33)-(34) in (35). The corresponding mean (13) and variance (15) of the 1st order Taylor series are not derived explicitly, due to space constraints. However, the derivation is very similar.

APPENDIX C
DERIVATION OF SP-DOA ESTIMATION BIAS AND VARIANCE

For SP-DoA estimation with DBS, we have $\hat{\varphi}_{ij} = f(\mathbf{p}) = \lambda_{ij} \pm b_{ij}\,g(\mathbf{p})$ with $\mathbf{p} = (p_{k,i}, p_{k,j})^T$. This leads to the 2×1 gradient vector $\mathbf{j}$ with elements

$$\mathbf{j}_1 = [f]_{p_{k,i}}(\boldsymbol{\mu}) = \pm\frac{\beta_i\beta_j}{4\,p_{k,i}\,g(\boldsymbol{\mu})} \quad (36)$$

$$\mathbf{j}_2 = [f]_{p_{k,i}}(\boldsymbol{\mu}) = \mp\frac{\beta_i\beta_j}{4\,p_{k,j}\,g(\boldsymbol{\mu})} \quad (37)$$

and the 2×2 Hessian matrix $\mathbf{H}$ with elements

$$\mathbf{H}_{11} = [f]_{p_{k,i}p_{k,i}}(\boldsymbol{\mu}) = \mp\beta_i\beta_j\,\frac{4[g(\boldsymbol{\mu})]^2 + \Delta\beta_{ij}}{16\,p_{k,i}^2\,[g(\boldsymbol{\mu})]^3} \quad (38)$$

$$\mathbf{H}_{22} = [f]_{p_{k,j}p_{k,j}}(\boldsymbol{\mu}) = \pm\beta_i\beta_j\,\frac{4[g(\boldsymbol{\mu})]^2 - \Delta\beta_{ij}}{16\,p_{k,j}^2\,[g(\boldsymbol{\mu})]^3} \quad (39)$$

$$\mathbf{H}_{12} = \mathbf{H}_{21} = [f]_{p_{k,i}p_{k,j}}(\boldsymbol{\mu}) = \pm\frac{\beta_i\beta_j\,\Delta\beta_{ij}}{16\,p_{k,i}\,p_{k,j}[g(\boldsymbol{\mu})]^3} \quad (40)$$

both evaluated at $\mathbf{p} = \boldsymbol{\mu}$. We furthermore obtain

$$\mathrm{trace}(\mathbf{HQ}) = \mathbf{H}_{11}\sigma_1^2 + \mathbf{H}_{22}\sigma_2^2 \quad (41)$$

$$\mathrm{trace}(\mathbf{HQ})^2 = \left(\mathbf{H}_{11}\sigma_1^2\right)^2 + 2\mathbf{H}_{12}^2\sigma_1^2\sigma_2^2 + \left(\mathbf{H}_{22}\sigma_2^2\right)^2. \quad (42)$$

since $\mathbf{Q}$ is diagonal. Inserting (38)-(40) in (41) and using (41) in (14) yields $\mathrm{E}[\hat{\varphi}_{k,ij}^{(2)}]$ and, after subtraction of the DoA φ_k, the bias (18). (19) results from (15) and (36)-(37). Finally, inserting (42) in (16) and using the results from (19) leads to (20).

REFERENCES

[1] L. Kaplan, "Global node selection for localization in a distributed sensor network," *IEEE Trans. Aerosp. Electron. Syst.*, vol. 42, no. 1, pp. 113–135, Jan. 2006.

[2] H. Celebi and H. Arslan, "Utilization of location information in cognitive wireless networks," *IEEE Wireless Commun. Mag.*, vol. 14, no. 4, pp. 6–13, Aug. 2007.

[3] K. Ho and Y. Chan, "Solution and performance analysis of geolocation by TDOA," *IEEE Trans. Aerosp. Electron. Syst.*, vol. 29, no. 4, pp. 1311–1322, Oct. 1993.

[4] A. Weiss, "On the accuracy of a cellular location system based on RSS measurements," *IEEE Trans. Veh. Technol.*, vol. 52, no. 6, pp. 1508–1518, Nov. 2003.

[5] R. Martin and R. Thomas, "Algorithms and bounds for estimating location, directionality, and environmental parameters of primary spectrum users," *IEEE Trans. Wireless Commun.*, vol. 8, no. 11, pp. 5692 –5701, Nov. 2009.

[6] F. Penna and D. Cabric, "Bounds and tradeoffs for cooperative DoA-only localization of primary users," in *Proc. IEEE Global Telecommunications Conf., GLOBECOM*, 2011, pp. 1–5.

[7] J. Wang, J. Chen, and D. Cabric, "Cramer-Rao bounds for joint RSS/DoA-based primary-user localization in cognitive radio networks," *IEEE Trans. Wireless Commun.*, vol. 12, no. 3, pp. 1363–1375, Mar. 2013.

[8] J. Werner, A. Hakkarainen, and M. Valkama, "Cramer-Rao bounds for hybrid RSS-DOA based location and transmit power estimation in cognitive radio systems," in *Proc. IEEE 78th Vehicular Technology Conf., VTC Fall*, 2013.

[9] R. Schmidt, "Multiple emitter location and signal parameter estimation," *IEEE Trans. Antennas Propag.*, vol. 34, no. 3, pp. 276 – 280, Mar. 1986.

[10] T. Ohira, "Adaptive array antenna beamforming architectures as viewed by a microwave circuit designer," in *Proc. 2000 Asia-Pacific Microwave Conf.*, 2000, pp. 828 –833.

[11] J. Werner, J. Wang, A. Hakkarainen, M. Valkama, and D. Cabric, "Primary user localization in cognitive radio networks using sectorized antennas," in *Proc. 10th Annu. Conf. on Wireless On-demand Network Systems and Services, WONS*, 2013, pp. 155–161.

[12] ——, "Primary user DoA and RSS estimation in cognitive radio networks using sectorized antennas," in *Proc. 8th Int. Conf. on Cognitive Radio Oriented Wireless Networks, CROWNCOM*, 2013, pp. 43–48.

[13] J. Wang, J. Werner, M. Valkama, and D. Cabric, "Performance analysis of primary user RSS/DoA estimation and localization in cognitive radio networks using sectorized antennas," *IEEE Wireless Commun. Lett.*, vol. 3, no. 2, pp. 237–240, Apr. 2014.

[14] D. Piazza, D. Michele, and K. Dandekar, "Two port reconfigurable CRLH leaky wave antenna with improved impedance matching and beam tuning," in *Proc. 3rd European Conf. Antennas and Propagation, EuCAP*, 2009, pp. 2046–2049.

[15] C. Sun and N. C. Karmakar, "Direction of arrival estimation with a novel single-port smart antenna," *EURASIP J. Advances in Signal Process.*, vol. 2004, no. 9, pp. 1364–1375, Aug. 2004.

[16] K. Gotsis, K. Siakavara, and J. Sahalos, "On the direction of arrival (DoA) estimation for a switched-beam antenna system using neural networks," *IEEE Trans. Antennas Propag.*, vol. 57, no. 5, pp. 1399–1411, May 2009.

[17] M. Sharawi, F. Sultan, and D. Aloi, "An 8-element printed v-shaped circular antenna array for power-based vehicular localization," *IEEE Antennas Wireless Propag. Lett.*, vol. 11, pp. 1133–1136, 2012.

[18] M. S. Sharawi, F. Sultan, and D. N. Aloi, "A comparative performance analysis of two printed circular arrays for power-based vehicle localization applications," *Int. J. of Antennas and Propagation*, vol. 2012, pp. 1–8, Sep. 2012.

[19] X. Yu and H. Xin, "Direction of arrival estimation utilizing incident angle dependent spectra," in *Proc. IEEE MTT-S Int. Microwave Symp. Dig.*, 2012, pp. 1–3.

[20] V. Vakilian, J.-F. Frigon, and S. Roy, "Direction-of-arrival estimation in a clustered channel model," in *Proc. IEEE 10th Int. New Circuits and Systems Conf., NEWCAS*, 2012, pp. 313–316.

[21] H. Paaso, A. Mammela, D. Patron, and K. R. Dandekar, "DoA estimation through modified unitary MUSIC algorithm for CRLH leaky-wave antennas," in *Proc. IEEE 24th Int. Symp. Personal Indoor and Mobile Radio Communications, PIMRC*, 2013, pp. 311–315.

[22] D. N. Aloi and M. S. Sharawi, "Comparative analysis of single-channel direction finding algorithms for automotive applications at 2400 MHz in a complex reflecting environment," *Physical Commun. J.*, vol. 3, no. 1, pp. 19–27, Mar. 2010.

[23] M. S. Sharawi and D. N. Aloi, "Characterizing the performance of single-channel pseudo-doppler direction finding systems at 915 MHz for vehicle localization," *Int. J. of Communication Systems*, vol. 24, no. 1, pp. 27–39, Jan. 2011.
[24] S. Abielmona, H. Nguyen, and C. Caloz, "Analog direction of arrival estimation using an electronically-scanned CRLH leaky-wave antenna," *IEEE Trans. Antennas Propag.*, vol. 59, no. 4, pp. 1408 –1412, Apr. 2011.
[25] T. Ohira and K. Gyoda, "Hand-held microwave direction-of-arrival finder based on varactor-tuned analog aerial beamforming," in *Proc. 2001 Asia-Pacific Microwave Conf.*, 2001, pp. 585–588.
[26] F. Gunnarsson, M. Johansson, A. Furuskar, M. Lundevall, A. Simonsson, C. Tidestav, and M. Blomgren, "Downtilted base station antennas - a simulation model proposal and impact on HSPA and LTE performance," in *Proc. IEEE 68th Vehicular Technology Conf., VTC Fall*, Sep. 2008, pp. 1–5.
[27] *Evolved Universal Terrestrical Radio Access (E-UTRA).* 3GPP TR 25.814 V. 7.10, 2011.
[28] R. Stansfield, "Statistical theory of d.f. fixing," *J. Institution Elect. Engineers - Part IIIA: Radiocommunication*, vol. 94, no. 15, pp. 762–770, Mar. 1947.
[29] J. Werner, J. Wang, A. Hakkarainen, M. Valkama, and D. Cabric, "Performance and Cramer-Rao bounds for DoA/RSS estimation and transmitter localization using sectorized antennas," *submitted to IEEE Trans. Veh. Technol.*, 2014.
[30] N. I. Fisher and T. Lewis, "Estimating the common mean direction of several circular or spherical distributions with differing dispersions," *Biometrika*, vol. 70, no. 2, pp. 333–341, Aug. 1983.
[31] A. Hakkarainen, J. Werner, N. Gulati, D. Patron, D. Pfeil, H. Paaso, A. Mammela, K. Dandekar, and M. Valkama, "Reconfigurable antenna based DoA estimation and localization in cognitive radios: Low complexity algorithms and practical measurements," in *Proc. 9th Int. Conf. on Cognitive Radio Oriented Wireless Networks, CROWNCOM*, 2014.
[32] "Mango communications WARP v3 kit," 2014. [Online]. Available: http://mangocomm.com/products/kits/warp-v3-kit
[33] A. M. Mathai and S. B. Provost, *Quadratic Forms in Random Variables: Theory and Applications*, 1st ed. New York: M. Dekker, 1992.

Janis Werner was born in Berlin, Germany, in 1986. He received the Dipl. Ing. degree in electrical engineering from Dresden University of Technology (TUD), Germany in 2011. Currently he is working towards a Ph.D. degree at Tampere University of Technology (TUT), Finland, where he is a researcher at the Department of Electronics and Communications Engineering. His main research interests are localization with an emphasis on directional antenna-based systems as well as the utilization and further processing of location information in future generation mobile networks.

Jun Wang received his B.Eng. degree in electronic information engineering from Beijing University of Technology and M.Phil. degree in electrical engineering from City University of Hong Kong, in 2006 and 2009, respectively. He received his Ph.D. degree in electrical engineering from University of California Los Angeles in 2014, advised by Prof. Danijela Cabric. He joined Broadcom Corporation as a research scientist in wireless communication systems design in 2014. His research interests include acquisition and utilization of primary-user location information and various issues related to spectrum sensing in cognitive radio networks.

Aki Hakkarainen received the M.Sc. (with honors) in Communication Electronics from Tampere University of Technology (TUT), Finland in 2007. From 2007 to 2009, he was working as a RF Design Engineer with Nokia, Salo. From 2009 to 2011, he was working as a Radio System Specialist with Elisa, Tampere. Currently, he is working towards a Ph.D. degree at TUT. He is a Researcher and Doctoral Student at the Department of Electronics and Communications Engineering, TUT. His research interests include digital signal processing methods for RF impairment mitigation and digital signal processing for localization.

Nikhil Gulati received the B.Eng. degree in Electronics Instrumentation and Control from the University of Rajasthan, India, in 2005 and the M.S. degree in Electrical Engineering with major in Systems and Control from Drexel University, Philadelphia, PA, USA, in 2007, where he conducted research on sensor networks, autonomous systems and real-time control. He worked as a Software Engineer from 2007–2010. He is currently pursuing his Ph.D. degree in Electrical Engineering at Drexel University. His research is focused on developing adaptive learning algorithms for cognitive radios employing electrical reconfigurable antennas. He also works on developing distributed algorithms for interference management and heterogeneous wireless networks.

Damiano Patron received the B.S. Degree in Electronics Engineering from University of Padua, Italy in 2010 and the M.S. in Electrical and Computer Engineering from Drexel University, Philadelphia, PA in 2013, where he is currently pursuing his Ph.D. in Telecommunication Engineering. From 2002 to 2010, Patron worked with Euro-Link S.r.l. as a system integrator of RFID systems. In 2010 he joined the start-up company Adant Inc. as an RF and antenna Engineer, designing reconfigurable antennas for WiFi and RFID applications. His research focuses on the design of reconfigurable antennas for throughput maximization and DoA estimation in wireless networks. He also works in the development of wearable sensors and power harvesting systems. Patron is the author and coauthor of several patents in the field of reconfigurable antennas, antennas miniaturization and wearable technologies. He received several awards including the Drexel Frank and Agnes Seaman Fellowship Award in 2013 and the Young Scientist Best Paper Award at the ICEAA – IEEE APWC – EMS 2013 Conference.

Doug Pfeil received his B.S. and M.S. degrees in Computer Engineering in 2007 from Drexel University, Philadelphia, PA. He is currently pursuing his Ph.D. from Drexel University where he is also a member of the research staff in the Wireless Systems Lab. His current research interests include software defined radio, free space optical communication, physical layer design, and FPGA baseband processing with an emphasis on the practical implementation of novel hybrid RF and optical communication techniques.

Kapil Dandekar received the B.S. degree in electrical engineering from the University of Virginia in 1997. He received the M.S. and Ph.D. degrees in Electrical and Computer Engineering from the University of Texas at Austin in 1998 and 2001, respectively. In 1992, he worked at the U.S. Naval Observatory and from 1993-1997, he worked at the U.S. Naval Research Laboratory.

In 2001, Dandekar joined the Electrical and Computer Engineering Department at Drexel University in Philadelphia, Pennsylvania. He is currently a Professor of Electrical and Computer Engineering at Drexel University; the Director of the Drexel Wireless Systems Laboratory (DWSL); Associate Dean for Research and Graduate Studies in the Drexel University College of Engineering. DWSL has been supported by the U.S. National Science Foundation, Army CERDEC, National Security Agency, Office of Naval Research, and private industry. Dandekar's current research interests and publications involve wireless, ultrasonic, and optical communications, reconfigurable antennas, and smart textiles. Intellectual property from DWSL has been licensed by external companies for commercialization. Dandekar is a member of the IEEE Educational Activities Board and co-founder of the EPICS-in-IEEE program.

Danijela Cabric received the Dipl. Ing. degree from the University of Belgrade, Serbia, in 1998, and the M.Sc. degree in electrical engineering from the University of California, Los Angeles, in 2001. She received her Ph.D. degree in electrical engineering from the University of California, Berkeley, in 2007, where she was a member of the Berkeley Wireless Research Center. In 2008, she joined the faculty of the Electrical Engineering Department at the University of California, Los Angeles, where she is now Associate Professor. Dr. Cabric received the Samueli Fellowship in 2008, the Okawa Foundation Research Grant in 2009, Hellman Fellowship in 2012 and the National Science Foundation Faculty Early Career Development (CAREER) Award in 2012. She serves as an Associate Editor in IEEE Journal on Selected Areas in Communications (Cognitive Radio series) and IEEE Communications Letters, and TPC Co-Chair of 8th International Conference on Cognitive Radio Oriented Wireless Networks (CROWNCOM) 2013. Her research interests include novel radio architecture, signal processing, and networking techniques to implement spectrum sensing functionality in cognitive radios.

Mikko Valkama was born in Pirkkala, Finland, on November 27, 1975. He received the M.Sc. and Ph.D. Degrees (both with honors) in electrical engineering (EE) from Tampere University of Technology (TUT), Finland, in 2000 and 2001, respectively. In 2002, he received the Best Ph.D. Thesis–award by the Finnish Academy of Science and Letters for his dissertation entitled "Advanced I/Q signal processing for wideband receivers: Models and algorithms". In 2003, he was working as a visiting researcher with the Communications Systems and Signal Processing Institute at SDSU, San Diego, CA. Currently, he is a Full Professor and Department Vice-Head at the Department of Electronics and Communications Engineering at TUT, Finland. He has been involved in organizing conferences, like the IEEE SPAWC'07 (Publications Chair) held in Helsinki, Finland. His general research interests include communications signal processing, estimation and detection techniques, signal processing algorithms for software defined flexible radios, cognitive radio, full-duplex radio, radio localization, 5G mobile cellular radio, digital transmission techniques such as different variants of multicarrier modulation methods and OFDM, and radio resource management for ad-hoc and mobile networks.

Publication 3

J. Werner, A. Hakkarainen, and M. Valkama, "Estimating the primary user location and transmit power in cognitive radio systems using extended Kalman filters," in *Proceedings of the 10th Annual Conference on Wireless On-Demand Network Systems and Services (WONS)*, Banff, AB, 2013, pp. 155–161.

Estimating the Primary User Location and Transmit Power in Cognitive Radio Systems Using Extended Kalman Filters

(Invited Paper)

Janis Werner, Aki Hakkarainen and Mikko Valkama
Department of Electronics and Communications Engineering
Tampere University of Technology, P.O. Box 553, FI-33101 Tampere, Finland
Emails: {janis.werner, aki.hakkarainen, mikko.e.valkama}@tut.fi

***Abstract*—In cognitive radio systems, the primary user location and transmit power are valuable information in order to create an efficient secondary network that uses spatial spectrum holes without introducing interference to the primary users. Since primary users cannot be assumed to cooperate, their locations and transmit powers need to be estimated at the secondary users. Existing localization techniques, based on the received signal strength require a high amount of secondary users in order to achieve a high accuracy while direction of arrival based methods alone suffer from the random secondary user positions and the requirements for making the associated devices portable. In this paper we propose a hybrid solution using an extended Kalman filter that is able to localize a moving primary user and estimate its transmit power under the aforementioned conditions. Its performance is compared to an extended Kalman filter that uses only direction of arrival estimation by means of Monte Carlo simulations, and shown to clearly outperform the DOA-only based processing.**

I. Introduction

The ever-increasing demands for higher transmission rates in combination with the emergence of more and more mobile devices and services require an efficient use of the electromagnetic spectrum. Traditionally, dedicated parts of the RF spectrum have been licensed for exclusive use, leading to temporally and spatially unused frequency bands. A lot of recent research has therefore focused on cognitive radio (CR) networks, where cognitive, secondary users (SU) sense the spectrum and dynamically access those bands that are available. However, these secondary networks need to assure that the interference introduced to the primary users (PU) is kept at minimum [1], [2].

When aiming for the usage of temporal spectral holes, it is sufficient to check whether a PU is transmitting or not. As opposed to this, accessing spatial spectrum opportunities with directional antennas as e.g. in [3] requires more detailed information about the primary network. At the transmitting SU, the locations of the PUs must be known in order to direct transmission away from them. In addition, once the PU locations are available, they can be used for routing in the secondary network [4], [5]. The PU locations need to be estimated by observing the PU-transmitted signals as normally no cooperation between the primary and secondary network exists. Localization based on emissions has been studied in various applications such as indoor positioning or in the military context and very recently also in the CR context.

Algorithms for PU localization based on the received signal strength (RSS) exist in the literature, e.g. [6]. The downside of this approach is that many secondary sensors need to collaborate in order to obtain accurate results since the RSS is heavily influenced by the channel (e.g. shadowing and other uncertainties). Furthermore, the localization works only for a single PU in the observation area because the distinction between multiple PUs is impossible in the RSS domain.

Direction of arrival (DOA) estimation, on the other hand, makes it possible to detect multiple transmitters by means of directional antennas as long as at least few SUs cooperate. The DOA can be estimated using antenna array techniques such as MUSIC [7]. For the directional transmission at the SUs, it is actually sufficient to have knowledge about the angles (instead of locations) to all present PUs. However, a problem arises when the signal to noise ratio (SNR) at the SU is too low or the antenna amount in the SU is very small. Then, the DOA estimation becomes inaccurate [8] or even worse, the PU is not detected at all. A situation commonly denoted as the hidden node problem. Since the SNR depends on the distance, transmit power and shadowing situation, a transmitting SU might still introduce interference to the hidden PU. But it also means that, at the same time, the PU might be visible to other SUs. Therefore, in analogy to the requirement to cooperatively sense the spectrum [9] it is also necessary to cooperatively localize the PUs in order to protect them from interference by means of directional transmission in the secondary network.

A widely used approach to estimate and track the position of an emitter source based on DOA estimation is the extended Kalman filter (EKF) [10]. Several different implementations can be found in the literature, including a completely decentralized version that does not require any central processing unit [11], making it an interesting choice for secondary ad-hoc networks. It is known that the accuracy of localization

The research leading to these results was financially supported by the Doctoral Programme of the President of Tampere University of Technology, the Tuula and Yrjö Neuvo Fund and the Finnish Funding Agency for Technology and Innovation (Tekes, under the project "Reconfigurable Antenna-based Enhancement of Dynamic Spectrum Access Algorithms").

based on DOA depends on the relative positions of the PU and the SUs as well as on the quality of DOA estimation [12], [13]. In a secondary network where the SUs also act as the sensors for localization, the sensor positions are random rather than optimal with respect to their capability to localize the PU. Furthermore, the SU devices are expected to have only few antennas (e.g. 2-4) in order to assure portability and affordability. This means that, in addition to the random distribution of nodes, the quality of individual DOA estimation is quite low. Therefore, the localization of PUs requires collaborative techniques that can cope with adverse conditions.

Due to these conditions and the requirement for high accuracy, all available information should be utilized in the localization. The authors of [14] propose hybrid localization based on both RSS and time-of-arrival (TOA) or time-difference-of-arrival (TDOA) and derive the respective Cramer-Rao bounds. However, timing information requires synchronization with the PU (TOA) or between the SUs (TDOA), which is not realistic in CR systems [4]. Hybrid localization in CR can therefore only be based on RSS and DOA. In [15] maximum likelihood (ML) and linear least-squares (LS) estimators are introduced for emitter localization based on sensors that either measure the RSS or estimate the DOA. The solution derived in [15] is limited to the stationary (non-moving) PU scenario which is not realistic in mobile radio communications.

In addition to the location of the PU, its transmit power is useful information in the secondary network. On the one hand, it can be used to obtain a better picture of the radio environment [16]. On the other hand, the estimates could be used to distinguish real measurements from noise [17] or for the association in case of multiple PUs [18].

In this paper, we propose a novel hybrid EKF that utilizes both RSS and DOA measurements at multiple SUs to estimate the PU location. We show that our hybrid solution outperforms the conventional DOA-only EKF when faced with the challenging conditions that can be found in CR systems. In addition we demonstrate the capability to estimate the PU transmit power which is not possible with the DOA-only EKF. In contrast to the estimators presented in [15], our solution can be used to localize and track a moving PU. Furthermore, we propose that each SU should measure both DOA and RSS. Finally, the method we introduce can also be used to estimate the transmit power which is not possible with the solution in [15].

This paper is organized as follows: In Section II, we describe the applied system model. The classical DOA-based EKF is summarized in Section III. In the subsequent section we introduce our proposed hybrid RSS-DOA EKF. This hybrid solution is compared to the classical approach in SectionV. The paper concludes with a short summary in Section VI.

II. Principal System Model

In this paper, we consider a secondary network, where cooperating SUs are trying to localize a single PU on a two-dimensional Cartesian coordinate system (Figure 1). On that account, all SUs communicate their observations which are

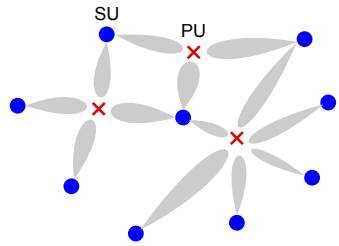

Fig. 1. Collaborative localization of a PU.

then either combined in a central fusion center or alternatively each of the SUs individually processes the communicated observations according to [11]. Since the approaches can easily be transformed from one to another and produce the same results, we describe only the centralized approach in the following.

A. DOA Model

We assume that all SUs are equipped with directional antennas (e.g. antenna arrays) such that DOA estimation is possible. For SU i at position (x_i, y_i) and the PU at position (x, y), the estimation is modeled as in e.g. [13]:

$$\vartheta_i = \arctan\left(\frac{y - y_i}{x - x_i}\right) + \gamma_i \tag{1}$$

with an estimation error $\gamma_i \sim \mathcal{N}\left(0, \sigma_\mathrm{a}^2\right)$ that has the same variance σ_a^2 for all SUs. In reality the variance varies across the SUs, depending on the configuration of the antenna array, e.g. its size and orientation. In addition, the variance is also influenced by the receiver SNR [8]. As a consequence, the quality of DOA estimates is dependent on the the RSS. However, in this paper we want to analyze the benefit of using RSS in addition to the DOA, in the case where the quality of DOA estimates is low. Therefore, we want to be able to control the quality of DOA estimates independently and use the aforementioned simplified model.

B. RSS Model

Besides providing angular information, DOA estimation techniques make it possible to determine the RSS associated with the DOA [7]. The dependence of the RSS on the distance between transmitter and receiver is typically assumed to be logarithmic. For SU i and the PU transmitting with power P_PU, the received power $P_{\mathrm{SU},i}$ is commonly (e.g. [6]) expressed by

$$P_{\mathrm{SU},i}[\mathrm{dBm}] = P_\mathrm{PU}[\mathrm{dBm}] - 10\alpha \lg\left(d_i\right) + m_i \tag{2}$$

where $d_i = \sqrt{(x - x_i)^2 + (y - y_i)^2}$ and α is a constant known as the path loss coefficient. The influence of fading is modeled by the random process $m_i \sim \mathcal{N}\left(0, \sigma_\mathrm{f}^2\right)$. Here, we analyze only the influence of slow fading due to shadowing since the influence of fast fading may be diminished by a sufficiently long RSS measurement window. Therefore, m_i is dependent only on the positions of the PU and SU i. Since shadowing is determined by the surrounding, two successive

RSS measurements are subject to correlated shadowing. We assume the model introduced in [19], where the correlation of shadow fading decreases exponentially with the distance. For an RSS measurement period of T and a static SU, the correlation between two consecutive RSS measurements can be written as

$$R_m(T) = \sigma_{\mathrm{f}}^2 \exp\left(-\frac{vT}{d_{\mathrm{c}}}\right) \tag{3}$$

and is therefore dependent on the PU velocity v and an environmental parameter, d_{c}, referred to as the correlation distance.

III. Kalman Filter

A. Extended Kalman Filter

The EKF is a version of the popular Kalman filter that makes it possible to iteratively estimate the state of an object based on the previous state and some measured data (see e.g. [20]). In contrast to the classical Kalman filter, the EKF can also treat models where both the state transition $\mathbf{f}(\cdot)$ and measurement function $\mathbf{h}(\cdot)$ are nonlinear. At time step k, the state is represented by the $M \times 1$ state vector $\mathbf{p}(k)$ where M is equal to the amount of variables necessary to describe the state of the object. The measurement vector, $\mathbf{z}(k)$, is composed of all N measurements and has the dimension $N \times 1$. Then, the following model can be formulated as

$$\mathbf{p}(k) = \mathbf{f}(\mathbf{p}(k-1)) + \boldsymbol{\eta}(k-1) \tag{4}$$

$$\mathbf{z}(k) = \mathbf{h}(\mathbf{p}(k)) + \boldsymbol{\gamma}(k-1). \tag{5}$$

Thereby, the $M \times 1$ vector $\boldsymbol{\eta}(k-1)$ and the $N \times 1$ vector $\boldsymbol{\gamma}(k-1)$ are additive, Gaussian distributed noise vectors with zero mean and covariance $\mathbf{Q}(k-1)$ and $\mathbf{R}(k-1)$. The actual filtering equations are divided into a prediction step

$$\hat{\mathbf{p}}(k|k-1) = \mathbf{f}(\hat{\mathbf{p}}(k-1|k-1)) \tag{6}$$

$$\mathbf{K}(k|k-1) = \mathbf{F}_{\mathbf{p}}(k-1|k-1)\,\mathbf{K}(k-1|k-1) \tag{7}$$

$$\mathbf{F}_{\mathbf{p}}{}^{T}(k-1|k-1) + \mathbf{Q}(k-1) \tag{8}$$

and an update step

$$\mathbf{v}(k) = \mathbf{z}(k) - \mathbf{h}(\hat{\mathbf{p}}(k|k-1)) \tag{9}$$

$$\mathbf{S}(k) = \mathbf{H}_{\mathbf{p}}(k|k-1)\mathbf{K}(k|k-1)\mathbf{H}_{\mathbf{p}}^{T}(k|k-1) + \mathbf{R}(k) \tag{10}$$

$$\mathbf{G}(k) = \mathbf{K}(k|k-1)\mathbf{H}_{\mathbf{p}}^{T}(k|k-1)\mathbf{S}^{-1}(k) \tag{11}$$

$$\hat{\mathbf{p}}(k|k) = \hat{\mathbf{p}}(k|k-1) + \mathbf{G}(k)\mathbf{v}(k) \tag{12}$$

$$\mathbf{K}(k|k) = \mathbf{K}(k|k-1) - \mathbf{G}(k)\mathbf{S}(k)\mathbf{G}^{T}(k) \tag{13}$$

where $\mathbf{F}_{\mathbf{p}}$ and $\mathbf{H}_{\mathbf{p}}$ are the Jacobian matrices of $\mathbf{f}$ and $\mathbf{h}$, defined as

$$[\mathbf{F}_{\mathbf{p}}(k)]_{i,j} = \left.\frac{\partial \mathbf{f}_i(\mathbf{p})}{\partial \mathbf{p}_j}\right|_{\mathbf{p}=\hat{\mathbf{p}}(k)} \tag{14}$$

$$[\mathbf{H}_{\mathbf{p}}(k)]_{i,j} = \left.\frac{\partial \mathbf{h}_i(\mathbf{p})}{\partial \mathbf{p}_j}\right|_{\mathbf{p}=\hat{\mathbf{p}}(k)}. \tag{15}$$

B. DOA-only Extended Kalman Filter

The EKF applied to localization based on DOA estimation has long been studied, e.g. [10]. In this context, $M = 4$ and the state can be expressed by

$$\mathbf{p} = (x, y, v_x, v_y)^T \tag{16}$$

where v_x and v_y are the PU velocity in x and y directions. For collaborative localization based on two SUs, $N = 2$ DOA estimates are available. Thus, the measurement vector becomes

$$\mathbf{z} = (\vartheta_1, \vartheta_2)^T \tag{17}$$

with the non-linear measurement equation (1) and $\mathbf{R}(k) = \sigma_{\mathrm{a}}^2\mathbf{I}$ where $\mathbf{I}$ denotes the 2×2 identity matrix. Then, the Jacobian matrix for the measurement function $\mathbf{h}$ can be easily shown to be

$$\mathbf{H}_{\mathbf{p}}(k) = \begin{pmatrix} -\frac{(y-y_1)}{(x-x_1)^2+(y-y_1)^2} & \frac{(x-x_1)}{(x-x_1)^2+(y-y_1)^2} & 0 & 0 \\ -\frac{(y-y_2)}{(x-x_2)^2+(y-y_2)^2} & \frac{(x-x_2)}{(x-x_2)^2+(y-y_2)^2} & 0 & 0 \end{pmatrix} \tag{18}$$

whereas $\mathbf{F}_{\mathbf{p}}(k)$ and $\mathbf{Q}(k)$ depend on the assumed PU movement model.

IV. Proposed Localization Using Both RSS and DOA

The combination of RSS and DOA for localization is very interesting since both DOA and especially RSS can be fairly easily measured in the SU devices. Furthermore, both quantities carry information about location - RSS in terms of distance and DOA in terms of direction. Thus it makes clearly sense to combine these two sources of information in the localization task. In theory, this makes the localization possible, even if only a single SU is involved. However, in the case of a non-cooperating PU, its transmit power in (2) is not available and needs to be estimated along with the position. Furthermore, the standard deviation of shadowing and its correlation are quite high such that it is hard to extract the distance from the RSS. On the other hand, when the DOA estimation is coarse and the tracking geometry suboptimal as the case in a CR network where the SUs do the sensing, localization performance may be improved by utilizing the RSS in addition to the DOA.

A. RSS-DOA Extended Kalman Filter

Since the PU transmit power is now assumed unknown and also estimated, it has to be considered as PU state in the model, yielding $M = 5$ and a state vector

$$\mathbf{p} = (x, y, v_x, v_y, P_{\mathrm{PU}})^T. \tag{19}$$

Utilizing the RSS in the EKF means that two additional measurements are available, i.e. $N = 4$ for two collaborating SUs. Then, the measurement vector can be modified to become

$$\mathbf{z} = (\vartheta_1, \vartheta_2, P_{\mathrm{SU},1}, P_{\mathrm{SU},2})^T. \tag{20}$$

Therefore, the measurement equations $\mathbf{h}_i$ remain (1) for $i = 1, 2$. For the RSS elements ($i = 3, 4$), we model

the measurement equations using (2) only. The measurement noise is then equal to the shadowing component in (2), i.e. $\gamma_{2+j}(k) = m_j(k)$. However, in the Kalman filter model we ignore the correlation (3) of the measurement noise. Thus, the error covariance becomes a diagonal matrix

$$\mathbf{R}(k) = \mathrm{diag}\left[\sigma_a^2, \sigma_a^2, \sigma_f^2, \sigma_f^2\right]. \tag{21}$$

The Jacobian matrix of the hybrid EKF is then equal to

$$\mathbf{H}_\mathbf{p}(k) = \begin{pmatrix} \mathbf{H}_\mathbf{p}^D & \mathbf{0} \\ \mathbf{H}_\mathbf{p}^R & \mathbf{1} \end{pmatrix} \tag{22}$$

where $\mathbf{0} = [0,0]^T$, $\mathbf{1} = [1,1]^T$ are the influence of the transmit power, $\mathbf{H}_\mathbf{p}^D$ is due to the DOA and equal to (18), $\mathbf{H}_\mathbf{p}^R$ is due to the RSS and given by

$$\mathbf{H}_\mathbf{p}^D(k) = \beta \begin{pmatrix} \frac{(x-x_1)}{(x-x_1)^2+(y-y_1)^2} & \frac{(y-y_1)}{(x-x_1)^2+(y-y_1)^2} & 0 & 0 \\ \frac{(x-x_2)}{(x-x_2)^2+(y-y_2)^2} & \frac{(y-y_2)}{(x-x_2)^2+(y-y_2)^2} & 0 & 0 \end{pmatrix} \tag{23}$$

with $\beta = -\frac{10\alpha}{\ln(10)}$.

V. Performance Examples and Simulations

The performance of the developed RSS-DOA EKF is studied for a PU moving with a constant velocity $v = \sqrt{v_x^2 + v_y^2}$ on an example trajectory as depicted in Figure 2. The PU is assumed to continuously transmit with the same power P_{PU} that is uniformly drawn from $[-35 \ldots 35]$ dBm for each simulation run. Two SUs are randomly placed on an area of $100 \times 100\mathrm{m}^2$ each of which measuring the DOA and RSS with a period of T. The DOA measurement is modeled according to (1) and the RSS measurement according to (2) with a correlation (3) for successive measurements at each SU but without correlation between the measurements of the two SUs. In order to avoid the problems associated with initialization such as divergence, the EKF is initialized with the actual PU coordinates whereas the velocities and PU power are all set to zero. Internally, the EKF works with a discretized Wiener velocity model [21] for the PU movement.

Figure 3 shows the root-mean squared error (RMSE) in the position estimate as a function of the correlation distance. The measurement distance $\Delta x = vT = 0.5$ m is fixed and the environment exhibits low shadowing with $\sigma_{\mathrm{f}} = 4$ dB. In this case, the RSS-DOA EKF outperforms the conventional DOA-only EKF for all considered σ_{a}. The RMSE of the RSS-DOA EKF increases with d_{c} which is explained by the model (21) getting worse. Furthermore, in case of high correlation, m_i remains practically constant for successive measurements, making it hard to distinguish m_i from the distance and transmit power component in (2). However, once $d_{\mathrm{c}} \approx 20$ m, the graphs level off. This coincides with the correlation distance where (21) approaches σ_{f}^2, i.e. the correlation is maximal. The gain in localization accuracy depends on the quality of DOA estimates. For $d_{\mathrm{c}} > 20$ m and $\sigma_{\mathrm{a}} = 0.3$ rad the RSS-DOA EKF outperforms the DOA-only EKF by $\approx 3\%$ (0.3m) while the gain for $\sigma_a = 0.7$ rad is $\approx 13\%$ (2m). In case of power estimation (Figure 4), the mean absolute error (MAE) also

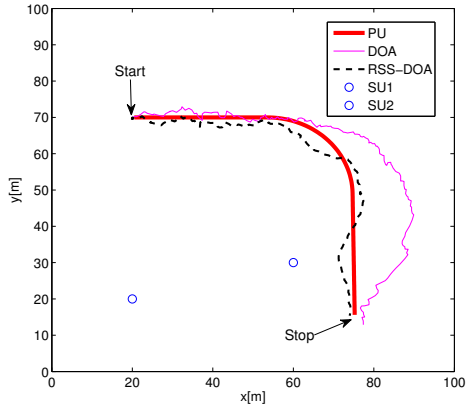

Fig. 2. PU trajectory and temporary divergence of the DOA-only EKF estimate due to disadvantageous PU-SU geometry. The proposed hybrid RSS-DOA processing, in turn, demonstrates accurate tracking of the moving PU.

increases with the correlation distance. However, at $d_{\mathrm{c}} = 20$ m, the MAE does not flatten out but the biggest slope occurs prior to that point. As expected, the more coarse the DOA estimation the higher the MAE since an accurate transmit power estimation requires an accurate position estimate.

The influence of shadowing on the localization accuracy is depicted in Figure 5. Again, the simulations were run with a fixed $\Delta x = vT = 0.5$ m, this time keeping the correlation distance constant at $d_{\mathrm{c}} = 20$ m. The graphs reveal the intuitive result that the RSS-DOA EKF is beneficial in those situations where the DOA is coarse and shadowing is low. Moreover when the shadowing becomes too large for a given σ_a, the classical DOA-only EKF actually outperforms the RSS-DOA EKF. At this point, it is important to note though that in practice an increase in shadowing also influences the SNR and as a consequence the quality of DOA estimates. However, as discussed earlier, correlation between DOA and RSS measurement noise is not considered in the underlying model. The MAE in power estimation in this setup is shown in Figure 6.

Besides shadowing and the quality of DOA estimates, the performance of the two approaches is heavily influenced by the PU-SU geometry. By looking at individual realizations, it was noted that utilizing the RSS is beneficial in those situations where the PU-SU geometry resembles a straight line. In those cases, the DOA alone is not enough to properly localize the PU since small errors in the DOA estimates result in big errors in the position estimates. In the extreme case where PU and SUs are on a straight line, localization is possible only with respect to one dimension. An example of a disadvantageous PU-SU geometry is depicted in Figure 2. This result was obtained with the SUs located at $(20, 20)$ m and $(60, 30)$ m, $d_c = 20$ m, $\sigma_f = 4$ dB, $\Delta x = 0.5$ m and $\sigma_a = 0.3$ rad. As typical for these SU positions, the estimate of the DOA-

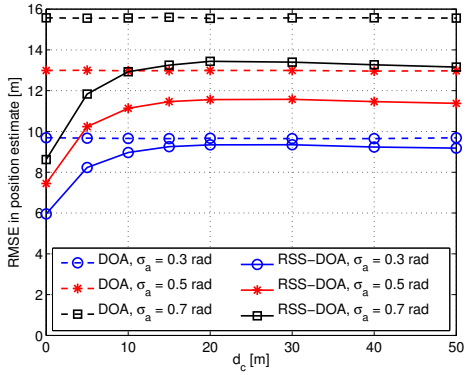

Fig. 3. RMSE in position estimate for $\Delta x = vT = 0.5$ m and $\sigma_f = 4$ dB.

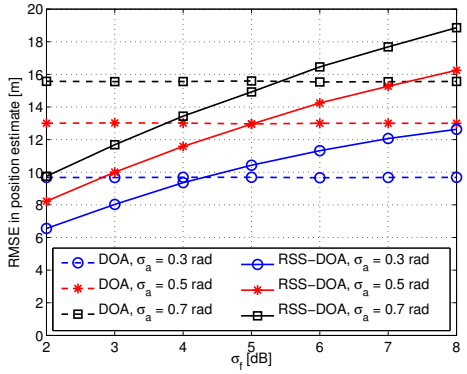

Fig. 5. RMSE in position estimate for $\Delta x = vT = 0.5$ m and $d_c = 20$ m.

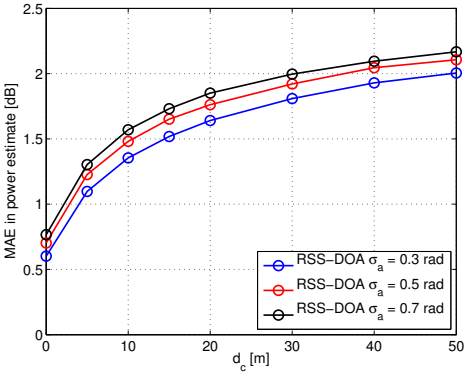

Fig. 4. MAE in power estimate for $\Delta x = vT = 0.5$ m and $\sigma_f = 4$ dB.

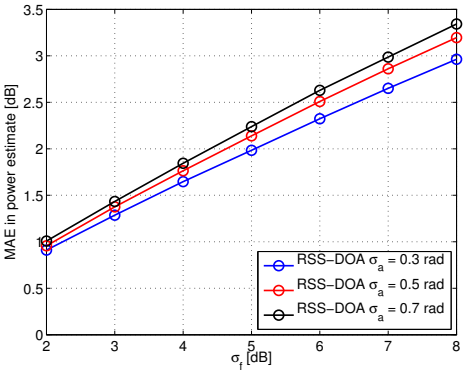

Fig. 6. MAE in power estimate for $\Delta x = vT = 0.5$ m and $d_c = 20$ m.

only EKF temporary diverges from the actual trajectory as the PU-SU geometry starts to resemble a line. The RSS-DOA on the other hand does not diverge. Several simulations were run with this setup resulting in a RMSE of around 14.2 m for the DOA-only EKF and a RMSE of around 9.6 m for the RSS-DOA EKF. Therefore, in contrast to the random SU placement, the RSS-DOA EKF outperforms the DOA-only EKF by $\approx 32\%$ if $\sigma_a = 0.3$ rad (as opposed to 11% with random SU positioning), proving the strong dependence of performance on the PU-SU geometry.

VI. Conclusions

In this paper, we studied hybrid RSS-DOA localization of a moving PU in the cognitive radio system context. More specifically, we proposed an EKF that, in contrast to the classical DOA-only EKF, also utilizes the RSS associated with the DOA. We showed that our hybrid EKF significantly outperforms the classical DOA-only EKF when the DOA estimation is coarse. Our evaluation revealed that the increase in accuracy is in particular due to cases where the PU-SU geometry resembles a straight line. Then, localization based on DOA only becomes very inaccurate. Since the RSS carries information about the distance to the PU, the hybrid solution, on the other hand, does not suffer from the same, strong dependence on the PU-SU geometry. Another benefit of the proposed hybrid solution is that the transmit power of the PU, which is assumed unknown in CR, can be estimated along with the PU location. This can greatly help in optimizing the SU network operation while protecting the PUs.

References

[1] I. Mitola, J. and J. Maguire, G.Q., "Cognitive radio: making software radios more personal," *Personal Communications, IEEE*, vol. 6, pp. 13 –18, Aug. 1999.

[2] S. Haykin, "Cognitive radio: brain-empowered wireless communications," *Selected Areas in Communications, IEEE Journal on*, vol. 23, pp. 201 – 220, Feb. 2005.

[3] S. Huang, Z. Ding, and X. Liu, "Non-intrusive cognitive radio networks based on smart antenna technology," in *Global Telecommunications Conference, 2007. GLOBECOM '07. IEEE*, pp. 4862 –4867, Nov. 2007.

[4] F. Penna, J. Wang, and D. Cabric, "Cooperative localization of primary users by directional antennas or antenna arrays: Challenges and design issues," in *Antennas and Propagation (APSURSI), 2011 IEEE International Symposium on*, pp. 1113 –1115, July 2011.

[5] L. D. Nardis, M.-G. D. Benedetto, A. Akthar, and O. Holland, "Combination of DOA and beamforming in position-based routing for underlay cognitive wireless networks," in *Cognitive Radio Oriented Wireless Networks and Communications (CROWNCOM), 2012 Seventh International ICST Conference on*, 2012.

[6] J. Wang, P. Urriza, Y. Han, and D. abri, "Weighted centroid algorithm for estimating primary user location: Theoretical analysis and distributed implementation," *arXiv:1011.2313*, Nov. 2010.

[7] R. Schmidt, "Multiple emitter location and signal parameter estimation," *Antennas and Propagation, IEEE Transactions on*, vol. 34, pp. 276 – 280, Mar. 1986.

[8] P. Stoica and A. Nehorai, "MUSIC, maximum likelihood and cramer-rao bound," in *Acoustics, Speech, and Signal Processing, 1988. ICASSP-88., 1988 International Conference on*, pp. 2296 –2299 vol.4, Apr. 1988.

[9] D. Cabric, S. Mishra, and R. Brodersen, "Implementation issues in spectrum sensing for cognitive radios," in *Signals, Systems and Computers, 2004. Conference Record of the Thirty-Eighth Asilomar Conference on*, vol. 1, pp. 772 – 776 Vol.1, Nov. 2004.

[10] V. Aidala, "Kalman filter behavior in bearings-only tracking applications," *Aerospace and Electronic Systems, IEEE Transactions on*, vol. AES-15, pp. 29 –39, Jan. 1979.

[11] B. Rao and H. Durrant-Whyte, "Fully decentralised algorithm for multisensor kalman filtering," *Control Theory and Applications, IEE Proceedings D*, vol. 138, pp. 413 –420, Sept. 1991.

[12] I. Kadar, "Optimum geometry selection for sensor fusion," *Proceedings of SPIE*, vol. 3374, pp. 96–107, July 1998.

[13] L. Kaplan, "Global node selection for localization in a distributed sensor network," *Aerospace and Electronic Systems, IEEE Transactions on*, vol. 42, pp. 113 – 135, Jan. 2006.

[14] A. Catovic and Z. Sahinoglu, "The cramer-rao bounds of hybrid TOA/RSS and TDOA/RSS location estimation schemes," *Communications Letters, IEEE*, vol. 8, pp. 626 – 628, Oct. 2004.

[15] S. Wang, B. Jackson, and R. Inkol, "Hybrid RSS/AOA emitter location estimation based on least squares and maximum likelihood criteria," in *2012 26th Biennial Symposium on Communications (QBSC)*, pp. 24 –29, May 2012.

[16] R. Martin and R. Thomas, "Algorithms and bounds for estimating location, directionality, and environmental parameters of primary spectrum users," *Wireless Communications, IEEE Transactions on*, vol. 8, pp. 5692 –5701, Nov. 2009.

[17] Y. Bar-Shalom and E. Tse, "Tracking in a cluttered environment with probabilistic data association," *Automatica*, vol. 11, pp. 451–460, Sept. 1975.

[18] T. Fortmann, Y. Bar-Shalom, and M. Scheffe, "Sonar tracking of multiple targets using joint probabilistic data association," *Oceanic Engineering, IEEE Journal of*, vol. 8, pp. 173 – 184, July 1983.

[19] M. Gudmundson, "Correlation model for shadow fading in mobile radio systems," *Electronics Letters*, vol. 27, pp. 2145 –2146, Nov. 1991.

[20] S. O. Haykin, *Adaptive Filter Theory*. Prentice Hall, 4 ed., Sept. 2001.

[21] Y. Bar-Shalom, X. R. Li, and T. Kirubarajan, *Estimation with Applications to Tracking and Navigation: Theory Algorithms and Software*. Wiley-Blackwell, July 2001.

[22] K. Phan, S. Vorobyov, N. Sidiropoulos, and C. Tellambura, "Spectrum sharing in wireless networks via QoS-Aware secondary multicast beamforming," *Signal Processing, IEEE Transactions on*, vol. 57, pp. 2323 –2335, June 2009.

Publication 4

J. Werner, A. Hakkarainen, J. Wang, D. Cabric, and M. Valkama, "Primary user localization in cognitive radio networks using sectorized antennas," in *Proceedings of the 10th Annual Conference on Wireless On-Demand Network Systems and Services (WONS)*, Banff, AB, 2013, pp. 68–73.

Primary User Localization in Cognitive Radio Networks Using Sectorized Antennas

(Invited Paper)

Janis Werner*, Jun Wang†, Aki Hakkarainen*, Mikko Valkama* and Danijela Cabric†
* Department of Communications Engineering
Tampere University of Technology, P.O. Box 553, FI-33101 Tampere, Finland
Emails: {janis.werner, aki.hakkarainen, mikko.e.valkama}@tut.fi
† Electrical Engineering Department
University of California Los Angeles, Los Angeles, CA 90095, USA
Emails: {eejwang, danijela}@ee.ucla.edu

***Abstract*—Information about primary user (PU) location can enable several key capabilities in cognitive radio (CR) networks. In this paper we consider PU localization using received-signal-strength (RSS) and direction-of-arrival (DoA) estimates from sectorized antenna. Abstracting from practical antenna types, we define a sectorized antenna as an antenna that can be set to different operating modes, each of which resulting in a selectivity of those signals that arrive from within a certain, continuous range of angles, i.e. a sector. We propose a low complexity algorithm, the MaxE algorithm, that provides coarse RSS and DoA estimates, and derive the asymptotic bounds for its root mean square error (RMSE) as a function of the antenna parameters. We then propose a modified Stansfield algorithm with a novel RSS-based weighting scheme based on the Stansfield DoA fusion method, which obtains PU location estimates from measurements of the MaxE algorithm. The modified Stansfield algorithm improves the accuracy of the Stansfield algorithm with equal weights. Simulation results studying the impact of various system parameters, such as number of sectors, number of samples and signal-to-noise ratio, on the DoA/RSS estimation and localization accuracy are presented to provide design guidelines for localization systems based on sectorized antennas.**

I. Introduction

Information about primary user (PU) location can enable several key capabilities in cognitive radio (CR) networks including improved spatio-temporal sensing, intelligent location-aware routing, as well as aiding spectrum policy enforcement [1]. The PU localization requires cooperation of a large amount of CRs performing passive localization, since they need to detect and localize non-cooperative PU in the whole coverage area at a very low signal-to-noise ratio (SNR) [2]. Prior research on passive localization can be categorized into three classes based on the types of measurements shared among sensors, namely received-signal-strength (RSS), time-difference-of-arrival (TDoA) and direction-of-arrival (DoA) [3]. TDoA-based algorithms are not suitable for CR applications since they require perfect synchronization among CRs. Therefore, RSS and DoA-based algorithms are the proper choices for the PU localization problem. Furthermore, our earlier work shows DoA-based and joint RSS/DoA-based algorithms outperform RSS-based algorithms [2].

One specific challenge to the PU localization problem is the difficulty to apply classical DoA estimation approach. The classical approach for DoA estimation assumes each sensor is equipped with a digital antenna array that includes a separate receiver chain for all antenna branches. The samples from all branches are then digitally processed by array processing algorithms such as MUSIC [4] and ESPRIT [5] to obtain DoA estimates. However, considering the large network size of the CR network, CR sensors should be portable and cheap devices with limited hardware and computation capability. Therefore, the cost of the antenna arrays and complexity of the array processing algorithms may make it impractical to apply the classical DoA estimation approach in CR networks.

In this paper we address low-cost and low-complexity DoA estimation and PU localization using sectorized antennas. We define a sectorized antenna as an antenna structure that can be set to selectively receive energy from different sectors. Thereby, a sector denotes a continuous range of angles and selectivity means that signals, arriving from outside of the activated sector, are strongly attenuated. We further assume that sectorized antennas have unique reception capabilities, i.e. only a single sector can be activated at a time. Examples of antenna structures that can be used as sectorized antennas are switched-beam systems (SBSs) and leaky-wave antennas (LWAs). An SBS consists of an antenna array and a beamforming network that can be configured to activate one of several fixed beam patterns [6], [7]. The SBS is more suitable for CR devices since the antenna branches are combined in the RF stage and several key receiver components, such as the analog-to-digital converters, are required only once, compared to one for each antenna branch in case of the digital antenna array [6]. An LWA [8] consists of a single antenna whose electrical properties can be modified such that the antenna's beam is steered to the desired direction, which makes it a very promising candidate for DoA estimation in portable devices. In

The research leading to these results was financially supported by the Doctoral Programme of the President of Tampere University of Technology, the Tuula and Yrjö Neuvo Fund and the Finnish Funding Agency for Technology and Innovation (Tekes, under the project "Reconfigurable Antenna-based Enhancement of Dynamic Spectrum Access Algorithms").

This work was also supported by the National Science Foundation under Grant No.1117600.

terms of our definition of sectorized antennas, different beams of SBSs and LWAs can be used to achieve the selectivity in each of the sectors.

For DoA estimation using sectorized antennas, the prior work requires knowledge of RSS or additional hardware cost. A DoA estimation algorithm based on neural networks is proposed in [7] for multiple DS-CDMA signals impinging on a base station equipped with an SBS. However, the algorithm requires either the RSS to be known or an additional, nearly omnidirectional, antenna at the receiver that is used to normalize the received energies to be independent of the RSS. Analog DoA estimation using an LWA is presented in [9]. However, it is based on continuously changing the antenna's beam, i.e. scanning the received energy as a function of the angle, instead of measurements in sectors.

In order to provide DSP-based DoA estimates that are independent of the underlying technology, we propose the so-called MaxE algorithm which is a low complexity algorithm providing coarse DoA as well as RSS estimates. It uses the orientation of the sector that measures the largest PU energy as the DoA estimate, and then obtains an RSS estimate as a byproduct. We derive the asymptotic bounds for the root mean square error (RMSE) of DoA and RSS estimates obtained using the proposed MaxE algorithm, and study the impact of important system parameters, such as SNR, number of sectors and number of samples, on the accuracy of the MaxE algorithm theoretically and via simulations.

We then proceed to consider the PU localization problem using RSS and DoA measurements from sectorized antennas. Prior work on joint RSS/DoA-based passive localization uses known or estimated DoA estimation error variance as weights for DoA fusion [2]. The most popular algorithm is the Stansfield algorithm which has a low-complexity and high accuracy compared with other candidate DoA fusion algorithms, such as the maximum likelihood algorithm and linear least squares [10]. However, a specific challenge to the fusion of measurements from the MaxE algorithm is that there is no theoretical model on the DoA estimation error variance, and it is difficult to estimate in practical systems using limited number of samples.

To further improve the PU localization accuracy based on the MaxE algorithm, we then propose a modified Stansfield algorithm with a RSS-based weighting scheme. The proposed algorithm uses the RSS estimate of the MaxE algorithm as the weight for each DoA in the DoA fusion process. The modified Stansfield algorithm improves the accuracy of the classical Stansfield algorithm with equal weighting, as shown in our simulation results in Section V.

The rest of the paper is organized as follows. The system model is introduced in Section II. The MaxE algorithm for DoA and RSS estimation and the asymptotic bounds for its accuracy are presented in Section III. The proposed modified Stansfield algorithm for DoA fusion is formulated in Section IV. Numerical results evaluating the impact of various parameters on DoA and RSS estimation and PU localization are discussed in Section V. Finally, the paper is concluded in Section VI.

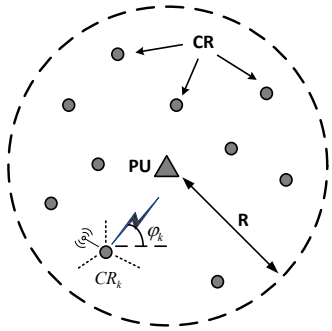

Fig. 1. Illustration of the PU-centric circular model of CR placement. Details of the sectorized antenna are shown for the k^{th} CR, which contains 3 sectors and the antenna is currently measuring in the top-left sector.

II. System Model

In this paper we consider K CRs localizing a single PU on a two-dimensional Cartesian coordinate system. We denote the PU location as $\boldsymbol{\ell}_P = [x_P, y_P]^T$ and the position of CR k as $\boldsymbol{\ell}_k = [x_k, y_k]^T$, which we assume are known to the fusion center. We assume the CRs that can hear the PU are located within a circle with radius R and are uniformly placed in the area, as shown in Fig.1. Each of the CRs is equipped with an antenna whose properties can be modified such that measurements in M different sectors are possible. Thereby, sectors are characterized by the radiation pattern, which we use to describe the attenuation of the PU signal as a function of its DoA. We assume a radiation pattern, $p(\varphi_k - \vartheta_m)$, that is equal for all CRs $k = 1 \dots K$ and whose attenuation depends only on the distance between the PU signal's DoA, φ_k, and orientation ϑ_m of sector m, $m = 1 \dots M$. In practice this is not necessarily the case as the shape of the radiation pattern might be different for every sector. However, since the exact shape in each sector depends on the type of the antenna (e.g. SBS, LWA) and its particular implementation (e.g. SBS with linear array) we adopt this somewhat general model. For the same reason, we further simplify the model of the radiation pattern by approximating only the antenna's main-beam using a Gaussian-like shape as proposed in [11]. Then, the radiation pattern can be expressed as

$$p(\varphi) = \exp\left(-\frac{[\mathcal{M}(\varphi)]^2}{\omega}\right) \tag{1}$$

where $\mathcal{M}(\varphi) = \text{mod}_{2\pi}(\varphi + \pi) - \pi$ is used to restrict the input angle to $[-\pi, \pi]$ and ω is a parameter influencing the width of the beam. With respect to the orientation of the sectors we make the assumption that spacing between sectors, $\Delta\vartheta = \frac{2\pi}{M}$, is constant such that the orientation of sector m may be expressed as $\vartheta_m = m\Delta\vartheta$. We then propose to parameterize the radiation pattern via a value that we denote the side-sector

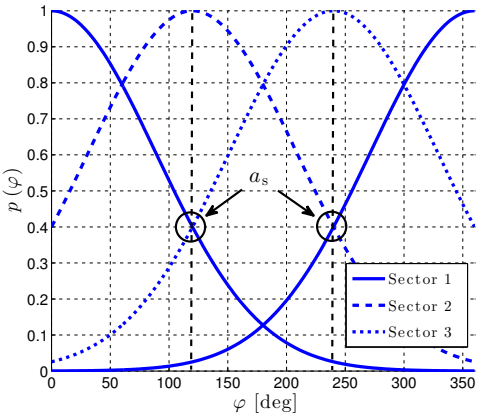

Fig. 2. Illustration of the side-sector suppression of a sectorized antenna with Gaussian radiation pattern, $M = 3$ sectors and $a_s = 0.4$.

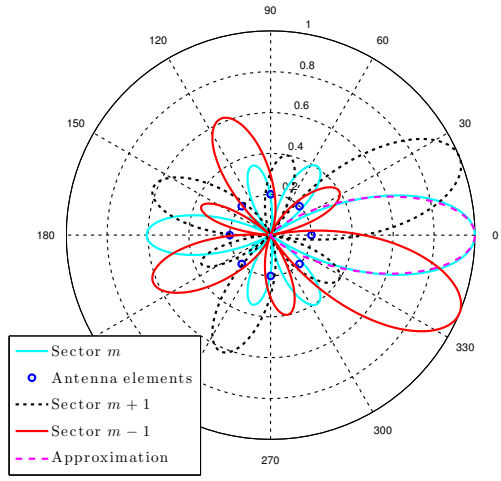

Fig. 3. Radiation pattern of an SBS with $M = 16$ sectors with three of them depicted. The underlying antenna array is circular with 8 antenna elements. The radiation pattern is approximated with a Gaussian pattern, which is parameterized with $\omega = 0.2\,\text{rad}^2$ or $a_s \approx 0.46$.

suppression, a_s. We define the side-sector suppression as the attenuation that a signal, arriving at the orientation ϑ_m of the m^{th} sector, experiences in the neighboring sectors $m-1$ and $m+1$, i.e. $a_s = p(\Delta\vartheta)$. An illustration of this definition can be found in Fig.2. This way of parameterizing makes it possible to examine how strongly beams in neighboring sectors are overlapping, independent of the number of sectors. The result is a beam-width that is determined by

$$\omega = -\frac{(2\pi)^2}{M^2 \ln(a_s)}. \tag{2}$$

Fig.3 shows the radiation pattern of an SBS based on a uniform circular array with 8 antennas. The SBS is configured to yield $M = 16$ equally spaced sectors out of which three are depicted. As can be seen, the main-beam of the sectors is very well approximated by a Gaussian radiation pattern with $\omega = 0.2\,\text{rad}^2$ or $a_s = 0.4625$, demonstrating the practical relevance of our model.

During the measurement period, each of the CRs successively switches through M sectors and receives N complex samples for each sector, which results in $M \times N$ complex samples in total. In order to simplify the presentation we assume that the channel attenuation h_k between PU and CR k is constant over the whole localization period. As a consequence, the complex received signal samples at CR k originating from the m-th sector, with the sample index range $n = (m-1)N+1 \ldots mN$, can be written as

$$x_k(n) = h_k p(\varphi_k - \vartheta_m)\, s(n - \tau_k) + w_k(n). \tag{3}$$

Thereby, τ_k is the delay determined by the propagation time between the PU and CR k and $w_k(n) \sim \mathcal{CN}(0, \sigma_w^2)$ is additive noise assumed to be circular symmetric complex Gaussian. Likewise, the PU signal is modeled as circular symmetric complex Gaussian, i.e. $s(n) \sim \mathcal{CN}(0, E_s)$, which is a good approximation for e.g. OFDM-based transmission. Our channel model for h_k is given as

$$h_k^2 = \frac{c_0 10^{-u_k/10}}{d_k^\alpha}, \tag{4}$$

where c_0 is the (constant) average multiplicative gain at reference distance, $d_k = \|\boldsymbol{\ell}_k - \boldsymbol{\ell}_P\|$ is the distance between the k^{th} CR and PU, α is the path loss exponent, $10^{-u_k/10}$ is a random variable that reflects shadowing, and $u_k \sim \mathcal{N}(0, \sigma_u^2)$ are i.i.d for different CRs.

III. DoA and RSS Estimation Using the MaxE Algorithms

Given the assumptions that the PU signal resembles white Gaussian noise and that the CRs do not have any detailed knowledge about the PU transmission, it is impossible to distinguish between noise and PU signal at the CRs. Therefore, estimations of DoA and RSS should be based on the received energies. At CR k, the energy in sector m is calculated according to

$$\epsilon_{m,k} = \frac{1}{N} \sum_{n=(m-1)N+1}^{mN} |x_k(n)|^2 \tag{5}$$

which results in an expected value equal to

$$\mathrm{E}[\epsilon_{m,k}] = [p(\varphi_k - \vartheta_m)]^2 \gamma_k + \sigma_w^2, \tag{6}$$

where $\gamma_k = h_k^2 E_s$ is the RSS at CR k.

Based on these energy estimates, a very rough DoA estimate may be obtained using the orientation of the sector with the

maximum energy, i.e.

$$\hat{\varphi}_k = \vartheta_{i,k} \,|\, i = \arg\max_i \epsilon_{k,i}. \tag{7}$$

Likewise, the RSS can be estimated using the maximum energy and subtracting the noise variance:

$$\hat{\gamma}_k = \max_i \epsilon_{i,k} - \sigma_{\mathrm{w}}^2. \tag{8}$$

Here, we assume that σ_{w}^2 is known at the CRs, e.g. using reference measurements. However, an estimate of it may easily be obtained by averaging over those sectors with low energies which contain close to no PU signal components, given the antenna has good directionality.

In the following we will refer to (7) and (8) as the MaxE estimators. While these estimators are easily implemented and have a very low complexity, both of them are biased and asymptotically lower bounded. This can be easily verified by considering an estimation with very large N. Then, according to the law of large numbers, (5) yields a value close to the expected value (6). Now, algorithm (7) will always find the correct sector, c. However, for any DoA $\varphi_k \neq \vartheta_{\mathrm{c},k}$ the estimator $\hat{\varphi}_k$ then has a bias of $\vartheta_{\mathrm{c},k} - \varphi_k$, which is a result of the discretization inherent to (7). If we assume a uniform distribution of DoAs, i.e. in (1) we have $\varphi \sim \mathcal{U}(-\pi;\pi)$, we can calculate the asymptotic lower bound on the RMSE of $\hat{\varphi}_k$ that is achieved for $N \to \infty$ according to:

$$\hat{\varphi}_{\mathrm{b}} = \sqrt{\frac{2}{\Delta\vartheta}\int_0^{\frac{1}{2}\Delta\vartheta} \varphi^2 d\varphi} = \frac{\Delta\vartheta}{\sqrt{12}} = \frac{\pi}{M\sqrt{3}}. \tag{9}$$

Similar considerations can be made to verify that the RSS MaxE estimator (8) is biased as well. The respective asymptotic lower bound for $N \to \infty$ on the RMSE of MaxE RSS estimation at SU k is determined by

$$\hat{\gamma}_{k,\mathrm{b}} = \gamma_k \sqrt{\frac{2}{\Delta\vartheta}\int_0^{\frac{1}{2}\Delta\vartheta} \left[1 - p(\varphi)\right]^2 d\varphi}. \tag{10}$$

However, in contrast to (9) this bound depends on the radiation pattern of the antenna. For the Gaussian radiation pattern (1) we obtain the bound

$$\hat{\gamma}_{k,\mathrm{b}} = \gamma_k \left[1 + \frac{1}{2}\sqrt{\frac{\pi}{\ln a_s}}\mathrm{erf}\left(\sqrt{\ln a_s}\right) - \sqrt{\frac{2\pi}{\ln a_s}}\mathrm{erf}\left(\sqrt{\frac{\ln a_s}{2}}\right)\right]^{\frac{1}{2}} \tag{11}$$

where $\mathrm{erf}(x)$ is the error function defined by $\mathrm{erf}(x) = \frac{2}{\sqrt{\pi}}\int_0^x \exp\left(-t^2\right) dt$.

IV. Localization With Modified Stansfield Algorithm

In this section we present the proposed modified Stansfield algorithm for fusion of DoAs obtained from multiple CRs using the MaxE algorithm. We first introduce the basic Stansfield algorithm, which is closely related to the maximum likelihood (ML) DoA fusion algorithm. The ML DoA fusion scheme is a nonlinear least square function that has to be solved by iterative algorithms such as the Gauss-Newton method. The iterative algorithms suffer from divergence which makes the ML DoA fusion scheme not reliable in practical scenarios [12]. The Stansfield algorithm is a linear approximation of the ML fusion scheme resulting in the following closed-form PU location estimate

$$\hat{\boldsymbol{\ell}}_P = (\mathbf{A}^T\mathbf{W}^{-1}\mathbf{A})^{-1}\mathbf{A}^T\mathbf{W}^{-1}\mathbf{b}, \tag{12}$$

where

$$\mathbf{A} = \begin{bmatrix} \sin(\hat{\varphi}_1) & -\cos(\hat{\varphi}_1) \\ \vdots & \vdots \\ \sin(\hat{\varphi}_K) & -\cos(\hat{\varphi}_K) \end{bmatrix},$$
$$\mathbf{b} = \begin{bmatrix} x_1\sin(\hat{\varphi}_1) - y_1\cos(\hat{\varphi}_1) \\ \vdots \\ x_N\sin(\hat{\varphi}_N) - y_N\cos(\hat{\varphi}_N) \end{bmatrix} \tag{13}$$

and the weighting matrix is defined as $\mathbf{W} = \mathrm{diag}[\omega_1^2, \ldots, \omega_K^2]$. The weights ω_k's are usually the DoA estimation error variance, which can be modelled mathematically as a function of array parameters and the RSS for digital antenna arrays [2]. Such a weighting scheme assumes the DoA estimator is asymptotically unbiased for a sufficient number of samples, and the statistical model of the DoA estimation is available (which is true for, for example, the MUSIC algorithm [4]). The geometric interpretation of the Stansfield algorithm is based on minimization of the weighted summation of distances from PU location estimate to lines formed by each CR location and its DoA estimate.

It is not possible to use the weighting scheme in the orginal Stansfield algorithm when using the MaxE algorithm as the DoA estimator, since the MaxE algorithm is biased as we discussed in Section III, and the statistical model for its DoA estimation is not available. Therefore, we propose to use the estimated RSS for each CR as the weights by setting $\mathbf{W} = \mathrm{diag}[\hat{\gamma}_1, \ldots, \hat{\gamma}_K]$, as the RSS estimates reflect the measurement quality of the DoAs. It is shown in our simulation results that the proposed modified Stansfield algorithm provides a proper weighting scheme to further improve the localization accuracy using the MaxE DoA estimator, compared with the Stansfield algorithm with equal weights (by setting $\mathbf{W} = \mathbf{I}_K$).

V. Simulation Results

A. RSS and DoA Estimation

The RSS estimation performance is best when the radiation pattern resembles that of an omnidirectional antenna, i.e. $a_{\mathrm{s}} = 1$. With respect to DoA estimation on the other hand, the directional properties of the antenna obviously need to be preserved, requiring $a_{\mathrm{s}} < 1$. However, for very small a_{s}, if the signal arrives in the middle of orientations of two sectors, the attenuation will be relatively severe, which leads to difficulty in detection and inaccurate RSS and DoA estimates.

As determined with computer simulations, the value of a_s that results in the lowest RMSE in DoA estimation is around 0.4. Since this value seems to always result in the lowest RMSE, independent of parameters such as M, N and SNR, $a_s = 0.4$ is therefore assumed as the default value in the following. Furthermore, our results show that varying the RSS while keeping the SNR constant does not influence the estimation performance. The RSS is thus simply set to a fixed value of $\gamma = 1$pW and σ_w^2 is adjusted in order to control the SNR. The RMSEs on DoA and RSS estimation in Fig.4 – Fig.7 are obtained using a uniform distribution of DoAs, $\varphi \sim \mathcal{U}(-\pi;\pi)$, emulated via averaging over 100 equidistant steps in the interval $\vartheta_k \in \left[0;\frac{\Delta\vartheta}{2}\right]$ and 10^3 realizations per DoA-step.

Fig.4 shows the RMSE of DoA estimation as a function of the SNR. As expected, increasing the number of sectors M from 4 to 10 leads to increasingly better performance. Independent of M, and a low number of samples, $N = 50$, the lower bound is attained for all SNRs in excess of 5 dB. In contrast to this, the RMSE of RSS estimation is almost independent of the amount of samples, with differences in the curves only visible for very low SNR (Fig.5). In addition, the bound is not attained, even for large SNR. Instead the curves saturate at a higher RMSE level from SNR $\approx$ 10 dB onwards. This different behavior in RSS and DoA estimation is explained by the respective requirements for attaining the bound. In case of DoA estimation, it is sufficient that the highest energy measurement occurs in the correct sector while in case of RSS estimation the energy, in addition, needs to be close to its expected value (6). The same behavior is observed when plotting the RMSE of DoA and RSS estimation as a function of the amount of samples, N, as depicted in Fig.6 and Fig.7. Then, for a low SNR of 0 dB, the DoA RMSE approaches the bounds already for around $N = 200$ samples, while in case of RSS estimation, the bound is not attained even for $N = 500$ samples. However, as this asymptotic bound is for $N \to \infty$, a further increase of the amount of samples does result in a RMSE that approaches the bound increasingly close.

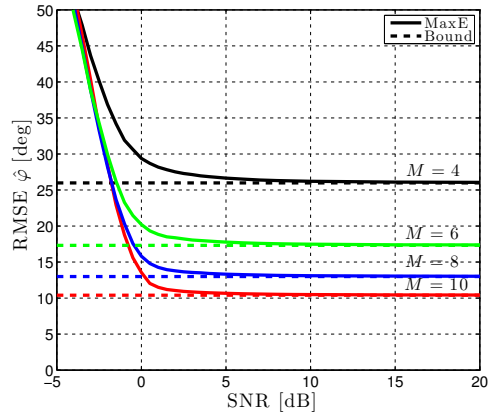

Fig. 4. Dependence of DoA estimation performance on the SNR for uniform distribution of DoAs. Parameters: N = 50, $a_s = 0.4$, $\gamma = 1$ mW, $M = \{4, 6, 8, 10\}$.

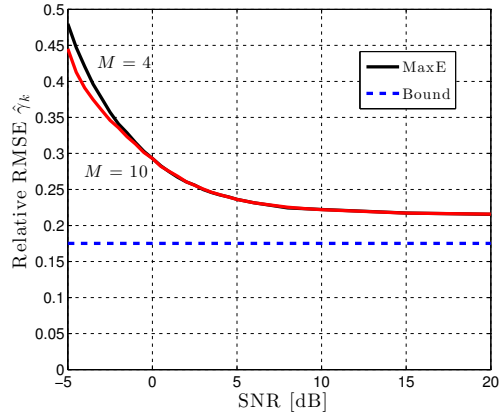

Fig. 5. Dependence of RSS estimation performance on the SNR for uniform distribution of DoAs. Depiction of the relative RMSE, i.e. $^{(\text{RMSE}\,\hat{\gamma}_k)}/_{\gamma_k}$. Parameters: N = 50, $a_s = 0.4$, $\gamma = 1$ mW, $M = \{4, 10\}$.

B. PU Localization

The basic parameter settings for PU localization are summarized as follows. The CRs are uniformly placed within a circle of radius $R = 150$m, centered around the PU with location $\boldsymbol{\ell}_P = [0, 0]^T$ for simplicity and without loss of generality. The PU signal power E_s is 20dBm (100mW) which is the typical radiation power of IEEE 802.11b/g wireless LAN transmitters for 20MHz channels in ISM bands. The measurement noise power σ_w^2 is -80dBm (10pW) which is a moderate estimate of the noise introduced in the DoA estimation process, compared to the -100dBm (0.1pW) thermal noise power of the 802.11 WLAN channel. The path-loss exponent and shadowing standard deviation are $\alpha = 5$ and $\sigma_u = 6$dB respectively. The sampling rate at each CR is 40MHz. The power and channel settings result in an averaged received SNR of 1dB. Each data point in the figures is obtained from averages of 200 CR placements and 200 realization of RSS/DoA measurements per placement.

Fig.8 illustrates the performance of the Stansfield algorithm with equal weighting (EW-Stan.) and the modified Stansfield algorithm (M-Stan.) versus the number of CRs K, with varying number of sectors M. The number of samples $N = 50$. Results in the figure show that increasing the number of CRs provides steady performance gain for both algorithms. Comparing the performance of the two algorithms, we observe that the modified Stansfield algorithm outperforms the Stansfield algorithm with equal weighting for all simulated number of sectors, indicating using the RSS estimates from the MaxE

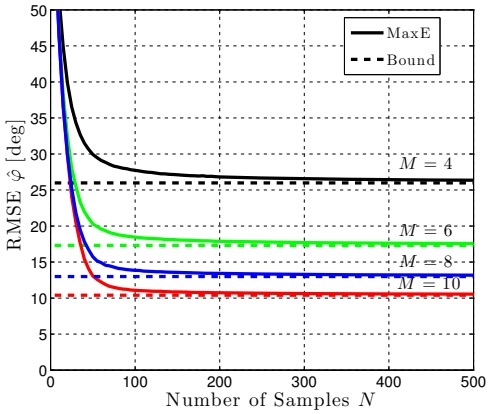

Fig. 6. Dependence of DoA estimation performance on the SNR for uniform distribution of DoAs. Parameters: SNR = 0 dB, $a_s = 0.4$, $\gamma = 1$ mW, $M = \{4, 6, 8, 10\}$

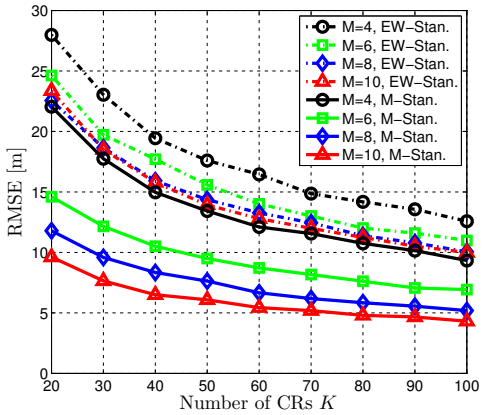

Fig. 8. RMSE of PU localization using Stansfield algorithm with equal weights (EW-Stan.) and the modified Stansfield algorithm (M-Stan.) versus number of CRs K, with varying number of sectors M. The number of samples $N = 50$.

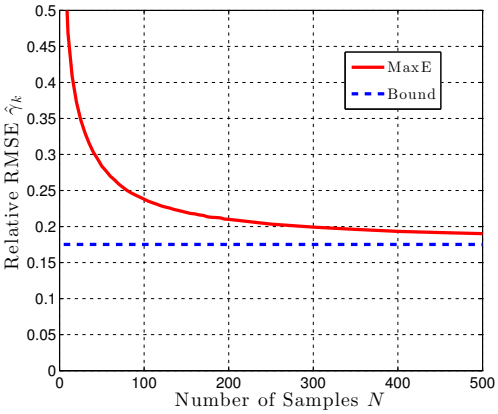

Fig. 7. Dependence of RSS estimation performance on the amount of samples for uniform distribution of DoAs. Depiction of the relative RMSE, i.e. $^{(\text{RMSE}\,\hat{\gamma}_k)}/_{\gamma_k}$. Parameters: SNR = 0 dB, $a_s = 0.4$, $\gamma = 1$ mW. At this SNR, the result is the same for either of the values $M = \{4, 6, 8, 10\}$.

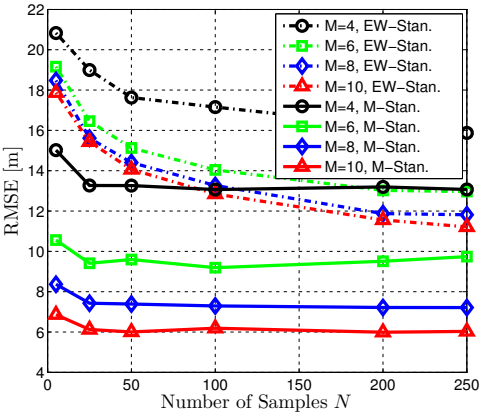

Fig. 9. RMSE of PU localization using Stansfield algorithm with equal weights (EW-Stan.) and the modified Stansfield algorithm (M-Stan.) versus number of samples N, with varying number of sectors M. The number of CRs $K = 50$.

algorithm as weights is beneficial. It is also observed that the benefit of adding number of sectors from 4 to 6 is about twice compared with 6 to 8; and the benefit continues to saturate for adding even more sectors. This indicates that in practical systems, using a small number of sectors at each node is good from both implementation cost and localization accuracy point of view.

Fig.9 compares the accuracy of the Stansfield algorithm with equal weighting and the modified Stansfield algorithm versus the number of samples N, with a varying number of sectors M. The number of CRs $K = 50$. Fig.9 shows that the modified Stansfield algorithm provides a performance gain compared with the Stansfield algorithm with equal weights for all simulated number of sectors. Another observation is that when the number of samples increases, the RMSE saturates for the modified Stansfield algorithm after a certain threshold, at around 50. This agrees with the results shown in Fig.6 since the RMSE on DoA estimation saturates after about 50 samples.

VI. Conclusion

In this paper we focused on the usage of energy measurements from sectorized antennas to solve the PU localization

problem. We first proposed the MaxE algorithm which provides low-complexity RSS and DoA estimates, and derived the asymptotic bounds for the RMSE of the estimates as the number of samples and sectors increases. We then proposed the modified Stansfield algorithm to fuse the DoAs obtained by the MaxE algorithm at each CR. The proposed algorithm uses the RSS estimates of the MaxE algorithm as weights for DoA fusion, and reduces the RMSE of the standard Stansfield algorithm with equal weights by 8 meters with 10 sectors, 50 samples and 50 CRs. Our future work includes advanced RSS and DoA estimators that exploit the knowledge of the antenna radiation pattern and measurement noise variance, as well as the Cramer-Rao bounds for RSS/DoA estimation and PU localization using sectorized antenna.

REFERENCES

[1] H. Celebi and H. Arslan, "Utilization of location information in cognitive wireless networks," *IEEE Wireless Commun. Mag.*, vol. 14, no. 4, pp. 6 –13, Aug. 2007.

[2] J. Wang, J. Chen, and D. Cabric, "Cramer-rao bounds for joint rss/doa-based primary-user localization in cognitive radio networks," *accepted for publication in IEEE Trans. Wireless Commun.*, December 2012, [Online] http://arxiv.org/abs/1207.1469.

[3] N. Patwari, J. Ash, S. Kyperountas, A. Hero, R. Moses, and N. Correal, "Locating the nodes: cooperative localization in wireless sensor networks," *IEEE Signal Process. Mag.*, vol. 22, no. 4, pp. 54–69, July 2005.

[4] P. Stoica and N. Arye, "Music, maximum likelihood, and cramer-rao bound," *IEEE Trans. Acoust., Speech, Signal Process.*, vol. 37, no. 5, pp. 720 –741, May 1989.

[5] R. Roy and T. Kailath, "Esprit-estimation of signal parameters via rotational invariance techniques," *IEEE Trans. Acoust., Speech, Signal Process.*, vol. 37, no. 7, pp. 984–995, Jul. 1989.

[6] T. Ohira, "Adaptive array antenna beamforming architectures as viewed by a microwave circuit designer," in *Asia-Pacific Microwave Conference*, 2000, pp. 828 –833.

[7] K. Gotsis, K. Siakavara, and J. Sahalos, "On the direction of arrival (DoA) estimation for a switched-beam antenna system using neural networks," *IEEE Trans. Antennas Propag.*, vol. 57, no. 5, pp. 1399 – 1411, May 2009.

[8] D. Piazza, D. Michele, and K. Dandekar, "Two port reconfigurable crlh leaky wave antenna with improved impedance matching and beam tuning," in *3rd European Conference on Antennas and Propagation 2009 (EuCAP09)*, Mar. 2009, pp. 2046–2049.

[9] S. Abielmona, H. Nguyen, and C. Caloz, "Analog direction of arrival estimation using an electronically-scanned CRLH leaky-wave antenna," *IEEE Trans. Antennas Propag.*, vol. 59, no. 4, pp. 1408 –1412, Apr. 2011.

[10] J. Wang and D. Cabric, "A cooperative doa-based algorithm for localization of multiple primary-users in cognitive radio networks," in *Proc. IEEE GLOBECOM*, Dec. 2012.

[11] R. Martin and R. Thomas, "Algorithms and bounds for estimating location, directionality, and environmental parameters of primary spectrum users," *IEEE Trans. Wireless Commun.*, vol. 8, no. 11, pp. 5692 –5701, Nov. 2009.

[12] M. Gavish and A. Weiss, "Performance analysis of bearing-only target location algorithms," *IEEE Trans. Aerosp. Electron. Syst.*, vol. 28, no. 3, pp. 817–828, Jul. 1992.

Publication 5

J. Werner, A. Hakkarainen, J. Wang, D. Cabric, and M. Valkama, "Primary user DoA and RSS estimation in cognitive radio networks using sectorized antennas," in *Proceedings of the 8th International Conference on Cognitive Radio Oriented Wireless Networks (CROWNCOM)*, Washington, DC, 2013, pp. 43–48.

Primary User DoA and RSS Estimation in Cognitive Radio Networks Using Sectorized Antennas

Janis Werner*, Jun Wang†, Aki Hakkarainen*, Mikko Valkama* and Danijela Cabric†
* Department of Electronics and Communications Engineering
Tampere University of Technology, P.O. Box 553, FI-33101 Tampere, Finland
Emails: {janis.werner, aki.hakkarainen, mikko.e.valkama}@tut.fi
† Electrical Engineering Department
University of California Los Angeles, Los Angeles, CA 90095, USA
Emails: {eejwang, danijela}@ee.ucla.edu

***Abstract*—Received-signal-strength (RSS) and direction-of-arrival (DoA) are the sufficient measurements to solve the primary user localization problem in cognitive radio networks. In this paper we consider using energy measurements from sectorized antenna to estimate RSS and DoA of a primary user. Abstracting from practical antenna types, we define a sectorized antenna as an antenna that can be set to different operating modes, each of which resulting in a selectivity of those signals that arrive from within a certain, continuous range of angles, i.e. a sector. We first characterize the achievable performance of RSS and DoA estimations using energy measurements from sectorized antennas by means of the Cramer-Rao Bound (CRB), which provides a lower bound on the estimation accuracy of any unbiased estimator. We then propose a practical RSS and DoA estimator, namely the simplified least squares (SLS) algorithm. The SLS algorithm minimizes a cost function obtained from two largest energy measurements among all sectors, and its accuracy closely approaches the CRB. Simulation results studying the impact of important system parameters, such as SNR, number of sectors and number of samples, on the achievable accuracy specified by the CRB and the SLS algorithm are presented.**

I. Introduction

Information about primary user (PU) location can enable several key capabilities in cognitive radio (CR) networks including improved spatio-temporal sensing, intelligent location-aware routing, as well as aiding spectrum policy enforcement [1]. The PU localization requires cooperation of a large amount of CRs performing passive localization, since they need to detect and localize non-cooperative PU or PUs in the whole coverage area at a very low signal-to-noise ratio (SNR) [2]. Prior research on passive localization can be categorized into three classes based on the types of measurements shared among sensors, namely received-signal-strength (RSS), time-difference-of-arrival (TDoA) and direction-of-arrival (DoA) [3]. TDoA-based algorithms are not suitable for CR applications since they require perfect synchronization among CRs. Therefore, RSS and DoA-based algorithms are the proper choices for the PU localization problem. Furthermore, our earlier work shows DoA-based and joint RSS/DoA-based algorithms outperform RSS-based algorithms [2].

One specific challenge to the PU localization problem is the difficulty to apply the classical DoA estimation approach [4], [5]. The classical approach for DoA estimation assumes each sensor is equipped with an antenna array that includes a separate receiver chain for all antenna branches. The samples from all branches are then digitally processed by array processing algorithms such as MUSIC [4] and ESPRIT [5] to obtain DoA estimates. However, considering the large network size of the CR network, CR sensors should be portable and cheap devices with limited hardware and computation capability. Therefore, the cost of the antenna arrays and the complexity of array processing algorithms may make it impractical to apply the classical DoA estimation approach in CR networks.

In this paper we address low-cost and low-complexity DoA estimation using sectorized antennas. We define a sectorized antenna as an antenna structure that can be set to selectively receive energy from different sectors. Thereby, a sector denotes a continuous range of angles and selectivity means that signals, arriving from outside of the activated sector, are strongly attenuated. We further assume that sectorized antennas have unique reception capabilities, i.e. only a single sector can be activated at a time. Examples of antenna structures that can be used as sectorized antennas are switched-beam systems (SBSs) and leaky-wave antennas (LWAs). An SBS consists of an antenna array and a beamforming network that can be configured to activate one of several fixed beam patterns [6], [7]. The SBS is more suitable for CR devices since the antenna branches are combined in the RF stage and several key receiver components, such as the analog-to-digital converters, are required for only the combined signal branch, compared to having one for each antenna branch like in case of the digital antenna array [6]. An LWA [8] consists of a single antenna whose electrical properties can be modified such that the antenna's beam is steered to the desired direction, which makes it a very promising candidate for DoA estimation in portable devices. In terms of our definition of sectorized antennas, different beams of SBSs and LWAs can be used to achieve the selectivity in each of the sectors.

The research leading to these results was financially supported by the Doctoral Programme of the President of Tampere University of Technology, the Tuula and Yrjö Neuvo Fund and the Finnish Funding Agency for Technology and Innovation (Tekes, under the project "Reconfigurable Antenna-based Enhancement of Dynamic Spectrum Access Algorithms").

This work was also supported by the National Science Foundation under Grant No. 1117600.

For DoA estimation using sectorized antennas, the prior work requires knowledge of RSS or additional hardware cost. A DoA estimation algorithm based on neural networks is proposed in [7] for multiple DS-CDMA signals impinging on a base station equipped with an SBS. However, the algorithm requires either the RSS to be known or an additional, nearly omnidirectional, antenna at the receiver that is used to normalize the received energies properly. Analog DoA estimation using an LWA is presented in [9]. However, it is based on continuously changing the antenna's beam, i.e. scanning the received energy as a function of the angle, instead of measurements in sectors.

In this paper, we consider digital signal processing (DSP)-based DoA estimation algorithms using sectorized antennas, that are independent of the underlying technology, as well as the achievable performance of such algorithms. We first formulate the Cramer-Rao Bound (CRB) for RSS and DoA estimates obtained from energy measurements of sectorized antennas. The CRB provides a lower bound on the estimation accuracy of any unbiased estimator. We then propose a practical algorithm, namely the simplified least square algorithm (SLS), for RSS and DoA estimation. The SLS algorithm exploits the fact that for any given DoA, only a few sectors contain considerable signal energy, if the antenna pattern is adequately selective. Therefore, the SLS algorithm formulates the RSS and DoA estimation as a least square problem using only the two largest energy measurements from all sectors. In general a grid search can then be used to estimate DoA and RSS. However, we also derive a closed-form solution for those antennas that can be approximated using a Gaussian radiation pattern. The SLS algorithm provides a better estimation accuracy than the MaxE algorithm, which is a simple RSS and DoA estimator we proposed in our early work [10], and closely approaches the CRB. Simulation results studying the impact of important system parameters, such as SNR, number of sectors and number of samples, on the achievable accuracy and the SLS algorithm are presented.

The rest of the paper is organized as follows. The system model is introduced in Section II. The CRB for DoA and RSS estimates obtained from sectorized antennas is presented in Section III. The RSS and DoA estimation algorithms are formulated in Section IV. Numerical results evaluating the impact of various parameters on DoA and RSS estimators and the CRB are discussed in Section V. Finally, the paper is concluded in Section VI.

II. System Model

In this paper we consider a CR device estimating the DoA and RSS of a PU signal without any detailed information about the transmission. On that account, the CR is equipped with an antenna whose properties can be modified such that measurements in M different sectors are possible. Thereby, sectors are characterized by the radiation pattern, which describes the attenuation of the PU signal as a function of its DoA. In this paper we first develop the CRBs and algorithms in a general form such that they are applicable to any sectorized antenna. However, in order to identify some general trends, we then assume that the radiation pattern, $p(\varphi - \vartheta_m)$, depends only on the angular distance between the PU signal's DoA, φ, and orientation ϑ_m of sector m, $m = 1 \dots M$. In addition, for analysis purposes, we further simplify the model of the radiation pattern by approximating only the antenna's main beam using a Gaussian-like shape as proposed in [11]. Then, the radiation pattern can be expressed as

$$p(\varphi) = \exp\left(-\left[\mathcal{M}(\varphi)\right]^2 / \beta\right) \tag{1}$$

where $\mathcal{M}(\varphi) = \mathrm{mod}_{2\pi}(\varphi + \pi) - \pi$ is used to restrict the input angle to $[-\pi, \pi]$ and β is a parameter determining the width of the beam. The spacing between the sectors, $\Delta\vartheta = \frac{2\pi}{M}$, is assumed to be constant, such that the orientation of sector m becomes $\vartheta_m = m\Delta\vartheta$. Instead of parameterizing the radiation pattern via the beamwidth, we use a value that we denote the side-sector suppression, a_s. We define the side-sector suppression as the attenuation that a signal, arriving at the orientation ϑ_m of the m^{th} sector, experiences in the neighboring sectors $m-1$ and $m+1$, i.e. $a_\mathrm{s} = p(\Delta\vartheta)$. Therefore, the side-sector suppression determines the amount of overlap between neighboring sectors, independent of the number of sectors. The result is a beamwidth determined by

$$\beta = -(2\pi)^2 \left[M^2 \ln(a_\mathrm{s})\right]^{-1}. \tag{2}$$

During the measurement period, the CR successively switches through the M sectors and receives N complex samples for each sector, which results in $M \times N$ complex samples in total. Then, the baseband complex received signal sample originating from the m-th sector, with the sample index range $n = (m-1)N + 1 \dots mN$, can be written as

$$x(n) = p(\varphi - \vartheta_m)\, s(n) + w(n), \tag{3}$$

where $w(n) \sim \mathcal{CN}\left(0, \sigma_\mathrm{w}^2\right)$ is additive noise assumed to be circular symmetric complex Gaussian. Likewise, the noiseless part of the received PU signal is modeled as circular symmetric complex Gaussian, i.e. $s(n) \sim \mathcal{CN}(0, \gamma)$, which is a good approximation for e.g. OFDM-based transmission.

Given the above stated assumptions, it is impossible to distinguish between the PU signal and noise at the CR. Therefore, the estimations of RSS γ and DoA φ should be based on the received energies. The power in sector m is calculated according to

$$\epsilon_m = \frac{1}{N} \sum_{n=(m-1)N+1}^{mN} |x(n)|^2, \tag{4}$$

resulting in chi-squared distributed values ϵ_m with $2N$ degrees of freedom. For moderate to large values of N, the energies can therefore be well approximated using a Gaussian distribution (see e.g. [12]), i.e. $\epsilon_m \sim \mathcal{N}\left(\mu_m, \sigma_m^2\right)$, with the parameters

$$\mu_m = \sigma_\mathrm{w}^2 + \rho_m \gamma \tag{5}$$

$$\sigma_m^2 = \frac{1}{N}\left(\sigma_\mathrm{w}^2 + \rho_m \gamma\right)^2 \tag{6}$$

where $\rho_m = \left[p(\varphi - \vartheta_m)\right]^2$.

III. Cramer-Rao Bounds

The CRB is a lower bound on the covariance matrix of any unbiased estimator. For the estimation of a $K \times 1$ parameter vector $\mathbf{r}$, given the $L \times 1$ vector $\boldsymbol{\epsilon}$ composed of the observations, the CRB is obtained as the inverse of the Fisher information matrix (FIM). The FIM is element-wise defined as

$$\mathbf{F}_{i,j} = -\mathrm{E}\left(\frac{\partial^2}{\partial \mathbf{r}_i \partial \mathbf{r}_j} \ln\left[f\left(\boldsymbol{\epsilon}|\mathbf{r}\right)\right]\right),\ i,j = 1 \dots K \tag{7}$$

where $f\left(\boldsymbol{\epsilon}|\mathbf{r}\right)$ is the posterior probability distribution of $\boldsymbol{\epsilon}$ given $\mathbf{r}$.

Here, $K = 2$ since we estimate $\mathbf{r} = [\varphi, \gamma]^T$, using the $L = M$ energies $\boldsymbol{\epsilon} = [\epsilon_1, \epsilon_2, \dots \epsilon_M]^T$. Given the Gaussian approximation of the energy distribution, (5) and (6), the posterior probability distribution becomes

$$f\left(\boldsymbol{\epsilon}|\mathbf{r}\right) = \frac{1}{(2\pi)^{\frac{M}{2}} \left|\mathbf{Q}\right|^{\frac{1}{2}}} \exp\left\{-\frac{1}{2}\left(\boldsymbol{\epsilon} - \mathbf{g}\right)^T \mathbf{Q}^{-1}\left(\boldsymbol{\epsilon} - \mathbf{g}\right)\right\} \tag{8}$$

with $\mathbf{g} = [\mu_1, \mu_2, \dots, \mu_M]^T$ and $\mathbf{Q} = \mathrm{diag}\left[\sigma_1^2, \sigma_2^2, \dots, \sigma_M^2\right]$. In this paper we only present the final result for the resulting FIM while the detailed derivation, that will be part of a more extensive journal article, can be found in [13]. With the $\mathrm{SNR} = \frac{\gamma}{\sigma_{\mathrm{w}}^2}$, the elements of the FIM can be expressed as

$$\mathbf{F}_{11} = (N+2) \sum_{m=1}^{M} \frac{\tilde{\rho}_m^2}{\left(\rho_m^{-1}\mathrm{SNR}^{-1} + 1\right)^2} \tag{9}$$

$$\mathbf{F}_{12} = \mathbf{F}_{21} = \frac{(N+2)}{\gamma} \sum_{m=1}^{M} \frac{\tilde{\rho}_m}{\left(\rho_m^{-1}\mathrm{SNR}^{-1} + 1\right)^2} \tag{10}$$

$$\mathbf{F}_{22} = \frac{(N+2)}{\gamma^2} \sum_{m=1}^{M} \frac{1}{\left(\rho_m^{-1}\mathrm{SNR}^{-1} + 1\right)^2}. \tag{11}$$

Thereby, the value of $\tilde{\rho}_m = \frac{[\rho_m]_\varphi}{\rho_m}$ is a function of the radiation pattern and its derivative with respect to the DoA, i.e. $[\rho_m]_\varphi$. For the Gaussian radiation pattern (1), $\tilde{\rho}_m$ is equal to $\tilde{\rho}_m = -4\mathcal{M}\left(\varphi - \vartheta_m\right)/\beta$. Finally, we obtain the following relations for the lower bound on the root mean square error (RMSE) of DOA estimation

$$\mathrm{RMSE}\,\hat{\varphi} \geq \sqrt{\left[\mathbf{F}^{-1}\right]_{11}} \tag{12}$$

and on the relative RMSE (RRMSE) of RSS estimation

$$\mathrm{RRMSE}\,\hat{\gamma} = \frac{\mathrm{RMSE}\,\hat{\gamma}}{\gamma} \geq \frac{\sqrt{\left[\mathbf{F}^{-1}\right]_{22}}}{\gamma} \tag{13}$$

that we have normalized to be independent of the RSS.

IV. DoA and RSS Estimators

A. MaxE Estimator

A rough estimate of the DoA and RSS can be obtained using the following intuitive estimator that we refer to as the MaxE estimator [10]. The MaxE estimator finds the maximum power and uses the orientation of the associated sector as the DoA estimate, while the RSS estimate is obtained by subtracting the noise variance from the maximum energy:

$$\hat{\varphi}_{\mathrm{m}} = \left\{\vartheta_i \,|\, i = \arg\max_i \epsilon_i\right\} \tag{14}$$

$$\hat{\gamma}_{\mathrm{m}} = \max_i \epsilon_i - \sigma_{\mathrm{w}}^2. \tag{15}$$

It is easily verified that the resulting estimates are biased. Therefore, the performance of the MaxE estimator cannot be compared to the CRB. However, since the computational complexity of the MaxE estimator is very low, it serves anyway as a practical performance benchmark for more advanced estimators.

B. Proposed Simplified Least Squares Estimator

Using the same notation as in Sec. III, the received energies can be written in vector-form as

$$\boldsymbol{\epsilon} = \mathbf{g}\left(\varphi, \gamma\right) + \mathbf{e}, \tag{16}$$

where $\mathbf{e}$ is an $M \times 1$ random vector that is independent of the RSS and DoA. In the LS approach the RSS and DoA estimates are then estimated such that the LS error criterion,

$$J\left(\varphi, \gamma\right) = \left[\boldsymbol{\epsilon} - \mathbf{g}\left(\varphi, \gamma\right)\right]^T \left[\boldsymbol{\epsilon} - \mathbf{g}\left(\varphi, \gamma\right)\right], \tag{17}$$

is minimized. However, $\mathbf{g}\left(\varphi, \gamma\right)$ is nonlinear in φ and γ. Therefore, the minimization of (17) requires iterative algorithms whose convergence depends on the initial guess and is not guaranteed. Intuitively, the energy measurements indicate the contribution that each sector has in the RSS and DoA estimation process. If the sectorized antenna exhibits good directionality, if the SNR is at a practical level (above 0 dB) and if the number of samples is finite, then the PU signal component, i.e. $\rho_m\gamma$, is of meaningful strength only in very few sectors, while the remaining measurements are too noisy to exploit their PU signal component. Let $r = (r_1, r_2 \dots r_M)$ denote a permutation such that $\epsilon_{r_1} < \epsilon_{r_2} < \dots < \epsilon_{r_M}$. Then, the PU signal DoA is most likely in-between the sectors with the highest energy, i.e. $\vartheta_{r_M} < \varphi < \vartheta_{r_{M-1}}$. Sectors r_M and r_{M-1} also contribute most to the DoA and RSS estimation. Therefore, a good approximation of the LS solution is obtained by finding the DoA $\hat{\varphi}_{\mathrm{SLS}}$ that minimizes

$$J_{\mathrm{SLS}} = \left(\overline{\Delta\epsilon} - \frac{\rho_{r_M}}{\rho_{r_{M-1}}}\right)^2 \tag{18}$$

with

$$\overline{\Delta\epsilon} = \frac{\epsilon_{r_M} - \sigma_{\mathrm{w}}^2}{\epsilon_{r_{M-1}} - \sigma_{\mathrm{w}}^2} = \frac{\rho_{r_M}\gamma + e_{r_M}}{\rho_{r_{M-1}}\gamma + e_{r_{M-1}}}. \tag{19}$$

Since (18) is independent of the RSS and the DoA is restricted to the finite interval $\varphi \in [-\pi; \pi]$, a solution may be obtained using a simple grid search. However, if the antenna's main beam can be approximated using the Gaussian pattern (1), the DoA estimate minimizing (18) can also be obtained in closed-form according to

$$\hat{\varphi}_{\mathrm{SLS}} = \frac{\frac{1}{2}\beta \ln\overline{\Delta\epsilon} + \vartheta_{r_M}^2 - \vartheta_{r_{M-1}}^2}{2\left(\vartheta_{r_M} - \vartheta_{r_{M-1}}\right)}. \tag{20}$$

Note that the closed-form solution (20) is also applicable to antennas whose main beams differ in every sector, as long as all of them may be approximated by the Gaussian radiation pattern. In that case the parameter β in (20) is sector-dependent. An estimation of the attenuation in each of the sectors follows directly from the estimated DoA, according to $\hat{\rho}_m = \left[p\left(\hat{\varphi}_{\text{SLS}} - \vartheta_m\right)\right]^2$. As a consequence, an RSS estimate can be calculated for each of the sectors. In order to reduce the effect of statistical fluctuations, we then obtain a final estimate of the RSS by averaging over the RSS estimates from the two sectors with the highest energies, i.e.

$$\hat{\gamma}_{\text{SLS}} = \frac{1}{2}\left[\left(\epsilon_{r_M} - \sigma_{\text{w}}^2\right)/\hat{\rho}_M + \left(\epsilon_{r_{M-1}} - \sigma_{\text{w}}^2\right)/\hat{\rho}_{M-1}\right]. \quad (21)$$

In the following we refer to the algorithm that estimates the DoA based on the minimization of (18) and the respective RSS estimation (21) as the SLS estimator. In order to prevent large estimation errors when the signal is severely attenuated, we have added a validation check that reduces the SLS to the MaxE algorithm in the following cases:

1) If $\epsilon_{r_{M-2}} < \sigma_{\text{w}}^2$ then DoA estimation is according to (14).
2) If the estimated angle, $\hat{\varphi}_{\text{SLS}}$, is not in-between the two sectors with the highest energies then RSS estimation is according to (15).

V. Simulation Results

The bounds and algorithms for DoA and RSS estimation are studied assuming a uniform distribution of incoming DoAs, i.e. $\varphi \sim \mathcal{U}(-\pi;\pi)$. We emulate this distribution via 10^2 equidistant steps in the interval $\varphi_k \in \left[-\frac{\Delta\vartheta}{2};\frac{\Delta\vartheta}{2}\right]$, and simulate 10^3 realizations per algorithm and DoA-step, and average over the result at each step in order to obtain the RMSE and absolute value of bias (AB). The CRB on the RMSE of DoA estimation (12) and the CRB on the RRMSE of RSS estimation (13) depend only on the SNR, not on the RSS. The same conclusion applies for the algorithms presented in Sec. IV. Therefore, we set the RSS to a fixed value $\gamma = 1\text{pW}$ and adjust the noise power σ_{w}^2 in order to control the SNR.

Fig. 1 shows the dependence of DoA estimation performance on the side-sector suppression a_{s}. For high values of $a_{\text{s}} \approx 1$, the antenna is close to omnidirectional and as a consequence, DoA estimation becomes impossible and the RMSE is very high. This trend, observed for the CRB as well as the algorithms, is very intuitive. However, if the side-sector suppression is too low, the RMSE for the CRB and algorithms is also high. In order to understand this behavior, we consider Fig. 2, which depicts the DoA estimation RMSE as a function of the incoming DoA. Since we assume the same radiation pattern for all sectors and since the assumed Gaussian radiation pattern (1) is symmetric with respect to $\varphi = 0$, the resulting RMSE curves are periodic with the period $\Delta\vartheta$ and it is sufficient to consider the normed DoA, $\varphi' = \frac{\varphi}{\Delta\vartheta}$, over the finite interval $\varphi' \in [0;0.5]$. Then, the value $\varphi' = 0$ represents all DoAs that arrive at the orientation ϑ_m of a sector $m = 1\ldots M$, while $\varphi' = 0.5$ represents DoAs that arrive in-between two sectors. For the sake of clarity we have not added the curves of MaxE estimation to Fig. 2. However, due to its simplicity it is easy to see that the RMSE of the MaxE estimator increases with φ'. This is explained by the discretization of $\varphi \in [-\pi;\pi]$ to $\hat{\varphi} \in \{\vartheta_m | m = 1\ldots M\}$ as well as due to the attenuation of signals that is increasing with φ'. This signal attenuation, which is stronger for smaller a_{s}, explains the high RMSE resulting from MaxE estimation in combination with low values of a_{s} in Fig. 1. With respect to the CRB, on the other hand, the RMSE decreases with φ'. This is due to the estimation of the DoA that is dependent on the shape of the radiation pattern, which has its lowest slope (=0) at the orientation of a sector. With a low slope, small variations in the measured energies appear as big changes of the DoA, while the pattern's high slope at around $\varphi' \approx 0.5$ makes the DoA estimation more stable towards variations in the measured energies. For a medium value a_{s}, information not only from the sector at which the signal is arriving, but also from the neighboring sectors is available, resulting in a more even distribution of the RMSE over the whole DoA range. Due to the validity checks discussed in Sec. IV-B, the behavior of SLS estimation depends on the operating conditions. Whenever the operating conditions are disadvantageous for the estimation, it is likely that the validity checks result in the reduction of SLS to MaxE. As observed in Fig. 1, the quality of operating conditions for estimation and therefore the reduction of SLS to MaxE is, among other parameters, influenced by a_{s}. As discussed in Sec. IV-A, the MaxE algorithm is biased and therefore not necessarily bounded by the CRB, which is a lower bound only on unbiased estimators. As a consequence, SLS estimation in disadvantageous operating conditions is also biased and therefore not always lower bounded by the CRB either, as can be seen in Fig. 1 and Fig. 2 (note, that SLS is biased as soon as AB $\neq 0$ for any $\varphi/\Delta\vartheta$) for low values of a_{s}. However, for moderate values of a_{s}, the bias of SLS is close to zero. Then, we observe in Fig. 2 a behavior similar to that of the CRB, i.e. the RMSE decreases with φ'.

Fig. 3 depicts the RRMSE of RSS estimation as a function of a_{s}. For RSS estimation, performance increases with a_{s}, i.e. the more the radiation pattern resembles that of an omnidirectional antenna. An exception is the small positive slope in the RRMSE of MaxE and SLS estimation for very large values of a_{s}. As a practical guideline, we would like to determine the value, $a_{\text{s,o}}$, of the side-sector suppression that results in the lowest RMSE for both DoA and RSS estimation in relevant operating conditions. However, we have seen that the best performance of DoA estimation is achieved for a medium value of a_{s}, while best performance of RSS estimation is, at least from the theoretical point of view, achievable for $a_{\text{s}} \approx 1$. With respect to the CRB on DoA estimation, the value $a_{\text{s,o}}$ seems to be independent of the parameters M and N. Merely an increase of the SNR results in a small shift of $a_{\text{s,o}}$ towards a more directional antenna. With respect to the algorithms on the other hand, not only increasing the SNR but also a decrease of M results in a shift of $a_{\text{s,o}}$ towards smaller values. Overall, the value $a_{\text{s}} = 0.4$ has proven to be a good tradeoff between RSS and DoA estimation and is henceforth

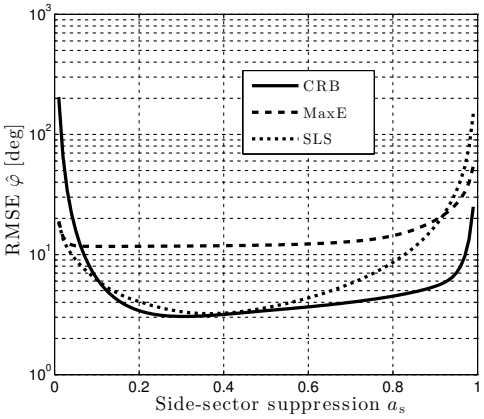

Fig. 1. Performance of DoA estimation as a function of the side-sector suppression for a uniform distribution of DoAs. Parameters: $M = 9$, $N = 50$, SNR = 5 dB.

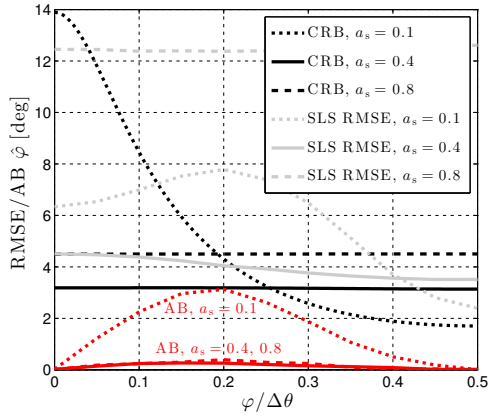

Fig. 2. Dependence of DoA estimation on the incoming DoA. Parameters: $M = 9$, $N = 50$, SNR = 5 dB.

used as the default value. Fig. 4 and Fig. 5 show the influence of the SNR on the DoA and RSS estimation performance. Since the SNR also influences the operating conditions for estimation and as a consequence the bias of SLS estimation, Fig. 4 and Fig. 5 depict the AB/relative AB (RAB $\hat{\gamma} = \mathrm{AB}/\gamma$) along with the RMSE/RRMSE. As expected, the CRBs and the RMSE/RRMSE of SLS estimation decrease with increasing SNR. Furthermore, we observe that the SLS yields biased DoA and RSS estimates for SNR values that are smaller than 5 dB. However, very low SNR values have little practical relevance as they make it difficult to detect the PU signal in the first place [12]. Thus, for most of the practical relevant cases and a well parameterized antenna ($a_s \approx 0.4$) the SLS algorithm is unbiased and therefore lower bounded by the CRB. In contrast to the behavior observed in CRB and SLS estimation, the RMSE and RRMSE of MaxE estimation decrease only up to SNR $\approx$ 5 dB. For an SNR $>$ 5 dB the performance is

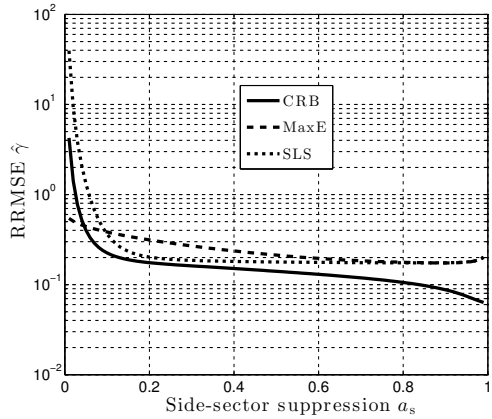

Fig. 3. Performance of RSS estimation as a function of the side-sector suppression for a uniform distribution of DoAs. Parameters: $M = 9$, $N = 50$, SNR = 5 dB.

constant due to the bias in the estimation [10]. In case of DoA estimation, the performance of the MaxE estimator is significantly worse than the CRB. While the RMSE of SLS-based DoA estimates is larger than the CRB, the algorithm always results in a smaller RMSE than the MaxE estimator. For an SNR = -2 dB, the difference between the MaxE and SLS RMSE is only $\approx 5°$. Performance starts to differ significantly from an SNR ≈ 0 dB onwards. Then, the MaxE RMSE does not decrease anymore, while the SLS estimator starts to perform close to the CRB ($1°$ difference at 5 dB). This coincides also with the level of SNR where the SLS algorithm starts to yield almost unbiased DoA estimates. For RSS estimation, the MaxE and SLS estimator have a lower RRMSE than the CRB if the SNR is very low (< -1 dB), i.e. an SNR region were both algorithms are biased. Otherwise, MaxE estimation results in the largest RMSE while the RMSE of SLS estimation is only slightly larger than the CRB.

Finally, Fig. 6 depicts the estimation performance as a function of the number of samples N and with two different numbers of sectors $M \in \{5, 9\}$. Since the dependence of RSS and DoA estimation on N is very similar, we chose to include only the curve for DoA estimation in this paper. As with the SNR, an increase of N results in a smaller SLS-RMSE and a lower CRB, while the performance of MaxE estimation saturates for comparably low N and at a high RMSE. Again, the CRB is lower than the RMSE of the estimators, while SLS is outperforming the MaxE estimator significantly. An increase of M is always beneficial for DoA estimation. In contrast to this, the RSS RRMSE is almost independent of M since the attenuation in neighboring sectors is constant due to the parametrization via (2), such that only a limited amount of sectors contribute to RSS estimation anyways.

VI. Conclusion

We considered the problem of estimating RSS and DoA of the primary user in cognitive radio networks using energy mea-

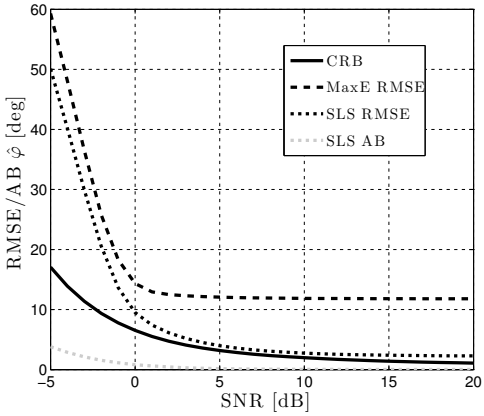

Fig. 4. Performance and bias of DoA estimation as a function of the SNR for a uniform distribution of DoAs. Parameters: $a_s = 0.4$, $M = 9$, $N = 50$.

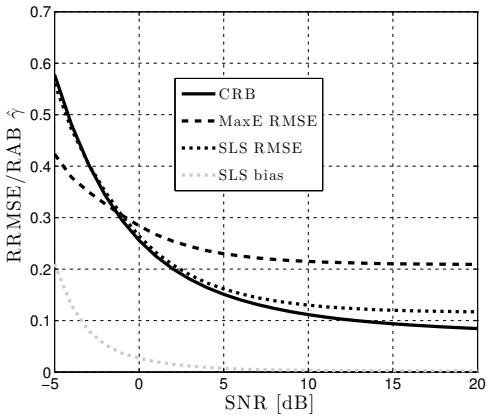

Fig. 5. Performance and bias of RSS estimation as a function of the SNR for a uniform distribution of DoAs. Parameters: $a_s = 0.4$, $M = 9$, $N = 50$.

surements from sectorized antennas. We first formulated the CRBs for such problem, which provides the lower bound on the achievable accuracy of any unbiased estimators. We then proposed the SLS algorithm, which is a simple estimator based on the two largest energy measurements among all antenna sectors. Simulation results of the impact of various important system parameters, such as side-sector suppression, number of antennas and samples, and SNR, on the CRB and SLS algorithm were presented to provide guidelines for practical systems and algorithm design. Our results showed that the SLS algorithm closely approaches the CRB for positive SNR values and also outperforms the simple MaxE reference algorithm. Overall, the obtained results indicate that sectorized antenna systems can be used for accurate PU DoA and RSS estimation, and thereon for PU localization, in fairly low-complexity SU devices, compared to e.g. classical digital antenna arrays.

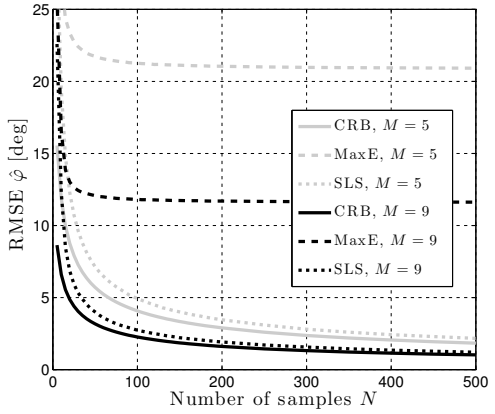

Fig. 6. Performance of DoA estimation as a function of the number of samples for a uniform distribution of DoAs. Parameters: $a_s = 0.4$, SNR = 5 dB.

REFERENCES

[1] H. Celebi and H. Arslan, "Utilization of location information in cognitive wireless networks," *IEEE Wireless Commun. Mag.*, vol. 14, no. 4, pp. 6 –13, Aug. 2007.

[2] J. Wang, J. Chen, and D. Cabric, "Cramer-rao bounds for joint rss/doa-based primary-user localization in cognitive radio networks," *accepted for publication in IEEE Trans. Wireless Commun.*, December 2012, [Online] http://arxiv.org/abs/1207.1469.

[3] N. Patwari, J. Ash, S. Kyperountas, A. Hero, R. Moses, and N. Correal, "Locating the nodes: cooperative localization in wireless sensor networks," *IEEE Signal Process. Mag.*, vol. 22, no. 4, pp. 54–69, July 2005.

[4] P. Stoica and N. Arye, "Music, maximum likelihood, and cramer-rao bound," *IEEE Trans. Acoust., Speech, Signal Process.*, vol. 37, no. 5, pp. 720 –741, May 1989.

[5] R. Roy and T. Kailath, "Esprit-estimation of signal parameters via rotational invariance techniques," *IEEE Trans. Acoust., Speech, Signal Process.*, vol. 37, no. 7, pp. 984–995, Jul. 1989.

[6] T. Ohira, "Adaptive array antenna beamforming architectures as viewed by a microwave circuit designer," in *Asia-Pacific Microwave Conference*, 2000, pp. 828 –833.

[7] K. Gotsis, K. Siakavara, and J. Sahalos, "On the direction of arrival (DoA) estimation for a switched-beam antenna system using neural networks," *IEEE Trans. Antennas Propag.*, vol. 57, no. 5, pp. 1399 – 1411, May 2009.

[8] D. Piazza, D. Michele, and K. Dandekar, "Two port reconfigurable crlh leaky wave antenna with improved impedance matching and beam tuning," in *3rd European Conference on Antennas and Propagation 2009 (EuCAP09)*, Mar. 2009, pp. 2046–2049.

[9] S. Abielmona, H. Nguyen, and C. Caloz, "Analog direction of arrival estimation using an electronically-scanned CRLH leaky-wave antenna," *IEEE Trans. Antennas Propag.*, vol. 59, no. 4, pp. 1408 –1412, Apr. 2011.

[10] J. Werner, J. Wang, A. Hakkarainen, M. Valkama, and D. Cabric, "Primary user localization in cognitive radio networks using sectorized antennas," *10th Annual Conference on Wireless On-Demand Network Systems and Services (WONS2013)*, Jan. 2013.

[11] R. Martin and R. Thomas, "Algorithms and bounds for estimating location, directionality, and environmental parameters of primary spectrum users," *IEEE Trans. Wireless Commun.*, vol. 8, no. 11, pp. 5692 –5701, Nov. 2009.

[12] R. Tandra and A. Sahai, "SNR walls for signal detection," *IEEE Journal of Selected Topics in Signal Processing*, vol. 2, no. 1, pp. 4 –17, Feb. 2008.

[13] J. Werner, "Technical report." [Online]. Available: http://www.cs.tut.fi/%7ewerner/ccrb/sector-crb.pdf

Publication 6

J. Werner, A. Hakkarainen, and M. Valkama, "Cramer-Rao bounds for hybrid RSS-DOA based emitter location and transmit power estimation in cognitive radio networks," in *Proceedings of the IEEE 78th Vehicular Technology Conference (VTC fall)*, Las Vegas, NV, 2013, pp. 1–7.

Cramer-Rao Bounds for Hybrid RSS-DOA Based Emitter Location and Transmit Power Estimation in Cognitive Radio Systems

Janis Werner, Aki Hakkarainen and Mikko Valkama
Department of Electronics and Communications Engineering
Tampere University of Technology, P.O. Box 553, FI-33101 Tampere, Finland
Emails: {janis.werner, aki.hakkarainen, mikko.e.valkama}@tut.fi

***Abstract*—In this paper, we consider cooperating secondary users (SUs) that are estimating the location and transmit power of an emitter that may be either a primary user (PU) or another SU in the cognitive radio (CR) context. Since SU devices need to be affordable and portable, their capabilities to estimate e.g. the direction of arrival (DOA) are very limited. In addition, the geographical distribution of SUs is random rather than optimized resulting in very stringent conditions for the localization. We therefore analyze possible benefits and performance of hybrid received signal strength (RSS)-DOA based emitter transmit power and position estimation by means of the Cramer-Rao bound (CRB). We show that the RSS-DOA hybrid approach can lead to significantly lower bounds compared to estimation based on only RSS or DOA. Assuming a special case of two SUs at equal distance from the emitter, we derive the CRBs in closed-form and demonstrate that for certain SU-emitter geometries, the RSS-only and DOA-only CRBs become infinite due to the inability to estimate one of the emitter's coordinates. Since those coordinates are orthogonal for RSS and DOA, the hybrid approach does not suffer from these geometries, resulting in a finite CRB. Results from Monte-Carlo simulations are provided which illustrate that significant theoretic gains are possible also for random SU and emitter placements. The results also show that biggest performance gains from joint processing of RSS and DOA are available when the number of cooperating SUs is fairly small, in the order of 2-5.**

I. Introduction

Efficient use of the available radio spectrum is of high importance in order to meet future demands in mobile communications. However, recent measurement campaigns have revealed that the current approach to license parts of the spectrum for exclusive use only, lead to great variances of the actual spectrum usage. In order to increase efficiency, CRs have been proposed that sense the environment for idle spectrum and dynamically access those parts that are available. During the access phase it has to be guaranteed, however, that the interference introduced to the PUs is kept at minimum [1], [2].

The research leading to these results was financially supported by the Doctoral Programme of the President of Tampere University of Technology, the Tuula and Yrjö Neuvo Fund, the Academy of Finland (under the project 251138 "Digitally-Enhanced RF for Cognitive Radio Devices") and the Finnish Funding Agency for Technology and Innovation (Tekes, under the project "Reconfigurable Antenna-based Enhancement of Dynamic Spectrum Access Algorithms").

In this context, the localization of the PU has received much attention recently, e.g. [3], [4], [5], [6]. The knowledge of PU positions is considered as valuable information to reliably protect the PU from interference and enable directional transmission as well as routing in the secondary network [5]. In order for estimation to be possible and to enable techniques such as routing, the positions of all observing SUs must be available as well. While some SUs might have knowledge about their location using e.g. global navigation satellite system (GNSS), others might not. Thus, the positions of certain SUs must be estimated as well. In addition to the location of the PU, its transmit power is useful information in the secondary network since it gives a better picture of the radio environment [3].

In a CR network, localization can only be based on the RSS or the DOA [5], while the transmit power can only be estimated using the RSS. However, the radio environment heavily influences the PU-transmitted signal. As a consequence, the quality of DOA estimates as well as the RSS varies with the measurement location. In the extreme case, the surroundings might interfere so strongly that the PU is not at all detected at some locations. Therefore, the estimation should be collaborative and even if dedicated sensor nodes exist, the SUs should at least assist in the localization. Since SU devices need to be portable and affordable, they will have only few antennas (e.g. 2-4), making the DOA estimation very coarse. In addition, the SU distribution on the observation area is random which negatively influences the quality of position estimates for both RSS- and DOA-only based localization [7] [8].

A. Related Work

The CRB is often used to determine a lower bound on the localization variance for any unbiased estimator. It is equal to the inverse of the fisher information matrix (FIM). In [9], the CRB on localization using RSS-only is derived. The authors of [3] argue that most devices do not transmit with omnidirectional antennas. Therefore, they calculate the CRBs on both position and transmit power estimation when the PU transmits with directional antennas and estimation is based on RSS-only. A derivation of the CRB in case of DOA-only based localization in CR can be found in [4].

The CRB on localization based on both the RSS and the time of arrival or time-difference of arrival is derived in [10], showing that hybrid localization is potentially beneficial. An example of actual signal processing for hybrid RSS-DOA based localization, stemming from maximum likelihood and linear least-squares estimation, is given in [11].

Due to the adverse conditions for localization in CR and the requirement for high accuracy, all available information needs to be utilized, making the combined RSS-DOA based localization a promising approach. Most existing research has studied the CRB on localization based on either RSS-only [3], [9] or DOA-only [4]. Recently, the CRB on hybrid RSS-DOA localization has been derived in [12]. However, in their derivation the authors implicitly assume the transmit power to be known, resulting in an overly optimistic CRB for a CR network where the PU is non-cooperative and its transmit power therefore unknown. Furthermore, the emphasis of the article is on a large number of SUs which is not necessarily feasible since reporting overhead to the fusion center becomes prohibitive. Moreover, our results in this paper show that the hybrid approach is in particular beneficial if the number of nodes is low. This is a more practical scenario then also from the reporting overhead perspective.

B. Contributions

Our contributions in this paper are the following:

- We are the first to consider the CRB on hybrid RSS-DOA localization with unknown transmit power. For that case we derive the FIMs for localization and transmit power estimation in closed-form.
- While the general closed-form solution for the CRB is easily evaluated using e.g. symbolic computation software, it is not very meaningful due to the dimensions of the respective FIM. Instead, we explicitly consider geometries that are disadvantageous for RSS-only and DOA-only localization and identify the two SU-case as an important abstraction that lets us explain what ultimately makes the hybrid approach beneficial. Therefore, we derive the CRB in closed-form for the two SU-case and demonstrate that the hybrid approach does not suffer from the same disadvantageous geometries as RSS-only and DOA-only localization.
- Extensive simulations for arbitrary geometries and varying number of SUs then confirms our hypothesis and show that the biggest benefit of the hybrid approach is obtained when the number of CR devices is low and therefore the probability of disadvantageous geometries high.

The rest of this paper is organized as follows: In Section II, we describe the applied system model. The CRB in general and for RSS- and DOA-only based localization are shortly revised in Section III, followed by the derivation of the CRBs on combined RSS-DOA based estimation. In the subsequent section we solve and analyze the CRBs for the special case of two SUs at equal distance from the emitter. Numerical evaluation of the CRBs are presented in Section V and the conclusions and a summary can be found in Section VI.

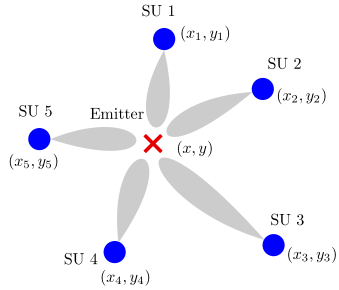

Fig. 1. Illustration of the principal system model with $M = 5$ collaborating SUs.

II. Principal System Model

In this paper, we consider a cognitive radio network, where M cooperating SUs with known positions are trying to localize an emitting source on a two-dimensional Cartesian coordinate system, as depicted in Fig. 1. This emitter may be a PU or another SU with unknown location and unknown transmit power.

A. DOA Model

We assume that all SUs are equipped with directional antennas (e.g. small antenna arrays) such that coarse DOA estimation is possible. Denote $\boldsymbol{\vartheta}$ as the $M \times 1$ vector composed of all DOA estimates and let (x, y) be the emitter location and (x_i, y_i) the location of observing SU i. We assume an additive white Gaussian DOA estimation error $\boldsymbol{\gamma} \sim \mathcal{N}(0, \mathbf{Q})$ as in [4]. Then, the DOA estimates become

$$\boldsymbol{\vartheta} = \boldsymbol{\varphi}(x, y) + \boldsymbol{\gamma}. \tag{1}$$

where $\boldsymbol{\varphi}(x, y)$ is composed of the elements

$$[\boldsymbol{\varphi}(x, y)]_i = \arctan\left(\frac{y - y_i}{x - x_i}\right). \tag{2}$$

Furthermore, we assume the DOA estimation errors to be independent but with equal variance, resulting in an error covariance matrix $\mathbf{Q} = \sigma_{\mathrm{a}}^2 \mathbf{I}$. This is an idealization we make in order to simplify the CRBs. In reality the variance varies across the SUs, depending on factors such as size and orientation of the antenna arrays, and the receiver signal-to-noise ratio and thus as a consequence also on the RSS [13].

B. RSS Model

Besides providing angular information, DOA estimation techniques make it possible to determine the RSS associated with the DOA [14]. We assume the commonly used (e.g. [3], [6]) logarithmic path loss model for the dependence of the RSS on the emitter-SU distance. All powers are expressed in a logarithmic scale such as dBm. Then, fading $\mathbf{m}$ becomes additive, yielding the RSSs

$$\mathbf{S} = \mathbf{g}(x, y, P) + \mathbf{m} \tag{3}$$

where $\mathbf{g}(x, y, P)$ is the statistical mean dependent on the transmit power P and the distance $d_i = \sqrt{(x - x_i)^2 + (y - y_i)^2}$ to the individual observing SUs. The statistical mean is element-wise modeled as

$$[\mathbf{g}(x, y, P)]_i = P - 10\alpha \lg (d_i) . \tag{4}$$

where α is a constant known as the path loss coefficient. Here, we analyze only the influence of slow fading due to shadowing since the influence of fast fading may be diminished by a sufficiently long RSS measurement window. Therefore, $\mathbf{m}$ is dependent only on the positions of the emitter and observing SUs. Since shadowing is determined by the surroundings, RSS measurements are subject to correlated shadowing. We assume the model introduced in [15], where the correlation of shadow fading decreases exponentially with the distance. This leads to $\mathbf{m} \sim \mathcal{N}(0, \mathbf{K})$ and an $M \times M$ covariance matrix with the elements

$$[\mathbf{K}]_{ij} = \sigma_{\mathrm{f}}^2 \exp\left(-\frac{\Delta d_{i,j}}{d_{\mathrm{c}}}\right) \tag{5}$$

where $\Delta d_{i,j} = \sqrt{(x_i - x_j)^2 + (y_i - y_j)^2}$ is the distance between observing SU i and j and d_{c} is an environmental parameter commonly referred to as the correlation distance.

III. Cramer-Rao Lower Bounds

The CRB is a lower bound on any unbiased estimator. Let $\hat{\mathbf{q}}$ be an estimator for the N dimensional parameter vector $\mathbf{q}$ given the measurements $\mathbf{r}$ and let $f(\mathbf{r}|\mathbf{q})$ be the conditional probability density function (PDF). Then, the covariance matrix of $\hat{\mathbf{q}}$ is lower bounded by the inverse of the Fisher information matrix (FIM), defined as (e.g. [16])

$$[\mathbf{F}]_{ij} = -\mathrm{E}_{\mathbf{r}}\left\{\frac{\partial^2}{\partial \mathbf{q}_i \partial \mathbf{q}_j} \ln\left[f(\mathbf{r}|\mathbf{q})\right]\right\}, \quad i, j = 1 \ldots N. \tag{6}$$

Therefore, the variances of the estimates are lower bounded by the elements on the main diagonal of $\mathbf{F}^{-1}$:

$$\mathrm{var}\left([\hat{\mathbf{q}}]_i\right) \geq \left[\mathbf{F}^{-1}\right]_{ii} . \tag{7}$$

For the sake of simplicity, whenever referring to the CRB of a parameter in the following, we will omit the inequality. Instead, e.g. $\mathrm{var}\left([\hat{\mathbf{q}}]_i\right)$ is used to denote the CRB on the variance of $[\hat{\mathbf{q}}]_i$. With respect to the transmit power we distinguish two cases:

1) *Unknown P*: If the transmit power is unknown it has to be estimated along with the emitter location, leading to the parameter vector $\mathbf{q} = (x, y, P)$ and a 3×3 FIM. This case is typical for PU localization since the exact PU transmit power is normally not available due to the non-cooperative nature of the primary network.
2) *Known P*: For known transmit power, the parameter vector consists only of the location, $\mathbf{q} = (x, y)$, thus the FIM becomes a 2×2 matrix. As will be shown in the following, the knowledge of the transmit power is beneficial for the localization and should therefore be communicated if possible. Therefore, this case is typical for the localization of another SU.

Let $\Delta x = x - x_i$, $\Delta y = y - y_i$ and $\beta = \frac{10\alpha}{\ln 10}$. Then, the partial derivatives of $\boldsymbol{\varphi}$ and $\mathbf{g}$ with respect to $\mathbf{q}$ that are needed for the calculation of the FIMs are given by

$$[\boldsymbol{\varphi}_x]_i = -\frac{\Delta y_i}{\Delta^2 x_i + \Delta^2 y_i} \qquad [\mathbf{g}_x]_i = -\beta \frac{\Delta x_i}{\Delta^2 x_i + \Delta^2 y_i} \tag{8}$$

$$[\boldsymbol{\varphi}_y]_i = \frac{\Delta x_i}{\Delta^2 x_i + \Delta^2 y_i} \qquad [\mathbf{g}_y]_i = -\beta \frac{\Delta y_i}{\Delta^2 x_i + \Delta^2 y_i} \tag{9}$$

$$[\boldsymbol{\varphi}_P]_i = 0 \qquad [\mathbf{g}_P]_i = 1. \tag{10}$$

A. DOA-only

The CRB for localization based on DOA-only has been derived in [4]. It is obtained by setting $\mathbf{r} = \boldsymbol{\vartheta}$ and noting that the resulting conditional PDF $f_{\mathrm{DOA}}(\boldsymbol{\vartheta}|\mathbf{q})$ is Gaussian distributed with mean (2) and covariance $\mathbf{Q}$. Since the transmit power has no influence and cannot be estimated, the FIM is a 2×2 matrix with the elements (Note that $\mathbf{F}_{i,j} = \mathbf{F}_{j,i}$):

$$[\mathbf{F}_{\mathrm{DOA}}]_{11} = \boldsymbol{\varphi}_x^T \mathbf{Q}^{-1} \boldsymbol{\varphi}_x \tag{11}$$

$$[\mathbf{F}_{\mathrm{DOA}}]_{22} = \boldsymbol{\varphi}_y^T \mathbf{Q}^{-1} \boldsymbol{\varphi}_y \tag{12}$$

$$[\mathbf{F}_{\mathrm{DOA}}]_{12} = \boldsymbol{\varphi}_x^T \mathbf{Q}^{-1} \boldsymbol{\varphi}_y. \tag{13}$$

Thus, the root-mean squared error (RMSE) of the localization is lower bounded by

$$\mathrm{RMSE}_{\mathrm{DOA}} = \sqrt{[\mathbf{F}_{\mathrm{DOA}}^{-1}]_{11} + [\mathbf{F}_{\mathrm{DOA}}^{-1}]_{22}}. \tag{14}$$

B. RSS-only

In the case of localization based on RSS-only, the measurement vector becomes $\mathbf{r} = \mathbf{S}$ and the conditional PDF $f_{\mathrm{RSS}}(\mathbf{S}|\mathbf{q})$ is likewise Gaussian distributed with mean (4) and covariance $\mathbf{K}$.

1) Unknown Transmit Power: The CRB for RSS-only based localization with unknown transmit power is studied in [9]. The 3×3 FIM is composed of the elements:

$$[\mathbf{F}_{\mathrm{RSS,u}}]_{11} = \mathbf{g}_x^T \mathbf{K}^{-1} \mathbf{g}_x \qquad [\mathbf{F}_{\mathrm{RSS,u}}]_{12} = \mathbf{g}_x^T \mathbf{K}^{-1} \mathbf{g}_y \tag{15}$$

$$[\mathbf{F}_{\mathrm{RSS,u}}]_{22} = \mathbf{g}_y^T \mathbf{K}^{-1} \mathbf{g}_y \qquad [\mathbf{F}_{\mathrm{RSS,u}}]_{13} = \mathbf{g}_x^T \mathbf{K}^{-1} \mathbf{g}_P \tag{16}$$

$$[\mathbf{F}_{\mathrm{RSS,u}}]_{33} = \mathbf{g}_P^T \mathbf{K}^{-1} \mathbf{g}_P \qquad [\mathbf{F}_{\mathrm{RSS,u}}]_{23} = \mathbf{g}_y^T \mathbf{K}^{-1} \mathbf{g}_P \tag{17}$$

leading to the CRBs on the RMSE and variance of the transmit power estimation according to

$$\mathrm{RMSE}_{\mathrm{RSS,u}} = \sqrt{[\mathbf{F}_{\mathrm{RSS,u}}^{-1}]_{11} + [\mathbf{F}_{\mathrm{RSS,u}}^{-1}]_{22}} \tag{18}$$

$$\mathrm{var}(\hat{P}_{\mathrm{RSS,u}}) = [\mathbf{F}_{\mathrm{RSS,u}}^{-1}]_{33}. \tag{19}$$

2) Known Transmit Power: The FIM for RSS-only based localization with known transmit power is a submatrix of $\mathbf{F}_{\mathrm{RSS,u}}$ given by

$$\mathbf{F}_{\mathrm{RSS,k}} = \begin{pmatrix} [\mathbf{F}_{\mathrm{RSS,u}}]_{11} & [\mathbf{F}_{\mathrm{RSS,u}}]_{12} \\ [\mathbf{F}_{\mathrm{RSS,u}}]_{21} & [\mathbf{F}_{\mathrm{RSS,u}}]_{22} \end{pmatrix}. \tag{20}$$

Then, the CRB on the RMSE is equal to

$$\mathrm{RMSE}_{\mathrm{RSS,k}} = \sqrt{[\mathbf{F}_{\mathrm{RSS,k}}^{-1}]_{11} + [\mathbf{F}_{\mathrm{RSS,k}}^{-1}]_{22}}. \tag{21}$$

C. Proposed Hybrid RSS-DOA

For hybrid localization based on both RSS and DOA, the conditional PDF becomes

$$f_{\mathrm{H}}\left(\boldsymbol{\vartheta}, \mathbf{S}|\mathbf{q}\right) = f_{\mathrm{RSS}}\left(\mathbf{S}|\mathbf{q}\right) f_{\mathrm{DOA}}\left(\boldsymbol{\vartheta}|\mathbf{q}_{\mathrm{u}}\right) \tag{22}$$

due to the assumed independence of $\boldsymbol{\vartheta}$ and $\mathbf{S}$. As a consequence of (6) and (22), the FIM for hybrid RSS-DOA localization is the sum of the FIMs for DOA- and RSS-only based localization.

1) Unknown Transmit Power: Since localization with unknown transmit power results in a 3×3 matrix, the FIM for DOA estimates needs to be complemented with zeros that represent the independence of DOA estimates from the transmit power. With $\mathbf{0} = (0, 0)$, this leads to the following FIM

$$\mathbf{F}_{\mathrm{H,u}} = \mathbf{F}_{\mathrm{RSS,u}} + \begin{pmatrix} \mathbf{F}_{\mathrm{DOA}} & \mathbf{0}^T \\ \mathbf{0} & 0 \end{pmatrix} \tag{23}$$

and CRBs on RMSE of position and variance of transmit power estimation of the form

$$\mathrm{RMSE}_{\mathrm{H,u}} = \sqrt{\left[\mathbf{F}_{\mathrm{H,u}}^{-1}\right]_{11} + \left[\mathbf{F}_{\mathrm{H,u}}^{-1}\right]_{22}} \tag{24}$$

$$\mathrm{var}(\hat{P}_{\mathrm{H,u}}) = \left[\mathbf{F}_{\mathrm{H,u}}^{-1}\right]_{33}. \tag{25}$$

2) Known Transmit Power: With known transmit power the 2×2 FIM is calculated according to

$$\mathbf{F}_{\mathrm{H,k}} = \mathbf{F}_{\mathrm{RSS,k}} + \mathbf{F}_{\mathrm{DOA}} \tag{26}$$

which results in the CRB

$$\mathrm{RMSE}_{\mathrm{H,k}} = \sqrt{\left[\mathbf{F}_{\mathrm{H,k}}^{-1}\right]_{11} + \left[\mathbf{F}_{\mathrm{H,k}}^{-1}\right]_{22}}. \tag{27}$$

In the following we will use (14), (18), (19), (21), (24), (25) and (27) to study how a hybrid RSS-DOA approach can improve RSS-only and DOA-only localization as well as transmit power estimation.

IV. Closed-Form Solution

Although inverting the general FIMs derived in the previous section in closed form is in principle possible, the results of the inversion and thus the associated CRBs, in particular for the hybrid RSS-DOA localization case, are not very intuitive. Therefore, we make some simplifying assumptions and solve (14), (21), (24), (25) and (27) under such assumptions. We are particularly interested in a comparison of the CRBs for the case where the emitter-SU geometry is disadvantageous for position estimates using only DOAs or RSSs. In a CR network where the localization is carried out by mobile SU devices, the placement of the localizing SUs is arbitrary. In addition, the amount of SUs that contribute to the localization needs to be low, in order to prevent an overhead in the fusion center. As a consequence, the probability for disadvantageous geometries is comparably high in a CR network. In general, these disadvantageous geometries are the result of a non-uniform placement of multiple SUs around the emitter. However, a good abstraction of these disadvantageous geometries may be obtained with only $M = 2$ cooperating PUs at a distance of $2R_0$ apart from each other. By making the assumption $R_0 \gg d_{\mathrm{c}}$ we do not need to consider the shadow correlation in RSS measurements, resulting in $\mathbf{K} = \sigma_{\mathrm{f}}^2\mathbf{I}$. Furthermore, we assume that both SUs are at equal distance, R, to the emitter. Without loss of generality, we define the angles towards the emitter to be $\varphi_1 = \varphi$ for SU 1 and $\varphi_2 = \pi - \varphi$ for SU 2. Then, the following equation relates the distance to the angle φ:

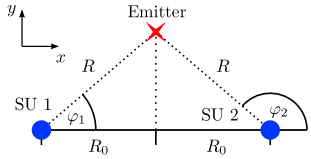

Fig. 2. Illustration of the considered special case that we use to study and demonstrate the main benefit of hybrid RSS-DOA localization.

$$R = \frac{R_0}{\cos\varphi}. \tag{28}$$

The resulting special case is illustrated in Fig. 2. We first derive the CRB for the RSS-DOA hybrid. Then, the CRB for the DOA-only and RSS-only estimation is obtained by calculating the limit as σ_{f} or σ_{a} approach infinity. In the following, the CRB on the variance of x- and y-coordinate estimation, i.e. $\mathrm{var}(\hat{x})$ and $\mathrm{var}(\hat{y})$ is presented instead of the RMSE which is obtained by recalling that $\mathrm{RMSE} = \sqrt{\mathrm{var}(\hat{x}) + \mathrm{var}(\hat{y})}$.

A. Hybrid RSS-DOA

1) Unknown Transmit Power: With the angle defined as in (2) and the made assumptions it follows that $\Delta x_1 = R_0$, $\Delta x_2 = -R_0$ and $\Delta y_1 = \Delta y_2 = R_0 \tan\varphi$. These results are used to calculate the partial derivatives (8) - (10) which are then plugged into the calculation of the FIM according to (11) - (13), (15) - (17) and (23). Finally, after inverting the FIM the following CRBs are obtained:

$$\mathrm{var}\left(\hat{x}_{\mathrm{H,u}}\right) = \frac{\sigma_{\mathrm{a}}^2\sigma_{\mathrm{f}}^2R_0^2}{2\cos\varphi\left(\sigma_{\mathrm{a}}^2\beta^2\cos^2\varphi + \sigma_{\mathrm{f}}^2\sin^2\varphi\right)} \tag{29}$$

$$\mathrm{var}\left(\hat{y}_{\mathrm{H,u}}\right) = \frac{\sigma_{\mathrm{a}}^2R_0^2}{2\cos^3\varphi} \tag{30}$$

$$\mathrm{var}\left(\hat{P}_{\mathrm{H,u}}\right) = \frac{\sigma_{\mathrm{f}}^2}{2} + \frac{\sigma_{\mathrm{a}}^2\beta^2}{2}\tan^2\left(\varphi\right). \tag{31}$$

2) Known Transmit Power: Following the same steps while using (26) instead of (23) leads to CRBs for known transmit power equal to

$$\mathrm{var}\left(\hat{x}_{\mathrm{H,k}}\right) = \frac{\sigma_{\mathrm{a}}^2\sigma_{\mathrm{f}}^2R_0^2}{2\cos\varphi\left(\sigma_{\mathrm{a}}^2\beta^2\cos^2\varphi + \sigma_{\mathrm{f}}^2\sin^2\varphi\right)} \tag{32}$$

$$\mathrm{var}\left(\hat{y}_{\mathrm{H,u}}\right) = \frac{\sigma_{\mathrm{a}}^2\sigma_{\mathrm{f}}^2R_0^2}{2\cos\varphi\left(\sigma_{\mathrm{a}}^2\beta^2\sin^2\varphi + \sigma_{\mathrm{f}}^2\cos^2\varphi\right)}. \tag{33}$$

B. DOA-only

The CRBs for DOA-only based localization may be calculated by $\mathrm{var}\left(\hat{x}_{\mathrm{DOA}}\right) = \lim_{\sigma_{\mathrm{f}}\to\infty}\mathrm{var}\left(\hat{x}_{\mathrm{H,u}}\right)$ and $\mathrm{var}\left(\hat{y}_{\mathrm{DOA}}\right) =$

$\lim_{\sigma_f \to \infty} \mathrm{var}\,(\hat{y}_{\mathrm{H,u}})$, resulting in

$$\mathrm{var}\,(\hat{x}_{\mathrm{DOA}}) = \frac{\sigma_a^2 R_0^2}{2\cos\varphi \sin^2\varphi} \tag{34}$$

$$\mathrm{var}\,(\hat{y}_{\mathrm{DOA}}) = \frac{\sigma_a^2 R_0^2}{2\cos^3\varphi}. \tag{35}$$

Alternatively, the same results for the DOA-only case are obtained by either solving (14) or by applying the made assumptions to the results presented in [4].

C. RSS-only

The CRBs for RSS-only localization can be calculated in a similar manner. However, $M = 2$ SUs are not enough to localize an emitter with unknown transmit power as indicated by the singularity of the FIM [17] that is obtained when applying the assumptions to (15)-(17). Therefore, the limits should only be calculated for the case of known transmit power, i.e. $\mathrm{var}\,(\hat{x}_{\mathrm{RSS,k}}) = \lim_{\sigma_a \to \infty} \mathrm{var}\,(\hat{x}_{\mathrm{H,k}})$ and $\mathrm{var}\,(\hat{y}_{\mathrm{RSS,k}}) = \lim_{\sigma_a \to \infty} \mathrm{var}\,(\hat{y}_{\mathrm{H,k}})$. This results in the CRBs:

$$\mathrm{var}\,(\hat{x}_{\mathrm{RSS,k}}) = \frac{\sigma_f^2 R_0^2}{2\beta^2 \cos^3\varphi} \tag{36}$$

$$\mathrm{var}\,(\hat{y}_{\mathrm{RSS,k}}) = \frac{\sigma_f^2 R_0^2}{2\beta^2 \cos\varphi \sin^2\varphi}. \tag{37}$$

D. Illustrations and Discussion

Fig. 3 and Fig. 4 depict the derived CRBs as functions of the angle φ. The hybrid solution is always lower bounded than the DOA-only or respective RSS-only estimation. Obviously, the limit of all CRBs is infinity as φ approaches $90°$. This is an intuitive result since the distance to the emitter (28) also grows with φ and $\lim_{\varphi \to 90°} R = \infty$. Furthermore, we notice that the limit is also infinite as φ approaches zero in case of RSS-only and DOA-only based localization, while the RMSE CRB for the hybrid approach is finite and attains its minimum for $\varphi = 0$. This can be explained by analyzing the CRBs on x and y estimation individually. For DOA-only based localization we obtain

$$\lim_{\varphi \to 0} \mathrm{var}\,(\hat{x}_{\mathrm{DOA}}) = \infty \tag{38}$$

$$\mathrm{var}\,(\hat{y}_{\mathrm{DOA}})\,|_{\varphi=0} = \frac{\sigma_a^2 R_0^2}{2}. \tag{39}$$

and for RSS-only localization the CRBs become

$$\mathrm{var}\,(\hat{x}_{\mathrm{RSS,k}})\,|_{\varphi=0} = \frac{\sigma_f^2 R_0^2}{2\beta^2} \tag{40}$$

$$\lim_{\varphi \to 0} \mathrm{var}\,(\hat{y}_{\mathrm{RSS,k}}) = \infty. \tag{41}$$

Thus, both RSS-only and DOA-only based localization fail in case of the SU-emitter geometry resembling a straight line. Obviously, this also applies to the multiple SU case. However, since the localization is failing in orthogonal coordinates, the hybrid solution may overcome this problem. In fact, the CRBs for the hybrid approach at $\varphi = 0$ are determined by either the RSS-only or the DOA-only CRB:

$$\mathrm{var}\,(\hat{x}_{\mathrm{H,u}})\,|_{\varphi=0} = \mathrm{var}\,(\hat{x}_{\mathrm{H,k}})\,|_{\varphi=0} = \mathrm{var}\,(\hat{x}_{\mathrm{RSS,k}})\,|_{\varphi=0} \tag{42}$$

$$\mathrm{var}\,(\hat{y}_{\mathrm{H,u}})\,|_{\varphi=0} = \mathrm{var}\,(\hat{y}_{\mathrm{H,k}})\,|_{\varphi=0} = \mathrm{var}\,(\hat{y}_{\mathrm{DOA,k}})\,|_{\varphi=0}. \tag{43}$$

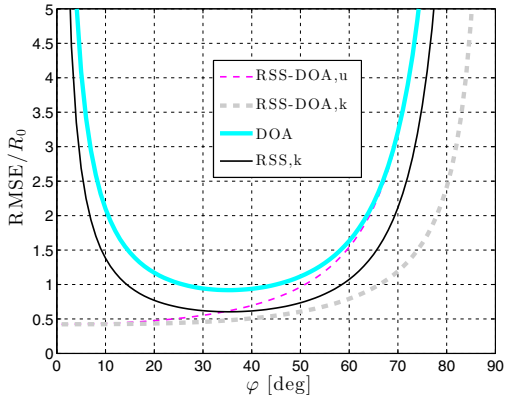

Fig. 3. Closed-form CRB on position estimation with the parameters $\alpha = 3.5$, $\sigma_a = 0.5$ rad, and $\sigma_f = 5$ dB. Indices: k - transmit power known, u - transmit power unknown.

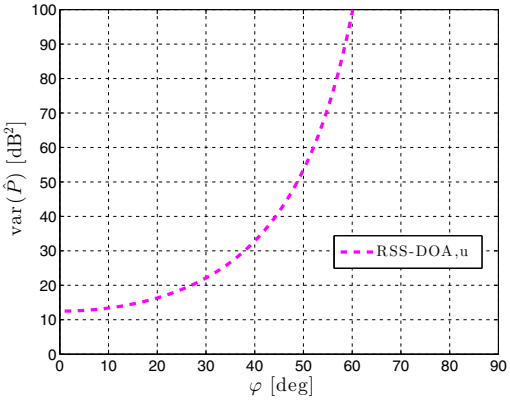

Fig. 4. Closed-form CRB on transmit power estimation based on RSS-DOA with the parameters $\alpha = 3.5$, $\sigma_a = 0.5$ rad, and $\sigma_f = 5$ dB.

This shows that the hybrid RSS-DOA based localization is finitely bounded for this type of SU-emitter geometry, with the individual CRB on x estimation stemming from RSS-only based localization and the individual CRB on y estimation stemming from DOA-only based localization.

V. Numerical Evaluations for Arbitrary Geometries

In order to evaluate and illustrate the derived CRBs for arbitrary scenarios, the SUs and the emitter are randomly placed on an area of $100 \times 100\mathrm{m}^2$ and (14), (18), (19), (21), (24), (25) and (27) are evaluated numerically. Fig. 5 depicts an exemplary realization of the random placement. Note that the depicted realization is an example of a disadvantageous geometry that we abstracted with the two SU-model in Sec. IV. In general, we observed that cases where the hybrid RSS-DOA based localization is significantly lower bounded than DOA-only based localization, were almost exclusively the result of a

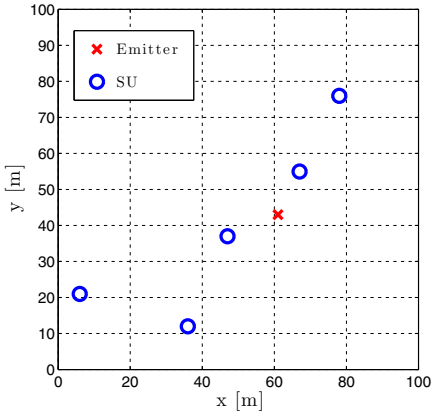

Fig. 5. Example realization of random SU and emitter placements with $M = 5$ SUs.

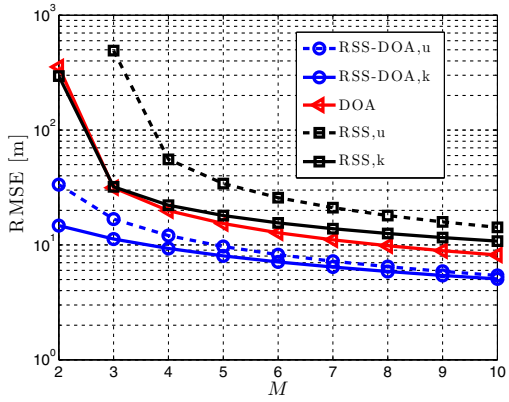

Fig. 6. Numerical evaluation of the derived CRBs on position estimation with different numbers of cooperating SUs, M. Parameters $\alpha = 3.5$, $\sigma_a = 0.3$ rad, $\sigma_f = 5$ dB, $d_c = 30$ m. Indices: k - transmit power known, u - transmit power unknown.

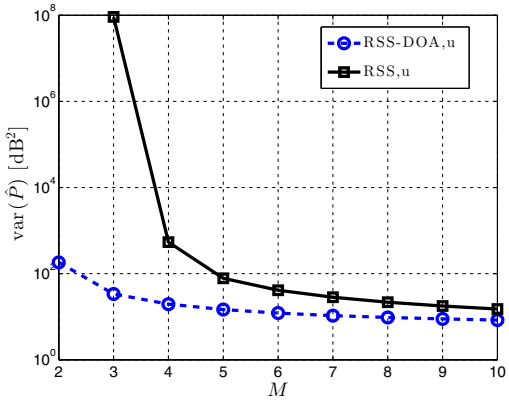

Fig. 7. Numerical evaluation of the derived CRBs on transmit power estimation with different numbers of cooperating SUs, M. Parameters $\alpha = 3.5$, $\sigma_a = 0.3$ rad, $\sigma_f = 5$ dB, $d_c = 30$ m.

SU-emitter geometry that resembles a straight line. This again shows the relevance of our abstraction.

The dependence of the CRBs on the amount of SUs involved, M, in the estimation is shown in Fig. 6 and Fig. 7. As expected, the RMSE bounds are lower if the transmit power is known. However, the differences between the CRBs for the known and unknown transmit power cases decrease as M increases. The CRB on the hybrid estimation is always lower compared to the RSS-only or DOA-only based approach. Furthermore, in this example the estimation based on DOA-only is also lower bounded than the RSS-only based estimation. This, however, is dependent on the choice of the parameters σ_a and σ_f. The highest decrease in the CRB on position as well as transmit power estimation occurs prior to $M = 5$ SUs for the RSS-only and DOA-only case. This is due to the problems associated with disadvantageous SU-emitter geometries that become increasingly unlikely with increasing M. As discussed in Section IV, the combination of RSS and DOA is not affected by these problems. Therefore, the curves for the hybrid approach are not subject to the same change in slope and the associated CRBs for small M are much lower as compared to the RSS-only and DOA-only based estimation. This again demonstrates clearly the benefits and novelty of the hybrid RSS-DOA based localization, especially when the number of observing SU devices is low.

The influence of the correlation distance on the CRBs is depicted in Fig. 8 and Fig. 9. Except for RSS-only based estimation with unknown transmit power, d_c has practically no influence on the RMSE. With increasing d_c, the CRB on $\text{RMSE}_{\text{RSS,u}}$ is decreasing. This is due to the value of the shadowing term m_i in (3) becoming increasingly equal for all SUs $i = 1 \dots M$ until in the extreme case, $d_c \to \infty$, $m_1 = m_2 = \dots m_M$. With less variance in shadowing across the SUs, the distance-dependent term in (4) is more easily extracted from the measurements (3) and the localization becomes more accurate. With respect to transmit power estimation on the other hand, an increase in shadowing correlation is disadvantageous since the transmit power P and $\mathbf{m}$ in (3) and (4) appear as a single constant offset making a distinction between the two unknowns impossible. Therefore, the RSS-DOA hybrid CRB on transmit power estimation is increasing with increasing d_c. In case of the RSS-only transmit power estimation, the CRB decreases with d_c. This, however, is due to the increase in localization accuracy making a more accurate transmit power estimation possible.

VI. Conclusions

In this paper we considered multiple SUs collaborating in order to estimate the location and transmit power of an emitter in a CR network. In the context of this scenario, we derived the CRBs on hybrid RSS-DOA location and transmit power estimation that we compared to the estimation based on either DOA- or RSS-only. On that account, we derived the FIMs

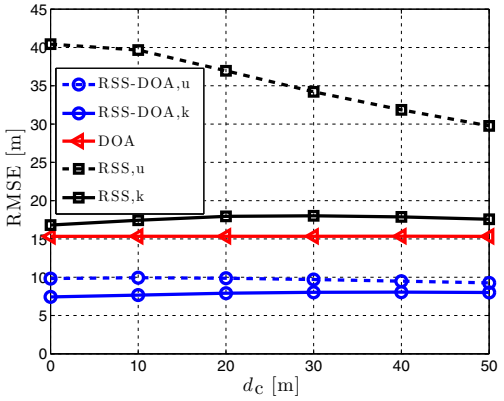

Fig. 8. Numerical evaluation of the derived CRBs on position estimation versus correlation distance d_c, with the parameters $\alpha = 3.5$, $\sigma_a = 0.3$ rad, $\sigma_f = 5$ dB, $M = 5$ SUs. Indices: k - transmit power known, u - transmit

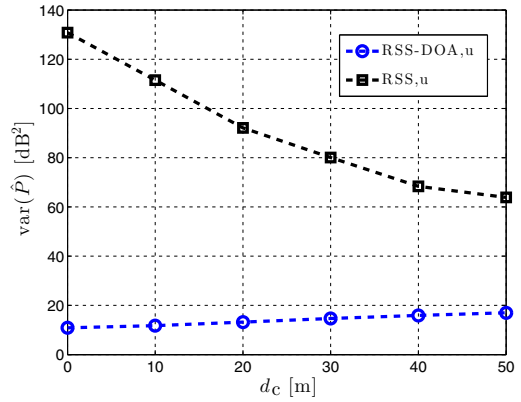

Fig. 9. Numerical evaluation of the derived CRBs on transmit power estimation versus correlation distance d_c, with the parameters $\alpha = 3.5$, $\sigma_a = 0.3$ rad, $\sigma_f = 5$ dB, $M = 5$ SUs.

for localization and transmit power estimation in closed-form. Although inversion of the FIMs in order to obtain the CRBs is possible with arbitrary SU geometries, the results are not very intuitive. Therefore, we focused on the important special case of two SUs at equal distance from the emitter that lets us study and understand geometries that are disadvantageous for localization based on RSS-only and DOA-only and derived the CRBs for that case in closed-form. With these results we were able to demonstrate that the CRB on the RMSE for DOA-only and RSS-only based localization is infinite when the SU-emitter geometry resembles a straight line, while the hybrid RSS-DOA approach results in a finite CRB. We showed that this is due to an infinite variance of one of the coordinate estimates for both RSS-only and DOA-only processing. However, since these coordinates are orthogonal the RSS-DOA hybrid estimation results in a finite RMSE. Using numerical evaluations of the derived CRBs in more general scenarios, we furthermore showed that even for arbitrary geometries, the hybrid approach results in significantly lower CRBs, in particular when the amount of observing SUs is comparably low. Furthermore, our results reveal that the CRB on hybrid RSS-DOA transmit power estimation is significantly lower compared to the CRB on estimation based on RSS-only. This demonstrates that using both RSS and DOA is indeed beneficial for localization and transmit power estimation of an emitter. The derived results form a solid theoretical framework for designing and optimizing collaborative SU networks, especially in case of mobile devices and mobile networks where minimizing the complexity of the devices and network reporting overhead are essential, and thus the realistic numbers of collaborating devices can easily be only in the order of 2-5. In such scenarios, based on the results of this paper, the hybrid RSS-DOA solutions are particularly attractive.

REFERENCES

[1] I. Mitola, J. and J. Maguire, G.Q., "Cognitive radio: making software radios more personal," *Personal Communications, IEEE*, vol. 6, pp. 13 –18, Aug. 1999.

[2] S. Haykin, "Cognitive radio: brain-empowered wireless communications," *Selected Areas in Communications, IEEE Journal on*, vol. 23, pp. 201 – 220, Feb. 2005.

[3] R. Martin and R. Thomas, "Algorithms and bounds for estimating location, directionality, and environmental parameters of primary spectrum users," *Wireless Communications, IEEE Transactions on*, vol. 8, pp. 5692 –5701, Nov. 2009.

[4] F. Penna and D. Cabric, "Bounds and tradeoffs for cooperative DoA-Only localization of primary users," in *Global Telecommunications Conference (GLOBECOM 2011), 2011 IEEE*, pp. 1 –5, Dec. 2011.

[5] F. Penna, J. Wang, and D. Cabric, "Cooperative localization of primary users by directional antennas or antenna arrays: Challenges and design issues," in *Antennas and Propagation (APSURSI), 2011 IEEE International Symposium on*, pp. 1113 –1115, July 2011.

[6] J. Wang, P. Urriza, Y. Han, and D. Čabrić, "Weighted centroid algorithm for estimating primary user location: Theoretical analysis and distributed implementation," *arXiv:1011.2313*, Nov. 2010.

[7] N. Patwari, I. Hero, A.O., M. Perkins, N. Correal, and R. O'Dea, "Relative location estimation in wireless sensor networks," *IEEE Transactions on Signal Processing*, vol. 51, pp. 2137 – 2148, Aug. 2003.

[8] I. Kadar, "Optimum geometry selection for sensor fusion," *Proceedings of SPIE*, vol. 3374, pp. 96–107, July 1998.

[9] A. Weiss, "On the accuracy of a cellular location system based on RSS measurements," *Vehicular Technology, IEEE Transactions on*, vol. 52, pp. 1508 – 1518, Nov. 2003.

[10] A. Catovic and Z. Sahinoglu, "The cramer-rao bounds of hybrid TOA/RSS and TDOA/RSS location estimation schemes," *Communications Letters, IEEE*, vol. 8, pp. 626 – 628, Oct. 2004.

[11] S. Wang, B. Jackson, and R. Inkol, "Hybrid RSS/AOA emitter location estimation based on least squares and maximum likelihood criteria," in *2012 26th Biennial Symposium on Communications (QBSC)*, pp. 24 –29, May 2012.

[12] J. Wang, J. Chen, and D. Cabric, "Cramer-rao bounds for joint rss/doa-based primary-user localization in cognitive radio networks," *accepted for publication in IEEE Trans. Wireless Commun.*, December 2012. [Online] http://arxiv.org/abs/1207.1469.

[13] P. Stoica and A. Nehorai, "MUSIC, maximum likelihood and cramer-rao bound," in *Acoustics, Speech, and Signal Processing, 1988. ICASSP-88., 1988 International Conference on*, pp. 2296 –2299 vol.4, Apr. 1988.

[14] R. Schmidt, "Multiple emitter location and signal parameter estimation," *Antennas and Propagation, IEEE Transactions on*, vol. 34, pp. 276 – 280, Mar. 1986.

[15] M. Gudmundson, "Correlation model for shadow fading in mobile radio systems," *Electronics Letters*, vol. 27, pp. 2145 –2146, Nov. 1991.

[16] S. M. Kay, *Fundamentals of Statistical Signal Processing, Volume I: Estimation Theory*. Prentice Hall, 1 ed., Apr. 1993.

[17] P. Stoica and T. Marzetta, "Parameter estimation problems with singular information matrices," *IEEE Transactions on Signal Processing*, vol. 49, pp. 87 –90, Jan. 2001.

Publication 7

J. Werner, M. Costa, A. Hakkarainen, K. Leppänen, and M. Valkama, "Joint user node positioning and clock offset estimation in 5G ultra-dense networks," accepted for publication in *Proceedings of the IEEE Global Communications Conference (GLOBECOM), San Diego, CA, 2015.*

Joint User Node Positioning and Clock Offset Estimation in 5G Ultra-Dense Networks

Janis Werner*, Mário Costa†, Aki Hakkarainen*, Kari Leppänen† and Mikko Valkama*
* Department of Electronics and Communications Engineering, Tampere University of Technology
Emails: {janis.werner, aki.hakkarainen, mikko.e.valkama}@tut.fi
† Huawei Technologies Oy (Finland) Co., Ltd, Finland R&D Center
Emails: {mariocosta, kari.leppanen}@huawei.com

***Abstract*—It is commonly expected that network densification will play an important role in achieving the capacity demands of 5G communication networks. While densification is introduced to improve the spectral efficiency and area-capacity, it also results in an infrastructure that is perfectly suitable for user node (UN) positioning. However, so far this compelling opportunity has not been clearly recognized in the literature. In this paper, we therefore propose to make "always on" positioning an integral part of 5G networks such that highly accurate UN position estimates are available at any given moment but without draining the UN batteries. We furthermore propose an extended Kalman filter (EKF) that tracks the UN position based on the fusion of direction of arrival (DoA) and time of arrival (ToA) estimates obtained at the access nodes (ANs) of the 5G network. Since ToA estimates are typically not useful for positioning unless the UN is synchronized with the network, we include a realistic clock model within the DoA/ToA EKF. This addition makes it possible to estimate the offset of the imperfect UN clock, along with the UN position. In an extensive analysis that is based on specific 5G simulation models, we then quantify the enormous potential of high accuracy positioning in 5G networks, in general, and the proposed DoA/ToA EKF, in particular. Moreover, we demonstrate that the proposed DoA/ToA EKF substantially outperforms the classical DoA-only EKF and is furthermore also able to handle practically extremely relevant situations where the DoA-only EKF fails to position the UN.**

***Index Terms*—Angle-of-arrival, direction-of-arrival, localization, location-awareness, time-of-arrival, tracking, ultra-dense networks, 5G networks**

I. Introduction

In order to achieve the demands expected for 5G wireless communication networks, it is likely that access nodes (ANs) with high spatial density are deployed (see, e.g., [1]). Consequently, user nodes (UNs) in 5G will operate within the range of several ANs simultaneously, such that devices are likely to be in the line of sight (LoS) of a few ANs for most of the time. In addition to meeting the increased communication demand, this also creates the opportunity for accurate device positioning based on time of arrival (ToA) estimates, obtained at the LoS ANs. Since it is expected that the ANs are also equipped with antenna arrays, ANs can furthermore estimate the direction of arrivals (DoAs), which can, in turn, be used to improve the device positioning accuracy. Overall, this results in great potential to develop and provide highly accurate device positioning within 5G networks that has significant advantages compared to already existing approaches.

On the technical side, the envisioned wide waveform bandwidths in 5G systems make it possible to obtain highly accurate ToA estimates that, in combination with the DoA estimates, can be fused into position estimates with extremely high accuracy. Therefore, 5G device positioning has the potential to substantially outperform existing techniques such as global navigation satellite systems (GNSSs) ($\approx 5\,\mathrm{m}$ [2]), LTE observed time difference of arrival (OTDoA) ($\approx 25\,\mathrm{m}$ [3]) or WLAN fingerprinting (3 – $4\,\mathrm{m}$ [4]). Second, since 5G positioning can potentially be carried out entirely on the network side, the power consumption within the user devices is exceptionally low. In fact, in the network-centric scenario, the only contribution to 5G positioning on the UN side is the transmission of uplink signals that are used to estimate the ToA and DoA within the ANs. However, these signals do not necessarily need to be dedicated positioning signals, but can be basically the same reference/pilot signals that are anyways exchanged between the devices and ANs for multiple-input multiple-output (MIMO) channel estimation [5]. Thus, the power consumption within the UNs, due to positioning capabilities, could be even a 100 times less compared to that of global positioning system (GPS) (≈ 100 – $150\,\mathrm{mW}$ [6]). As a consequence, and in contrast to GPS and other GNSSs, 5G positioning can continuously run in the background, providing highly accurate position estimates at any given moment. Third, the 5G positioning concepts will also work indoors, opening business opportunities to an important market. In contrast, classical GNSS-based solutions are not able to provide accurate positioning indoors as they require direct visibility to the satellites. Finally, 5G positioning would also allow for the determination of altitude, which is of particular importance in indoor positioning.

With all of these advantages, 5G positioning is expected to meet the high demands of future location based services and applications. Moreover, an accurate positioning infrastructure will be needed also for the navigation and mutual coordination of, e.g., robots that are expected to be commonplace by 2020-2030. Similarly, vehicles would benefit from fast, reliable and accurate positioning that enables advanced collision-avoidance as well as automatic driving gains. Ultimately, the UN position

This work was supported by the Doctoral Program of the President of Tampere University of Technology and the Finnish Funding Agency for Technology and Innovation (Tekes, under the project "5G Networks and Device Positioning").

Online video material available at `www.tut.fi/5G/GLOBECOM15`.

can also be capitalized in the 5G radio network itself in order to predict mobility and overall to carry out enhanced location-based radio resource management (RRM), for example.

In summary, the deployment of 5G networks with a high density of ANs provides an unprecedented opportunity to create an advanced positioning system that will be able to meet the demands of future location-based services and applications and greatly enhance the RRM of the 5G radio network. However, so far this opportunity has not been clearly recognized in the academy and industry. In this paper, we propose and demonstrate the capabilities of a positioning system that is specifically designed for high accuracy user device position estimation and tracking in 5G ultra-dense networks. More specifically, we propose an extended Kalman filter (EKF) that fuses the ToA and DoA estimates from a single or multiple LoS ANs into a position estimate. In the past, EKFs have been proposed for tracking the position of a target using DoA estimates only [7]. However, the fusion of both ToA and DoA estimates has not been considered, to the best of our knowledge.

It is well known that the use of ToA estimates in positioning requires nearly perfect synchronization within the network as well as with the device to be positioned. While synchronization within the network is a reasonable assumption, it is very unrealistic to assume a synchronization with the UN. The latter form of synchronization is particularly challenging due to the cheap oscillators that are commonly installed in user devices. These imperfect oscillators result in large and time-varying clock offsets, which, if not corrected, render the respective ToA estimates useless for positioning. In this paper, we address this problem by including a realistic clock offset model from [8] within the EKF. The resulting joint DoA/ToA EKF is then able to estimate both the UN position as well as the clock offset of the user device. To test the proposed positioning system, we first demonstrate the achievable DoA/ToA estimation performance using the respective Cramer-Rao bound (CRB) in conjunction with the 5G simulation models from the "Mobile and wireless communications enablers for the twenty-twenty information society (METIS)" project [9], [10]. Thereafter, we use these results to show that the proposed joint DoA/ToA EKF provides position estimates with significantly higher accuracy than the classical DoA-only EKF [7], while, at the same time, obtaining also highly accurate clock offset estimates. Moreover, we show that, in contrast to DoA-only based solutions, the proposed joint DoA/ToA EKF is capable of tracking the user position even if only a single LoS AN exists.

In summary, the contributions of this paper are as follows:

- We propose and discuss "always on" UN positioning in 5G.
- We simulate and analyze the achievable DoA/ToA estimation performance in 5G networks using the respective CRB in combination with the METIS channel model.
- We propose and test a novel joint DoA/ToA-EKF for joint UN positioning and clock offset estimation using realistic simulation models.

The paper is organized as follows. In Section II we discuss the proposed 5G positioning engine as well as the applied clock offset models. The CRB that we use to evaluate the achievable DoA and ToA estimation performance is shortly summarized in Section III. The joint DoA/ToA EKF for positioning is proposed in Section IV. A numerical evaluation and analysis of the algorithms can be found in Section V. Finally, the paper is concluded in Section VI. As supporting material for this paper, we have created two videos that can be found online under: *www.tut.fi/5G/GLOBECOM15*.

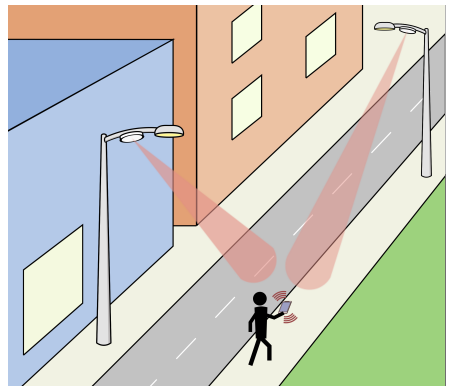

Fig. 1. Example of UN positioning in 5G ultra-dense networks. Positioning and tracking is carried out by the network in order to minimize the power consumption at the UN.

II. System Model

A. 5G Network and Positioning Engine

In this paper, we consider a dense network of ANs as depicted in Fig. 1. We assume that the location $\mathbf{p}_k = (x_k, y_k)$ of each AN k is known and that the ANs are equipped with antennas that make DoA estimation possible. As an example, we model the AN antennas as concentric circular antenna array consisting of nine cross-dipoles arranged in the horizontal plane $10\,\mathrm{m}$ above the ground. However, other antenna choices are possible as well. We further assume that the ANs composing the network are synchronized among each other but not with the UN. This AN synchronization does not have to be perfect, but should not exceed the range of the ToA estimation errors, which are about $1 - 4\,\mathrm{ns}$ with the setup that we consider in this paper. In the considered network, the UN periodically sends uplink signals that we will be referring to as beacons. Here we investigate the utilization of these beacons for network-based positioning. However, the beacons could also be used to acquire channel state information (CSI) at the ANs as proposed in [5]. Hence, dedicated signals for positioning may not be required in future 5G networks.

Based on the received beacons, ANs will detect whether they are in LoS with the UN. Such LoS detection schemes can be based on the Rice factor of the received signal strength (RSS) [11] or on the kurtosis of the estimated channel impulse response [12], for example. In case of an LoS link, an AN will then estimate the DoA and ToA of the beacon signal. Thereafter, the network gathers the DoA and ToA estimates from all LoS-ANs, which are finally fused into a UN position estimate $\hat{\mathbf{p}} = (\hat{x}, \hat{y})$ by means of the proposed joint DoA/ToA-EKF. For simplicity

of presentation and analysis, we only study 2D positioning based on azimuth DoA estimation. However, an extension to 3D positioning based on azimuth and elevation DoA estimation is possible and follows straightforwardly from the work presented in this paper.

B. Clock offset

In the literature, it is generally agreed that the clock offset ρ is a time-varying quantity due to imperfections of the device oscillators, see e.g., [8], [13]. For a measurement period T, the clock offset can therefore be written in a recursive form as [8]

$$\rho[n] = \rho[n-1] + \alpha[n]T \tag{1}$$

where $\alpha[n]$ is known as the clock skew. Some authors, e.g., those of [13] assume the clock skew to be constant, while some recent research based on measurements suggests that the clock skew is in fact time-dependent, at least over the large observation period ($1.5\,\text{months}$) considered in [8]. However, taking the research and measurement results in [14], [15] into account, where devices are identified remotely based on an estimate of the average clock skew, one could assume that the *average clock skew* is indeed constant. This also matches with the measurement results in [8], where the clock skew seems to be fluctuating around a mean value. Nevertheless, the measurements in [8], [14], [15] were obtained indoors, i.e., in a temperature controlled environment. In practice, it would be surprising if large changes in the ambient temperature due to, e.g., a transition from indoors to outdoors would not affect the clock skew at all. Therefore, we adopt the more general model [8] of a time-varying clock skew, which also encompasses the constant clock skew model.

The clock skew in [8] is modeled as an auto-regressive (AR) process of order P. While the measurement results in [8] reveal that modeling the clock offset as an AR process results in large performance gains compared to a constant clock skew model, an increase of the order beyond $P = 1$ does not seem to increase the accuracy of clock offset tracking significantly. In here, we consequently model the clock skew as an AR model of first order according to

$$\alpha[n] = \beta\alpha[n-1] + \eta[n] \tag{2}$$

where β is a (constant) parameter and $\eta[n] \sim \mathcal{N}(0, \sigma_\eta^2)$ is additive white Gaussian noise (AWGN). Note that the joint DoA/ToA EKF proposed in Section IV could easily be extended to AR processes of higher orders.

III. CRB on DoA and ToA Estimation

The CRB is a lower bound on the estimation variance of any unbiased estimator. This section derives the CRB on 2D DoA and delay estimation of the LoS path on a dense multipath channel. In this paper, the DoA and ToA estimates used by the EKF proposed in Section IV follow a distribution that is given by the CRB. We choose such an approach in order to identify the ultimate performance limits of DoA/ToA estimation in ultra-dense networks, independent of a particular estimator. In practice, the DoA and ToA estimates used by the EKF may be found from the RIMAX algorithm, for example [16]. Interestingly, the RIMAX algorithm is known to be statistically efficient in the asymptotic regime, and very close to the CRB in practice [16]. Thus, this approach *does not* limit the generality of the proposed EKF and is moreover also a good indication for the performance that can be achieved with practical estimators.

We model each uplink (UL)-single input multiple output (SIMO) channel as a superposition of a single specular component and diffuse components. As motivated in Section II, we consider the channels corresponding to the ANs that are in LoS with the UN, only. In particular, let $\bar{\mathbf{z}}_k \in \mathbb{C}^{M_f N_k \times 1}$ denote the UL-SIMO channel of the kth AN for all of the M_f subcarriers, i.e. $\bar{\mathbf{z}}_k = [\hat{\mathbf{z}}_k(1), \ldots, \hat{\mathbf{z}}_k(M_f)]^T$. The UL-SIMO channel may be estimated from UL pilot signals, and it is also needed in multiantenna wireless communications for spatial-division multiple-access and beamforming.

In this paper, the UL-SIMO channel is parameterized as follows:

$$\bar{\mathbf{z}}_k(\boldsymbol{\xi}) = \left([\mathbf{a}_k^H(\vartheta,\varphi),\ \mathbf{a}_k^V(\vartheta,\varphi)] \otimes \mathbf{a}_k(\tau)\right)\boldsymbol{\gamma} + \mathbf{n}, \tag{3}$$

where $\otimes$ denotes the Kronecker product and the LoS-parameter vector $\boldsymbol{\xi} \in \mathbb{R}^{3\times 1}$ is given by $\boldsymbol{\xi} = [\tau, \vartheta, \varphi]^T$. In particular, $\tau \in \mathbb{R}_0^+$, $\vartheta \in [0, \pi]$, and $\varphi \in [0, 2\pi)$ denote the ToA of the LoS path as well as the elevation and azimuth DoAs, respectively. Moreover, vectors $\mathbf{a}_k^H(\vartheta,\varphi) \in \mathbb{C}^{N_k\times 1}$ and $\mathbf{a}_k^V(\vartheta,\varphi) \in \mathbb{C}^{N_k\times 1}$ in (3) denote the array steering vectors of the kth AN for a horizontal and vertical polarization, respectively. Furthermore, $\mathbf{a}_k(\tau) \in \mathbb{C}^{M_f\times 1}$ denotes the frequency-response of the UL-SIMO channel, including the Tx/Rx RF-chains, and $M_f \in \mathbb{N}$ denotes the number of subcarriers. For the sake of simplicity, we assume that the Rx RF-chains are identical. Finally, vector $\boldsymbol{\gamma} \in \mathbb{C}^{2\times 1}$ denotes the complex-valued weights of the LoS path in both horizontal and vertical polarizations while $\mathbf{n} \in \mathbb{C}^{M_f N_k \times 1}$ models both the diffuse components of the channel and the measurement noise. Vector $\mathbf{n}$ is zero-mean complex-circular multivariate Gaussian distributed with a covariance matrix given by $\mathbf{R}_n \in \mathbb{C}^{M_f N_k \times M_f N_k}$.

The CRB for the LoS-parameters is given by $\mathbf{CRB}(\boldsymbol{\theta}) = \mathbf{I}^{-1}(\boldsymbol{\theta})$ where $\mathbf{I}(\boldsymbol{\theta}) \in \mathbb{R}^{7\times 7}$ denotes the Fisher information matrix (FIM). The parameter vector $\boldsymbol{\theta} \in \mathbb{R}^{7\times 1}$ is given by $\boldsymbol{\theta} = [\boldsymbol{\xi}^T, \Re\{\boldsymbol{\gamma}\}^T, \Im\{\boldsymbol{\gamma}\}^T]^T$. The FIM can be shown to equal

$$\mathbf{I}(\boldsymbol{\theta}) = 2\Re\{\mathbf{D}_f^H\mathbf{R}_f^{-1}\mathbf{D}_f \odot \mathbf{D}_\gamma^H\mathbf{D}_\gamma \odot \mathbf{D}_g^H\mathbf{R}_g^{-1}\mathbf{D}_g\}, \tag{4}$$

where $\odot$ denotes the Hadamard-Schur product and $\mathbf{R}_f$ and $\mathbf{R}_g$ denote the covariance matrices of the diffuse components in the delay and angular domain, respectively. Moreover, matrices $\mathbf{D}_f \in \mathbb{C}^{M_f\times 7}$, $\mathbf{D}_\gamma \in \mathbb{C}^{1\times 7}$, and $\mathbf{D}_g \in \mathbb{C}^{N_k\times 7}$ are given by:

$$\mathbf{D}_f = [\frac{\partial}{\partial\tau}\mathbf{a}(\tau),\ \mathbf{1}^T \otimes \mathbf{a}(\tau)], \quad \mathbf{D}_\gamma = [\mathbf{1}^T,\ j,\ 1,\ j] \tag{5a}$$

$$\mathbf{D}_g = [\bar{\mathbf{a}}(\vartheta,\varphi),\ \frac{\partial}{\partial\vartheta}\bar{\mathbf{a}}(\vartheta,\varphi),\ \frac{\partial}{\partial\varphi}\bar{\mathbf{a}}(\vartheta,\varphi),\ \bar{\mathbf{a}}(\vartheta,\varphi) \otimes \mathbf{1}^T], \tag{5b}$$

where $\mathbf{1}$ denotes a vector of 1's with appropriate dimensions.

Note that the FIM expression in (4) assumes a noise covariance matrix given by $\mathbf{R}_n = \mathbf{R}_f \otimes \mathbf{R}_g$. This is a common assumption in channel modeling [16]. It is also important to note that $\mathbf{R}_n$ is unknown in practice and needs to be estimated, in addition to the LoS-parameters. However, the corresponding CRB block related to the LoS-parameters is still given by (4).

IV. Proposed EKF for Joint Tracking of User Position and Clock Offset

The EKF is a non-linear extension of the popular Kalman filter that iteratively estimates the state of a dynamic system. In this section, we first propose the joint DoA/ToA EKF and then shortly discuss how to properly initialize the EKF for good tracking performance.

A. EKF Iterations

Within the joint DoA/ToA EKF, we estimate the UN position along with the clock offset and clock skew. Therefore, we obtain a state vector $\mathbf{s}[n] = [x[n], y[n], v_x[n], v_y[n], \rho[n], \alpha[n]]^T$ that evolves according to the state transition

$$\mathbf{s}[n] = \mathbf{F}\mathbf{s}[n-1] + \mathbf{w}[n], \tag{6}$$

$$\mathbf{F} = \begin{bmatrix} \mathbf{I}_2 & T\cdot\mathbf{I}_2 & \mathbf{0}_2 \\ \mathbf{0}_2 & \mathbf{I}_2 & \mathbf{0}_2 \\ \mathbf{0}_2 & \mathbf{0}_2 & \mathbf{F}_\mathrm{c} \end{bmatrix}, \quad \mathbf{F}_\mathrm{c} = \begin{bmatrix} 1 & T \\ 0 & \beta \end{bmatrix} \tag{7}$$

with $\mathbf{w}[n] \sim \mathcal{N}(0, \mathbf{Q})$, $\mathbf{Q} = \mathrm{diag}[0, 0, \sigma_v^2, \sigma_v^2, 0, \sigma_\eta^2]$. From (7), we can see that (6) consists of two decoupled parts. On the one hand, we have the part that corresponds to the movement of the user, i.e., position and velocity. This part originates from a conventional movement model as described in, e.g., [17, p. 459]. On the other hand, we have the part that describes the evolution of the clock offset and skew according to (1) and (2), respectively. Note that both (1) and (2) have been shown to be suitable for clock tracking in [8] using practical measurements. Unfortunately, the authors of [8] do not state values for β as determined in their experiments. However, they argue that the clock skew is quasi-stationary, even for very long measurement periods ($1.5\,\mathrm{months}$) such that we can calculate $\beta = \sqrt{(\sigma_\alpha^2 - \sigma_\eta^2)/\sigma_\alpha^2}$, which becomes $\beta \approx 0.98$ for the values of σ_α^2 and σ_η^2 given in [8]. In general, and although the authors of [8] propose some techniques to estimate β, it is rather difficult for a network to obtain those estimates. Therefore, we set $\hat{\beta} = 1$ within the EKF. However, according to our observations, the joint DoA/ToA EKF is not very sensitive to mismatches between $\hat{\beta}$ and the actual β.

For every time step n, denote $K[n]$ as the number of ANs with a LoS to the UN and $\ell = \{l_1, l_2, \ldots, l_{K[n]}\}$ as the indices of those ANs. At an individual AN $k \in \ell$, the measurement equation then consists of two parts, i.e., the DoA estimate $\hat{\varphi}_k[n] = \varphi_k[n] + \delta\varphi_k[n]$ as well as the ToA estimate $\hat{\tau}_k[n] = \tau_k[n] + \delta\tau_k[n]$ with estimation errors $\delta\varphi_k[n]$ and $\delta\tau_k[n]$. We can hence write in short $\mathbf{y}_k = [\hat{\varphi}_k[n], \hat{\tau}_k[n]]^T = \mathbf{h}_k(\mathbf{s}[n]) + \mathbf{u}[n]$, where $\mathbf{u}_k = [\delta\varphi_k, \delta\tau_k]^T$ is the estimation error with covariance $\mathbf{R}_k = \mathrm{E}[\mathbf{u_k}\mathbf{u}_k^T]$ and $\mathbf{h}_k(\mathbf{s}[n]) = [h_{k,1}(\mathbf{s}[n]),\, h_{k,2}(\mathbf{s}[n])]^T$. The vector function $\mathbf{h}_k : \mathbb{R}^6 \to \mathbb{R}^2$ relates the measurement vector $\mathbf{y}_k$ to the UN state through the nonlinear equations

$$h_{k,1}(\mathbf{s}[n]) = \arctan\frac{\Delta y_k[n]}{\Delta x_k[n]} \tag{8}$$

$$h_{k,2}\left(\mathbf{s}[n]\right) = \frac{d_k[n]}{c} + \rho[n] \tag{9}$$

with $\Delta x_k[n] = x[n] - x_k$, $\Delta y_k[n] = y[n] - y_k$, $d_k[n] = \sqrt{\Delta^2 x_k[n] + \Delta^2 y_k[n]}$ and the speed of light c. Finally, we write the complete measurement equation at time-step n by combining the $\mathbf{y}_k$ from all $L[n]$ LoS-ANs into the $L[n]\times 1$ vector

$$\mathbf{y}[n] = \mathbf{h}(\mathbf{s}[n]) + \mathbf{u}[n] \tag{10}$$

where $\mathbf{y} = [\mathbf{y}_1^T, \mathbf{y}_2^T, \ldots, \mathbf{y}_{L[n]}^T]^T$, $\mathbf{h} = [\mathbf{h}_1^T, \mathbf{h}_2^T, \ldots, \mathbf{h}_{L[n]}^T]^T$ and $\mathbf{u} \sim \mathcal{N}(0, \mathbf{R})$ with an $L[n]\times L[n]$ block diagonal covariance matrix $\mathbf{R} = \mathrm{blkdiag}(\mathbf{R}_{l_1}, \mathbf{R}_{l_1}, \ldots, \mathbf{R}_{l_{L[n]}})$.

We are now ready to state the well known EKF equations. In this paper, we use the same notation as in [18] where $\mathbf{s}^-[n]$ denotes an *a priori* state estimate, i.e., an estimate obtained from the measurements up to but not including $\mathbf{y}[n]$, while $\mathbf{s}^+[n]$ denotes an *a posteriori* estimate, i.e., an estimate obtained from measurements up to and including $\mathbf{y}[n]$. With this notation we can write the *a priori* estimates of the state and its covariance at time-step n as

$$\hat{\mathbf{s}}^-[n] = \mathbf{F}\hat{\mathbf{s}}^+[n-1] \tag{11}$$

$$\mathbf{P}^-[n] = \mathbf{F}\mathbf{P}^+[n-1]\mathbf{F}^T + \mathbf{Q}[n] \tag{12}$$

while the *a posteriori* estimates can be written as

$$\mathbf{K}[n] = \mathbf{P}^-[n]\mathbf{H}[n]^T(\mathbf{H}[n]\mathbf{P}^-[n]\mathbf{H}^T[n] + \mathbf{R}[n])^{-1} \tag{13}$$

$$\hat{\mathbf{s}}^+[n] = \hat{\mathbf{s}}^-[n] + \mathbf{K}[n]\left[\mathbf{y}[n] - \mathbf{h}(\hat{\mathbf{s}}^-[n])\right] \tag{14}$$

$$\mathbf{P}^+[n] = (\mathbf{I} - \mathbf{K}[n]\mathbf{H}[n])\,\mathbf{P}^-[n]. \tag{15}$$

In (13-15) we use the Jacobian matrix $\mathbf{H} = \frac{\partial \mathbf{h}[n]}{\partial \mathbf{s}[n]}$ evaluated at $\mathbf{s}^-[n]$. For the joint DoA/ToA EKF, the elements of $\mathbf{H}$ become $\mathbf{H}_{2k-1,1}[n] = [\mathbf{h}_{k,1}]_x(\hat{\mathbf{s}}^-[n])$, $\mathbf{H}_{2k-1,2}[n] = [\mathbf{h}_{k,1}]_y(\hat{\mathbf{s}}^-[n])$, $\mathbf{H}_{2k,1}[n] = [\mathbf{h}_{k,2}]_x(\hat{\mathbf{s}}^-[n])$, $\mathbf{H}_{2k,2}[n] = [\mathbf{h}_{k,2}]_y(\hat{\mathbf{s}}^-[n])$, $\mathbf{H}_{2k,5} = [\mathbf{h}_{k,2}]_\rho(\hat{\mathbf{s}}^-[n])$ for $k = 1 \ldots L[n]$ and zero otherwise. It is then straight forward to show that

$$\left[\mathbf{h}_{k,1}\right]_x(\mathbf{s}[n]) = -\frac{\Delta y_k[n]}{d_k^2[n]}, \quad \left[\mathbf{h}_{k,1}\right]_y(\mathbf{s}[n]) = \frac{\Delta x_k[n]}{d_k^2[n]} \tag{16}$$

$$\left[\mathbf{h}_{k,2}\right]_x(\mathbf{s}[n]) = \frac{\Delta x_k[n]}{c\,d_k[n]}, \quad \left[\mathbf{h}_{k,2}\right]_y(\mathbf{s}[n]) = \frac{\Delta y_k[n]}{c\,d_k[n]} \tag{17}$$

$$\left[\mathbf{h}_{k,2}\right]_\rho(\mathbf{s}[n]) = 1. \tag{18}$$

The UN position estimate at time step n is finally obtained as $(\hat{\mathbf{s}}_1^+[n], \hat{\mathbf{s}}_2^+[n])$ with an estimated covariance found as the upper-left-most 2×2 submatrix of $\mathbf{P}^+[n]$. An estimate of the clock-offset is given through $\hat{\mathbf{s}}_5^+[n]$.

B. EKF Initialization

In general, the initialization, i.e., the choice of $\hat{\mathbf{s}}^+[0]$ and $\mathbf{P}^+[0]$ is very important for the performance of an EKF. In the worst case, bad choices of $\hat{\mathbf{s}}^+[0]$ might lead to divergence in the EKF. Fortunately, in ultra dense networks divergence of the UN position estimates is relatively easily noticed by checking whether the obtained estimates match with the locations of the ANs that can hear the UN. Nevertheless, we would obviously like to avoid divergence in the first place. Therefore, in the following we will briefly discuss possible initialization methods.

For the initialization of the UN position estimates, we can resort to one of the many RSS/DoA/time difference of arrival (TDoA)-based positioning techniques that are available in the literature. If available, the UN could even communicate a position estimate that it obtained itself using, e.g., GNSSs. It is

important though that the chosen technique provides not only position estimates but also an estimate of the position covariance such that the respective elements in both $\mathbf{s}^+[0]$ and $\mathbf{P}^+[0]$ can be initialized. Unless the chosen positioning technique also provides a velocity estimate, the EKF can be initialized with a very coarse estimate of the average velocity that is easily obtained for a given location considering e.g. speed limits and available means of transportation.

The UN clock offset can be limited to fairly low values by simply communicating the time from one of the LoS-ANs. Upon arrival at the UN, the communicated time can be used to set the time within the UN. Thereafter, the UN clock offset is determined by the transmission and reception delays occurring within the involved AN and UN, respectively, as well as the signal propagation time.

Manufactures typically report the clock skew of their oscillators in parts per million (ppm). An oscillator with a specification of $20\,\mathrm{ppm}$, as an example, can be expected to result in a maximum clock offset of $\pm 20\,\mu\mathrm{s}$ per $1\,\mathrm{s}$ of runtime. However, based on the results in [8], [14], [15] positive clock skews seem to be much more common than negative ones. In [14], the clock skews of 69 desktop computers have been estimated using transmission control protocol (TCP) timestamps over a period of 38 days. Out of the 69 machines, only two had slightly negative clock skews ($>-6\,\mathrm{ppm}$), while the average clock skew was about $21\,\mathrm{ppm}$ with a standard deviation (STD) of about $12\,\mathrm{ppm}$. Similar results can be found in [15], where the clock skews of five smartphones have been estimated using internet control message protocol (ICMP) timestamps. Again, only a single smartphone had a slightly negative clock skew ($\approx -3\,\mathrm{ppm}$), while the average clock skew and STD were about $29\,\mathrm{ppm}$ and $34\,\mathrm{ppm}$, respectively. Finally, in [8] the average clock skews of a low-powered micro controller in combination with a $16\,\mathrm{MHz}$ and a $32.768\,\mathrm{kHz}$ clock were determined to be approximately $78\,\mathrm{ppm}$ and $39\,\mathrm{ppm}$, respectively. Therefore, as a very general rule, we could initialize the clock skew to $\hat{\alpha}[0] = 25\,\mathrm{ppm}$ with an STD of a few $10\,\mathrm{ppm}$.

V. Numerical Evaluations and Analysis

In our evaluation, we first use the geometry-based stochastic METIS channel model [10] to determine the CRB on DoA/ToA estimation. The obtained CRB then serves as the basis to simulate the performance of the proposed DoA/ToA EKF. This approach greatly reduces the overall simulation run-time and moreover also simplifies the repeatability of our results.

A. DoA and Delay Estimation

The METIS geometry-based stochastic channel model (GSCM) stems from the WINNER+ channel model [19]. Our focus has been on the 3D urban micro (UMi) propagation scenario. In particular, the maximum number of clusters in the 3D UMi scenario is 12 for LoS and 19 for a NLoS condition. The clusters that are at least $25\,\mathrm{dB}$ weaker than the cluster with largest power are discarded. Each cluster comprises 20 propagation paths. Each propagation path is characterized by a power, delay, elevation angle, azimuth angle, complex-path weights and a cross-polarization ratio. Details regarding the calculation of the aforementioned parameters of the propagation paths may be found in [10], in addition to the corresponding probability distributions. The LoS propagation path is also included in case of a LoS condition. The Ricean K-factor is used to weight the LoS propagation path as well as the remaining clusters accordingly. The parameters of the LoS propagation path, namely the elevation angle, azimuth angle, delay and path-weights, follow from the distance between the AN and UN as well as their relative locations.

For the beacons transmitted by the UNs we assume an OFDM waveform with a bandwidth of $B = 200\,\mathrm{MHz}$ and a total number of $N_{\mathrm{s,m}} = 640$ subcarriers. However, we exploit only $N_{\mathrm{s}} = 64$ subcarriers for positioning purposes (1 every 10). The receiver noise in the ANs is modeled as *iid* circular symmetric complex Gaussian thermal noise with a variance of $kTB_{\mathrm{s}} = -119\,\mathrm{dBm}$ per subcarrier, where $T = 295\,\mathrm{K}$, k is the Boltzmann's constant, and $B_{\mathrm{s}} = B/N_{\mathrm{s,m}}$. The radio frequency interference (RFI) at an AN is assumed to stem from UNs outside of the AN's coordination area which we model as a circle of radius $250\,\mathrm{m}$ around the AN. In a separate simulation study (not included here due to lack of space), we have determined the RFI by placing the interferring UNs on a ring around the AN with outer and inner radius of $250\,\mathrm{m}$ and $500\,\mathrm{m}$, respectively. The placement of the interferring UNs was according to a non-homogeneous Poisson process leading to an overall density of about 1000 UNs per $1\,\mathrm{km}^2$. This value is according to the car density recommended by METIS [9]. Next, we assumed that the interfering UNs transmit an OFDM-based signal with 640 active subcarriers and a transmit power of $23\,\mathrm{dBm}$. According to our simulation results, the overall interference at an AN can then be well approximated as normally distributed with a variance of $-86\,\mathrm{dBm}$ per subcarrier. Finally, the RFI is modeled as a spatially white process. Such an assumption significantly reduces the complexity of the simulations and it is in agreement with the recommendations in [20]. Finally, we have calculated the transmit power of the UNs to be positioned such that a LoS-AN $60\,\mathrm{m}$ away from the UN receives the positioning beacons with a signal-to-interference-plus-noise ratio (SINR) of $15\,\mathrm{dB}$. This results in a UN transmit power of about $3\,\mathrm{dBm}$.

Using the aforementioned setup, we have determined the CRB on the STD of DoA/ToA estimation as depicted in Fig. 2. The depicted results were obtained by numerically averaging over the CRB for $3 \cdot 10^5$ channel realizations drawn randomly according to the METIS channel model [10]. The CRB for the METIS channel model has been obtained by fitting the multipath-components of the channel to the covariance matrix in (4). We have observed that in rare cases channel realizations occur which lead to a CRB on DoA estimates much larger than $[180°]^2$. This is a limitation of the CRB in use, which was derived neglecting the fact that DoAs are circular values defined on an interval of $360°$. In order to avoid that the average CRB is dominated by these rare but very large and faulty values, we have removed the corresponding channel realizations. In a practical system we would also recommend to remove DoA/ToA estimates that do not match our earlier observations in any way. Thus, we believe that the removal of such channel realizations is

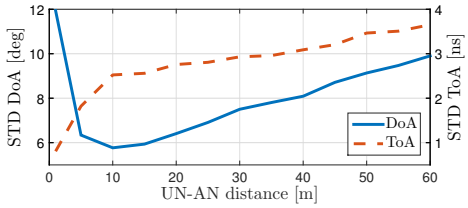

Fig. 2. CRB on the STD of DoA and ToA estimation as a function of the AN-UN distance using the stochastic METIS channel model [10].

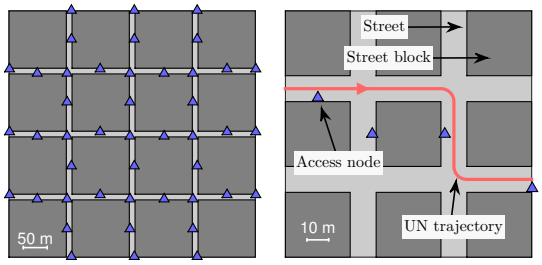

(a) Multiple LoS-AN map. (b) Single LoS-AN map.

Fig. 3. Maps used to test the tracking performance of the proposed joint DoA/ToA-EKF.

in fact a very practical approach to solve the shortcomings of the CRB in use.

As expected, the CRB on ToA estimation increases monotonically with the UN-AN distance. This is caused by the propagation path loss that increases with the UN-AN distance. Obviously, an increasing path loss also results in a reduction of the UN SINR at the AN. This, in turn, leads to the observed worsening of the ToA estimates. However, for the CRB on DoA estimation we observe a slightly different behavior. In fact, the CRB on DoA estimation decreases up to around $10\,\mathrm{m}$ and only thereafter, we observe the same monotonic increase with the UN-AN distance. While this initial decrease of the CRB might seem counter-intuitive at first, it is explained by the geometry of our estimation problem. According to our assumptions, the AN's planar antenna array is mounted in a horizontal plane $8.5\,\mathrm{m}$ above the UN. Now if a UN is located directly underneath the AN azimuth DoA estimation is in fact impossible with the assumed array. The conditions for azimuth DoA estimation only improve when the UN is moving away from the AN. In theory, the best performance is achieved when both the AN and UN are approximately co-planar. However, this also means that the UN is very far from the AN, which as discussed above significantly reduces the SINR. Due to these counteracting mechanisms we thus observe the lowest value for the CRB on DoA estimation at around $10\,\mathrm{m}$. Finally, the CRB also reveals that DoA and ToA estimation errors are statistically independent since the off-diagonal elements of the CRB are practically zero (even in comparison to the small values of the CRB on ToA estimation).

B. User Position and Clock Offset Tracking

In this section, the performance of the proposed joint DoA/ToA-EKF is evaluated by tracking a UN moving through an urban environment similar to METIS' Madrid model [9]. In accordance with the Madrid model, each block has dimensions of $120\,\mathrm{m} \times 120\,\mathrm{m}$ and the street width is set to $12\,\mathrm{m}$. The density of ANs is assumed to be $60\,\mathrm{m}$, which is well in line with the assumptions in [5]. Overall, our street model consists of 4×4 blocks, resulting in the map depicted in Fig. 3a.

TABLE I. Tracking RMSE of UN position (Pos.) and clock offset (Clk.).

	DoA-only EKF [7]		proposed joint DoA/ToA-EKF	
N_T	Pos.	Clk.	Pos.	Clk.
100	$5.3\,\mathrm{m}$	–	$0.4\,\mathrm{m}$	$4\,\mathrm{ns}$
500	$8.2\,\mathrm{m}$	–	$0.6\,\mathrm{m}$	$4\,\mathrm{ns}$
1000	$10.3\,\mathrm{m}$	–	$1.0\,\mathrm{m}$	$4\,\mathrm{ns}$

A new UN is randomly and uniformly placed at the start of the N, E, S or W ends of either of the streets. When the UN approaches an intersection, its route continues in a randomly and uniformly chosen direction excluding the direction the UN is coming from. The route ends when the UN moves out of the map or when it has crossed a maximum of 6 intersections. For the sake of simplicity, it is assumed that the UN is moving in the middle of the street and with a constant velocity $v = \sqrt{v_x^2 + v_y^2} = 15\,\mathrm{km/h}$. Whenever a new UN is placed on the map, its clock offset and clock skew are randomly initialized according to $\rho[0] \sim \mathcal{N}(0, \sigma_{\rho,0}^2)$, $\sigma_{\rho,0} = 100\,\mu\mathrm{s}$ and $\alpha[0] \sim \mathcal{N}(\mu_{\alpha,0}, \sigma_{\alpha,0}^2)$, $\mu_{\alpha,0} = 25\,\mathrm{ppm}$, $\sigma_{\alpha,0} = 30\,\mathrm{ppm}$, respectively, as motivated in Section IV-B. Based on the measurement results in [8], we set the STD of the clock skew driving noise to $\sigma_\eta = 6.3 \cdot 10^{-8}$.

We assume that an initial estimate $\hat{\mathbf{p}}[0] = (\hat{x}[0], \hat{y}[0])^T$ of the UN position $\mathbf{p}[0]$ is available through, e.g., GNSS where $\hat{\mathbf{p}}[0] \sim \mathcal{N}(\mathbf{p}[0], \sigma_{\mathrm{p},0}^2 \mathbf{I}_2)$, $\sigma_{\mathrm{p},0} = 5\,\mathrm{m}$. For each new UN, we then initialize the joint DoA/ToA-EKF as well as the classical DoA-only EKF [7] that serves as our positioning benchmark. The state vector and covariance of the joint DoA/ToA-EKF are initialized as $\hat{\mathbf{s}}^+[0] = (\hat{\mathbf{p}}^T[0], 0, 0, 0, \mu_{\alpha,0})^T$ and $\mathbf{P}^+[0] = \mathrm{diag}(\sigma_{p,0}^2, \sigma_{p,0}^2, \sigma_{v,0}^2, \sigma_{v,0}^2, \sigma_{\rho,0}^2, \sigma_{\alpha,0}^2)^T$, $\sigma_{v,0} = 5\,\mathrm{m}$, respectively. The same values are then also used for the initialization of the DoA-only EKF. Thereafter, the EKFs are updated in an interval of $T = N_\mathrm{T} T_\mathrm{f}$, where $T_\mathrm{f} = 167.3\,\mu\mathrm{s}$ is the duration of the 5G radio frame proposed in [5] and N_T is a positive integer. At every time-step n, we assume that the two closest ANs not obscured by building blocks are in LoS with the UN. These LoS-ANs then produce a DoA and ToA estimate according to (10) using the CRBs obtained in the previous section. Thereby, the block matrix $\mathbf{R}_{l_i}$ of covariance $\mathbf{R}$ becomes the CRB that was obtained for the distance closest to the actual distance between AN l_i and the UN. Within the EKFs, we have tuned the STD of the driving noises to $\sigma_v = 0.1\,\mathrm{m/s}$ and $\sigma_\eta' = 10^{-4}$. The latter value is much larger than the actual value, but leads to a much improved overall performance. Based on our observation, very small σ_η' lead to a divergence in the joint DoA/ToA-EKF whenever the clock offset and clock skew estimates are very inaccurate as, e.g., the case in the initial tracking phase.

Table I summarizes the tracking performance of the proposed joint DoA/ToA-EKF in comparison to the classical DoA-only EKF. These results were obtained by averaging over 10^3 different UN routes, each with individual realizations of DoA/ToA

estimation errors. In order to avoid that the tracking root-mean-squared errors (RMSEs) are dominated by the initial state estimates $\hat{\mathbf{s}}^+$, we have excluded the first 20 EKF iterations in the RMSE calculation. Considering the clock offset, for example, we notice that the tracking RMSE in Table I is significantly smaller than the STD of the initial estimate ($100\,\mu\mathrm{s}$). However, these initial errors are not determined by the EKFs and should therefore also not be included in the tracking RMSE calculation.

As expected, we can improve the estimation accuracy by decreasing the tracking period. Overall, the results also show that the proposed joint DoA/ToA-EKF greatly improves the positioning accuracy of the classical DoA-only EKF. Depending on the tracking period, the joint DoA/ToA-EKF achieves a positioning RMSE of 0.4 – $1.0\,\mathrm{m}$, which is *an improvement by a magnitude compared to the RMSE of the DoA-only EKF*. Moreover and in contrast to the DoA-only EKF, the joint DoA/ToA-EKF also achieves highly accurate UN-network synchronization with an RMSE of only $4\,\mathrm{ns}$.

The performance of the DoA-only EKF suffers in particular when the geometry of the two LoS-ANs and the UN resembles a line. In such cases information about the AN-UN angles suffices only to determine that the UN is located somewhere on that line, but not exactly where. This is a known problem of DoA-only based positioning in general and it has been shown that this problem can be solved by including the RSS, i.e., a measurement of the AN-UN distance into the positioning process along with the DoA [21]. Since the ToA is also a measurement of the AN-UN distance, the proposed joint DoA/ToA-EKF therefore does not suffer from such disadvantageous geometries either. In a 5G network, this is a very important property as the network is not primarily designed for positioning such that situations with geometries disadvantageous for positioning are inevitable. In fact, we cannot even guarantee that UNs are always in LoS with multiple ANs. Therefore, we have tested the tracking capabilities of the proposed joint DoA/ToA-EKF also for a second map with extremely challenging conditions as depicted in Fig. 3b. In this map the UN is in LoS with only a single AN for most of the time. *Therefore, the classical DoA-only EKF is not able to track the UN at all. The proposed joint DoA/ToA-EKF on the other hand estimates the UN position and clock offset with a RMSE of about* $3.0\,\mathrm{m}$ *and* $10.3\,\mathrm{ns}$*, respectively for* $N_T = 100$. By increasing the number of antennas, we should be able to further increase the positioning accuracy. This makes the proposed joint DoA/ToA-EKF also interesting for positioning with massive MIMO systems, where the number of antennas is significantly larger compared to what we have assumed in this paper. This forms one of the aspects in our future research.

The behavior of both the DoA-only EKF and the joint DoA/ToA-EKF in tracking is also illustrated in the videos that we have uploaded to *www.tut.fi/5G/GLOBECOM15*.

VI. Conclusion

In this paper we showed that 5G ultra dense networks are able to provide UN positioning with an accuracy that may even be in the sub-meter range. More specifically, we have proposed a joint DoA/ToA-EKF that tracks both the clock offset and position of the UNs within a 5G network. Using the METIS channel models that were developed specifically for 5G networks, we then demonstrated the achievable DoA/ToA estimation performance by means of the respective CRB. Finally, we used the obtained results to simulate the performance of the proposed joint DoA/ToA-EKF and showed that the joint DoA/ToA-EKF significantly outperforms existing DoA-only solutions, while at the same time obtaining highly accurate UN clock offset estimates as a byproduct. Moreover, we also demonstrated that the joint DoA/ToA-EKF is able to handle situations where DoA-only solutions are not able to estimate the UN position at all.

References

[1] Huawei, "5G: A technology vision (white paper)," 2013. [Online]. Available: http://www.huawei.com/5gwhitepaper/

[2] D. Dardari, P. Closas, and P. M. Djurić, "Indoor tracking: Theory, methods, and technologies," *accepted for publication in IEEE Trans. Vehicular Tech.*, 2015.

[3] J. Medbo, I. Siomina, A. Kangas, and J. Furuskog, "Propagation channel impact on LTE positioning accuracy: A study based on real measurements of observed time difference of arrival," in *Proc. IEEE 20th Int. Symp. Personal, Indoor and Mobile Radio Communications*, Sep. 2009, pp. 2213–2217.

[4] H. Liu, Y. Gan, J. Yang, S. Sidhom, Y. Wang, Y. Chen, and F. Ye, "Push the limit of WiFi based localization for smartphones," in *Proc. 18th Annu. Int. Conf. Mobile Computing and Networking (MobiCom)*. New York, NY, USA: ACM, 2012, pp. 305–316.

[5] P. Kela, M. Costa, J. Salmi, K. Leppänen, J. Turkka, T. Hiltunen, and M. Hronec, "A novel radio frame structure for 5G dense outdoor radio access networks," in *Proc. IEEE 81st Vehicular Technology Conference (VTC spring)*, 2015.

[6] X. Chen, Y. Chen, M. Dong, and C. Zhang, "Demystifying energy usage in smartphones," in *Proc. 51st Design Automation Conference*, Jun. 2014, pp. 1–5.

[7] V. Aidala, "Kalman filter behavior in bearings-only tracking applications," *IEEE Trans. Aerosp. Electron. Syst.*, vol. AES-15, no. 1, pp. 29 –39, 1979.

[8] H. Kim, X. Ma, and B. Hamilton, "Tracking low-precision clocks with time-varying drifts using Kalman filtering," *IEEE/ACM Trans. Netw.*, vol. 20, no. 1, pp. 257–270, Feb. 2012.

[9] METIS, "D6.1 simulation guidelines," Oct. 2013.

[10] METIS, "D1.4 channel models," February 2015.

[11] F. Benedetto, G. Giunta, A. Toscano, and L. Vegni, "Dynamic LOS/NLOS statistical discrimination of wireless mobile channels," in *Proc. Vehicular Technology Conference*, Dublin, Ireland, 2007, pp. 3071–3075.

[12] J. Zhang, J. Salmi, and E. Lohan, "Analysis of kurtosis based LOS/NLOS identification using indoor MIMO channel measurement," *IEEE Trans. Vehicular Tech.*, vol. 62, no. 6, pp. 2871–2874, 2013.

[13] Y.-C. Wu, Q. Chaudhari, and E. Serpedin, "Clock synchronization of wireless sensor networks," *IEEE Signal Process. Mag.*, vol. 28, no. 1, pp. 124–138, Jan. 2011.

[14] T. Kohno, A. Broido, and K. Claffy, "Remote physical device fingerprinting," *IEEE Trans. on Dependable Secure Comput.*, vol. 2, no. 2, pp. 93–108, Apr. 2005.

[15] M. Cristea and B. Groza, "Fingerprinting smartphones remotely via ICMP timestamps," *IEEE Commun. Lett.*, vol. 17, no. 6, pp. 1081–1083, Jun. 2013.

[16] R. Thoma, M. Landmann, and A. Richter, "RIMAX - a maximum likelihood framework for parameter estimation in multidimensional channel sounding measurement," in *Proc. Int. Symp. Antennas and Propagation*, Sendai, Japan, Aug. 2004, pp. 53–56.

[17] S. M. Kay, *Fundamentals of Statistical Signal Processing, Volume I: Estimation Theory*, 1st ed. Prentice Hall, Apr. 1993.

[18] D. Simon, *Optimal State Estimation: Kalman, H Infinity, and Nonlinear Approaches*, 1st ed. Hoboken, N.J: Wiley-Interscience, Jun. 2006.

[19] CELTIC, "D5.3: WINNER+ final channel models," June 2010.

[20] 3GPP, "TR 25.996 v12 UMTS, spatial channel model for MIMO simulations," September 2014.

[21] J. Werner, A. Hakkarainen, and M. Valkama, "Cramer-Rao bounds for hybrid RSS-DOA based location and transmit power estimation in cognitive radio systems," in *Proc. IEEE 78th Vehicular Technology Conf. (VTC fall)*, 2013.

Tampereen teknillinen yliopisto
PL 527
33101 Tampere

Tampere University of Technology
P.O.B. 527
FI-33101 Tampere, Finland

ISBN 978-952-15-3634-2
ISSN 1459-2045